STEFAN KOFLER

PARTON DISTRIBUTIONS: APPLICATIONS AND MODELS

DOCTORAL THESIS

For obtaining the academic degree of Doktor der Naturwissenschaften.

Institute of Physics, Department of Theoretical Physics,

University of Graz

Betreuer: Ao. Univ.-Prof. Mag. Dr. Wolfgang Schweiger

Graz, January 2017

Stefan Kofler: *Parton Distributions: Applications and Models*

Supervisor:
Ao. Univ.-Prof. Mag. Dr. Wolfgang Schweiger

ABSTRACT

High energy scattering processes are an essential tool for understanding the substructure of hadrons in terms of their constituents, i.e. quarks and gluons. The theory which describes the dynamics of quarks and gluons inside hadrons is called quantum chromodynamics (QCD). Using QCD for the description of high energy particle collisions is a very challenging task. Its applicability rests on the concept of factorization: the scattering process is separated into a part where one can use well established perturbative methods and into a part where the complicated hadron structure is parameterized by phenomenological functions. Those functions are the, so called, *parton distribution functions*. Factorization can be rigorously proved (so-called factorization theorems) only for a few specific examples. But it is plausibly assumed to hold at high-energies. The thesis is organized as follows: After a short introduction we investigate the exclusive production of charmed hadrons using a factorization based approach in the first main part of this thesis. To be more specific, we consider the following two processes: $\pi^- \; p \to D^- \; \Lambda_c^+$ and $\gamma \; p \to \overline{D}^* \; \Lambda_c^+$. Using physical plausible assumptions, the scattering amplitude factorizes into a perturbatively calculable partonic subprocess and hadronic matrix elements, which contain the non-perturbative bound-state dynamics of the hadronic constituents. These hadronic matrix elements are parameterized in terms of generalized parton distributions (GPDs) and a meson distribution amplitude (DA). We show estimates for the cross sections and spin correlation functions. In the second main part we use the, so called, *meson-cloud model* to model (collinear) parton distribution functions (PDFs) of the proton. We discuss the unpolarized, polarized and transversity PDFs of the proton as well as the flavor asymmetries in the unpolarized and polarized proton sea.

ZUSAMMENFASSUNG

Hochenergie-Streuprozesse sind unverzichtbar um die Substruktur der Hadronen auf Konstituentenniveau, d.h. auf Niveau von Quarks und Gluonen, zu studieren. Die Theorie, welche die Dynamik von Quarks und Gluonen innerhalb von Hadronen beschreibt, nennt man Quantenchromodynamik (QCD). Deren Anwendung auf Hochenergie-Streuprozesse gestaltet sich als sehr schwierig. Um QCD auf Hochenergie-Streuprozesse anwenden zu können, verwendet man das Konzept der Faktorisierung. Dabei trennt man den Streuprozess in zwei verschiedene Teile auf: In einem Teil, auf den man gut etablierte störungstheoretische Methoden anwenden kann und ein anderer Teil, der die komplizierte Substruktur der Hadronen durch phänomenologische Funktionen parametrisiert. Diese Funktionen sind die so genannten *Partonverteilungsfunktionen*. Faktorisierung kann man rigoros nur für ein paar bestimmte Prozesse beweisen, aber man ist im allgemeinen der Ansicht, dass Faktorisierung auch generell bei sehr hohen Energien gelten soll. Die Dissertation ist wie folgt aufgebaut: Nach einer kurzen Einleitung diskutieren wir im ersten Teil dieser Arbeit die exklusive Produktion von Teilchen mit "Charm". Genauer gesagt, untersuchen wir die folgenden zwei Prozesse $\pi^- \; p \to D^- \; \Lambda_c^+$ und $\gamma \; p \to \overline{D}^* \; \Lambda_c^+$, indem wir eine durch Faktorisierung motivierte Herangehensweise benützen. Unter physikalisch plausiblen Annahmen faktorisieren die Streuamplituden in einen störungstheoretisch behandelbaren partonischen Teilprozess und hadronische Matrixelemente, welche die Formation der Partonen zu Hadronen beschreiben. Diese Matrixelemente werden durch sogenannte generalisierte Parton-Distributionen und Meson-Distributionsamplituden paramterisiert. Wir erhalten numerische Vohersagen für differentielle und integrierte Wirkungsquerschnitte, sowie Spin-Korrelationsfunktionen. Im zweiten Teil der Dissertation benützen wir ein *Meson-cloud Modell* um (kollineare) Partonverteilungsfunktionen des Protons zu modellieren. Wir diskutieren insbesondere nicht polarisierte, polarisierte und transversale Partonverteilungsfunktionen, sowie die dazugehörigen "flavor"- Asymmetrien im (nicht) polarisierten See des Protons.

CONTENTS

1 Introduction

Quantum chromodynamics (QCD) is the quantum field theory of the strong interaction. It is formulated as a gauge theory with $SU(3)_{color}$ as the corresponding gauge group which gives the theory its non-abelian character. The fundamental building blocks of QCD are spin $\frac{1}{2}$ particles, called the quarks, and spin 1 gauge bosons, called the gluons. QCD has two remarkable features which are predominant in different energy regimes

- In the high energy regime (or equivalently short space-time distances): **Asymptotic freedom**.
  Asymptotic freedom means that the coupling constant of QCD, α_s, becomes small at high energies and hence we can use well established perturbative methods to make theoretical predictions. This branch of QCD is termed perturbative QCD (pQCD) [1].

- In the low energy regime (or equivalently at large space-time distances): **Confinement**.
  Confinement stands, loosely speaking, for the fact that quarks and gluons cannot be isolated from each other, i.e. colored particles are not observable in nature. Furthermore in the low energy regime the coupling α_s becomes large, so that perturbative methods are not applicable. Rather we have to stick to some modeling or use non-perturbative methods such as lattice QCD [2].

Up to now it is not fully understood how quarks and gluons (which do not exist as isolated particles) form the observed hadrons. The missing link to fully describe all phenomena of the strong interaction within QCD is the transition from its elementary building blocks, i.e. quarks and gluons, to the real objects observed in experiments, i.e. hadrons. Therefore, QCD confronts us with a problem: On the macroscopic level our detectors can only detect hadrons. But with *hard processes*[1] we can also probe their substructure. How is it possible to learn something about the microscopic structure, that is on the level of quarks and gluons, from the experiments if we do not understand the transition from there to the observable hadrons? The answer and the way out of the dilemma is provided by factorization which is also the basis of the *parton model*. Thereby the process of interest is divided into two parts: a short-distance partonic subprocess that can be calculated by means of pQCD and the long

[1] These are generally high-energy processes that involve at least one hard scale such as a high photon virtuality or a large momentum transfer which justifies the use of pQCD

distance binding effects that are described by hadronic matrix elements of parton field operators. The short distance effects (hard physics) and the long distance effects (soft physics) decouple from each other and to a good approximation do not influence each other. The former are in principle calculable to arbitrary accuracy, but going beyond tree level becomes soon very tricky and quite tedious. The soft physics part is parameterized in the form of, a priori, unknown functions. Depending on the process of interest these functions can be

- Form factors (FFs)
- Parton distribution functions (PDFs)
- Generalized parton distributions (GPDs)
- ...

The predictive power of the formalism with FFs, PDFs and GPDs rests on the property of *universality* which means that, once measured in a hard process, FFs, PDFs and GPDs can be used for the calculation of other processes (requiring the same type of distributions). It is beyond the scope of this chapter to give a comprehensive introduction to these functions. We rather want to state their definition and we also want show typical examples whose description involves the above mentioned phenomenological functions[2]. We note that this will be done in a schematic and strongly simplified manner.

The nucleon structure has been extensively investigated by two main classes of scattering processes since the late 60's: Elastic scattering processes and inclusive (deep) inelastic scattering.
Let us start to consider the *elastic* process $e^- N \to e^- N$, see left panel of Fig. 1.1. An electron e^- exchanges a highly virtual photon γ^* with the nucleon N. The nucleon changes its momentum but it remains a nucleon. The photon interacts with a single quark inside the nucleon. The "soft" physics is factorized into the FFs $F_1^q(t)$ and $F_2^q(t)$ where $t = (p_N - p'_N)^2 = -Q^2$ and Q^2 being minus the photon four-momentum squared. They are related to the following vector QCD local operators (since we need them later we also define at this point the axial vector operators[3]), see right panel of Fig.1.1

$$\begin{aligned}
\langle N : p'_N | \bar{\Psi}^q(0) \gamma^+ \Psi^q(0) | N : p \rangle &= \bar{u}\left(p'_N\right) \left[F_1^q(t) \gamma^+ + F_2^q(t) \frac{i\sigma^{+\nu}\Delta_\nu}{2m_N} \right] u\left(p_N\right), \\
\langle N : p'_N | \bar{\Psi}^q(0) \gamma^+ \gamma_5 \Psi^q(0) | N : p \rangle &= \bar{u}\left(p'_N\right) \left[G_A^q(t) \gamma^+ \gamma_5 + G_P^q(t) \gamma_5 \frac{\Delta^+}{2m_N} \right] u\left(p_N\right).
\end{aligned} \tag{1.1}$$

[2] We follow here closely chapter 1 of Ref. [3]
[3] Those cannot be accessed in elastic lepton nucleon scattering

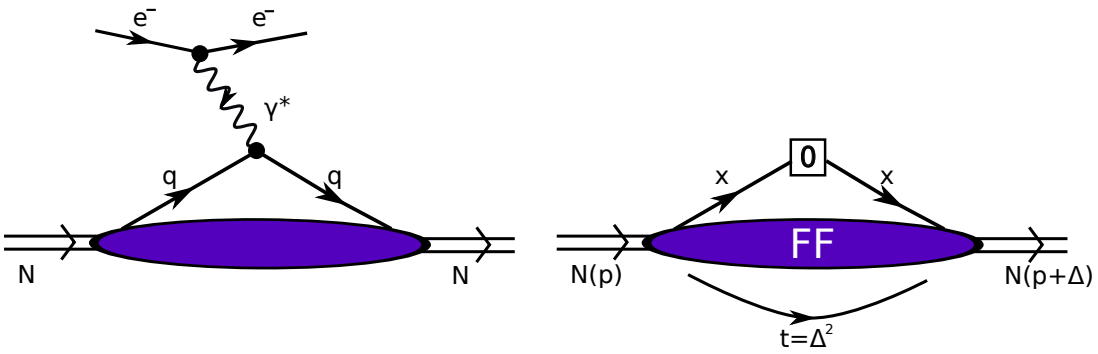

Figure 1.1: Left panel: Elastic scattering. Right panel: Illustration of the associated local non-diagonal matrix element which can be accessed in the elastic scattering process as shown in the left panel.

These operators are non-diagonal since the momenta of the initial and final nucleons are different and they are local since the initial and final quarks are created (annihilated) at the same space-time point.

The second class is inclusive deep inelastic scattering (DIS) $e^- N \to e^- X$, where X denotes an undefined final state. The electron scatters through one photon exchange[4]. For sufficiently high Q^2 we can "see" the inner structure of the nucleon[5], see left panel of Fig. 1.2. The photon interacts with a single quark of the nucleon. The struck quark is hit so hard that it "escapes" its parent nucleon and hadronizes. The nucleon also breaks-up into many fragments leaving the final state undetermined. The complex quark and gluon structure as governed by QCD is factorized into the unpolarized PDF $f_1^q(x)$ and polarized PDF $g_1^q(x)$. They correspond to the following QCD operators[6]

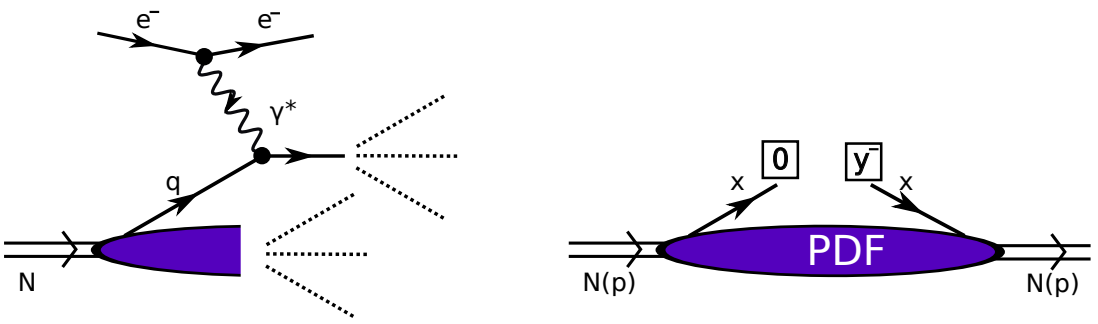

Figure 1.2: Left panel: Deep inelastic scattering. Right panel: Illustration of the associated diagonal non-local matrix element which can be accessed in DIS.

[4]This is only a first approximation. The effects of two photon exchanges are beyond the scope of this text.

[5]The approximate Q^2-independence of the cross section in the early days of the experiment was (correctly) interpreted as a signature of a process where the photon interacts with a pointlike constituent inside the nucleon. QCD modified this picture and gave an explanation of the Q^2-dependence of the cross section.

$$
\begin{aligned}
f_1^q(x) &= \frac{1}{2}\int \frac{\mathrm{d}z^-}{2\pi} e^{i\,x\,p^+\,z^-}\ \langle N:p|\bar{\Psi}^q\left(0\right)\gamma^+\Psi^q\left(y^-\right)|N:p\rangle\,, \\
g_1^q(x) &= \frac{1}{2}\int \frac{\mathrm{d}z^-}{2\pi} e^{i\,x\,p^+\,z^-}\ \langle N:p,S_\parallel|\bar{\Psi}^q\left(0\right)\gamma^+\gamma_5\Psi^q\left(y^-\right)|N:p,S_\parallel\rangle\,.
\end{aligned}
\tag{1.2}
$$

$S_\parallel$ denotes the longitudinal nucleon spin projection and x is the longitudinal momentum fraction carried by the struck quark. Since space-time coordinates of the initial and final nucleon are different, the operators in Eq. (1.2) are non-local and since the momenta of the initial and final nucleon are identical they are diagonal. The operators are illustrated in the right panel of Fig. 1.2. These PDFs are a 1-dimensional momentum distribution of the quarks inside the nucleon and therefore also called *collinear* PDFs.
The PDFs $f_1^q(x)$ and $g_1^q(x)$ do not exhaust all the possible collinear distribution functions which can be defined. It is also possible to define the transversity $h_1^q(x)$ by

$$
h_1^q(x) = -\frac{1}{2}\int \frac{\mathrm{d}z^-}{2\pi} e^{i\,x\,p^+\,z^-}\ \langle N:p,S_\perp|\bar{\Psi}^q\left(0\right)\ i\sigma^{+1}\gamma_5\,\Psi^q\left(y^-\right)|N:p,S_\perp\rangle\,, \tag{1.3}
$$

with $S_\perp$ being the transverse spin projection. Equation (1.3) is a chiral odd quantity and cannot be accessed in DIS. In order to measure h_1 the chirality must be flipped twice: We must either have two hadrons in the initial state or one hadron in the initial state and at least one hadron in the final state. Thus it is very challenging to extract information about the transversity from experiments. From a phenomenological point of view, the unpolarized PDF is a very well know quantity, the polarized PDF is know to some extent and the transversity is poorly know.

In the 90's another class of reactions attracted much interest: *Hard exclusive reactions*. Such reactions are experimentally very challenging, since it is very difficult to hit a complex composite object very hard (to resolve its substructure) on the one hand and to avoid a break-up into fragments (to detect a specific final state) on the other hand. The consequence is low counting rates in an experiment. As an example we consider the exclusive electroproduction of a photon on the nucleon at large Q^2 , i.e. $\gamma^* N \to \gamma N$, see left panel of Fig. 1.3. Such a diagram is also called a "handbag" diagram. The factorization theorem states that the handbag mechanism is the dominant one for sufficiently high virtuality of the initial photon. It scatters on the quark and the *same* quark radiates away the final photon. The factorizing functions are the so called GPDs[7] $H^q\left(x,\xi,t\right)$, $E^q\left(x,\xi,t\right)$, $\tilde{H}^q\left(x,\xi,t\right)$ and $\tilde{E}^q\left(x,\xi,t\right)$. They correspond to the Fourier transform of non-local and non-diagonal QCD operators (which are also

[6] We are working in light-cone gauge, i.e. $A^+ = 0$.
[7] Omitting their Q^2-dependence. It is a consequence of Lorentz invariance that the GPDs depend on the three variables x, ξ and t.

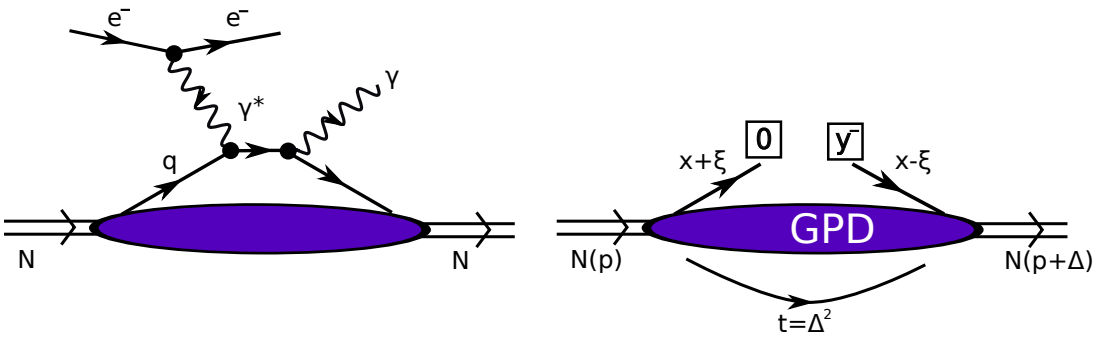

Figure 1.3: Left panel: Deep inelastic scattering. Right panel: Illustration of the associated diagonal non-local matrix element which can be accessed in DIS.

illustrated in the right panel of Fig. 1.3)

$$\begin{aligned}
&\frac{1}{2}\int\frac{dz^-}{2\pi}e^{ixP^+z^-}\left\langle N:p'|\bar{\Psi}^q\left(0\right)\gamma^+\Psi\left(y^-\right)|N:p\right\rangle \\
&=\frac{1}{2P^+}\overline{u}(p')\left[H^q(x,\xi,t)\gamma^+ + E^q(x,\xi,t)\,\frac{i\sigma^{+\nu}\Delta_\nu}{2m_N}\right]u(p), \\
&\frac{1}{2}\int\frac{dz^-}{2\pi}e^{ixP^+z^-}\left\langle N:p'|\bar{\Psi}^q\left(0\right)\gamma^+\gamma_5\Psi\left(y^-\right)|N:p\right\rangle \\
&=\frac{1}{2P^+}\overline{u}(p')\left[\tilde{H}^q(x,\xi,t)\gamma^+\gamma_5 + \tilde{E}^q(x,\xi,t)\,\gamma_5\frac{\Delta^+}{2m_N}\right]u(p),
\end{aligned} \tag{1.4}$$

where P is the average nucleon momentum, i.e. $P = \left(p_N + p'_N\right)/2$, $t = \Delta^2 = \left(p'_N - p_N\right)^2$ and $\xi = \frac{-\Delta^+}{2P^+}$, respectively. If we look at Eq. (1.4), we see that the quark field operator structure is helicity conserving. It is also possible to define transversity GPDs involving the use of the $\sigma^{+\nu}$ operator between the quark fields, see Ref. [4] for more details.
For a comprehensive review on GPDs we refer the interested reader to Ref. [5]. However, we do mention a few important properties:

- *Partonic content*:
  x can vary between -1 and 1 and ξ could in principle also vary in that range but due to time reversal invariance the range of ξ is reduced to be between 0 and 1. If $|x| > \xi$ the GPDs represent the probability amplitude of taking out a quark (or an antiquark if $x < -\xi$) from the nucleon with a plus momentum fraction $x + \xi$ $(\xi - x)$ and reinsert it back to the nucleon with a momentum fraction $x - \xi$ $(-\xi - x)$ plus some "kick" in the transverse momentum represented by t. In the region $-\xi < x < \xi$ the GPDs are the probability amplitude of finding a quark-antiquark pair in the nucleon with a momentum fraction $x + \xi$ and $\xi - x$ of the plus momentum, respectively. This partonic interpretation of the GPDs also reveal their novelty: The correlations between (anti-)quarks with different momenta or the information on $q\bar{q}$ configurations are relatively unknown.

  The region $|x| > \xi$ is also called $DGLAP$-region[8] and the region $-\xi < x < \xi$ is

[8] Dokshitzer-Gribov-Lipatov-Altarelli-Parisi

called the $ERBL$-region[9] following the different patterns of the evolution in the factorization scale.

- *Helicity content*:
  At the nucleon level H^q and $\tilde{H}^q$ leave the nucleon helicity unchanged, whereas E^q and $\tilde{E}^q$ are associated with a flip of the nucleon helicity. On the quark level H^q and E^q correspond to the average of quark helicities and are therefore called *unpolarized* GPDs. The GPDs $\tilde{H}^q$ and $\tilde{E}^q$ involve differences of quark helicities and are called *polarized* GPDs. Thus, the four GPDs of Eq. (1.4) reflect the independent quark-nucleon helicity combinations[10].

- *Forward limit*:
  In the forward limit, i.e. $\xi, t \to 0$, the GPDs $H^q(x,0,0)$ and $E^q(x,0,0)$ reduce to the collinear PDFs $f_1^q(x)$ and $g_1^q(x)$, respectively.

- *First moment*:
  The first moments of the GPDs of Eq. (1.4) are related to the FFs of Eq. (1.1) by

$$\begin{aligned} \int_{-1}^{1} \mathrm{d}x H^q(x,\xi,t) &= F_1^q(t), \quad \int_{-1}^{1} \mathrm{d}x E^q(x,\xi,t) = F_2^q(t), \\ \int_{-1}^{1} \mathrm{d}x \tilde{H}^q(x,\xi,t) &= G_A^q(t), \quad \int_{-1}^{1} \mathrm{d}x \tilde{E}^q(x,\xi,t) = G_P^q(t). \end{aligned} \tag{1.5}$$

- *Second moment*:
  The second moment of the GPDs, Ji's sum rule, is relevant for the spin structure of the nucleon. In Ref. [6] it was shown that the nucleon spin can be decomposed as follows: $\frac{1}{2} = J_q + J_g$, where J_q is the total quark contribution to the nucleon spin and J_g is the total gluon contribution to the nucleon spin, respectively. Ji's sum rule relates J_q to the GPDs:

$$J_q = \frac{1}{2} \int_{-1}^{1} \mathrm{d}x\, x \Big[H^q(x,\xi,t=0) + E^q(x,\xi,t=0) \Big]. \tag{1.6}$$

The first and the second moment of the GPDs are a particular case of a more general sum rule: x^n moments of the GPDs must be a polynomial in ξ of order n. This property is called *polynomiality* [5].

For the sake of completeness we mention that the FFs, PDFs and GPDs can be considered as a particular limit of more generalized objects, called *generalized parton correlation functions*, which provide a unified framework to discuss all the information on partons within hadrons.

In this thesis we deal not only with parton distributions of the nucleon and their modeling, but also with generalized parton distributions which describe the transition betweens hadrons– in our case $p \to \Lambda_c$ and $\pi \to D$ transitions. We analyze

[9] Efremov-Radyushkin-Brodsky-Lepage
[10] Conserving the quark helicity.

the handbag contributions to $\pi^- \; p \to D^- \; \Lambda_c^+$ and $\gamma \; p \to \overline{D}^*_{\lambda=0} \; \Lambda_c^+$, show how the transition GPDs arise in these processes, model the GPDs and make predictions for the corresponding reaction cross section. The thesis is organized as follows: It is divided into two main parts. In the first part, Sec. 2, we investigate the exclusive production of charmed hadrons. We start in Sec. 2.1 by pointing out that the situation on the description of charmed hadron production is controversial in the sense that the estimates of the production cross sections can differ by orders of magnitude for the different models available on the market. We discuss then how

- $\pi^- \; p \to D^- \; \Lambda_c^+$ (see Sec. 2.3),
- $\gamma \; p \to \overline{D}^*_{\lambda=0} \; \Lambda_c^+$ (see Sec. 2.4),

can be described within the generalized parton picture. The soft ingredients to these processes are $p \to \Lambda_c$ and $\pi \to D$ transition GPDs, which we model by means of valence quark light-cone wave functions for the hadrons involved. We conclude this chapter in Sec. 2.5 by discussing how the large differences in the cross section predictions as compared to our model come about.

In the second part, Sec. 3, we use a front form meson-cloud model to calculate collinear nucleon PFDs. We start in Sec. 3.2 to present the basics of the meson cloud model, explain in Sec. 3.3 how we can apply the meson-cloud model to get a convolution formula of the PDFs and finally present our results in Sec. 3.5.

2

Hard exclusive production of charmed particles

In this section we motivate why exclusive production of charmed particles is an interesting research field and then use a handbag approach to describe the following two processes:

- $\pi^- \; p \to D^- \; \Lambda_c^+$ (Sec. 2.3),
- $\gamma \; p \to \overline{D}^*_{\lambda=0} \; \Lambda_c^+$ (Sec. 2.4).

The pion induced process was published in Ref. [7] and the photoproduction of the longitudinally polarized $\overline{D}^*$ mesons (which we denote by $\overline{D}^*_{\lambda=0}$) is unpublished so far. We note that the photoproduction of the pseudoscalar $\overline{D}^0$ meson has been already studied and published in Refs. [8, 9][1]. Updated results with the same constituent kinematics as chosen now for the $\overline{D}^*_{\lambda=0}$ case are therefore included (and shown for the very first time) in this thesis in App. G.

2.1 Why should we study the production of charmed hadrons?

There is a vivid interest in the prediction of cross sections for the exclusive production of charmed hadrons. Be it for the planned $\bar{P}ANDA$ experiments [2], the new facility at *J-PARC* [3] with a high energy pion beam, or for the upgraded JLab [4]. To asses the capacity of the experiments and to plan the upcoming experiments it is important to know the amount of produced charmed mesons and baryons, i.e. to have a reliable estimate of the cross section. However the investigation of such processes is a very challenging task because of two main reasons:

- Lack of experimental data (to constrain parameters).

[1] The constituent kinematics chosen there is physically plausible, but violates four-momentum conservation on the constituent level.

[2] One of the key experiments at *FAIR* (Facility for Antiproton and Ion Research) in Darmstadt will be the $\bar{P}ANDA$ experiment. In this experiment one is, among other things, interested in charmed hadron spectroscopy and how charmed hadrons are modified when they are embedded in hadronic matter. One big advantage in using $\bar{p} \; p$ collisions to produce charmed particle pairs is that no extra particles are need to ensure charm conservation.

[3] *J-PARC* stands for Japan Proton Accelerator Research Complex. One experimental program is devoted to the study of (excited) charmed Lambda-particles. The reaction chosen to investigate these questions is $\pi \; p \to D^{(*)} \Lambda_c$.

[4] The energy of the photon beam after the 12 GeV upgrade at JLab (Jefferson Lab) is big enough to produce charmed mesons.

- The dominant production mechanism for charmed hadron production is not known.

The first point will become much less severe with the (above mentioned) upcoming experiments with which a considerable improvement of the experimental situation for charmed hadron production is to be expected. The second point is from the perspective of a theoretical physicist very exciting since several models can be used and compared with each other. In fact the situation is such, that the various predictions differ by several orders of magnitude as emphasized for example in Ref. [10] for $\bar{p}\ p \to \bar{\Lambda}_c^-\ \Lambda_c^+$. Let us illustrate this statement in some more detail. In particular we sketch the main features of the *generalized parton picture* (which we also use to investigate the processes mentioned in the very beginning of this section) and those of *hadronic models* and plot the estimates of the cross section.

In Fig. 2.1 we show the unpolarized cross section integrated over the forward hemisphere for $\bar{p}\ p \to \bar{\Lambda}_c^-\ \Lambda_c^+$ as predicted by the generalized parton picture. Its magnitude is of the order of 1 nb.

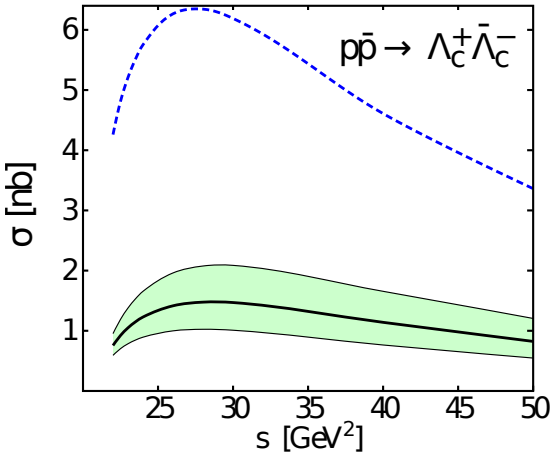

Figure 2.1: The cross section of $\bar{p}\ p \to \bar{\Lambda}_c^-\ \Lambda_c^+$ integrated over the forward hemisphere (i.e. $\cos\theta \leq 0$) using a handbag mechanism (see Fig. 2.2). This plot is taken from Ref. [11].

The main features of this approach are:

- The reaction mechanism is the handbag mechanism[5] shown in Fig. 2.2. The arguments why pole contributions (ERBL-region) can be neglected can be found in Ref. [11].
- The charm quarks are produced perturbatively.
- The transition GPDs for $p \to \Lambda_c^+$ and $\bar{p} \to \bar{\Lambda}_c^-$ are unknown: They need to be modeled.

In Fig. 2.3 we show the results for the integrated cross section using hadronic models. Their main features are

[5]Based on the hypothesis that hard and soft processes factorize.

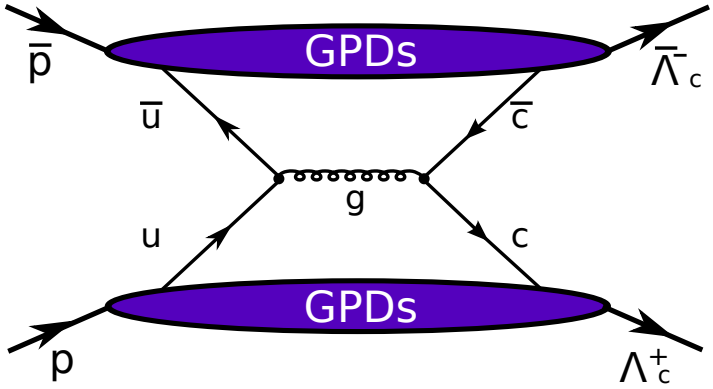

Figure 2.2: The double handbag contribution to $\bar{p}\ p \to \bar{\Lambda}_c^-\ \Lambda_c^+$.

- Charm is produced non-perturbatively via (single or reggeized) exchange of a hadron H, see Fig. 2.4.
- The strong coupling at the vertex is unknown. $SU(4)_f$-symmetry as a first approximation or for example QCD sum rules are used to determine the couplings.

When we compare Fig. 2.1 with Fig. 2.3 we note that there are differences in the predictions up to three orders of magnitude.

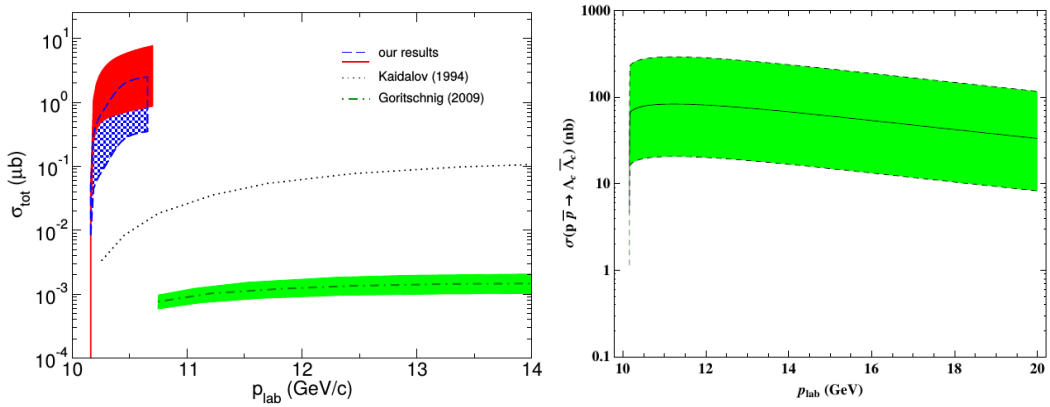

Figure 2.3: The integrated cross section for $\bar{p}\ p \to \bar{\Lambda}_c^-\ \Lambda_c^+$ predicted by hadronic models. On the left panel we show the result from an unreggeized hadronic model and on the right panel the result for a reggeized hadronic model. The figures are taken from Ref. [10] (left panel) and from Ref. [12] (right panel), respectively.

The differences are discussed in more detail in Sec. 2.5. We focus especially on the comparison with our model calculations.

Finally we note a complication in the theoretical description of the production of charmed hadrons. The presence of the charm quark introduces a mass scale which is much large than the confinement scale $\Lambda_Q \approx 300$ MeV. Since the mass scale of the lighter quarks is $\ll \Lambda_Q$ there are now two different scales. One way to deal with two different scales is to use effective theories such as heavy quark effective theories

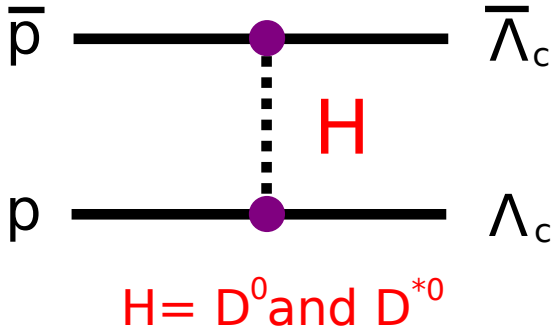

Figure 2.4: Graphical representation of the hadronic models used to describe $\bar{p}\ p \to \bar{\Lambda}_c^-\ \Lambda_c^+$. The intermediate line represents the (single or reggeized) exchange of a hadron H. For this particular process $H = D^0$ and D^{*0}.

(HQET)[6]. The large charm mass certainly justifies to apply HQET but is still not large enough to ignore corrections to it. Therefore, charmed hadrons are also ideal candidates to test and apply the predictions of HQET.

2.2 HARD EXCLUSIVE PRODUCTION OF CHARMED HADRONS WITHIN THE GENERALIZED PARTON PICTURE

Hard exclusive processes have attracted much attention in recent years by both, theoreticians and experimentalists. Above all the deeply virtual reactions as leptoproduction of mesons and photons have been theoretically studied and measured in great detail. This interest is based on the asymptotic factorization theorems which state that the process amplitudes can be represented as convolutions of perturbatively calculable partonic subprocess amplitudes with generalized parton distributions (GPDs). This, so-called, handbag approach is quite successful in describing the deeply virtual processes qualitatively as well as quantitatively. An alternative class of hard exclusive processes is characterized by large Mandelstam $-t$ (and $-u$) providing the hard scale. For this class the amplitudes factorize in a product of subprocess amplitudes and form factors representing moments of GPDs. Examples of such processes are wide-angle real Compton scattering or time-like reactions as, e.g., two-photon annihilations into pairs of hadrons. Also the time-reversed process proton-antiproton annihilation into two photons (or photon and meson) belong to this class. Again the handbag approach works very well in that case. A particular outstanding example is real Compton scattering. A GPD analysis of the nucleon form factors provides also results for the Compton form factors. Hence, Compton scattering in the wide-angle region can be evaluated free of parameters. The results are found to be in fair agreement with experiment. New measurements performed at the upgraded Jlab will provide another crucial test for the quality of these results. Future precise data from BELLE and FAIR may further probe the predictions for the time-like processes.

A third class of hard exclusive processes, which are amenable to the handbag approach, is formed by reactions involving heavy hadrons. Here the large scale is set

[6] Introductions to HQET can be found in Refs. [13, 14].

by the heavy-quark mass and the model can be applied to the forward hemisphere and Mandelstam s well above the reaction threshold. Like for the wide-angle processes the heavy-hadron amplitudes are represented by products of subprocess amplitudes and appropriate form factors. Till now the processes $\bar{p}p \to \bar{\Lambda}_c^- \Lambda_c^+$ [11], $\bar{p}p \to D^0 \overline{D}^0$ [15] and $\gamma p \to \overline{D}^0 \Lambda_c^+$ [8, 9] [7] have been investigated. In this thesis we add two further processes, namely $\pi^- \; p \to D^- \; \Lambda_c^+$ in Sec. 2.3 (published in Ref. [7]) and $\gamma \; p \to \overline{D}^*_{\lambda=0} \; \Lambda_c^+$ in Sec. 2.4 (unpublished).

[7] For an updated calculation see App. G.

2.3 $\pi^- \, p \to D^- \, \Lambda_c^+$

In this section we investigate a pion induced reaction for charmed particle production.

2.3.1 *Kinematics*

The momenta, light-cone (LC) helicities and masses of the incoming proton and π^- are denoted by p, μ, m_p and q, m_π, those of the outgoing Λ_c^+ and D^- by p', μ', M_{Λ_c} and q', M_D, respectively. We consider the reaction in a symmetric center-of-momentum system (CMS) which has the z-axis aligned along the three-vector part, $\bar{\mathbf{p}}$, of the average momentum $\bar{p} \equiv \frac{1}{2}(p + p')$. This reference frame is chosen such that the transverse component of the momentum transfer $\Delta \equiv (p' - p) = (q - q')$ is symmetrically shared between the particles. Introducing the skewness parameter

$$\xi \equiv \frac{p^+ - p'^+}{p^+ + p'^+} = -\frac{\Delta^+}{2\bar{p}^+}, \tag{2.1}$$

we parameterize the proton and the Λ_c^+ momenta as follows[8]

$$p = \left[(1+\xi)\bar{p}^+, \frac{m_p^2 + \boldsymbol{\Delta}_\perp^2/4}{2(1+\xi)\bar{p}^+}, -\frac{\boldsymbol{\Delta}_\perp}{2}\right], \quad p' = \left[(1-\xi)\bar{p}^+, \frac{M_{\Lambda_c}^2 + \boldsymbol{\Delta}_\perp^2/4}{2(1-\xi)\bar{p}^+}, \frac{\boldsymbol{\Delta}_\perp}{2}\right]. \tag{2.2}$$

The π^--meson and the D^--meson momenta can be written in an analogous way

$$q = \left[\frac{m_\pi^2 + \boldsymbol{\Delta}_\perp^2/4}{2(1+\eta)\bar{q}^-}, \, (1+\eta)\bar{q}^-, \, \frac{\boldsymbol{\Delta}_\perp}{2}\right], \quad q' = \left[\frac{M_D^2 + \boldsymbol{\Delta}_\perp^2/4}{2(1-\eta)\bar{q}^-}, (1-\eta)\bar{q}^-, -\frac{\boldsymbol{\Delta}_\perp}{2}\right], \tag{2.3}$$

with

$$\bar{q} \equiv \frac{1}{2}(q + q') \quad \text{and} \quad \eta \equiv \frac{q^- - q'^-}{q^- + q'^-} = \frac{\Delta^-}{2\bar{q}^-}. \tag{2.4}$$

The Mandelstam variable s is given by

$$s = (p+q)^2 = (p'+q')^2, \tag{2.5}$$

which is the invariant mass squared of our process. Mandelstam s has to be larger than $(M_{\Lambda_c} + M_D)^2 = 17.27\ \text{GeV}^2$ to produce the particles Λ_c^+ and D^-. The remaining two Mandelstam variables read

$$t = \Delta^2 = (p' - p)^2 = (q - q')^2 \tag{2.6}$$

and

$$u = (q' - p)^2 = (p' - q)^2, \tag{2.7}$$

[8] The notation that we use can be found in the App. A.

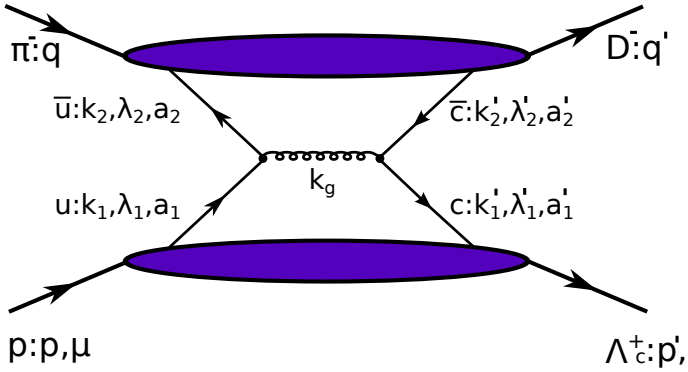

Figure 2.5: The double-handbag contribution to the process $\pi^- \; p \to D^- \; \Lambda_c^+$ (in the DGLAP region). The momenta, LC helicities and colors of the quarks are specified.

such that

$$s + t + u = m_p^2 + m_\pi^2 + M_{\Lambda_c}^2 + M_D^2. \tag{2.8}$$

The explicit expressions for $\bar{p}^+$, $\bar{q}^-$, ξ, η, $\boldsymbol{\Delta}_\perp^2$, t, u can be found in App. B with[9] $m_a = m_p = 0.938272$ GeV, $m_b = m_\pi = 0.139570$ GeV, $m_c = M_{\Lambda_c} = 2.286460$ GeV and $m_d = M_D = 1.869620$ GeV.

2.3.2 *Double-handbag mechanism*

As in Ref. [11] we argue that intrinsic (non-perturbative) charm of the proton (see also Sec. 2.5.3) can be neglected and the mechanism which dominates $\pi^- \; p \to D^- \; \Lambda_c^+$ well above the kinematical threshold $\left(\approx 17.27 \text{ GeV}^2\right)$ and in the forward hemisphere is the one depicted in Fig. 2.5. It is understood that the proton emits a u-quark[10] with momentum k_1 and helicity λ_1, the π^- a $\bar{u}$-quark with momentum k_2 and helicity λ_2, respectively. They undergo a scattering with each other, i.e. they annihilate into a gluon and subsequently produce the $c\bar{c}$ pair. The heavy partons, characterized by k_1', λ_1' and k_2', λ_2', are reabsorbed by the remnants of the proton and the π^- to form the final Λ_c^+ and D^-. To produce the $c\bar{c}$-pair the Mandelstam variable $\hat{s}$ of the subprocess[11] has to be

$$\hat{s} \geq 4m_c^2 \approx 6.50 \text{ GeV}^2. \tag{2.9}$$

The (heavy) quark mass m_c therefore serves as a natural scale which implies that the intermediate gluon has to be highly virtual.

2.3.2.1 *"Factorization" of the handbag diagram*

In the quantum-field-theoretical sense, factorization means that IR-sensitive contributions arising from radiative corrections to the partonic cross-sections or amplitudes can be unambiguously absorbed into appropriate hadronic quantities. We use the

[9] The values of the masses are taken from Ref. [16].
[10] The light quarks are treated as massless particles.
[11] Generally, the "hat" on Mandelstam variables indicates that those Mandelstam variables refer to the partonic subprocess.

word "factorization" in a more loose sense[12]: We just mean the physical situation of a hard subprocess on the partonic level ($u\bar{u} \to c\bar{c}$) at $\mathcal{O}(\alpha_s)$ and the soft emission (re-absorption) of partons by the proton and π^- (Λ_c^+ and D^-) described by soft hadronic matrix elements on the hadronic level. In order to justify such a picture we have to make the following assumptions [11, 17]:

- The parton virtualities and (intrinsic) transverse momenta[13] are restricted by a typical hadronic scale Λ which is of the order of 1 GeV:

$$k_i^2 \lesssim \Lambda^2 \text{ for } u\text{-quarks} \quad \text{and} \quad |k_i^2 - m_c^2| \lesssim \Lambda^2 \text{ for charm quarks,} \tag{2.10}$$

$$\frac{\mathbf{k}_\perp^{(\prime)2}}{x_i^{(\prime)}} \lesssim \Lambda^2. \tag{2.11}$$

The $u \to c$ ($\bar{u} \to \bar{c}$) transition GPDs are a function of three variables: The average momentum fraction defined by

$$\bar{x}_1 = \frac{k_1^+ + k_1'^+}{p^+ + p'^+} \left(\bar{x}_2 = \frac{k_1^- + k_1'^-}{q^- + q'^-} \right), \tag{2.12}$$

the skewness parameter ξ (η) and Mandelstam t.

- $p \to \Lambda_c$ ($\pi \to D$) GPDs exhibit a pronounced peak at a large value of $\bar{x}_1$ ($\bar{x}_2$) close to the ratio of charm-quark to charmed-hadron masses $\bar{x}_{10} = m_c/M_{\Lambda_c} \approx 0.56$ ($\bar{x}_{20} = m_c/M_D \approx 0.68$). Such a behavior parallels the theoretical expected and experimentally confirmed property of heavy-quark fragmentation functions, in particular for $c \to \Lambda_c^+$ [18] and is also analogous to the behavior of heavy-hadron distribution amplitudes (DAs) [19, 20]. It also ensures that the active u ($\bar{u}$) and c ($\bar{c}$) quarks which take part in the hard subprocess do not have large transverse momentum with respect to their parent hadron, cf. Ref. [21].

Under these assumptions, with m_c taken as the hard scale, the hadronic amplitude $\mathcal{M}$ is represented as a product of a hard partonic scattering kernel $\tilde{H}$ and soft hadronic matrix elements which describe the $p \to \Lambda_c$ and $\pi \to D$ transitions by emission and absorption of soft (anti)quarks. These quarks participate in the partonic subprocess $\bar{u}\,u \to \bar{c}\,c$, are approximately on-mass-shell and collinear with their parent hadron. Of course, this is by no means a proof for factorization but we rather take it as an assumption to be confronted with experimental data.

[12] We do not give a proof of factorization, but rather argue under which assumptions factorization may happen.

[13] The i-th parton carries a momentum fraction $x_i^{(\prime)}$ of its parent particle.

2.3.2.2 *The scattering amplitude I*

The scattering amplitude for the process can be written as[14]

$$\begin{aligned}\mathscr{M}_{\mu',\mu} = \sum_{a_i^{(\prime)},\alpha_i^{(\prime)}} \int \mathrm{d}^4\bar{k}_1 \; \Theta(\bar{k}_1^+) \int \frac{\mathrm{d}^4 z_1}{(2\pi)^4} e^{i\bar{k}z_1} \int \mathrm{d}^4\bar{k}_2 \; \Theta(\bar{k}_2^-) \int \frac{\mathrm{d}^4 z_2}{(2\pi)^4} e^{i\bar{k}_2 z_2} \\ \times \langle \Lambda_c^+ : p', \mu' | \mathscr{T} \overline{\Psi}^c_{a_1',\alpha_1'} \left(-\frac{z_1}{2}\right) \Psi^u_{a_1,\alpha_1} \left(\frac{z_1}{2}\right) | p : p, \mu \rangle \; \widetilde{H}_{a_i^{(\prime)},\alpha_i^{(\prime)}} \left(\bar{k}_1, \bar{k}_2\right) \\ \times \langle D^- : q' | \mathscr{T} \overline{\Psi}^u_{a_2,\alpha_2} \left(\frac{z_2}{2}\right) \Psi^c_{a_2',\alpha_2'} \left(-\frac{z_2}{2}\right) | \pi^- : q \rangle \,,\end{aligned} \tag{2.13}$$

where we have introduced[15] the average partonic momenta $\bar{k}_i \equiv \frac{k_i + k_i'}{2}$, $\alpha_i^{(\prime)}$, $a_i^{(\prime)}$ denote the Dirac and color indices, respectively, and $\widetilde{H}$ is the hard scattering kernel. Using Eqs. (2.10)-(2.11) the momenta of the active quarks can be approximated by on-mass shell vectors which are collinear to their parent hadrons, i.e.

$$\begin{aligned} k_1 &\to \left[k_1^+, \frac{x_1^2 \boldsymbol{\Delta}_\perp^2}{8k_1^+}, -x_1 \frac{\boldsymbol{\Delta}_\perp}{2}\right] && \text{with } \; k_1^+ = x_1 p^+, \\ k_1' &\to \left[k_1'^+, \frac{m_c^2 + x_1'^2 \boldsymbol{\Delta}_\perp^2/4}{2k_1'^+}, x_1' \frac{\boldsymbol{\Delta}_\perp}{2}\right] && \text{with } \; k_1'^+ = x_1' p'^+, \\ k_2 &\to \left[\frac{x_2^2 \boldsymbol{\Delta}_\perp^2}{8k_2^-}, k_2^-, x_2 \frac{\boldsymbol{\Delta}_\perp}{2}\right] && \text{with } \; k_2^- = x_2 q^-, \\ k_2' &\to \left[\frac{m_c^2 + x_2'^2 \boldsymbol{\Delta}_\perp^2/4}{2k_2'^-}, k_2'^-, -x_2' \frac{\boldsymbol{\Delta}_\perp}{2}\right] && \text{with } \; k_2'^- = x_2' q'^-. \end{aligned} \tag{2.14}$$

Or, in other words, using the fact that our subprocess is dominated by a large scale (the heavy quark mass m_c), the variation of the transverse and minus (plus) components of the active quarks in the proton and π (D and Λ_c) can be neglected in the hard-scattering kernel $\widetilde{H}$. Therefore the integrations over $\bar{k}_1^-$, $\bar{\mathbf{k}}_{\perp 1}$, $\bar{k}_2^+$ and $\bar{\mathbf{k}}_{\perp 2}$ in Eq. (2.13) can be done analytically. The line of arguments leading to Eq. (2.14) also puts an upper bound on $\boldsymbol{\Delta}_\perp^2$ which restricts the validity of our approach to a particular angular range around the forward direction. For the energies we are interested in this angular range is, however, sufficiently large to obtain reasonable estimates for integrated cross sections.

[14] We are working in light-cone gauge, i.e. $A^+ = 0$.

[15] The whole hadronic four-momentum transfer Δ is exchanged between the active partons in the partonic subprocess.

The simplified amplitude reads[16] (using $\bar{k}_1^+ = \bar{x}_1 \bar{p}^+$ and $\bar{k}_2 = \bar{x}_2 \bar{q}^-$)

$$\begin{aligned}\mathscr{M}_{\mu',\mu} = \sum_{a_i^{(\prime)},\alpha_i^{(\prime)}} \int \mathrm{d}\bar{x}_1\, \bar{p}^+ \int \frac{\mathrm{d}z_1^-}{(2\pi)} e^{i\bar{x}_1 \bar{p}^+ z_1^-} \int \mathrm{d}\bar{x}_2\, \bar{q}^- \int \frac{\mathrm{d}z_2^+}{(2\pi)} e^{i\bar{x}_2 \bar{q}^- z_2^+} \\ \times \langle \Lambda_c^+ : p', \mu' | \overline{\Psi}^c_{a_1',\alpha_1'} \left(-\frac{z_1^-}{2} \right) \Psi^u_{a_1,\alpha_1} \left(\frac{z_1^-}{2} \right) | p : p, \mu \rangle \, \widetilde{H}_{a_i^{(\prime)},\alpha_i^{(\prime)}} \left(\bar{x}_1 \bar{p}^+, \bar{x}_2 \bar{q}^- \right) \\ \times \langle D^- : q' | \overline{\Psi}^u_{a_2,\alpha_2} \left(\frac{z_2^+}{2} \right) \Psi^c_{a_2',\alpha_2'} \left(-\frac{z_2^+}{2} \right) | \pi^- : q \rangle \,. \end{aligned} \tag{2.15}$$

The process amplitude is a convolution of a hard scattering kernel with hadronic matrix elements Fourier transformed w.r.t. the momentum fraction $\bar{x}_1$ and $\bar{x}_2$. The soft part is encoded in Fourier transforms of two hadronic matrix elements (of a bilocal product of quark field operators):

- $p \to \Lambda_c^+$ transition

$$\bar{p}^+ \int \frac{\mathrm{d}z_1^-}{(2\pi)} e^{i\bar{x}_1 \bar{p}^+ z_1^-} \langle \Lambda_c^+ : p', \mu' | \overline{\Psi}^c_{a_1',\alpha_1'} \left(-\frac{z_1^-}{2} \right) \Psi^u_{a_1,\alpha_1} \left(\frac{z_1^-}{2} \right) | p : p, \mu \rangle \,, \tag{2.16}$$

- $\pi^- \to D^-$ transition

$$\bar{q}^- \int \frac{\mathrm{d}z_2^+}{(2\pi)} e^{i\bar{x}_2 \bar{q}^- z_2^+} \langle D^- : q' | \overline{\Psi}^u_{a_2,\alpha_2} \left(\frac{z_2^+}{2} \right) \Psi^c_{a_2',\alpha_2'} \left(-\frac{z_2^+}{2} \right) | \pi^- : q \rangle \,. \tag{2.17}$$

These matrix elements describe the non-perturbative part of our process and are called *transition matrix elements*. The subsequent section is devoted on how to manipulate those matrix elements to bring it to a form which is suitable for a parameterization in terms of GPDs.

2.3.2.3 *Transition matrix elements*

Using projection techniques as in Refs. [11, 17] we can pick out the "leading twist" contributions from the bilocal quark-field operator product $\overline{\Psi}^c(-z_1^-/2)\Psi^u(z_1^-/2)$ of Eq. (2.16)

$$\langle \Lambda_c^+ | \, \overline{\Psi}^c \Psi^u \, | p \rangle : \langle \Lambda_c^+ | \, \overline{\Psi}^c \left\{ \gamma^+, \gamma^+ \gamma_5, i\sigma^{+j} \right\} \Psi^u \, | p \rangle \tag{2.18}$$

and from $\overline{\Psi}^u(z_2^+/2)\Psi^c(-z_2^+/2)$ of Eq. (2.17)

$$\langle D^- | \, \overline{\Psi}^u \Psi^c \, | \pi^- \rangle : \langle D^- | \, \overline{\Psi}^u \left\{ \gamma^-, \gamma^- \gamma_5, i\sigma^{-j} \right\} \Psi^c \, | \pi^- \rangle \,, \tag{2.19}$$

respectively ($\sigma^{\pm j} = i\gamma^\pm \gamma^j$ with $j = 1, 2$ labeling transverse components). The three Dirac structures showing up in Eqs. (2.18) and (2.19) can be considered as $+$ or $-$ components of (bilocal) vector, pseudovector and tensor currents, respectively. These currents are then Fourier transformed (with respect to z_1^- or z_2^+) and decomposed into appropriate hadronic covariants. The coefficients in front of these covariants are

[16] The distance of the quark field operators is forced to be light-like with the replacement of Eq. (2.14) and thus we do not need time ordering anymore.

the quantities which are usually understood as GPDs. For the $p \to \Lambda_c^+$ transition this kind of analysis leads to 8 GPDs, as explained in detail in Ref. [11]. Matters become much simpler for the pseudoscalar to pseudoscalar $D^- \to \pi^-$ transition. Due to parity invariance the matrix element $\langle D^-| \overline{\Psi}^u \gamma^- \gamma_5 \Psi^c |\pi^-\rangle$ vanishes and the covariant decomposition of the remaining vector and tensor currents gives rise to two $\pi^- \to D^-$ transition GPDs. In App. C we use the aforementioned technique step by step and show how it can be used to parameterize the matrix element of Eq. (2.16) in terms of GDPs. Therefore we restrict the discussion in the remainder of this subsection to the transition matrix element, Eq. (2.17).

The $\pi^- \to D^-$-transition is described by the following matrix element[17]

$$\bar{q}^- \int \frac{\mathrm{d}z_2^+}{(2\pi)} e^{i\bar{x}_2 \bar{q}^- z_2^+} \langle D^- : q' | \overline{\Psi}^u \left(\frac{z_2^+}{2} \right) \Psi^c \left(-\frac{z_2^+}{2} \right) | \pi^- : q \rangle \,. \tag{2.20}$$

The quark field operator product of Eq. (2.20) can be written as (see Ref. [11] and App. C.1)

$$\begin{aligned}
&\overline{\Psi}^u \left(z_2^+/2 \right) \Psi^c \left(-z_2^+/2 \right) = -\frac{1}{2\sqrt{k_2^- k_2'^-}} \\
&\times \sum_{\lambda_2} \Big\{ \Big[\overline{\Psi}^u \left(z_2^+/2 \right) \gamma^- \frac{1 - 2\lambda_2 \gamma_5}{2} \Psi^c \left(-z_2^+/2 \right) \Big] \overline{v} \left(k_2, \lambda_2 \right) v \left(k_2', \lambda_2 \right) \\
&+ 2\lambda_2 \Big[\overline{\Psi}^u \left(z_2^+/2 \right) \frac{i\sigma^{-1}}{2} \Psi^c \left(-z_2^+/2 \right) \\
&+ 2i\lambda_2 \overline{\Psi}^u \left(z_2^+/2 \right) \frac{i\sigma^{-2}}{2} \Psi^c \left(-z_2^+/2 \right) \Big] \overline{v} \left(k_2, \lambda_2 \right) v \left(k_2', -\lambda_2 \right) \Big\}.
\end{aligned} \tag{2.21}$$

Inserting Eq. (2.21) into Eq. (2.20) we get

$$\begin{aligned}
&\bar{q}^- \int \frac{\mathrm{d}z_2^+}{(2\pi)} e^{i\bar{x}_2 \bar{q}^- z_2^+} \langle D^- : q' | \overline{\Psi}^u \left(\frac{z_2^+}{2} \right) \Psi^c \left(-\frac{z_2^+}{2} \right) | \pi^- : q \rangle = \\
&- \frac{1}{4\sqrt{k_2^- k_2'^-}} \bar{q}^- \int \frac{\mathrm{d}z_2^+}{(2\pi)} e^{i\bar{x}_2 \bar{q}^- z_2^+} \\
&\times \sum_{\lambda_2} \langle D^- : q' | \Big\{ \\
&\quad \overline{v} \left(k_2, \lambda_2 \right) v \left(k_2', \lambda_2 \right) \Big[\overline{\Psi}^u \left(z_2^+/2 \right) \gamma^- \Psi^c \left(-z_2^+/2 \right) - 2\lambda_2 \overline{\Psi}^u \left(z_2^+/2 \right) \gamma^- \gamma_5 \Psi^c \left(-z_2^+/2 \right) \Big] \\
&\quad + 2\lambda_2 \overline{v} \left(k_2, \lambda_2 \right) v \left(k_2', -\lambda_2 \right) \Big[\overline{\Psi}^u \left(z_2^+/2 \right) i\sigma^{-1} \Psi^c \left(-z_2^+/2 \right) \\
&\quad + 2i\lambda_2 \, \overline{\Psi}^u \left(z_2^+/2 \right) i\sigma^{-2} \Psi^c \left(-z_2^+/2 \right) \Big] \\
&\Big\} | \pi^- : q \rangle \,.
\end{aligned} \tag{2.22}$$

[17] For better legibility we suppress the Dirac and color indices of the quark fields.

Due to parity invariance $\langle D^-|\overline{\Psi}^u\gamma^-\gamma_5\Psi^c|\pi^-\rangle = 0$ [22]. We introduce now the following notation

$$V^\mu(-z_2^+/2,z_2^+/2) := \overline{\Psi}^c(-z_2^+/2)\gamma^\mu\Psi^u(z_2^+/2) - \overline{\Psi}^u(z_2^+/2)\gamma^\mu\Psi^c(-z_2^+/2),$$
$$T^{\mu\nu}(-z_2^+/2,z_2^+/2) := \overline{\Psi}^c(-z_2^+/2)i\sigma^{\mu\nu}\Psi^u(z_2^+/2) - \overline{\Psi}^u(z_2^+/2)i\sigma^{\mu\nu}\Psi^c(-z_2^+/2) \quad (2.23)$$

and

$$\mathscr{H}^{\overline{cu}} \equiv \bar{q}^- \int \frac{dz_2^+}{2\pi} e^{i\bar{x}_2\bar{q}^-z_2^+} \langle D^- : q'|\, V^-(-z_2^+/2,z_2^+/2)\,|\pi^- : q\rangle\,, \quad (2.24)$$

$$\mathscr{H}_j^{T\,\overline{cu}} \equiv \bar{q}^- \int \frac{dz_2^+}{2\pi} e^{i\bar{x}_2\bar{q}^-z_2^+} \langle D^- : q'|\, T^{-j}(-z_2^+/2,z_2^+/2)\,|\pi^- : q\rangle\,, \quad (2.25)$$

with

$$\mathscr{H}_{\lambda_2}^{T\,\overline{cu}} \equiv \frac{1}{2}\left(\mathscr{H}_1^{T\,\overline{cu}} - 2\lambda_2 i\mathscr{H}_2^{T\,\overline{cu}}\right). \quad (2.26)$$

Thus Eq. (2.20) reads

$$\bar{q}^- \int \frac{\mathrm{d}z_2^+}{(2\pi)} e^{i\bar{x}_2\bar{q}^-z_2^+} \langle D^- : q'|\overline{\Psi}^u\left(\frac{z_2^+}{2}\right)\Psi^c\left(-\frac{z_2^+}{2}\right)|\pi^- q\rangle =$$
$$\frac{1}{4\sqrt{k_2^-k_2'^-}}\sum_{\lambda_2}\left\{\mathscr{H}^{\overline{cu}}\,\overline{v}\,(k_2,\lambda_2)\,v\,(k_2',\lambda_2) + 4\lambda_2\mathscr{H}_{-\lambda_2}^{T\,\overline{cu}}\,\overline{v}\,(k_2,\lambda_2)\,v\,(k_2',-\lambda_2)\right\}. \quad (2.27)$$

This is the final form of the $\pi^- \to D^-$ transition matrix element. It is in a form which is suitable for a parameterization in terms of GPDs. The leading twist pseudoscalar GPDs are defined by[18] [22]

$$\bar{q}^- \int \frac{dz_2^+}{2\pi} e^{i\bar{x}_2\bar{q}^-z_2^+} \langle D^- : q'|\,\overline{\Psi}^u\left(\frac{z_2^+}{2}\right)\gamma^-\Psi^c\left(-\frac{z_2^+}{2}\right)|\pi^- : q\rangle = 2\bar{q}^-\,H_{\pi D}^{\overline{cu}}(\bar{x}_2,\eta,t) \quad (2.28)$$

and

$$\bar{q}^- \int \frac{dz_2^+}{2\pi} e^{i\bar{x}_2\bar{q}^-z_2^+} \langle D^- : q'|\,\overline{\Psi}^u\left(\frac{z_2^+}{2}\right)i\sigma^{-j}\Psi^c\left(-\frac{z_2^+}{2}\right)|\pi^- : q\rangle$$
$$= \frac{\bar{q}^-\Delta^j - \Delta^-\bar{q}^j}{m_\pi + M_D} E_{T\,\pi D}^{\overline{cu}}(\bar{x}_2,\eta,t), \quad (2.29)$$

respectively. These GPDs are functions of the average momentum fraction $\bar{x}_2$, the skewness parameter η and the Mandelstam variable $t = \Delta^2$. To model them, we employ an overlap representation in terms of LCWFs as discussed in Ref. [23]. We remark at this point that we take simple s-wave wave functions for the hadron ground states. This has the consequence that $\langle D^-|\, i\sigma^{-j}\,|\pi^-\rangle$ vanishes. The reason is that the

[18] This definition resembles also the one for the matrix elements $\langle\Lambda_c^+|\,\overline{\Psi}^c\gamma^+\Psi^u\,|p\rangle$ and $\langle\Lambda_c^+|\,\overline{\Psi}^c i\sigma^{+j}\Psi^u\,|p\rangle$ introduced in Ref. [11].

tensor structure requires the flip of a quark helicity which means that in at least one of the LCWFs, ψ_π or ψ_D, the helicity of the meson is not the sum of its parton helicities so that orbital excitations of the quarks have to come into play. For zero orbital angular momentum the $\pi^- \to D^-$ transition matrix element can thus be expressed in terms of a single GPD, namely $H_{\pi D}^{\overline{c}u}$. Likewise, for pure s-wave baryon wave functions five of the eight $p \to \Lambda_c^+$ transition GPDs vanish.

2.3.2.4 *The scattering amplitude II: final form*

The process amplitude, cf. Eq. (2.15), can be written with the help of Eqs. (2.27) and (C.24) as

$$\begin{aligned}\mathscr{M}_{\mu',\mu} = \frac{C}{16}\frac{1}{\bar{q}^+\bar{q}^-}\int\frac{\mathrm{d}\bar{x}_1}{\sqrt{\bar{x}_1^2-\xi^2}}\int\frac{\mathrm{d}\bar{x}_2}{\sqrt{\bar{x}_2^2-\eta^2}}\,\widetilde{H}\left(\bar{x}_1\bar{p}^+,\bar{x}_2\bar{q}^-\right)\\ \times\sum_{\lambda_1}\sum_{\lambda_2}\left\{\left[\mathscr{H}^{cu}_{\mu'\mu}+2\lambda_1\widetilde{\mathscr{H}}^{cu}_{\mu'\mu}\right]\overline{u}(k_2,\lambda_1)u(k_1,\lambda_1)-4\lambda_1\mathscr{H}^{Tcu}_{\lambda_1\mu'\mu}\overline{u}(k_2,-\lambda_1)u(k_1,\lambda_1)\right\}\\ \times\left\{\mathscr{H}^{\overline{c}u}\,\overline{v}\left(k_2,\lambda_2\right)v\left(k_2',\lambda_2\right)+4\lambda_2\mathscr{H}^{T\overline{c}u}_{-\lambda_1'}\,\overline{v}\left(k_2,\lambda_2\right)v\left(k_2',-\lambda_2\right)\right\},\end{aligned} \tag{2.30}$$

where $C = 1/2$ is the color factor. The decomposition of $\mathscr{H}^{cu}$, $\widetilde{\mathscr{H}}^{cu}$, $\mathscr{H}^{Tcu}$ in terms of GPDs is shown in Eqs. (C.26), (C.27), (C.32), respectively, the decomposition of $\mathscr{H}^{\overline{c}u}$ in terms of GPDs is shown in Eq. (2.28) and we have used the fact that

$$\frac{1}{\sqrt{k_1^+k_1'^+}}=\frac{1}{\bar{p}^+\sqrt{\bar{x}_1^2-\xi^2}}\quad\text{and}\quad\frac{1}{\sqrt{k_2^-k_2'^-}}=\frac{1}{\bar{q}^-\sqrt{\bar{x}_2^2-\eta^2}}. \tag{2.31}$$

The spinors of Eq. (2.30) and of Eq. (C.13) can be absorbed into the hard-scattering kernel[19]

$$H_{\lambda_1'\lambda_2',\lambda_1\lambda_2}=\overline{v}\left(k_2,\lambda_2\right)u(k_1,\lambda_1)\,\widetilde{H}\,\overline{u}(k_1',\lambda_1')v\left(k_2',\lambda_2'\right), \tag{2.32}$$

which defines the hard-scattering amplitude. It will be discussed in the subsequent section. We can now use Eq. (2.32) and the fact that[20] $\lambda_1 = -\lambda_2$ to obtain the final

[19] We note that in deriving Eq. (2.30) we have used one time that the quark helicity does not flip, i.e. $\lambda_1' = \lambda_1,\ \lambda_2' = \lambda_2$ and one time that the quark helicity flips, i.e. $\lambda_1' = -\lambda_1,\ \lambda_2' = -\lambda_2$.

[20] In the hard subprocess the massless $\bar{u}$-quark has to have opposite helicity compared to the massless u-quark since they cannot flip their helicities when interacting with a gluon.

expression of the process amplitude[21]:

$$\begin{aligned}\mathscr{M}_{\mu',\mu} = \frac{C}{8}\frac{1}{\bar{p}^+\bar{q}^-}\int\frac{\mathrm{d}\bar{x}_1}{\sqrt{\bar{x}_1^2-\xi^2}}\int\frac{\mathrm{d}\bar{x}_2}{\sqrt{\bar{x}_2^2-\eta^2}}\\ \Big[\frac{1}{2}H_{+-,+-}\Big\{\Big(\mathscr{H}^{cu}_{\mu'\mu}+\widetilde{\mathscr{H}}^{cu}_{\mu'\mu}\Big)\mathscr{H}^{\overline{cu}}+\Big(\mathscr{H}^{cu}_{\mu'\mu}-\widetilde{\mathscr{H}}^{cu}_{\mu'\mu}\Big)\mathscr{H}^{\overline{cu}}\Big\}\\ +H_{++,+-}\Big\{\mathscr{H}^{Tcu}_{-\mu'\mu}\mathscr{H}^{\overline{cu}}+\mathscr{H}^{Tcu}_{+\mu'\mu}\mathscr{H}^{\overline{cu}}\Big\}\Big].\end{aligned} \tag{2.33}$$

Here we have used that $H_{+-,+-} = H_{-+,-+}$ and $H_{++,+-} = -H_{-+,-+}$, which follows from parity invariance.
Let us summarize what we have achieved so far: Having expressed the soft hadronic matrix elements in Eq. (2.15) in terms of generalized parton distributions one ends up with an integral in which these parton distributions, multiplied with the hard partonic scattering amplitude $H_{\lambda_1'\lambda_2',\lambda_1\lambda_2}(\bar{x}_1\bar{p}^+,\bar{x}_2\bar{q}^-)$ are integrated over $\bar{x}_1$ and $\bar{x}_2$.

The supposition that the $p\to\Lambda_c^+$ and $D^-\to\pi^-$ GPDs (in Figs. 2.8, 2.9 and 2.13 we see that they indeed exhibit a peak) are strongly peaked at $\bar{x}_{10}$ and $\bar{x}_{20}$, respectively, leads to a further simplification of the $\pi^- p\to D^-\Lambda_c^+$ amplitude. One can thus replace the hard partonic scattering amplitude by its value at the peak position, $H_{\lambda_1'\lambda_2',\lambda_1\lambda_2}(\bar{x}_{10}\bar{p}^+,\bar{x}_{20}\bar{q}^-)$ and take it out of the integral. This is called *peaking approximation*. What one is left with are separate integrals over the GPDs which may be interpreted as generalized $p\to\Lambda_c^+$ and $D^-\to\pi^-$ transition form factors. In the formal limit of $m_c\to\infty$, $\bar{x}_{10}$ and $\bar{x}_{20}$ tend to 1 according to the heavy-quark effective theory [24]. With this peaking approximation our final expressions for our process amplitudes become:

$$\begin{aligned}\mathscr{M}_{+,+} &= \mathscr{M}_{-,-} = \frac{1}{4}\sqrt{1-\xi^2}\,H_{+-,+-}\,R_V\,G\,,\\ \mathscr{M}_{+,-} &= -\mathscr{M}_{-,+} = \frac{1}{4}\sqrt{1-\xi^2}\,H_{++,-+}\,S_T\,G,\end{aligned} \tag{2.34}$$

with the $\pi^-\to D^-$ transition form factor

$$G(\eta,t) = \int_\eta^1\frac{\mathrm{d}\bar{x}_2}{\sqrt{\bar{x}_2^2-\eta^2}}H^{\overline{cu}}_{\pi D}(\bar{x}_2,\eta,t). \tag{2.35}$$

In Eq. (2.34) we have restricted ourselves to the two most important $p\to\Lambda_c^+$ GPDs, $H^{cu}_{p\Lambda_c}$ and $H^{cu}_{Tp\Lambda_c}$, leading to the respective form factors R_V and S_T, defined in App. C.4.

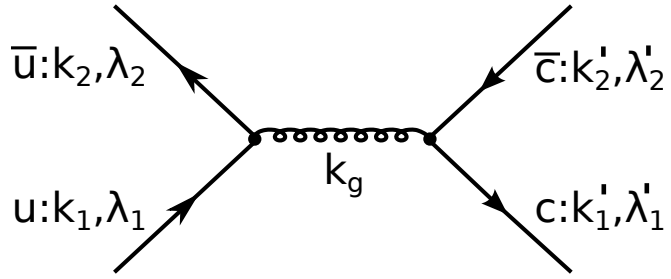

Figure 2.6: The leading order Feynman diagram of the hard scattering process $u\bar{u} \to c\bar{c}$.

2.3.2.5 *The hard scattering amplitude*

The $H_{\lambda_1'\lambda_2',\lambda_1\lambda_2}$ are LC helicity amplitudes for $u\bar{u} \to c\bar{c}$ via one-gluon exchange [22], see Fig. 2.6. Naive application of the collinear approximation gives (minus signs for primed momenta) $k_1^{(\prime)} = (\bar{x}_{10} \pm \xi)p^{(\prime)}/(1 \pm \xi)$ and $k_2^{(\prime)} = (\bar{x}_{20} \pm \eta)q^{(\prime)}/(1 \pm \eta)$ for the parton momenta (m_p and m_π are usually neglected). In order to match the subprocess kinematics (charm-quark mass m_c) with the one on the hadronic level (hadron masses $M_{\Lambda_c} \neq M_D$) some further approximations are required. As one can easily verify $k_1 + k_2 \neq k_1' + k_2'$, i.e. momentum conservation does not hold on the partonic level, in general. There are only two special cases in which momentum conservation is recovered. The first case is $\bar{x}_{10}, \bar{x}_{20} \to 1$, which one would obtain in the heavy-quark limit ($M_{\Lambda_c} = M_D = m_c \to \infty$). The second case is $\bar{x}_{10} = \bar{x}_{20}$ finite, but $\xi = \eta \simeq 0$, which holds for finite charm-quark mass in the limit of large (hadronic) Mandelstam s. In these two limiting cases the partonic amplitudes become formally the same if expressed in terms of the hadronic momentum components $p^{+(\prime)}$, $q^{-(\prime)}$, $\mathbf{\Delta}_\perp$ and Mandelstam s. They only differ in the argument of the strong coupling α_s which is Mandelstam s in the first case and $(\bar{x}_{10}\bar{x}_{20}\, s)$ in the second one. Since we want to apply our approach for physical masses of the heavy hadrons it seems more plausible to take $(\bar{x}_{10}\bar{x}_{20}\, s)$ as the scale which determines the strength of α_s. In both cases one demands that $\bar{x}_{10} = \bar{x}_{20}$ which means that an average mass must be taken for the heavy hadrons when calculating the partonic amplitude. We take the geometric mean value $M^2 = M_{\Lambda_c} M_D$. The resulting analytic expressions for $H_{+-,+-}$, $H_{+-,-+}$ and $H_{++,-+}$ are given by

[21] We write$\pm$ instead of $\pm\frac{1}{2}$ for the helicities for better legibility.
[22] The definition and normalization of the LC-helicity spinors can be found in App. E.

$$
\begin{aligned}
H_{+-,+-} &= \frac{4\pi\alpha_s(\bar{x}_{10}\bar{x}_{20}s)}{s}\,\frac{4(p^+p'^+ - \boldsymbol{\Delta}_\perp^2/8)^2 + 2M^2p^{+2}}{p^+p'^+}\,,\\
H_{+-,-+} &= -\frac{4\pi\alpha_s(\bar{x}_{10}\bar{x}_{20}s)}{s}\,\frac{\boldsymbol{\Delta}_\perp^2\left[2(p^+ + p'^+)^2 + M^2\right]}{4p^+p'^+}\,,\\
H_{++,-+} &= \frac{4\pi\alpha_s(\bar{x}_{10}\bar{x}_{20}s)}{s}\,\frac{M|\boldsymbol{\Delta}_\perp|\left[2p^+p'^+ - \boldsymbol{\Delta}_\perp^2/8 + p^{+2}\right]}{p^+p'^+}\,.
\end{aligned}
\tag{2.36}
$$

For the strong coupling constant α_s we take the one-loop expression with four flavors and $\Lambda_{QCD} = 0.24$ GeV.

2.3.3 *Modeling*

In order to make numerical predictions for $\pi^-\ p \to D^-\ \Lambda_c^+$ observables we need to know how the GPDs and, in particular, the form factors R_V, S_T and G look like. This requires some modeling. Proceeding along the lines of Ref. [23] the overlap representation for the transition GPDs is obtained by inserting the Fourier representation of the field operators and the Fock state decomposition of the corresponding hadron states in LC-quantum field theory. We restrict ourselves on the valence (anti)quarks sector. For the p and the π^- higher Fock states are most likely also important, but they do not contribute to the overlap with the valence Fock states of Λ_c and D^-, respectively.
For the rest of this section we use the following notation : The momenta of the partons belonging to the incoming hadron in the hadron-in frame are indicated with a " $\sim$". Likewise the momenta of the partons belonging to the outgoing hadron in the hadron-out frame are indicated with a "$\wedge$". The notation used in LC field theory can be found in App. A.

2.3.3.1 *The $p \to \Lambda_c^+$ transition*

The valence Fock state of the proton is written as [25]:

$$
|p:+,uud\rangle = \int [\mathrm{d}x]_3[\mathrm{d}^2\mathbf{k}_\perp]_3\left\{(\Psi_{123}\mathscr{M}^u_{+-+} + \Psi_{213}\mathscr{M}^u_{-++}) - (\Psi_{132}+\Psi_{231})\,\mathscr{M}^u_{++-}\right\},
\tag{2.37}
$$

where the color wave function has been omitted. Since we only consider ground state wave functions with zero orbital angular momentum the quark helicities sum up to $+1/2$, i.e. the helicity of the proton. $\mathscr{M}^q_{\lambda_1\lambda_2\lambda_3}$ are the three-quark states and defined as

$$
\mathscr{M}^q_{\lambda_1\lambda_2\lambda_3} \equiv \frac{1}{\sqrt{x_1x_2x_3}}\,|q:x_1,\mathbf{k}_{\perp 1},\lambda_1\rangle\,|u:x_2,\mathbf{k}_{\perp 2},\lambda_2\rangle\,|d:x_3,\mathbf{k}_{\perp 3},\lambda_3\rangle\,.
\tag{2.38}
$$

In Eq. (2.38) the active quark is denoted by q (for the proton $q = u$ for the Λ_c^+ $q = c$). According to Ref.[26] one needs only one independent scalar wave function Ψ_{ijk} if parity invariance and permutation symmetry between the u-quarks should hold and if the three quarks couple to an isospin 1/2-state. For the proton LCWF we choose the one proposed in Ref. [19] by Bolz and Kroll

$$\begin{aligned}\Psi_{123} &= \Psi_p(x_1, x_2, x_3; \mathbf{k}_{\perp 1}, \mathbf{k}_{\perp 2}, \mathbf{k}_{\perp 3}) \\ &= N_P(1 + 3x_1) \exp\left[-a_p^2 \sum \frac{\mathbf{k}_{\perp i}^2}{x_i}\right].\end{aligned} \tag{2.39}$$

The transverse momentum dependence of the wave function is contained in a Gaussian factor which keeps the model simple and allows one to perform $\mathbf{k}_\perp$-integrations analytically. Furthermore the Gaussian $\mathbf{k}_\perp$-dependence is conform to the requirement that we only need the soft part of the full wave function, i.e. the wave function with its perturbative tail removed and is supported by theoretical requirements, see for instance Ref. [27]. The LCWF in Eq. (2.39) has been constructed and its parameters N_p and a_p are chosen in such a way that it fulfills several constraints: It should provide the correct contribution to the Dirac form factors of the proton and neutron at large momentum transfer; it should provide an acceptable value for the $J/\Psi \to N\bar{N}$ decay width and it should be consistent with the common parameterization of the valence quark distributions. This proton LCWF is therefore a very well established one and has been applied, for example, to model the GPDs as an overlap of LCWFs to investigate wide-angle Compton scattering in the handbag approach and the results are found to be in good agreement with experiments, see Ref. [17]. The fit to various data implies values for the two free parameters, namely the normalization constant N_p and the oscillator parameter a_p, which in turn determine values for the valence Fock state probability and the root mean square (r.m.s) intrinsic transverse momentum, cf. App. D:

$$\left.\begin{aligned} N_p &= 160.93 \text{ GeV}^{-2} \\ a_p &= 0.75 \text{ GeV}^{-1} \end{aligned}\right\} \Rightarrow \begin{aligned} P_p &= 0.17, \\ \sqrt{\langle \mathbf{k}_\perp^2 \rangle} &= 411 \text{ MeV}. \end{aligned} \tag{2.40}$$

The valence Fock state of the Λ_c^+ is written as [11]

$$|\Lambda_c^+ : +, cud\rangle = \int [\mathrm{d}x]_3 [\mathrm{d}^2\mathbf{k}_\perp]_3 \Big\{ (\mathscr{M}^c_{++-} - \mathscr{M}^c_{+-+}) + \rho(x_2 - x_3)\mathscr{M}^c_{-++} \Big\} \Psi_\Lambda(x_i, \mathbf{k}_{\perp i}). \tag{2.41}$$

The valence Fock state of the Λ_c^+ consists of a contribution where the c-quark either has the same helicity as the Λ_c^+ and one where it has the opposite helicity. The strength of the latter contribution is controlled by the parameter[23] ρ and the factor $(x_2 - x_3)$ guarantees the correct isospin behavior. Although the opposite contribution is expected to be suppressed in comparison to the first one and should even vanish

[23] We take a value of $\rho = 2$ which amounts to a 15% contribution of the opposite helicity admixture to the overall valence Fock state probability of 0.9.

in the formal limit $m_c \to \infty$ according to HQET, it cannot be ruled out completely[24]. The LCWF of the Λ_c^+ is chosen to be

$$\Psi_\Lambda(x_1, x_2, x_3; \mathbf{k}_{\perp 1}, \mathbf{k}_{\perp 2}, \mathbf{k}_{\perp 3}) = N_\Lambda \exp\left[-f(x_1)\right] \exp\left[-a_\Lambda^2 \sum \frac{\mathbf{k}_{\perp i}^2}{x_i}\right], \tag{2.42}$$

where the function $f(x_1)$ takes care of the mass of the heavy c-quark inside the Λ_c^+ and should generate the expected peak at $x_1 \approx x_0 = m_c/M_{\Lambda_c} \sim 0.56$. We use two versions for $f(x_1)$. The first one is a slightly modified version of the one given in Ref. [29],

$$f_{KK}(x_1) = a_\Lambda^2 M^2 \frac{(x_1 - x_0)^2}{x_1(1 - x_1)}. \tag{2.43}$$

The second version was originally developed for the Λ_b within a QCD sum rule approach in Ref. [30] which we adapt to our case of a Λ_c:

$$f_{BB}(x_1) = a_\Lambda M(1 - x_1). \tag{2.44}$$

The two functions have the same x_1 dependence for large m_c up to corrections of order $(M - m_c)/M$. The normalization N_Λ and the oscillator parameter a_Λ are chosen such that they yield for the valence Fock state probability $P_\Lambda = 0.9$ and for the r.m.s. transverse momentum of the active c-quark $\sqrt{\langle \mathbf{k}_\perp \rangle} \approx 450$ MeV, cf. App. D:

$$\left.\begin{array}{rcl} N_\Lambda &=& 2117\ \text{GeV}^{-2}(\text{BB})/3477\ \text{GeV}^{-2}(\text{KK}) \\ a_\Lambda &=& 0.75\ \text{GeV}^{-1} \end{array}\right\} \Rightarrow \begin{array}{rcl} P_\Lambda &=& 0.9, \\ \sqrt{\langle \mathbf{k}_\perp \rangle} &\approx& 450\ \text{MeV}. \end{array} \tag{2.45}$$

The distribution amplitudes (DAs)[25] corresponding to Eqs. (2.39) and (2.42) are

$$\phi_p = 60\, x_1 x_2 x_3\, (1 + 3x_1)\,, \tag{2.46}$$

$$\phi_\Lambda \sim x_1 x_2 x_3\, e^{-f(x_1)} \tag{2.47}$$

and are plotted in Fig. 2.7. We see that the DAs of the proton and of the Λ_c^+ with mass exponential f_{BB} are very similar. The latter one exhibits only a mild peak at $x_1 \sim x_0$. The reason for that is that f_{BB} was originally proposed for the Λ_b, but the c-quark is relatively light compared to the b-quark. The Λ_c^+ DA with the variant $f = f_{KK}$, however, leads to a pronounced peak and is narrower and thus higher than the DA with $f = f_{BB}$.

As mentioned in the beginning of this section, the GPDs are modeled by overlaps

[24] This is supported by experimental investigations of the much heavier Λ_b where even there a contribution of an opposite b-quark helicity does not seem to be negligible (see Ref. [28] and references cited therein, in particular those of the ALEPH collaboration (1996) and of the OPAL collaboration (1998)).

[25] A distribution amplitude $\phi(x)$ is the probability amplitude for finding a quark with a momentum fraction x of its parent particle. It is normalized to 1, i.e. $\int_0^1 \mathrm{d}x\, \phi(x) = 1$. If one integrates the LCWF with respect to the intrinsic transverse components one gets the corresponding DA which is a function of the momentum fraction(s) only.

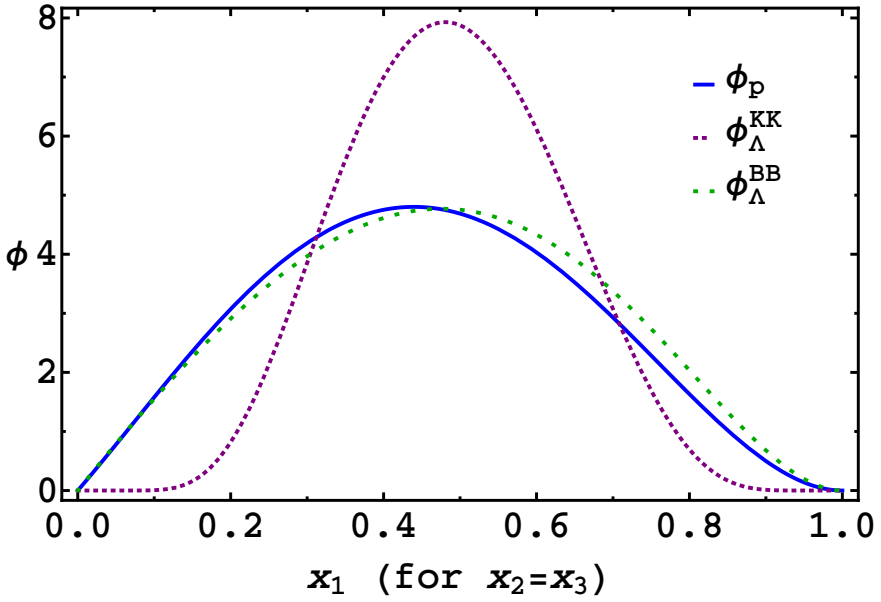

Figure 2.7: The DAs of the proton (solid) and the Λ_c^+ with the KK mass exponential (dashed) and the BB mass exponential (dotted) vs. the momentum fraction x.

of LCWFs. Using the baryon states of Eqs. (2.37) and (2.41), the LCWFs of Eqs. (2.39) and (2.42) and choosing the parameters as discussed above, we can now construct the GPDs $H^{cu}_{p\Lambda_c}$, $\widetilde{H}^{cu}_{p\Lambda_c}$ and $H^{cu}_{T\,p\Lambda_c}$ (all other GPDs vanish for the present choice of the p and Λ_c^+ LCWFs) by performing the overlap[26]. The result is, according to Ref. [11],

$$\begin{aligned} H^{cu}_{T\,p\Lambda_c}\left(\bar{x},\xi,\boldsymbol{\Delta}_\perp^2\right) = &-\frac{3}{4}\frac{N_\Lambda\, N_p}{4\pi^4}\frac{1}{1-\xi^2}\frac{\bar{x}^2-\xi^2}{a_p^2(1+\xi)+a_\Lambda^2(1-\xi)} \\ &\times\frac{(1-\bar{x})^3}{1+\xi}\frac{1+2\xi+\bar{x}}{a_p^2(1+\xi)^2(\bar{x}-\xi)+a_\Lambda^2(1-\xi)^2(\bar{x}+\xi)} \\ &\times\exp\left[-f\left(\frac{\bar{x}-\xi}{1-\xi}\right)\right]\exp\left[\frac{-(1-\bar{x})a_p^2a_\Lambda^2\boldsymbol{\Delta}_\perp^2}{a_p^2(1+\xi)^2(\bar{x}-\xi)+a_\Lambda^2(1-\xi)^2(\bar{x}+\xi)}\right] \end{aligned} \tag{2.48}$$

and for the ρ dependent part

$$\Delta H^{cu}_{p\Lambda_c}\left(\bar{x},\xi,\boldsymbol{\Delta}_\perp^2\right) = \frac{\rho}{15}\frac{1}{1-\xi}\frac{(1-\bar{x})^2}{1+2\xi+\bar{x}}H^{cu}_{T\,p\Lambda_c}\left(\bar{x},\xi,\boldsymbol{\Delta}_\perp^2\right), \tag{2.49}$$

such that

$$H^{cu}_{p\Lambda_c}\left(\bar{x},\xi,\boldsymbol{\Delta}_\perp^2\right) = H^{cu}_{T\,p\Lambda_c}\left(\bar{x},\xi,\boldsymbol{\Delta}_\perp^2\right) - \Delta H^{cu}_{p\Lambda_c}\left(\bar{x},\xi,\boldsymbol{\Delta}_\perp^2\right) \tag{2.50}$$

and

$$\widetilde{H}^{cu}_{p\Lambda_c}\left(\bar{x},\xi,\boldsymbol{\Delta}_\perp^2\right) = H^{cu}_{T\,p\Lambda_c}\left(\bar{x},\xi,\boldsymbol{\Delta}_\perp^2\right) + \Delta H^{cu}_{p\Lambda_c}\left(\bar{x},\xi,\boldsymbol{\Delta}_\perp^2\right). \tag{2.51}$$

The function $f(x)$ was defined in Eqs. (2.43) (KK mass exponential) and Eq. (2.44)

[26] Setting ρ to zero would lead to $H^{cu}_{p\Lambda_c} = \widetilde{H}^{cu}_{p\Lambda_c} = H^{cu}_{T\,p\Lambda_c}$.

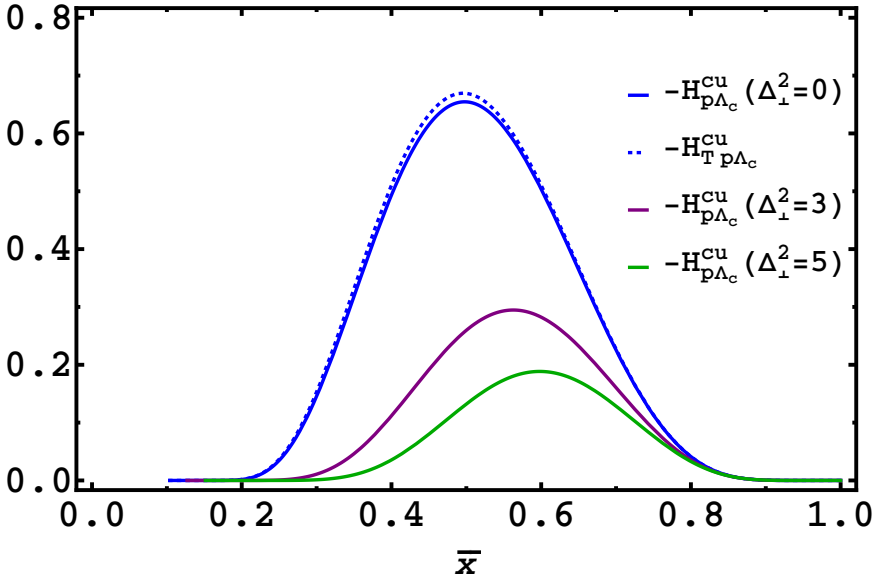

Figure 2.8: This plot shows the $p \to \Lambda_c$ transition GPDs $H^{cu}_{p\Lambda_c}$ and $H^{cu}_{T\,p\Lambda_c}$ vs. $\bar{x}$ at Mandelstam $s = 25$ Gev^2 for the hadron LCWFs introduced in the text (KK mass exponential, cf. Eq. (2.43)). The dependence of $H^{cu}_{p\Lambda_c}$ on $\boldsymbol{\Delta}^2_\perp$ is also shown: $\boldsymbol{\Delta}^2_\perp = 0$, 3.0, 5.0 GeV^2 (solid blue, solid purple and solid green), corresponding to $|t'| = |t - t_0| = 0$, 3.35, 5.78 GeV^2 ($\xi = 0.10$, 0.13, 0.15). t_0 is the (non-vanishing) value of t for forward scattering ($\boldsymbol{\Delta}_\perp = 0$, $p'^3 \geq 0$).

(BB mass exponential), respectively. We note that for $\pi^-\ p \to D^-\ \Lambda_c^+$ the GPD $\widetilde{H}^{cu}_{p\Lambda_c}$ does not contribute. Nevertheless we do mention it because we need it for the photoproduction process $\gamma\ p \to \overline{D^*_L}\ \Lambda_c^+$ in Sec. 2.4.

The $p \to \Lambda_c$ GPDs for $\pi^-\ p \to D^-\ \Lambda_c^+$ in our symmetric CMS are shown in Figs. 2.8 and 2.9. We observe that the GPDs exhibit a peak at $\bar{x} \approx x_0$. This peak is more pronounced for the f_{KK} mass exponential. We also learn that the differences between $H^{cu}_{p\Lambda_c}$ and $H^{cu}_{T\,p\Lambda_c}$ are marginal. The reason that $\Delta H^{cu}_{p\Lambda_c}$ (cf. Eq. (2.49)) is small, is due to the tiny overlap of the ρ-term of the Λ_c^+-LCWF with the LCWF of the proton. The GPDs exhibit the following behavior for increasing $\boldsymbol{\Delta}^2_\perp$: The peak height becomes smaller and the peak position is shifted towards larger values of $\bar{x}$. This behavior is independent of the choice of the mass exponential. The corresponding transition form factors, R_V and S_T are shown in Fig. 2.10 at Mandelstam $s = 25$ GeV^2. The energy dependence of R_V with the KK mass exponential is studied in Fig. 2.11. It turns out that the energy dependence is very mild.

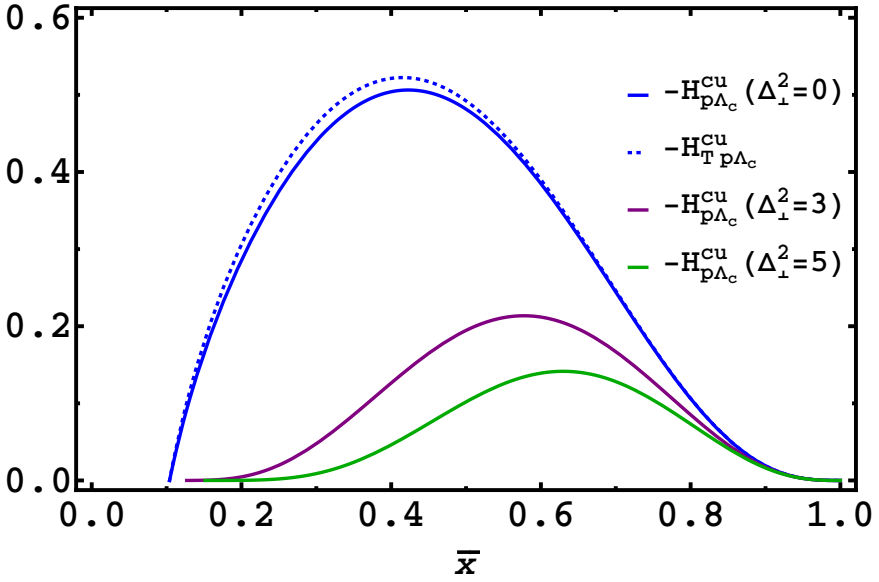

Figure 2.9: This plot shows the $p \to \Lambda_c$ transition GPDs $H^{cu}_{p\Lambda_c}$ and $H^{cu}_{T\,p\Lambda_c}$ vs. $\bar{x}$ at Mandelstam $s = 25$ Gev^2 for the hadron LCWFs introduced in the text (BB mass exponential, cf. Eq. (2.44)).

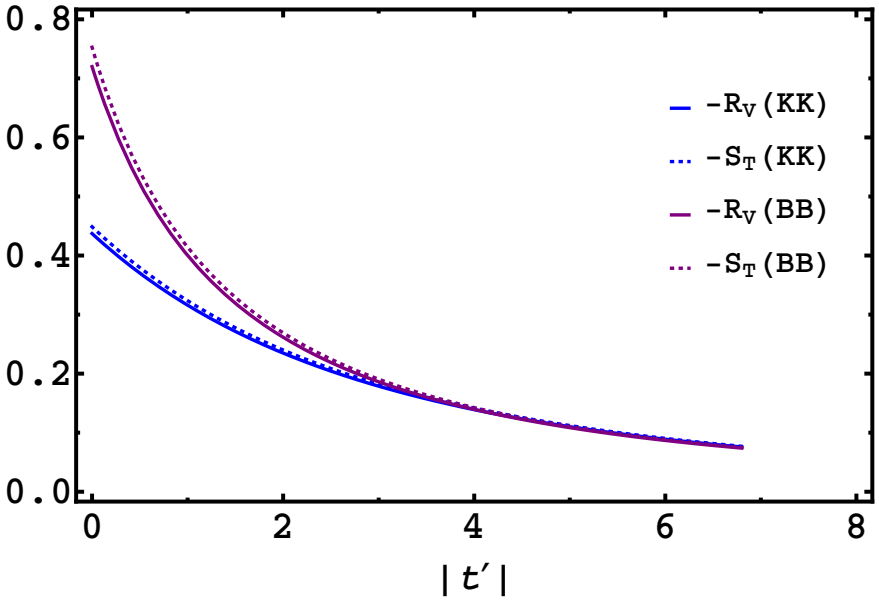

Figure 2.10: In this figure we show the $p \to \Lambda_c$ transition form factors at $s = 25$ GeV^2. R_V corresponds to the solid line and S_T to the dashed line, respectively. The color code is as follows: Blue for the KK mass exponential and purple for the BB mass exponential.

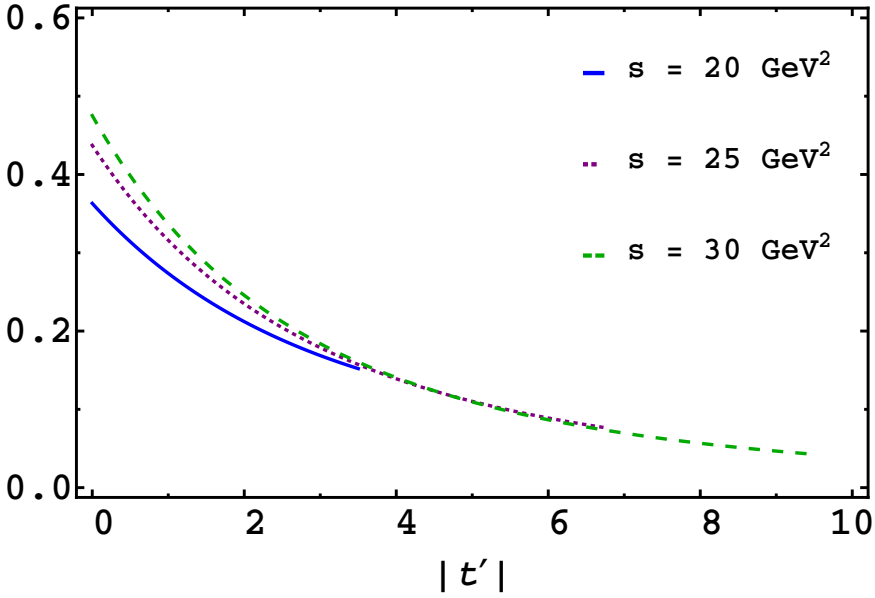

Figure 2.11: The energy dependence of R_V for the KK mass exponential.

2.3.3.2 *The $\pi^- \to D^-$ transition*

In this section we will derive a LCWF overlap representation of the $\pi^- \to D^-$ transition matrix element. As we mentioned in Sec. 2.3.2.3 this matrix element is described at leading twist and involves only one GPD which we denoted by $H^{\bar{c}u}_{\pi D}$ if we assume pure s-wave LCWFs for the π and D. For convenience we repeat its definition here

$$\bar{q}^- \int \frac{dz_2^+}{2\pi} e^{i\bar{x}_2 \bar{q}^- z_2^+} \langle D^- : q' | \overline{\Psi}^u \left(\frac{z_2^+}{2}\right) \gamma^- \Psi^c \left(-\frac{z_2^+}{2}\right) | \pi^- : q \rangle = 2\bar{q}^- H^{\bar{c}u}_{\pi D}(\bar{x}_2, \eta, t). \tag{2.52}$$

The bilocal product of quark-field operators in Eq. (2.52) can be written in terms of the "good" (independent) field components

$$\bar{\Psi}^u \left(\frac{z_2^+}{2}\right) \gamma^- \Psi^c \left(-\frac{z_2^+}{2}\right) = \sqrt{2} \phi^{\dagger u} \left(\frac{z_2^+}{2}\right) \phi^c \left(-\frac{z_2^+}{2}\right). \tag{2.53}$$

We note that due to our choice of kinematics for the $\pi \to D^-$ transition the "good" components are the minus components, see footnote 2 in App. B. The "good" field components have the following Fourier decomposition

$$\begin{aligned} \phi^{\dagger u} \left(\frac{z_2^+}{2}\right) = \int \frac{\mathrm{d}k_2^-}{k_2^-} \int \frac{\mathrm{d}^2 \mathbf{k}_{\perp 2}}{16\pi^2} \theta\left(k_2^-\right) \sum_{\lambda_2} \Big[& b_u^\dagger \left(k_2^-, \mathbf{k}_{\perp 2}, \lambda_2\right) u_-^\dagger \left(k_2, \lambda_2\right) e^{\frac{ik_2^- z_2^+}{2}} \\ & + d_u \left(k_2^-, \mathbf{k}_{\perp 2}, \lambda_2\right) v_-^\dagger \left(k_2, \lambda_2\right) e^{-\frac{ik_2^- z_2^+}{2}} \Big] \end{aligned} \tag{2.54}$$

and

$$\phi^c\left(-\frac{z'^+}{2}\right) = \int \frac{\mathrm{d}k_2'^-}{k_2'^-} \int \frac{\mathrm{d}^2\mathbf{k}'_{\perp 2}}{16\pi^2}\theta\left(k_2'^-\right) \sum_{\lambda_2'}\Big[b_c\left(k_2'^-, \mathbf{k}'_{\perp 2}, \lambda_2'\right) u_-\left(k_2', \lambda_2'\right) e^{\frac{ik_2'^- z'^+}{2}} + d_c^\dagger\left(k_2'^-, \mathbf{k}'_{\perp 2}, \lambda_2'\right) v_-\left(k_2', \lambda_2'\right) e^{-\frac{ik_2'^- z'^+}{2}}\Big]. \tag{2.55}$$

The spinors u_- and v_- are the "good" components of the (anti-)quark spinors u and v, i.e. $u_- = \mathscr{P}_- u$ and $(v_- = \mathscr{P}_- v)$. The operator b_q ($d_q^\dagger$) annihilates (creates) a quark (anti-quark) of flavor q, respectively. Its action on the vacuum gives the single-parton states, which are normalized as follows

$$\langle k'^-, \mathbf{k}'_\perp, \lambda' | k^-, \mathbf{k}_\perp, \lambda\rangle = 16\,\pi^3\, k^-\,\delta\left(k'^- - k^-\right)\delta^{(2)}\left(\mathbf{k}'_\perp - \mathbf{k}_\perp\right)\delta_{\lambda'\lambda}. \tag{2.56}$$

This normalization is in accordance with the anti-commutation relations

$$\begin{aligned}\left\{c_q\left(k'^-, \mathbf{k}'_\perp, \lambda'\right), c_q^\dagger\left(k^-, \mathbf{k}_\perp, \lambda\right)\right\} &= \left\{d_q\left(k'^-, \mathbf{k}'_\perp, \lambda'\right), d_q^\dagger\left(k^-, \mathbf{k}_\perp, \lambda\right)\right\} \\ &= 16\,\pi^3\, k^-\,\delta\left(k'^- - k^-\right)\delta^{(2)}\left(\mathbf{k}'_\perp - \mathbf{k}_\perp\right).\end{aligned} \tag{2.57}$$

The valence Fock state decomposition of the π^- meson is

$$\begin{aligned}|\pi^- : q\rangle = \int \mathrm{d}\tilde{x} \int \frac{\mathrm{d}^2\tilde{\mathbf{k}}'_\perp}{16\pi^3}\,\Psi_\pi(\tilde{x}, \tilde{\mathbf{k}}_\perp)\,\frac{1}{\sqrt{\tilde{x}(1-\tilde{x})}}\,\frac{1}{\sqrt{2}}\sum_\lambda 2\,\lambda \\ \times |\bar{u} : \tilde{x}q^-, \tilde{\mathbf{k}}_\perp + \tilde{x}\mathbf{q}_\perp, \lambda\rangle\,|d : (1-\tilde{x})q^-, -\tilde{\mathbf{k}}_\perp + (1-\tilde{x})\mathbf{q}_\perp, -\lambda\rangle\,,\end{aligned} \tag{2.58}$$

the one of the D^- meson is

$$\begin{aligned}|D^- : q'\rangle = \int \mathrm{d}\hat{x}' \int \frac{\mathrm{d}^2\hat{\mathbf{k}}'_\perp}{16\pi^3}\,\Psi_D(\hat{x}', \hat{\mathbf{k}}'_\perp)\,\frac{1}{\sqrt{\hat{x}'(1-\hat{x}')}}\,\frac{1}{\sqrt{2}}\sum_{\lambda'} 2\,\lambda' \\ \times |\bar{c} : \hat{x}'q'^-, \hat{\mathbf{k}}'_\perp + \hat{x}'\mathbf{q}'_\perp, \lambda'\rangle\,|d : (1-\hat{x}')q'^-, -\hat{\mathbf{k}}'_\perp + (1-\hat{x}')\mathbf{q}'_\perp, -\lambda'\rangle\,,\end{aligned} \tag{2.59}$$

respectively. The normalization of the Fock states is

$$\langle H : q'^-, \mathbf{q}'_\perp | H : q^-, \mathbf{q}_\perp\rangle = 16\,\pi^3\, q^-\,\delta\left(q'^- - q^-\right)\delta^{(2)}\left(\mathbf{q}'_\perp - \mathbf{q}_\perp\right). \tag{2.60}$$

Equations (2.58) and (2.59) are the Fock state expansions for pseudoscalar mesons consisting of partons with vanishing orbital angular momentum, i.e. the sum of the parton helicities is equal to the parent meson helicity. The parton helicity flip term, see Eq. (2.29), is therefore equal to zero in our model. This is also supported by an explicit calculation of this matrix element.
The arguments of the LCWFs of the active partons are related to the average momentum fraction $\bar{x}_2$ and the average transverse momentum $\bar{\mathbf{k}}_{\perp 2}$ by

$$\tilde{x}_2 = \frac{\bar{x}_2 + \eta}{1+\eta}, \qquad \tilde{\mathbf{k}}_{\perp 2} = \bar{\mathbf{k}}_{\perp 2} + \frac{1-\bar{x}_2}{1+\eta}\frac{\boldsymbol{\Delta}_\perp}{2} \tag{2.61}$$

and

$$\hat{x}_2' = \frac{\bar{x}_2 - \eta}{1-\eta}, \qquad \hat{\mathbf{k}}_{\perp 2}' = \bar{\mathbf{k}}_{\perp 2} - \frac{1-\bar{x}_2}{1-\eta}\frac{\boldsymbol{\Delta}_\perp}{2}, \tag{2.62}$$

respectively. Inserting Eqs. (2.54), (2.55), (2.59) and (2.58) into Eq. (2.52) and using the anti-commutation relations as specified above and Eqs. (2.61) and (2.62) we get

$$\begin{aligned} H_{\pi D}^{\overline{cu}}(\bar{x}_2,\eta,t) = \frac{1}{4\bar{q}^-}\int \frac{\mathrm{d}\bar{\mathrm{x}}}{\sqrt{\bar{x}^2-\eta^2}}\int \frac{\mathrm{d}^2\bar{\mathbf{k}}_{\perp 2}}{16\pi^3}\delta\left(\bar{x}-\bar{x}_2\right) \\ \Big[\Psi_D\left(\hat{x}'\left(\bar{x},\eta\right),\hat{\mathbf{k}}_\perp'\left(\bar{\mathbf{k}}_{\perp 2},\bar{x},\eta\right)\right)\Psi_\pi\left(\tilde{x}\left(\bar{x},\eta\right),\tilde{\mathbf{k}}_\perp\left(\bar{\mathbf{k}}_{\perp 2},\bar{x},\eta\right)\right) \\ \times\sum_\lambda \bar{v}_-^u\left(\tilde{x}\left(\bar{x},\eta\right),\tilde{\mathbf{k}}_\perp\left(\bar{\mathbf{k}}_{\perp 2},\bar{x},\eta\right)\right)\gamma_- v_-^c\left(\hat{x}\left(\bar{x},\eta\right),\hat{\mathbf{k}}_\perp'\left(\bar{\mathbf{k}}_{\perp 2},\bar{x},\eta\right)\right)\Big]. \end{aligned} \tag{2.63}$$

The spinor product is equal to

$$\sum_\lambda \bar{v}_-^u\gamma_- v_-^c = 4\bar{q}^-\sqrt{\bar{x}^2-\eta^2}. \tag{2.64}$$

Equation (2.63) therefore reads

$$\begin{aligned} H_{\pi D}^{\overline{cu}}(\bar{x}_2,\eta,t) = \int \mathrm{d}\bar{\mathrm{x}}\int \frac{\mathrm{d}^2\bar{\mathbf{k}}_{\perp 2}}{16\pi^3}\delta\left(\bar{x}-\bar{x}_2\right) \\ \Big[\Psi_D\left(\hat{x}'\left(\bar{x},\eta\right),\hat{\mathbf{k}}_\perp'\left(\bar{\mathbf{k}}_{\perp 2},\bar{x},\eta\right)\right)\Psi_\pi\left(\tilde{x}\left(\bar{x},\eta\right),\tilde{\mathbf{k}}_\perp\left(\bar{\mathbf{k}}_{\perp 2},\bar{x},\eta\right)\right)\Big]. \end{aligned} \tag{2.65}$$

We now specify the LCWFs Ψ_π and Ψ_D, appearing in the Fock state decomposition in Eqs. (2.58) and (2.59), which we need to evaluate the overlap in Eq. (2.65). For the valence Fock state of the π^- meson we use the following LCWF [31, 32]

$$\Psi_\pi\left(x,\mathbf{k}_\perp\right) = N_\pi x(1-x)\exp\left[\frac{-a_\pi^2\mathbf{k}_\perp^2}{x(1-x)}\right]. \tag{2.66}$$

The two free parameters of the π^- LCWF, N_π and a_π, are chosen such that they yield for the r.m.s. of the transverse momentum of the active quark $\sqrt{\langle\mathbf{k}_\perp^2\rangle}_u = 370$ MeV [31] and give the experimental value of the meson decay constant f_π taken from Ref. [16]. The (light) pseudoscalar meson decay constant is defined by the relation

$$\langle 0|\bar{\Psi}^u(0)\gamma^\mu\gamma_5\Psi^d(0)|\pi^-:q\rangle = if_\pi q^\mu. \tag{2.67}$$

Taking the minus component and inserting the π^- valence Fock state expansion we get (omitting phases)

$$2\sqrt{6}\int \mathrm{d}x\int\frac{\mathrm{d}^2\mathbf{k}_\perp}{16\pi^3}\Psi_\pi\left(x,\mathbf{k}_\perp\right) = f_\pi. \tag{2.68}$$

The two parameters of the π^- LCWF are, cf. App. D:

$$\left.\begin{array}{rcl} N_\pi &=& 18.56 \text{ GeV}^{-2} \\ a_\pi &=& 0.85 \text{ GeV}^{-1} \end{array}\right\} \Rightarrow \begin{array}{rcl} \sqrt{\langle \mathbf{k}_\perp^2 \rangle}_u &=& 370 \text{ MeV}, \; P_\pi = 0.25, \\ f_\pi &=& 132 \text{ MeV}. \end{array} \tag{2.69}$$

For the valence Fock state of the D^- we take the LCWF [29]

$$\Psi_D\left(x, \mathbf{k}_\perp\right) = N_D \, \exp\left[-f(x)\right] \, \exp\left[\frac{-a_D^2 \mathbf{k}_\perp^2}{x(1-x)}\right], \tag{2.70}$$

with either the KK mass exponential ($x_0 = m_c / M_D \sim 0.68$)

$$f(x) = a_D^2 M_D^2 \frac{(x - x_0)^2}{x\,(1-x)} \tag{2.71}$$

or with the BB mass exponential

$$f(x) = a_D M_D (1 - x), \tag{2.72}$$

respectively. The two free parameters of the D^--LCWF, N_D and a_D, are chosen such that they yield for the valence Fock state probability $P_D = 0.9$ and reproduce the experimental value of the meson decay constant f_D taken from Ref. [16]. The (heavy) pseudoscalar meson decay constant is defined by the relation

$$\langle 0 | \bar{\Psi}^c(0) \gamma^\mu \gamma_5 \Psi^d(0) | D^- : q' \rangle = i f_D q'^\mu. \tag{2.73}$$

Taking the minus component and inserting the D^- valence Fock state expansion we get (omitting phases)

$$2\sqrt{6} \int \mathrm{d}x \int \frac{\mathrm{d}^2 \mathbf{k}_\perp}{16\pi^3} \Psi_D\left(x, \mathbf{k}_\perp\right) = f_D. \tag{2.74}$$

The two parameters of the D^- LCWF are, cf. App. D:

$$\left.\begin{array}{rcl} N_{D_{KK(BB)}} &=& 54.92 \; (83.20) \text{ GeV}^{-2} \\ a_{D_{KK(BB)}} &=& 0.86 \; (0.96) \text{ GeV}^{-1} \end{array}\right\} \Rightarrow \begin{array}{l} P_D = 0.9, \\ f_D = 206.7 \text{ MeV}. \end{array} \tag{2.75}$$

The distributions amplitudes (DAs) corresponding to Eqs. (2.66) and (2.70) are

$$\phi_\pi = 6x(1-x), \tag{2.76}$$

$$\phi_D \sim x(1-x) \, \exp\left[-f(x)\right]. \tag{2.77}$$

They are shown in Fig. 2.12.

Employing the model wave functions, Eq. (2.66) and Eq. (2.70), the LCWF overlap

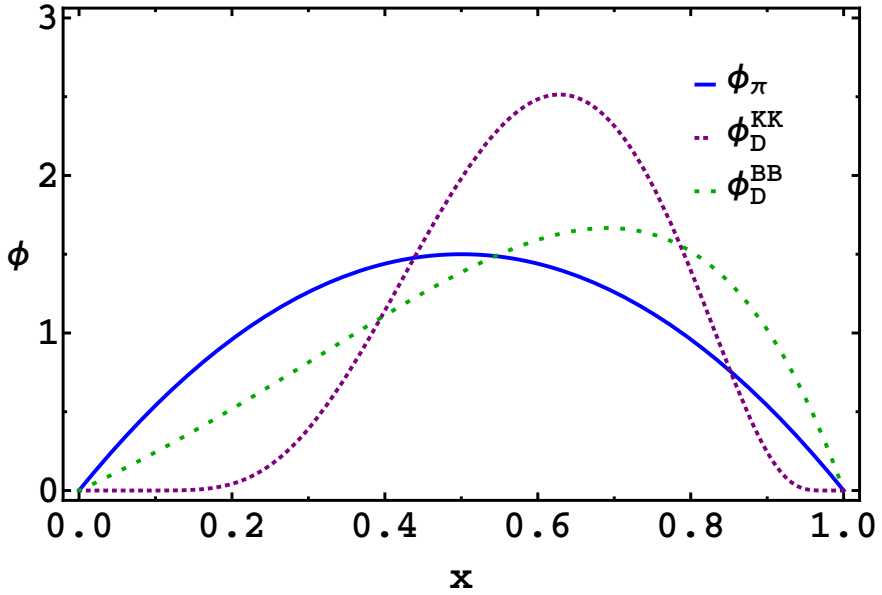

Figure 2.12: The DAs of the π^- (solid) and the D^- with the KK mass exponential (dashed) and the BB mass exponential (dotted) vs. the momentum fraction x.

for $H_{\pi D}^{\bar{c}u}$ reads

$$\begin{aligned} H_{\pi D}^{\bar{c}u}\left(\bar{x}_2,\eta,\boldsymbol{\Delta}_\perp^2\right) = & \frac{N_\pi N_D}{16\pi^2}\frac{\left(\bar{x}_2-1\right)\left(\bar{x}_2^2-\eta^2\right)}{a_\pi^2\left(\bar{x}_2-\eta\right)\left(1+\eta\right)^2+a_D^2\left(\bar{x}_2+\eta\right)\left(\eta-1\right)^2} \\ & \times\exp\left[\frac{-\boldsymbol{\Delta}_\perp^2 a_\pi^2 a_D^2\left(1-\bar{x}_2\right)}{a_\pi^2\left(\bar{x}_2-\eta\right)\left(1+\eta\right)^2+a_D^2\left(\bar{x}_2+\eta\right)\left(\eta-1\right)^2}\right] \\ & \times\exp\left[-f\left(\bar{x}_2\right)\right]. \end{aligned} \tag{2.78}$$

The function $f\left(\bar{x}_2\right)$ depends on the chosen mass exponential in the D meson LCWF. It is

$$f_{KK}\left(\bar{x}_2\right) = \frac{a_D^2 M_D^2\left(\bar{x}_2-\eta+\bar{x}_{20}\left(\eta-1\right)\right)^2}{\left(\bar{x}_2-\eta\right)\left(1-\bar{x}_2\right)} \tag{2.79}$$

for the KK mass exponential and

$$f_{BB}\left(\bar{x}_2\right) = \frac{a_D M_D\left(\bar{x}_2-1\right)}{\eta-1} \tag{2.80}$$

for the BB one. Results for $H_{\pi D}^{\bar{c}u}$ for the two different mass exponentials are presented in Fig. 2.13. The GPD $H_{\pi D}^{\bar{c}u}$ exhibits the expected pronounced peak near $\bar{x}_{20}=0.68$, with the peaking value being slightly shifted towards larger values of $\bar{x}_2$ for increasing $\boldsymbol{\Delta}_\perp^2$ (or $-t'$). If we had taken the BB mass exponential for the D^- wave function instead of the KK one the $\pi^-\to D^-$ transition GPD $H_{\pi D}^{\bar{c}u}$ would become broader and the shift of its maximum to larger $\bar{x}_2$ with increasing $\boldsymbol{\Delta}_\perp^2$ is somewhat faster than for the KK mass exponential. Fig. 2.14 shows the form factor corresponding to $H_{\pi D}^{\bar{c}u}$ for the KK mass exponential as function of $|t'|$ for different values of Mandelstam s. Interestingly

it exhibits only a weak dependence on s. For $|t'| \lesssim 3$ GeV^2 the BB mass exponential provides a considerably larger transition form factor G than the KK mass exponential. The results of the $\pi \to D^-$ GPDs and form factors resemble very much those of the $p \to \Lambda_c$ transition GPDs, discussed in detail in Sec. 2.3.3.1.

2.3.3.3 *Remarks on the LCWFs*

This section is taken from Ref. [7]. A few remarks concerning the choice of the hadron LCWFs are in order. Whereas our models for the proton and π LCWFs have already been successfully tested in other applications, we are not aware of models for the Λ_c and D LCWFs which are comparably well established. The concepts of heavy-quark effective theory, which are very useful in restricting LCWFs for bottom mesons and baryons and determining the renormalization-group evolution of the corresponding light-cone distribution amplitudes [33], could also be used for modeling LCWFs of charmed hadrons, but with the caveat that one is still far away from the heavy-quark limit and corrections of order $1/m_c$ can be large. We therefore decided to take simple two-parameter forms for the LCWFs with the mass exponentials providing a more (KK) or less (BB) pronounced peak in longitudinal direction around m_c/M_H ($H = \Lambda_c, \pi$). The BB mass exponential is inspired by a model for the Λ_b distribution amplitude which is based on QCD sum rules [30]. The two parameters of the D and Λ_c LCWFs are fixed by physical requirements, namely reasonable values for the valence Fock state probabilities, the experimentally known D-meson decay constant and a reasonable value for the average transverse momentum in case of the Λ_c, respectively. In the numerical calculations the renormalization-group evolution of our transition GPDs is neglected. We work in a rather restricted energy range, where we expect the corresponding effects to be less important than the variations due to the different modeling of the D and Λ_c LCWFs.

2.3.4 *Results*

In Sec. 2.3.2.5 we showed the results for the hard scattering amplitude and in Sec. 2.3.3 we thoroughly discussed the model input. i.e. the LCWFs and the GPDs used for describing our process. All parts of the scattering amplitude, cf. Eq. (2.34), are by now determined. We are therefore in the position to investigate the cross section and spin observables.

The differential cross section for $\pi p \to D^- \Lambda_c^+$ reads

$$\frac{d\sigma}{d\Omega} = \frac{1}{64\pi^2 s}\frac{|\mathbf{p}'|}{|\mathbf{p}|}\sigma_0 = \frac{1}{64\pi^2 s}\frac{\Lambda'}{\Lambda}\sigma_0 = \frac{1}{4\pi} s\Lambda\Lambda' \frac{d\sigma}{dt}, \tag{2.81}$$

where σ_0 is defined by

$$\sigma_0 := \frac{1}{2}\sum_{\mu,\mu'} |\mathscr{M}_{\mu',\mu}|^2 \tag{2.82}$$

and Λ and Λ' are given in Eqs. (B.12) and (B.13). The differential cross section predic-

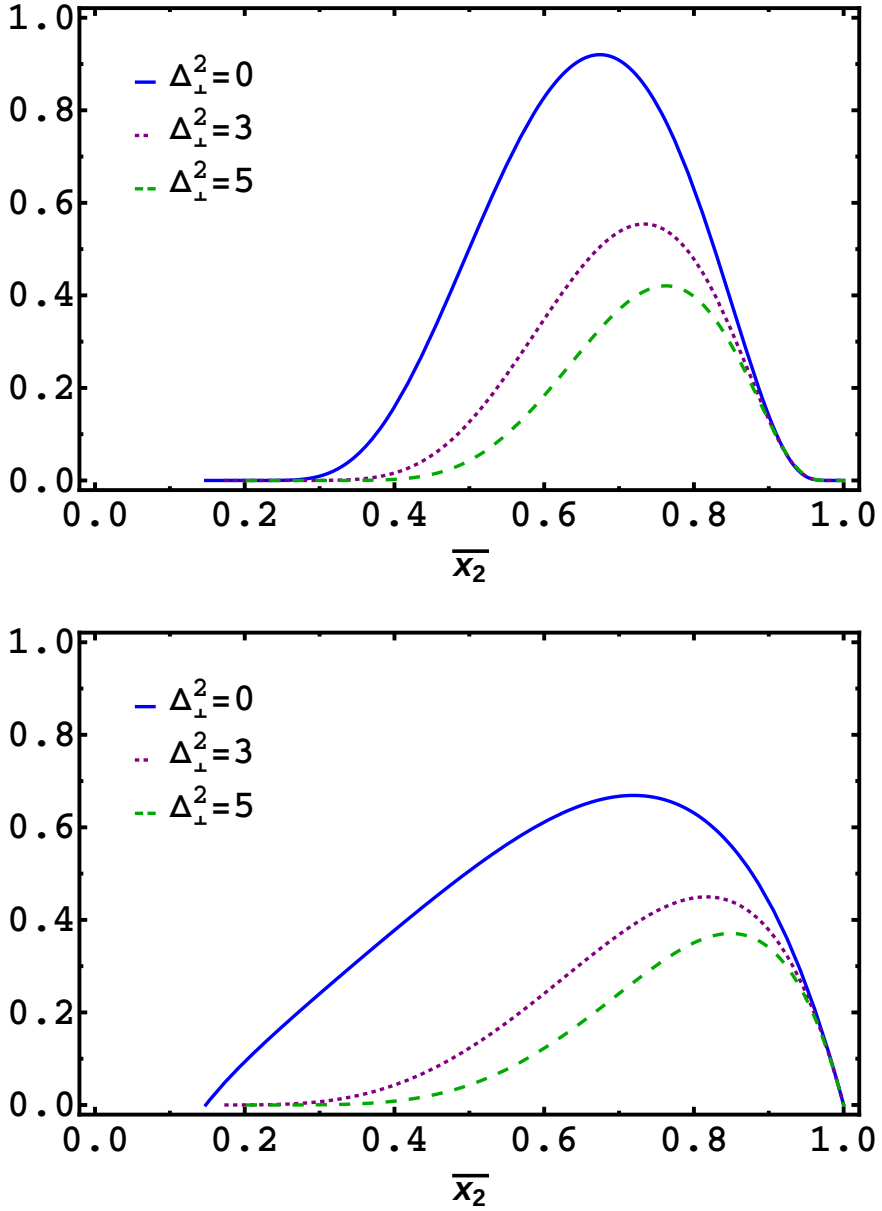

Figure 2.13: This plot shows the $\pi^- \to D^-$ transition GPD $H^{\overline{c}u}_{\pi D}$ vs. $\bar{x}_2$ at Mandelstam $s = 25\ \text{GeV}^2$ and $\Delta_\perp^2 = 0, 3.0, 5.0\ \text{GeV}^2$ (solid, dotted and dashed line), corresponding to $|t'| = |t - t_0| = 0, 3.35, 5.77\ \text{GeV}^2$ ($\eta = 0.15, 0.17, 0.20$), for the hadron LCWFs introduced in the text (KK mass exponential in the upper panel and BB mass exponential in the lower panel). t_0 is the (non-vanishing) value of t for forward scattering ($\boldsymbol{\Delta}_\perp = 0$, $p'^3 \geq 0$).

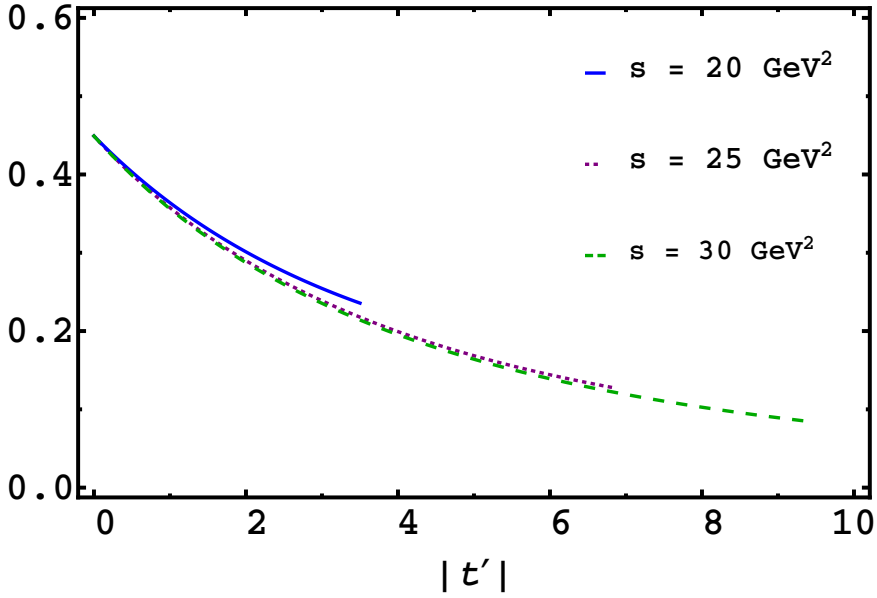

Figure 2.14: This figure shows the $\pi^- \to D^-$ transition form factor G (KK mass exponential) as function of $|t'|$ for $s = 20,\ 25$ and 30 GeV^2 (solid, dotted and dashed line)).

tions for several values of s are presented in Fig. 2.15 for the KK mass exponential (upper panel) and for the BB mass exponential (lower panel). The forward peak of the cross section is obviously more pronounced for the latter. The shaded bands take the uncertainties of the Λ_c and D^- LCWF parameters into account. The band corresponds to a variation of P_{Λ_c} and P_D between 0.8 and 1, of f_D within the experimental uncertainties and of $\langle \mathbf{k}_{\perp c}^2 \rangle_{\Lambda_c}^{1/2}$ within a range of 417 ± 42 MeV (see also Refs. [11] and [15]) and to taking s instead of $(\bar{x}_{10}\bar{x}_{20}s)$ as argument of α_s.

The integrated cross section is plotted in Fig. 2.16 for both, the KK and the BB mass exponentials. As for the differential cross section, we have also made an error assessment in case of the KK mass exponential. A comparable error band is also found for the BB mass exponential. The differences between the predictions obtained with different analytic forms of the Λ_c and D^- LCWFs are obviously much larger than the variations coming from parametric errors in the wave functions. The integrated cross sections are of the order of nb with the BB mass exponential giving the larger results. This is the order of magnitude that has also been found for $\bar{p}p \to \bar{\Lambda}_c^- \Lambda_c^+$ [11] and $\bar{p}p \to \overline{D}^0 D^0$ [15], when treated within the generalized parton framework. It is in accordance with old AGS experiments at $s \approx 25$ GeV^2 which found upper bounds of 7 nb for $\pi^- \; p \to D^{*-} \; \Lambda_c^+$ and ≈ 15 nb for $\pi p \to D^- \Lambda_c^+$ [34]. A new and more precise measurement of these cross sections would be highly welcome.

For $0 + 1/2 \to 0 + 1/2$ processes one has three linearly independent polarization observables, one single-spin observable and two spin correlations. Single-spin observables vanish in lowest order perturbation theory, but our approach provides

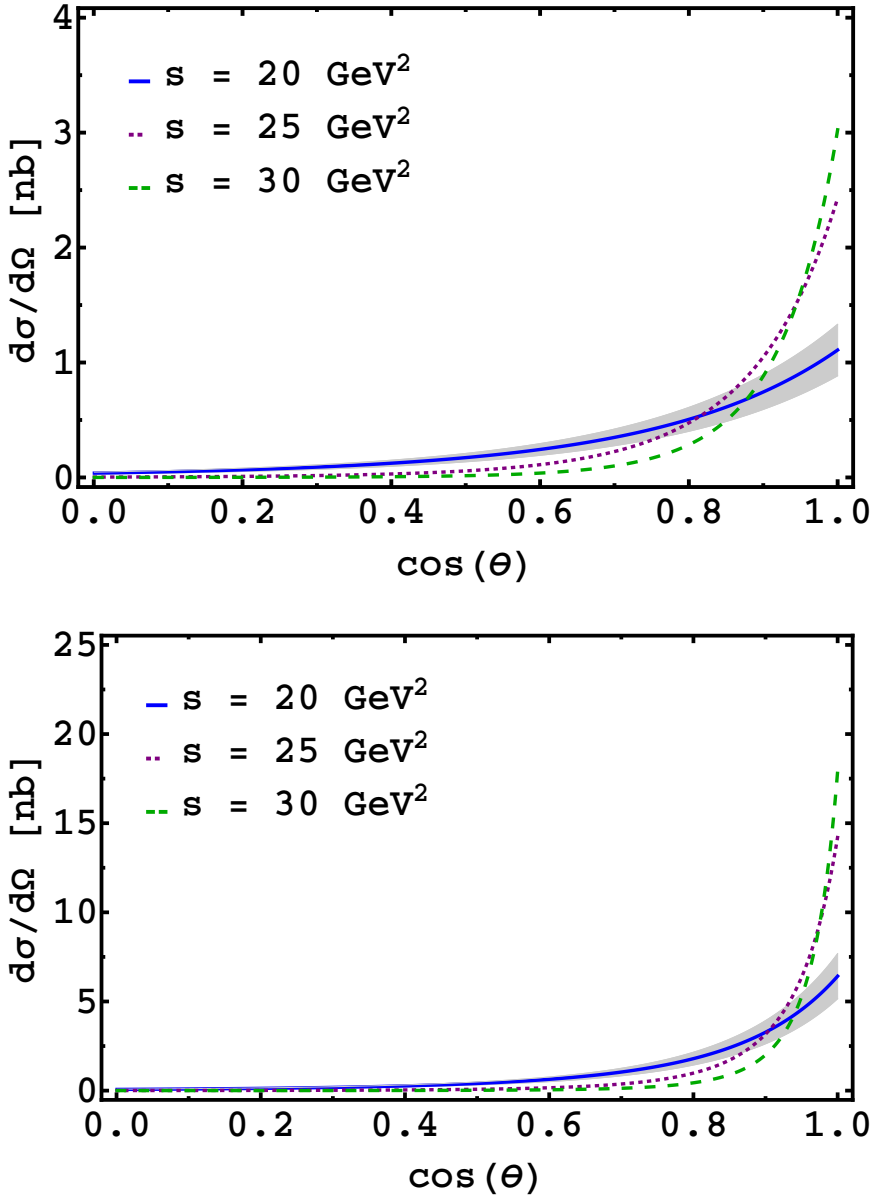

Figure 2.15: The differential $\pi p \to D^- \Lambda_c^+$ cross section versus $\cos\theta$ for $s = 20$, 25, 30 GeV^2 (solid, dotted and dashed line). This plot has been obtained with the wave function parameterizations described in the text using the KK mass exponential (upper panel) and using the BB mass exponential (lower panel). The effects of uncertainties in the Λ_c and the D^- wave function parameters are indicated by the shaded band around the curve for $s = 20$ GeV^2.

non-trivial predictions for spin correlations. We consider the polarization transfers

$$D_{LL} = D_{SS} = \frac{|\Phi_{++}|^2 - |\Phi_{+-}|^2}{|\Phi_{++}|^2 + |\Phi_{+-}|^2}\,, \tag{2.83}$$

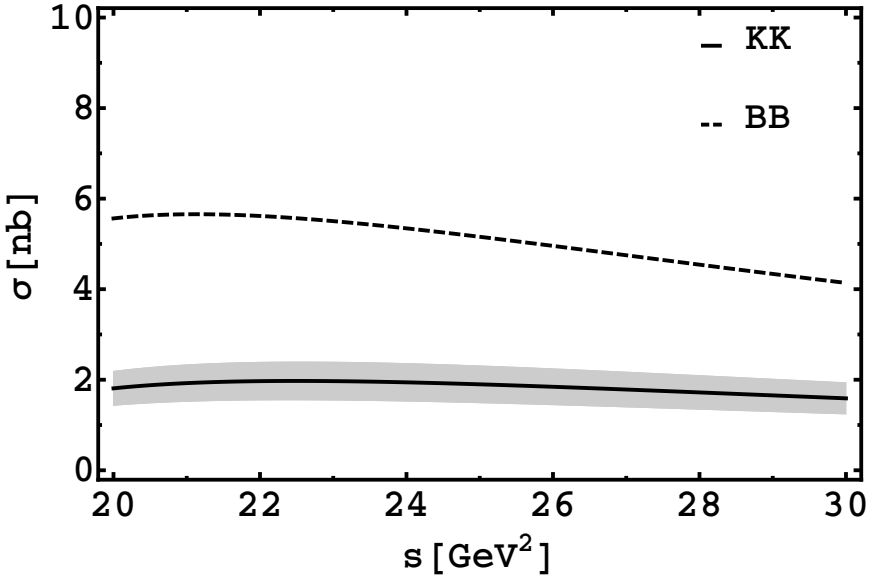

Figure 2.16: Our prediction for the integrated cross section σ versus Mandelstam s (solid line with error band). Solid line corresponds to the KK mass exponentials and the dashed line corresponds to the BB mass exponential.

and

$$D_{LS} = \frac{2\,\mathrm{Re}(\Phi_{++}\Phi_{+-}^*)}{|\Phi_{++}|^2 + |\Phi_{+-}|^2} \tag{2.84}$$

as the two independent, nontrivial spin correlations. The labels "S" and "L" denote longitudinal and sideways (in the scattering plane) polarization directions (cf. Ref. [11]). The $\Phi_{\tilde{\mu}'\tilde{\mu}}$ are CMS helicity amplitudes which are related to our LC helicity amplitudes $\mathcal{M}_{\mu'\mu}$, as defined in Eq. (2.34), by means of an appropriate Melosh rotation [27]. For a reasonable probability of about 10% to find the c quark with helicity opposite to the Λ_c helicity in the Λ_c, the form factors R_V and S_T differ by less then 2% [11]. As a consequence all the form factors and thereby the whole model dependence nearly cancel out in D_{LL} and D_{LS}. The energy dependence of D_{LL} and D_{LS} is plotted in Figs. 2.17 and 2.18 for the KK mass exponential. It occurs to be very mild over the considered energy range. The corresponding plots for the BB mass exponential look more or less the same, which confirms the approximate independence of D_{LL} and D_{LS} on the choice of the GPDs.

[27] Like in Ref. [11] only the Melosh transformation of the Λ_c helicity is considered since that of the p plays a minor role.

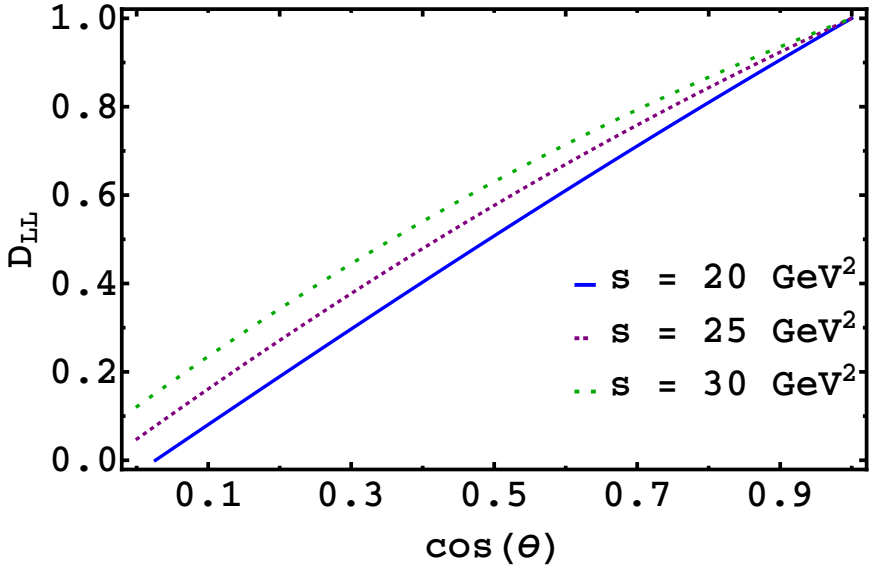

Figure 2.17: The spin-correlation parameters D_{LL} versus $\cos\theta$ for $s = 20$, 25 and 30 GeV^2.

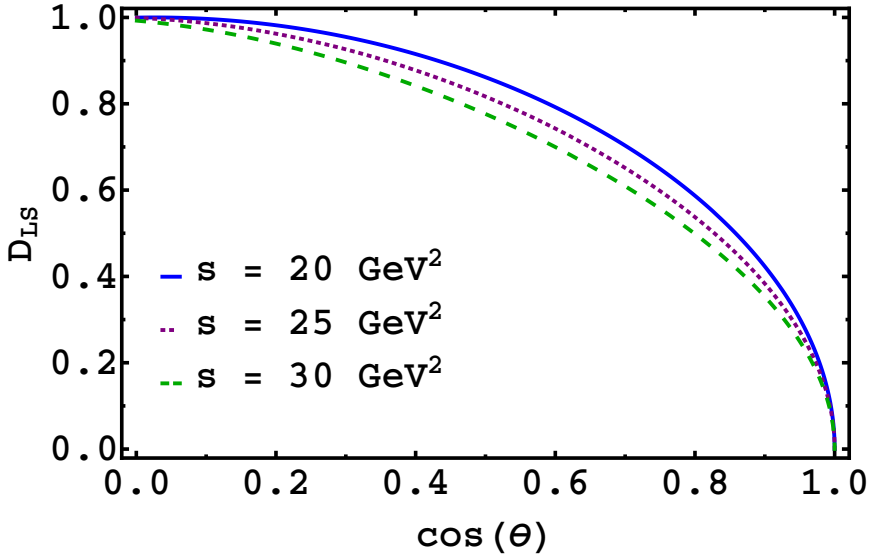

Figure 2.18: The spin-correlation parameters D_{LS} versus $\cos\theta$ for $s = 20$, 25 and 30 GeV^2.

2.3.5 *Summary*

We have investigated the exclusive process $\pi p \to D^- \Lambda_c^+$ within the generalized parton picture. Thereby we have extended previous work on $\bar{p}\, p \to \bar{\Lambda}_c^-\, \Lambda_c^+$ [11], where $p \to \Lambda_c$ transition GPDs were introduced for the first time. The analysis of $\pi p \to D^- \Lambda_c^+$ is analogous to the one for $\bar{p}\, p \to \bar{\Lambda}_c^-\, \Lambda_c^+$, the only new ingredients being the $\pi^- \to D^-$ transition GPDs which replace those for the $\bar{p} \to \bar{\Lambda}_c$ transition. Starting with a double-handbag-type mechanism for the production of the charmed

hadrons the arguments for factorization into the hard partonic subprocess $\bar{u}\,u \to \bar{c}\,c$ and soft hadronic matrix elements, which describe the $\pi^- \to D^-$ and $p \to \bar{\Lambda}_c$ transitions, are quite the same as for $\bar{p}\; p \to \bar{\Lambda}_c^-\; \Lambda_c^+$. Under the assumption that the transition GPDs are strongly peaked for momentum fractions close to $m_c / M_{\Lambda_c, D}$ the process amplitude simplified further and became just the product of the hard-scattering amplitude with generalized transition form factors, which are kind of moments of the GPDs. To model the GPDs and make numerical predictions we have employed an overlap representation in terms of LCWFs for the valence Fock states of the hadrons involved.

Interesting for planned experiments, e.g. at J-PARC or at COMPASS, we found the integrated cross section well above production threshold ($s \gtrsim 20$ GeV^2) to be of the order of nb, depending on the models for the hadron LCWFs. Our result is in accordance with experimental evidence on $\pi^- p \to D^{*-} \Lambda_c^+$ [34]. The size of the $\pi^- p \to D^- \Lambda_c^+$ cross section is typical for the exclusive production of charmed hadrons, like $\bar{p}\; p \to \bar{\Lambda}_c^-\; \Lambda_c^+$ [11] and $\bar{p}\; p \to D^0\; \overline{D}^0$ [15] when treated within the same kind of factorization approach that has been applied here. We expect a cross section of this size also for the case of a pion-induced production of longitudinally polarized D^* mesons in a straightforward extension of our model. The calculated spin correlation parameters, on the other hand, were seen to be nearly independent on the models for the LCWFs. This means that those spin correlations are mostly determined by the hard partonic subprocess and may thus give us some clues on how charm is produced on the partonic level.

2.4 $\gamma\, p \to \overline{D}^*_{\lambda=0}\, \Lambda_c^+$

In this section we investigate the exclusive photoproduction of charmed vector mesons. If we want to apply again our collinear framework and stay at leading twist, the production of transversely polarized vector mesons is power suppressed [35], so we focus on the production of longitudinally polarized vector mesons. To be more specific, we consider the process $\gamma\, p \to \overline{D}^*_{\lambda=0}\, \Lambda_c^+$. When we are speaking of a $\overline{D}^*$ we mean in the following the longitudinal polarized one.

2.4.1 *Kinematics*

The momenta, light-cone (LC) helicities and masses of the incoming proton and photon are denoted by $p,\ \mu,\ m_p$ and $q,\ \nu$, those of the outgoing Λ_c^+ and $\overline{D}^*$ by $p',\ \mu',\ M_{\Lambda_c}$ and $q',\ M_{D^*}$, respectively. As the reference frame we choose again a symmetric CMS, cf. Sec. 2.3.1. We parameterize the proton and the Λ_c^+ momenta as follows

$$p = \left[(1+\xi)\bar{p}^+, \frac{m_p^2 + \boldsymbol{\Delta}_\perp^2/4}{2(1+\xi)\bar{p}^+}, -\frac{\boldsymbol{\Delta}_\perp}{2}\right], \quad p' = \left[(1-\xi)\bar{p}^+, \frac{M_{\Lambda_c}^2 + \boldsymbol{\Delta}_\perp^2/4}{2(1-\xi)\bar{p}^+}, \frac{\boldsymbol{\Delta}_\perp}{2}\right], \tag{2.85}$$

with

$$\Delta \equiv (p'-p) = (q-q') \quad \text{and} \quad \xi \equiv \frac{p^+ - p'^+}{p^+ + p'^+} = -\frac{\Delta^+}{2\bar{p}^+}. \tag{2.86}$$

The photon and the $\overline{D}^*$-meson momenta can be written in an analogous way

$$q = \left[\frac{\boldsymbol{\Delta}_\perp^2/4}{2(1+\eta)\bar{q}^-},\ (1+\eta)\bar{q}^-,\ \frac{\boldsymbol{\Delta}_\perp}{2}\right], \quad q' = \left[\frac{M_{D^*}^2 + \boldsymbol{\Delta}_\perp^2/4}{2(1-\eta)\bar{q}^-}, (1-\eta)\bar{q}^-, -\frac{\boldsymbol{\Delta}_\perp}{2}\right], \tag{2.87}$$

with

$$\bar{q} \equiv \frac{1}{2}(q+q') \quad \text{and} \quad \eta \equiv \frac{q^- - q'^-}{q^- + q'^-} = \frac{\Delta^-}{2\bar{q}^-}. \tag{2.88}$$

The Mandelstam variable s is given by

$$s = (p+q)^2 = (p'+q')^2, \tag{2.89}$$

which is the invariant mass squared of our process. Mandelstam s has to be larger than $(M_{\Lambda_c} + M_{D^*})^2 = 18.43\ \text{GeV}^2$ to produce the particles Λ_c^+ and $\overline{D}^*$. The remaining two Mandelstam variables read

$$t = \Delta^2 = (p'-p)^2 = (q-q')^2 \tag{2.90}$$

and

$$u = (q'-p)^2 = (p'-q)^2, \tag{2.91}$$

such that

$$s + t + u = m_p^2 + m_\pi^2 + M_{\Lambda_c}^2 + M_{D^*}^2. \tag{2.92}$$

The explicit expressions for $\bar{p}^+,\ \bar{q}^-,\ \xi,\ \eta,\ \boldsymbol{\Delta}_\perp^2,\ t,\ u$ can be found in App. B with[28] $m_a = m_p = 0.938272$ GeV, $m_b = 0$ GeV, $m_c = M_{\Lambda_c} = 2.286460$ GeV and $m_d = M_{D^*} = 2.00697$ GeV.

2.4.2 *Handbag mechanism and scattering amplitude*

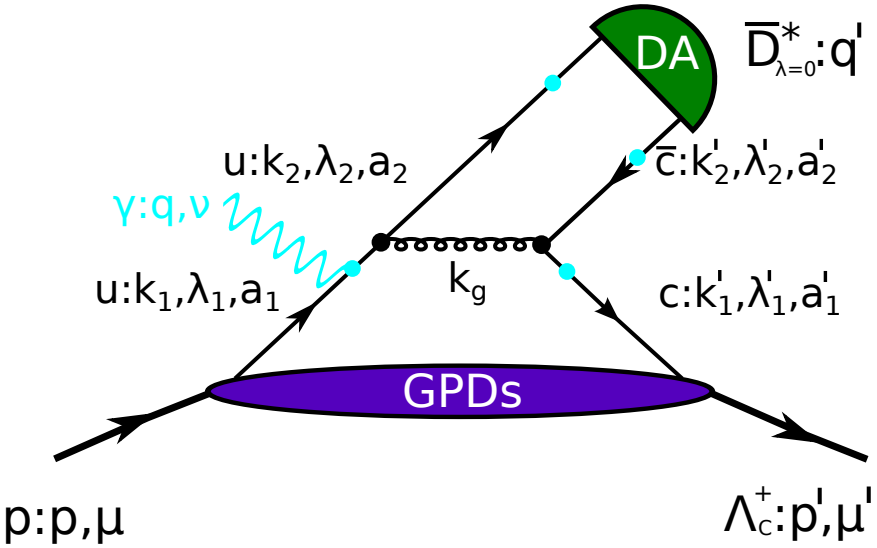

Figure 2.19: Handbag contribution to the process $\gamma\, p \to \overline{D}^*_{\lambda=0}\, \Lambda_c^+$ (in the DGLAP region). The momenta, LC helicities and colors of the quarks are specified. The photon can couple to either of the points indicated by the dots.

The mechanism we assume for the description of the $\gamma\, p \to \overline{D}^*_{\lambda=0}\, \Lambda_c^+$ reaction well above the kinematical threshold and in the forward scattering hemisphere is depicted in Fig. 2.19. A proton emits a u-quark with momentum k_1 and helicity λ_1 which itself emits a gluon and henceforth changes its momentum to k_2 and helicity to λ_2. The gluon subsequently decays into a charm-anticharm pair with momenta k_1', k_2' and helicities λ_1', λ_2', respectively. The "scattered" u-quark[29] and the produced $\bar{c}$-quark form the $\overline{D}^*$ meson and the residual c-quark is reabsorbed by the remainders of the proton and both form the Λ_c^+[30].
The heavy-quark mass m_c serves as a *natural hard scale* which requires the gluon to be highly virtual. This is easy to see for those graphs in which the photon couples to the u-quarks, but less obvious for those in which the photon couples to either the c- or $\bar{c}$-quark. When the photon couples to the u-quark it is obvious that $k_g^2 \geq 4m_c^2$. If it couples to the c- or $\bar{c}$-quark one can verify by a numerical calculation that also in this case the gluon propagator is highly virtual. Furthermore, we can also verify

[28] The values of the masses are taken from Ref. [16].
[29] The light quarks are treated as massless.
[30] We are neglecting the intrinsic charm of the proton, therefore only the emission of the u-quark from the proton leads to the Λ_c^+ in the final state.

by a numerical calculation that the propagators are sufficiently off-mass shell so that a perturbative treatment of the partonic subprocess is justified, even at small $-t$ and $-u$. The corresponding Feynman diagrams are investigated in Sec. 2.4.3. The non perturbative dynamics is encoded in hadronic matrix elements which can be parameterized in terms of transition GPDs (for the $p \to \Lambda_c^+$ transition) and a DA (for the $\overline{D}^*$ production).

The scattering amplitude for $\gamma p \to \overline{D}^*_{\lambda=0}\Lambda_c^+$ using the handbag mechanism can be written as

$$\begin{aligned}\mathscr{M}_{\mu' 0,\mu\nu} = \sum_{a_i^{(\prime)},\alpha_i^{(\prime)}} \int \mathrm{d}^4\bar{k}_1\, \Theta(\bar{k}_1^+) \int \frac{\mathrm{d}^4 z_1}{(2\pi)^4} e^{i\bar{k}_1 z_1} \int \mathrm{d}^4 k_2'\, \Theta(k_2'^-) \int \frac{\mathrm{d}^4 z_2}{(2\pi)^4} e^{i\frac{z_2}{2}(-q'+2k_2')} \\ \times \langle \Lambda_c^+ : p', \mu' | \mathscr{T} \overline{\Psi}^c_{a_1',\alpha_1'} \left(-\frac{z_1}{2}\right) \Psi^u_{a_1,\alpha_1} \left(\frac{z_1}{2}\right) | p : p, \mu \rangle \, \widetilde{H}^{\nu}_{a_i^{(\prime)},\alpha_i^{(\prime)}} \left(\bar{k}_1, k_2, k_2'\right) \\ \times \langle \overline{D}^* : q' | \mathscr{T} \overline{\Psi}^u_{a_2,\alpha_2} \left(\frac{z_2}{2}\right) \Psi^c_{a_2',\alpha_2'} \left(-\frac{z_2}{2}\right) | 0 \rangle \,,\end{aligned} \tag{2.93}$$

where the assignments of momenta and helicities can be read off from Fig. 2.19 and $a_i^{(\prime)}$ and $\alpha_i^{(\prime)}$ denote color and spinor labels, respectively, and $\widetilde{H}$ is the hard scattering kernel. The average momentum is defined by $\bar{k}_1 = \frac{k_1+k_1'}{2}$. As we explained in Sec. 2.3.2.1 in detail the crucial assumptions are that the parton virtualities and the intrinsic transverse momentum components of the parton divided by its momentum fraction are restricted by a hadronic scale of the order of 1 GeV, see Eqs. (2.10)-(2.11). The active parton momenta are then approximately on mass shell and collinear to their parent hadron

$$\begin{aligned} k_1 &\to \left[k_1^+, \frac{x_1^2 \boldsymbol{\Delta}_\perp^2}{8k_1^+}, -x_1 \frac{\boldsymbol{\Delta}_\perp}{2}\right] && \text{with } k_1^+ = x_1 p^+, \\ k_1' &\to \left[k_1'^+, \frac{m_c^2 + x_1'^2 \boldsymbol{\Delta}_\perp^2/4}{2k_1'^+}, x_1' \frac{\boldsymbol{\Delta}_\perp}{2}\right] && \text{with } k_1'^+ = x_1' p'^+, \\ k_2 &\to \left[\frac{(1-x_2')^2 \boldsymbol{\Delta}_\perp^2}{8k_2^-}, k_2^-, -(1-x_2')\frac{\boldsymbol{\Delta}_\perp}{2}\right] && \text{with } k_2^- = (1-x_2')\, q^-, \\ k_2' &\to \left[\frac{m_c^2 + x_2'^2 \boldsymbol{\Delta}_\perp^2/4}{2k_2'^-}, k_2'^-, -x_2' \frac{\boldsymbol{\Delta}_\perp}{2}\right] && \text{with } k_2'^- = x_2' q'^-. \end{aligned} \tag{2.94}$$

Therefore Eq. (2.93) can be simplified to

$$\begin{aligned}\mathscr{M}_{\mu' 0,\mu\nu} = &\sum_{a_i^{(\prime)},\alpha_i^{(\prime)}} \int \mathrm{d}\bar{x}_1\, \bar{p}^+ \int \frac{\mathrm{d}z_1^-}{(2\pi)} e^{i\bar{x}_1 \bar{p}^+ z_1^-} \int \mathrm{d}k_2'^- \int \frac{\mathrm{d}z_2^+}{(2\pi)} e^{i\frac{z_2^+}{2}\left(-q'^- + 2k_2'^-\right)} \\ &\times \langle \Lambda_c^+ : p', \mu' | \overline{\Psi}^c_{a_1',\alpha_1'} \left(-\frac{z_1^-}{2}\right) \Psi^u_{a_1,\alpha_1} \left(\frac{z_1^-}{2}\right) | p : p, \mu \rangle\, \widetilde{H}^\nu_{a_i^{(\prime)},\alpha_i^{(\prime)}} \left(\bar{x}_1 \bar{p}^+, k_2^-, k_2'^-\right) \\ &\times \langle \overline{D}^* : q' | \overline{\Psi}^u_{a_2,\alpha_2} \left(\frac{z_2^+}{2}\right) \Psi^c_{a_2',\alpha_2'} \left(-\frac{z_2^+}{2}\right) | 0 \rangle\,,\end{aligned} \tag{2.95}$$

with $\bar{x}_1 = \frac{\bar{k}_1^+}{\bar{p}^+}$. The soft part of our process is encoded in Fourier transforms of two hadronic matrix elements of a bilocal product of quark field operators:

$$\int \frac{\mathrm{d}z_1^-}{2\pi} e^{iz_1^- \bar{k}_1^+} \langle \Lambda_c^+ : p', \mu' | \overline{\Psi}^c_{a_1',\alpha_1'} \left(-\frac{z_1^-}{2}\right) \Psi^u_{a_1,\alpha_1} \left(\frac{z_1^-}{2}\right) | p : p, \mu \rangle\,, \tag{2.96}$$

for the soft $p \to \Lambda_c^+$ transition and

$$\int \frac{\mathrm{d}z_2^+}{2\pi} e^{i\frac{z_2^+}{2}\left(-q'^- + 2k_2'^-\right)} \langle \overline{D}^* : q' | \overline{\Psi}^u_{a_2,\alpha_2} \left(\frac{z_2^+}{2}\right) \Psi^c_{a_2',\alpha_2'} \left(-\frac{z_2^+}{2}\right) | 0 \rangle\,, \tag{2.97}$$

for the formation of the $\overline{D}^*$-meson. In Eq. (2.96), $\Psi^u(z_1^-/2)$ takes out a u-quark at space-time $z_1^-/2$ from the proton state $|p : p, \mu\rangle$, which then participates in the hard partonic subprocess, whereas $\overline{\Psi}^c(-z_1^-/2)$ reinserts the produced c-quark at space-time $-z_1^-/2$ into the remainder of the proton which gives the final Λ_c^+ hadron. Equation (2.97) is the amplitude for finding the u- and the $\bar{c}$-quark that leave the hard-scattering process at space-time $z_2^+/2$ and $-z_2^+/2$, respectively, in the state $|\overline{D}^* : q'\rangle$. Appendix C is devoted to the study of Eq. (2.96). In the remainder of this section we investigate Eq. (2.97).

We want to decompose the quark field operator product $\bar{\Psi}^u \Psi^c$ at leading twist. This can easily done in the *hadron-out* frame of the $\overline{D}^*$ which is a frame where it has zero transverse momentum. The scattering process is formulated in the CMS and therefore also the quark field operators are expressed in terms of CMS quantities. However, by performing a transverse boost we can transform from the CMS to the hadron-out frame where we will single out the leading twist components of the quark fields. The transverse boost does not alter our reasoning. Therefore we can then transform back to the CMS. Let us now investigate this procedure step by step for Eq. (2.97). By performing a transverse boost we can change from the CMS to the hadron-out frame of the outgoing $\overline{D}^*$. In this frame the momenta k_2 and k_2' of

Eq. (2.94) read

$$k_2 = \left[0, k_2^-, \mathbf{0}_\perp\right], \tag{2.98}$$

$$k_2' = \left[\frac{m_c^2}{2k_2'^-}, k_2'^-, \mathbf{0}_\perp\right]. \tag{2.99}$$

The energy projectors can therefore be written as

$$\sum_{\lambda_2} u\left(k_2, \lambda_2\right) \bar{u}\left(k_2, \lambda_2\right) = k_2 \cdot \gamma = k_2^- \gamma^+, \tag{2.100}$$

$$\sum_{\lambda_2'} v\left(k_2', \lambda_2'\right) \bar{v}\left(k_2', \lambda_2'\right) = k_2' \cdot \gamma - m_c = k_2'^- \gamma^+ + \frac{m_c^2}{2k_2'^-}\gamma^- - m_c. \tag{2.101}$$

Using $1 = \mathscr{P}_+ + \mathscr{P}_-$ with the projection operators $\mathscr{P}_\pm$ (see Eq. A.15) we get

$$\bar{\Psi}^u = \bar{\Psi}^u 1 = \bar{\Psi}^u \frac{1}{2}\left(\gamma^-\gamma^+ + \gamma^+\gamma^-\right), \tag{2.102}$$

$$\Psi^c = 1\Psi^c = \frac{1}{2}\left(\gamma^-\gamma^+ + \gamma^+\gamma^-\right)\Psi^c, \tag{2.103}$$

in which we can eliminate γ^+ by means of Eq. (2.100) to obtain[31]

$$\bar{\Psi}^u = \frac{1}{2k_2^-}\sum_{\lambda_2}\left(\bar{\Psi}^u \gamma^- u\left(k_2, \lambda_2\right)\right) \bar{u}\left(k_2, \lambda_2\right), \tag{2.104}$$

$$\Psi^c = \frac{1}{2k_2'^-}\sum_{\lambda_2'} v\left(k_2', \lambda_2'\right)\left(\bar{v}\left(k_2', \lambda_2'\right)\gamma^-\Psi^c\right). \tag{2.105}$$

In Eqs. (2.104)-(2.105) we have projected out the "good" field components of the quark fields. This is seen for Eq. (2.104) as follows

$$\begin{aligned}\bar{\Psi}^u\gamma^- &= \Psi^{\dagger u}\gamma^0\gamma^-\gamma^0\gamma^0 = \Psi^{\dagger u}\gamma^+\gamma^0 = \left(\gamma^0\gamma^-\Psi^u\right)^\dagger = \sqrt{2}\left(\mathscr{P}_-^2\Psi_-^u\right)^\dagger \\ &= \left(\gamma^0\gamma^-\Psi^u\right)^\dagger = \bar{\Psi}_-^u\gamma^-\end{aligned} \tag{2.106}$$

and for Eq. (2.105)

$$\gamma^-\Psi^c = \gamma^0\gamma^0\gamma^-\Psi^c = \sqrt{2}\gamma^0\mathscr{P}_-\Psi^c = \sqrt{2}\gamma^0\mathscr{P}_-^2\Psi_c = \gamma^-\Psi_-^c \tag{2.107}$$

respectively (Ψ_- denotes the "good" field component of the quark field). With Eqs. (2.104)-(2.105) we can write for the quark field operator product in the meson matrix element

$$\bar{\Psi}^u\Psi^c = \frac{1}{4k_2^-k_2'^-}\sum_{\lambda_2}\left(\bar{\Psi}_-^u\gamma^- u\left(k_2, \lambda_2\right)\right)\left(\bar{v}\left(k_2', -\lambda_2\right)\gamma^-\Psi_-^c\right)\bar{u}\left(k_2, \lambda_2\right) v\left(k_2', -\lambda_2\right), \tag{2.108}$$

[31] For $\bar{\Psi}^u$ there is an additional term $\bar{\Psi}^u u\left(k_2, \lambda_2\right)\bar{u}\left(k_2, \lambda_2\right)\gamma^-$ and for Ψ^c there is the following additional term $\gamma^-\left(v\left(k_2', \lambda_2'\right)\bar{v}\left(k_2', \lambda_2'\right)\Psi^c - 2m_c\Psi^c\right)$. However, these two term vanish when they are applied to the meson matrix element $\langle\overline{D}^*|\bar{\Psi}^u\Psi^c|0\rangle$.

where we have used that $\lambda_2' = -\lambda_2$ (see the Fock state expansion of the $\overline{D}^*$ in Eq. (2.119)). We note that a transverse boost from the hadron-out frame to the CMS does not alter Eq. (2.108). In the following we are again working in our CMS. Using appropriate spinor products such as[32]

$$-\frac{\bar{u}\left(k_2,\lambda_2\right)\gamma^- v\left(k_2',-\lambda_2\right)}{2\sqrt{k_2^- k_2'^-}} = 1, \tag{2.109}$$

we can write the product

$$\left(\bar{\Psi}^u_- \gamma^- u\left(k_2,\lambda_2\right)\right)\ 1\ \left(\bar{v}\left(k_2',-\lambda_2\right)\gamma^- \Psi^c_-\right) \tag{2.110}$$

as

$$-\frac{1}{2\sqrt{k_2^- k_2'^-}}\bar{\Psi}^u_- \gamma^- u\left(k_2,\lambda_2\right)\bar{u}\left(k_2,\lambda_2\right)\gamma^- v\left(k_2',-\lambda_2\right)\bar{v}\left(k_2',-\lambda_2\right)\gamma^-\Psi^c_-. \tag{2.111}$$

In principle there is also the following spinor product at our disposal

$$\sim \bar{u}\left(k_2,\lambda_2\right) i\sigma^{-j} v\left(k_2',\lambda_2'\right), \tag{2.112}$$

but for $\lambda_2' = -\lambda_2$ it is zero. The reason that we inserted Eq. (2.111) into (2.108) is that we can use the helicity projectors for the u-quark and the heavy c-quark

$$u\left(k_2,\lambda_2\right)\overline{u}\left(k_2,\lambda_2\right) = k_2\cdot\gamma\frac{1-2\lambda_2\,\gamma_5}{2} \tag{2.113}$$

and

$$v\left(k_2',-\lambda_2\right)\overline{u}\left(k_2',-\lambda_2\right) = \left(k_2'\cdot\gamma + m_c\right)\frac{1+\gamma_5\, S_2\cdot\gamma}{2} \tag{2.114}$$

with the covariant spin vector

$$S_2 = \frac{-2\lambda_2}{m_c}\left(k_2'^- - \frac{m_c^2}{k_2'^-}n^+\right). \tag{2.115}$$

Putting all pieces together, Eq. (2.108) becomes

$$\bar{\Psi}^u\Psi^c = \frac{1}{4k_2^- k_2'^-}\sum_{\lambda_2}\left(\bar{\Psi}^u_-\gamma^-\left(1-2\lambda_2\gamma_5\right)\Psi^c_-\right)\bar{u}\left(k_2,\lambda_2\right)v\left(k_2',-\lambda_2\right). \tag{2.116}$$

Now, when we insert the Fourier decomposition of the field operators we find that $\bar{\Psi}^u\gamma^-\gamma_5\Psi^c = 0$ since $\lambda_2' = -\lambda_2$. Thus, the final expression for the quark field operator product reads

$$\bar{\Psi}^u\Psi^c = -\frac{1}{4k_2^- k_2'^-}\sum_{\lambda_2}\bar{\Psi}^u_-\gamma^-\Psi^c_-\,\bar{u}\left(k_2,\lambda_2\right)v\left(k_2',-\lambda_2\right). \tag{2.117}$$

[32]The explicit form of the spinors can be found in App. E. We remark that $\left(k_2^{(\prime)}\right)_3 < 0$ so the corresponding spinors must be used.

After these manipulations the hadronic matrix element describing the formation of the $\overline{D}^*$ has the following form[33]:

$$-\int \frac{\mathrm{d}z_2^+}{2\pi} e^{i\frac{z_2^+}{2}\left(-q'^- + 2k_2'^-\right)} \frac{1}{4k_2^- k_2'^-} \langle \overline{D}^* : q' | \sum_{\lambda_2} \bar{\Psi}_-^u \left(\frac{z_2^+}{2}\right) \gamma^- \Psi_-^c \left(-\frac{z_2^+}{2}\right) |0\rangle \,. \tag{2.118}$$

In order to calculate this matrix element we have to specify the valence Fock state of the $\overline{D}^*$:

$$\begin{aligned} |\overline{D}^* : q'\rangle = \int \mathrm{d}\hat{x}_2' \int \frac{\mathrm{d}^2\hat{\mathbf{k}}_{\perp 2}'}{16\pi^3} \Psi_D(\hat{x}_2', \hat{\mathbf{k}}_\perp') \frac{1}{\sqrt{\hat{x}_2'(1-\hat{x}_2')}} \\ \times \frac{1}{\sqrt{2}} \Big[|\bar{c} : \hat{x}_2' q'^-, \hat{\mathbf{k}}_\perp' + \hat{x}_2' \mathbf{q}_\perp', +\frac{1}{2}\rangle \, |u : (1-\hat{x}') q'^-, -\hat{\mathbf{k}}_\perp' + (1-\hat{x}') \mathbf{q}_\perp', -\frac{1}{2}\rangle \\ + |\bar{c} : \hat{x}_2' q'^-, \hat{\mathbf{k}}_\perp' + \hat{x}_2' \mathbf{q}_\perp', -\frac{1}{2}\rangle \, |u : (1-\hat{x}') q'^-, -\hat{\mathbf{k}}_\perp' + (1-\hat{x}') \mathbf{q}_\perp', \frac{1}{2}\rangle \Big]. \end{aligned} \tag{2.119}$$

For the $\overline{D}^*$-LCWF we use the same as in Sec. 2.3.3.2 to describe the $\pi^- \to D^-$ transition, cf. Eq. (2.70). For convenience we also repeat the Fourier representation of the field operators

$$\bar{\Psi}_-^u \left(\frac{z_2^+}{2}\right) = \int \frac{\mathrm{d}k_2^-}{k_2^-} \frac{\mathrm{d}^2\mathbf{k}_{\perp 2}}{16\pi^3} \sum_{\lambda_2} b_u^\dagger \bar{u}\left(k_2, \lambda_2\right) e^{i\frac{k_2^- z_2^+}{2}} + \ldots, \tag{2.120}$$

$$\Psi_-^c \left(-\frac{z_2^+}{2}\right) = \int \frac{\mathrm{d}k_2'^-}{k_2'^-} \frac{\mathrm{d}^2\mathbf{k}_{\perp 2}'}{16\pi^3} \sum_{\lambda_2'} d_c^\dagger v\left(k_2', \lambda_2'\right) e^{-i\frac{k_2'^- z_2^+}{2}} + \ldots, \tag{2.121}$$

with $\lambda_2' = -\lambda_2$ and $\ldots$ denote terms which are equal to zero in $\langle \overline{D}^* | \bar{\Psi}_-^u \gamma^- \Psi_-^c | 0 \rangle$ using the valence Fock state for the $\overline{D}^*$ of Eq. (2.119). With the definition of the meson decay constant

$$\langle 0 | \bar{\Psi}^c \gamma^\mu \Psi^u | \overline{D}^* \rangle = i f_{D^*} M_D \epsilon^\mu \tag{2.122}$$

and inserting Eqs. (2.119)-(2.120) into Eq. (2.118) we get

$$\begin{aligned} &-\int \frac{\mathrm{d}z_2^+}{2\pi} e^{i\frac{z_2^+}{2}\left(-q'^- + 2k_2'^-\right)} \frac{1}{4k_2^- k_2'^-} \langle \overline{D}_L^* : q' | \sum_{\lambda_2} 2\lambda_2 \bar{\Psi}_-^u \left(\frac{z_2^+}{2}\right) \gamma^- \gamma_5 \Psi_-^c \left(-\frac{z_2^+}{2}\right) |0\rangle \\ &= -\frac{f_{D^*}}{2\sqrt{6}} \phi_{D^*}\left(x_2'\right). \end{aligned} \tag{2.123}$$

The value of the meson decay constant $f_{D^*} = 0.252 \pm 22.64$ MeV is taken from Ref. [36]. We note that we are not using the peaking approximation in the hadronic meson matrix element. The DA is peaked at values around $x_{20}' \sim \frac{m_c}{M_D} \sim 0.63$ (see Sec. 2.3.3.2), i.e. when integrating over x_2' only the region close to x_{20}' gives sizable con-

[33] The spinors of Eq. 2.117 (and also those of Eq. (C.13)) are absorbed into the hard scattering kernel of the scattering amplitude and define the hard scattering amplitude.

tributions. For convenience we repeat the $\overline{D}^*$ distribution amplitude (see Sec. 2.3.3.2 for more details) that we use[34]

$$\phi_{D^*}(x_2') \sim x_2'(1-x_2')\, \exp\left[-f(x_2')\right], \tag{2.124}$$

with the KK mass exponential ($x_{20}' = m_c/M_D \sim 0.68$)

$$f(x) = a_{D^*}^2 M_{D^*}^2 \frac{(x_2' - x_{20}')^2}{x_2'(1-x_2')} \tag{2.125}$$

and with the BB mass exponential

$$f(x) = a_D^* M_D^* (1 - x_2'). \tag{2.126}$$

The oscillator parameters are $a_D^* = 0.74$ GeV$^{-1}(KK)$ and $a_D^* = 0.80$ GeV$^{-1}(BB)$, respectively. The normalization $N_D^* = 43.94$ GeV$^2(KK)/64.82$ GeV$^2(BB)$ and the oscillator parameter of the $\overline{D}^*$-LCWF are chosen such that f_D^* is reproduced and that the probability to find the valence Fock state in the to $\overline{D}^*$ becomes 0.9.

Before we show the explicit form of the scattering amplitude in terms of the $p \to \Lambda_c$ transition form factors and the $\overline{D}^*$-DA, we make some remarks about the hard scattering amplitude:

- Naive application of the collinear approximation gives (minus signs for primed momenta) $k_1^{(\prime)} = (\bar{x}_{10} \pm \xi) p^{(\prime)}/(1 \pm \xi)$, $k_2 = (1 - x_2')q'$ and $k_2' = x_2' q'$ for the parton momenta where $\bar{x}_{10} = m_c/M_\Lambda = 0.55$. In order to match the subprocess kinematics (charm-quark mass m_c) with the one on the hadronic level (hadron masses $M_{\Lambda_c} \neq M_D$) some further approximations are required. As one can easily verify $k_1 + k_2 \neq k_1' + k_2'$, i.e. momentum conservation does not hold on the partonic level, in general. There is only one special case in which momentum conservation is recovered, namely in the heavy-quark limit $M_{\Lambda_c} = M_D = m_c \to \infty$, i.e. $\bar{x}_{10} \to 1$.

- We absorb the spinors coming from the quark field operator manipulations (cf. Eq. (C.24) and Eq. (2.118)) into the hard scattering kernel of the (hadronic) scattering amplitude:

  - The spinors of the meson matrix element give to a good approximation the covariant spin wave function of the outgoing $\overline{D}^*$-meson[35]:

$$\frac{1}{\sqrt{2}}\left[\bar{u}\left(q', \frac{1}{2}\right) v\left(q', -\frac{1}{2}\right) + \bar{u}\left(q', -\frac{1}{2}\right) v\left(q', \frac{1}{2}\right)\right] = \frac{(\not{q}' - M_D)\, \not{\epsilon}_{VM}}{\sqrt{2}}. \tag{2.127}$$

    This structure is absorbed into the hard scattering kernel $\widetilde{H}^\nu$ and we denote the modified hard scattering kernel by $\hat{H}^\nu$.

[34] The DA normalization condition is $\int \mathrm{d}x_2' \phi_D^*(x_2') = 1$.

[35] This is exactly the general spin structure we would have for the wave function of a heavy-light meson that obeys heavy-quark symmetry, see Ref. [37].

– We define the hard scattering amplitude then as

$$H^{\nu}_{\lambda_1',\lambda_1} = \bar{u}\left(p',\lambda_1'\right)\hat{H}^{\nu}u\left(p,\lambda_1\right). \tag{2.128}$$

With the preceding discussions and App. C we can show that the final expression of the scattering amplitude reads

$$\begin{aligned}
\mathscr{M}_{\frac{1}{2}0,\frac{1}{2}\nu} &= \frac{C}{4\sqrt{6}}\, f_D\sqrt{1-\xi^2} \\
&\quad \left[(R_V+R_A)\int \mathrm{d}z\ \phi_D(z) H^{\nu}_{\frac{1}{2},\frac{1}{2}} + (R_V-R_A)\int \mathrm{d}z\ \phi_D(z) H^{\nu}_{-\frac{1}{2},-\frac{1}{2}}\right], \\
\mathscr{M}_{-\frac{1}{2}0,-\frac{1}{2}\nu} &= \frac{C}{4\sqrt{6}}\, f_D\sqrt{1-\xi^2} \\
&\quad \left[(R_V-R_A)\int \mathrm{d}z\ \phi_D(z) H^{\nu}_{\frac{1}{2},\frac{1}{2}} + (R_V+R_A)\int \mathrm{d}z\ \phi_D(z) H^{\nu}_{-\frac{1}{2},-\frac{1}{2}}\right], \\
\mathscr{M}_{\frac{1}{2}0,-\frac{1}{2}\nu} &= \frac{C}{2\sqrt{6}}\, f_D\sqrt{1-\xi^2}\, S_T \int \mathrm{d}z\ \phi_D(z) H^{\nu}_{\frac{1}{2},-\frac{1}{2}}, \\
\mathscr{M}_{-\frac{1}{2}0,\frac{1}{2}\nu} &= \frac{C}{2\sqrt{6}}\, f_D\sqrt{1-\xi^2}\, S_T \int \mathrm{d}z\ \phi_D(z) H^{\nu}_{-\frac{1}{2},\frac{1}{2}},
\end{aligned} \tag{2.129}$$

with $C = \frac{4}{3}\frac{1}{\sqrt{3}}$ being the color factor.

To conclude this section let us summarize the assumptions we have made that lead to Eq. (2.129)

- *Peaking approximation*: The $p \to \Lambda_c$ GPDs have a peak at $\bar{x}_1 \sim \bar{x}_{10}$ and therefore can be taken out of the convolution integral with the hard scattering amplitude. We rather need the integral over the GPDs than the GPDs themselves. We call those integrals transition form factors.
- In modeling the GPDs as an overlap of LCWFs we restricted ourselves to s-wave functions, i.e. the helicity of the partons in the valence Fock states add up to the hadron helicity. This reduces the number of GPDs from 8 to 3.

2.4.3 *The hard scattering amplitude*

At leading order in α_s we have to evaluate 4 Feynman diagrams, i.e. 4 amplitudes which are shown in Fig. 2.20. The hard scattering amplitude $H^{\nu}_{\lambda_1',\lambda_1}$ is then a sum of those four amplitudes. With the collinear approximation in the heavy quark limit, $k_1 = p$ and $k_1' = p'$, the partonic momenta can be expressed in terms of momenta on the hadronic level. To match the subprocess kinematics (charm-quark mass m_c) with the one on the hadronic level (hadron masses $M_{\Lambda_c} \neq M_D$) we introduce $\overline{M} = \sqrt{M_{\Lambda_c} M_D}$

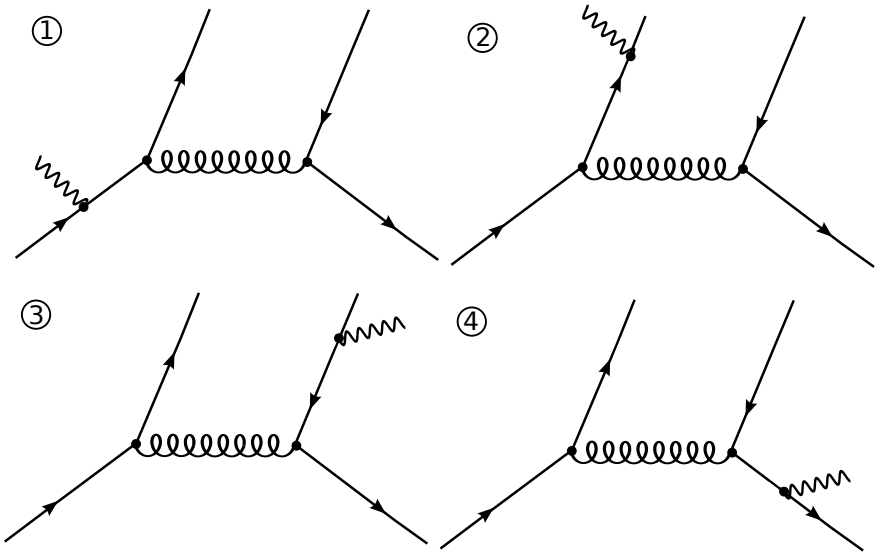

Figure 2.20: The 4 leading order Feynman graphs contributing to the partonic subprocess.

(the mass of the proton is chosen equal to zero in the hard scattering process). The kinematics is then such that we are again in a symmetric CMS and the kinematical quantities such as $\bar{p}^+,\ \xi,\ \boldsymbol{\Delta}_\perp^2, \ldots$ are given in App. B with $m_a = 0,\ m_b = 0, m_c = \overline{M}$ and $m_d = \overline{M}$. Before we discuss the structure of the amplitudes in more detail in Sec. 2.4.3.2, let us mention the following: When we simplify the amplitudes it turns out that the final expressions can be written in terms of 8 different spinor products and 8 different scalar products.

2.4.3.1 *Spinor and scalar products*

Let us start to list the 8 different spinor products and the 8 different scalar products that we have to calculate.

Spinor products:

- Spinor product 1 (SP1): $\bar{u}\,(p', \lambda_1')\, u\,(p, \lambda_1)$
- Spinor product 2 (SP2): $\bar{u}\,(p', \lambda_1')\, \not{\epsilon}_\gamma(q,1) u\,(p, \lambda_1)$
- Spinor product 3 (SP3): $\bar{u}\,(p', \lambda_1')\, \not{\epsilon}_M(q,0) u\,(p, \lambda_1)$
- Spinor product 4 (SP4): $\bar{u}\,(p', \lambda_1')\, \not{q} u\,(p, \lambda_1)$
- Spinor product 5 (SP5): $\bar{u}\,(p', \lambda_1')\, \not{\epsilon}_\gamma(q,1) \not{\epsilon}_M(q,0) u\,(p, \lambda_1)$
- Spinor product 6 (SP 6): $\bar{u}\,(p', \lambda_1')\, \not{q} \not{\epsilon}_\gamma(q,1) u\,(p, \lambda_1)$
- Spinor product 7 (SP7): $\bar{u}\,(p', \lambda_1')\, \not{q} \not{\epsilon}_M(q',0) u\,(p, \lambda_1)$
- Spinor product 8 (SP8): $\bar{u}\,(p', \lambda_1')\, \not{q} \not{\epsilon}_\gamma(q,1) \not{\epsilon}_M(q',0) u\,(p, \lambda_1)$

Scalar products:

- Scalar product 1 (ScP1): $p' \cdot \epsilon_\gamma(q,1)$
- Scalar product 2 (ScP2): $q' \cdot \epsilon_\gamma(q,1)$
- Scalar product 3 (ScP3): $q \cdot \epsilon_M(q',0)$
- Scalar product 4 (ScP4): $\epsilon_\gamma(q,1) \cdot \epsilon_M(q',0)$
- Scalar product 5 (ScP5): $q \cdot p'$
- Scalar product 6 (ScP6): $p' \cdot \epsilon_M(q',0)$
- Scalar product 7 (ScP7): $p \cdot \epsilon_M(q',0)$
- Scalar product 8 (ScP8): $p \cdot q$

The momenta in the hard scattering process are given by[36]

$$\begin{aligned} k_1 = p &= \Big[(1+\xi)\,\bar{p}^+, \ldots, -\frac{|\boldsymbol{\Delta}_\perp|}{2}, 0\Big], \\ k_1' = p' &= \Big[(1-\xi)\,\bar{p}^+, \ldots, \frac{|\boldsymbol{\Delta}_\perp|}{2}, 0\Big], \\ q &= \Big[\frac{\boldsymbol{\Delta}_\perp^2}{8\,(1+\xi)\,\bar{p}^+}, (1+\xi)\,\bar{p}^+, \frac{|\boldsymbol{\Delta}_\perp|}{2}, 0\Big] \end{aligned} \tag{2.130}$$

and

$$\begin{aligned} k_2 &= (1-x_2')\,q', \\ k_2' &= x_2' q', \\ \text{with } q' &= \Big[\frac{\overline{M}^2 + \boldsymbol{\Delta}_\perp^2/4}{2\,(1-\xi)\,\bar{p}^+}, (1-\xi)\,\bar{p}^+, -\frac{|\boldsymbol{\Delta}_\perp|}{2}, 0\Big]. \end{aligned} \tag{2.131}$$

The polarization vectors of the photon[37] ϵ_γ and of the longitudinally polarized vector mesons ϵ_M read

$$\epsilon_\gamma\,(q,1) = \Big[\frac{1}{2\sqrt{s}}|\boldsymbol{\Delta}_\perp|, -\frac{1}{2\sqrt{s}}|\boldsymbol{\Delta}_\perp|, \frac{2\,(1+\xi)\,\bar{p}^+}{\sqrt{s}} - \frac{1}{\sqrt{2}}, -\frac{i}{\sqrt{2}}\Big], \tag{2.132}$$

$$\epsilon_M(q',0) = \Big[\frac{\boldsymbol{\Delta}_\perp^2/4 - \overline{M}^2}{2\overline{M}\,(1-\xi)\,\bar{p}^+}, \frac{(1-\xi)\,\bar{p}^+}{\overline{M}}, -\frac{|\boldsymbol{\Delta}_\perp|}{2\overline{M}}, 0\Big]. \tag{2.133}$$

[36] The minus components of the proton and the Λ_c are not explicitly written because we do not need them in the following. They can be obtained by the on mass-shell conditions, i.e. $p^2 = 0$ and $p'^2 = \overline{M}^2$.

[37] We fix the photon helicity to 1. The photon helicity -1 amplitudes follow from parity relations.

We can now calculate the various spinor products for the four helicity combinations $(\lambda_1' = +, \lambda_1 = +)$, $(\lambda_1' = -, \lambda_1 = -)$, $(\lambda_1' = +, \lambda_1 = -)$ and $(\lambda_1' = -, \lambda_1 = +)$ [38]:

- $\bar{u}\,(p', \lambda_1')\, u\,(p, \lambda_1)$

$$(\lambda_1' = +, \lambda_1 = +): \quad \overline{M}\sqrt{\frac{1+\xi}{1-\xi}} \tag{2.134a}$$

$$(\lambda_1' = -, \lambda_1 = -): \quad \overline{M}\sqrt{\frac{1+\xi}{1-\xi}} \tag{2.134b}$$

$$(\lambda_1' = +, \lambda_1 = -): \quad \frac{|\boldsymbol{\Delta}_\perp|}{\sqrt{1-\xi^2}} \tag{2.134c}$$

$$(\lambda_1' = -, \lambda_1 = +): \quad -\frac{|\boldsymbol{\Delta}_\perp|}{\sqrt{1-\xi^2}} \tag{2.134d}$$

- $\bar{u}\,(p', \lambda_1')\, \not{\epsilon}_\gamma(q, 1) u\,(p, \lambda_1)$

$$(\lambda_1' = +, \lambda_1 = +): \quad -\frac{\sqrt{2}|\boldsymbol{\Delta}_\perp|}{\sqrt{1-\xi^2}} \tag{2.135a}$$

$$(\lambda_1' = -, \lambda_1 = -): \quad 0 \tag{2.135b}$$

$$(\lambda_1' = +, \lambda_1 = -): \quad 0 \tag{2.135c}$$

$$(\lambda_1' = -, \lambda_1 = +): \quad -\sqrt{2}\overline{M}\sqrt{\frac{1+\xi}{1-\xi}} \tag{2.135d}$$

- $\bar{u}\,(p', \lambda_1')\, \not{\epsilon}_M(q', 0) u\,(p, \lambda_1)$

$$(\lambda_1' = +, \lambda_1 = +): \frac{1}{32\overline{M}\bar{p}^{+2}\,(\xi-1)\,\sqrt{1-\xi^2}} \times \left[\boldsymbol{\Delta}_\perp^4 + 64\bar{p}^{+4}\,(1+\xi)\,(\xi-1)^3 - 4\boldsymbol{\Delta}_\perp^2\left(\overline{M}^2 - 4\bar{p}^{+2}\xi\,(\xi-1)\right)\right] \tag{2.136a}$$

$$(\lambda_1' = -, \lambda_1 = -) = (\lambda_1' = +, \lambda_1 = +) \tag{2.136b}$$

$$(\lambda_1' = +, \lambda_1 = -): \frac{|\boldsymbol{\Delta}_\perp|\left(\overline{M}^2 + \bar{p}^+\left(4\bar{p}^+ - \sqrt{2s}\right)\left(1+\xi\right)\right)}{4\bar{p}^{+2}\,(\xi-1)\,\sqrt{1-\xi^2}} \tag{2.136c}$$

$$(\lambda_1' = -, \lambda_1 = +) = -(\lambda_1' = +, \lambda_1 = -) \tag{2.136d}$$

[38] In order to simplify the results we use the following relation

$$\boldsymbol{\Delta}_\perp^2 = 4\sqrt{2\,s}\bar{p}^+\,(1+\xi) - 8\bar{p}^{+2}\,(1+\xi)^2\,.$$

- $\bar{u}\,(p',\lambda_1')\,\not{q}\,u\,(p,\lambda_1)$

$$(\lambda_1'=+,\lambda_1=+):\quad \left(2\sqrt{2s}\,\bar{p}^{+}-s\right)\sqrt{\frac{1+\xi}{1-\xi}} \tag{2.137a}$$

$$(\lambda_1'=-,\lambda_1=-)=-(\lambda_1'=+,\lambda_1=+) \tag{2.137b}$$

$$(\lambda_1'=+,\lambda_1=-):\quad -\frac{|\boldsymbol{\Delta}_\perp|\overline{M}\sqrt{s}}{2\sqrt{2}\,\bar{p}^{+}\sqrt{1-\xi^2}} \tag{2.137c}$$

$$(\lambda_1'=-,\lambda_1=+):\quad (\lambda_1'=+,\lambda_1=-) \tag{2.137d}$$

- $\bar{u}\,(p',\lambda_1')\,\not{\epsilon}_\gamma(q,1)\not{\epsilon}_M(q',0)u\,(p,\lambda_1)$

$$\begin{aligned}(\lambda_1'=+,\lambda_1=+):&-\frac{|\boldsymbol{\Delta}_\perp|}{4\sqrt{s}\,\bar{p}^{+2}\,(\xi-1)\,\sqrt{1-\xi^2}}\Big[16\bar{p}^{+3}\,(1+\xi)\\&+\left(1+\xi\right)\left(2s\bar{p}^{+}-8\sqrt{2s}\,\bar{p}^{+2}\right)+\overline{M}^2\left(2\bar{p}^{+}\,(1+\xi)-\sqrt{2s}\right)\Big]\end{aligned} \tag{2.138a}$$

$$(\lambda_1'=-,\lambda_1=-):-\frac{|\boldsymbol{\Delta}_\perp|}{2\bar{p}^{+}\sqrt{s}\,(\xi-1)}\left[\overline{M}^2+8\bar{p}^{+2}-2\sqrt{2s}\,\bar{p}^{+}\right]\sqrt{\frac{1+\xi}{1-\xi}} \tag{2.138b}$$

$$\begin{aligned}(\lambda_1'=+,\lambda_1=-):&\frac{2\,(1+\xi)}{\overline{M}\sqrt{s}\;(\xi-1)\,\sqrt{1-\xi^2}}\left(\overline{M}^2+8\bar{p}^{+2}-2\sqrt{2s}\,\bar{p}^{+}\right)\\&\times\left(2\bar{p}^{+}\,(1+\xi)-\sqrt{2s}\right)\end{aligned} \tag{2.138c}$$

$$\begin{aligned}(\lambda_1'=-,\lambda_1=+):&-\frac{(1+\xi)\,\left(1-\xi^2\right)^{-1/2}}{\overline{M}\sqrt{s}\,\bar{p}^{+}\,(\xi-1)}\Big[\bar{p}^{+}\left(1+\xi\right)\left(32\bar{p}^{+3}-24\sqrt{2s}\,\bar{p}^{+2}\right)\\&+12s\bar{p}^{+2}\,(1+\xi)-\sqrt{2}\,s^{3/2}\bar{p}^{+}\,(1+\xi)\\&+\overline{M}^2\left(s+4\bar{p}^{+2}\,(1+\xi)-\sqrt{2s}\,\bar{p}^{+}\,(3+\xi)\right)\Big]\end{aligned} \tag{2.138d}$$

- $\bar{u}\,(p',\lambda_1')\,\not{q}\not{\epsilon}_\gamma(q,1)u\,(p,\lambda_1)$

$$(\lambda_1'=+,\lambda_1=+):\quad -\frac{|\boldsymbol{\Delta}_\perp|\overline{M}\sqrt{s}}{2\bar{p}^{+}\sqrt{1-\xi^2}} \tag{2.139a}$$

$$(\lambda_1'=-,\lambda_1=-):\quad 0 \tag{2.139b}$$

$$(\lambda_1'=+,\lambda_1=-):\quad 0 \tag{2.139c}$$

$$(\lambda_1'=-,\lambda_1=+):\quad \left(\sqrt{2}\,s-4\sqrt{s}\,\bar{p}^{+}\right)\sqrt{\frac{1+\xi}{1-\xi}} \tag{2.139d}$$

- $\bar{u}\,(p',\lambda_1')\, \not{q} \not{\epsilon}_M(q',0) u\,(p,\lambda_1)$

$$(\lambda_1'=+,\lambda_1=+): \frac{1+\xi}{2\bar{p}^+\,(\xi-1)\,\sqrt{1-\xi^2}}\Big(\overline{M}^2+8\bar{p}^{+2}-2\sqrt{2s}\,\bar{p}^+\Big) \times\Big(2\bar{p}^+\,(1+\xi)-\sqrt{2s}\Big) \tag{2.140a}$$

$$(\lambda_1'=-,\lambda_1=-)=(\lambda_1'=+,\lambda_1=+) \tag{2.140b}$$

$$(\lambda_1'=+,\lambda_1=-): \frac{|\boldsymbol{\Delta}_\perp|\,(1+\xi)}{4\overline{M}\bar{p}^+\,(\xi-1)\,\sqrt{1-\xi^2}}\Big(4\bar{p}^+-\sqrt{2s}\Big)\Big(\overline{M}^2+8\bar{p}^{+2}-2\sqrt{2s}\,\bar{p}^+\Big) \tag{2.140c}$$

$$(\lambda_1'=-,\lambda_1=+)=-(\lambda_1'=+,\lambda_1=-) \tag{2.140d}$$

- $\bar{u}\,(p',\lambda_1')\, \not{q} \not{\epsilon}_\gamma(q,1) \not{\epsilon}_M(q',0) u\,(p,\lambda_1)$

$$(\lambda_1'=+,\lambda_1=+): \;\; 0 \tag{2.141a}$$

$$(\lambda_1'=-,\lambda_1=-): \;\; -\frac{|\boldsymbol{\Delta}_\perp|\,(1+\xi)}{4\overline{M}\bar{p}^+\,(\xi-1)\,\sqrt{1-\xi^2}}\Big(\sqrt{2}\,\overline{M}^2+8\sqrt{2}\,\bar{p}^{+2}-4\sqrt{s}\,\bar{p}^+\Big) \times\Big(4\bar{p}^+-\sqrt{2s}\Big) \tag{2.141b}$$

$$(\lambda_1'=+,\lambda_1=-): \;\; \frac{1+\xi}{2\bar{p}^+\,(\xi-1)\,\sqrt{1-\xi^2}}\Big(\sqrt{2}\,\overline{M}^2+8\sqrt{2}\,\bar{p}^{+2}-4\sqrt{s}\,\bar{p}^+\Big) \times\Big(2\bar{p}^+\,(1+\xi)-\sqrt{2s}\Big) \tag{2.141c}$$

$$(\lambda_1'=-,\lambda_1=+): \;\; 0 \tag{2.141d}$$

Finally we list the 8 scalar products:

$$p'\cdot\epsilon_\gamma(q,1)=-\frac{|\boldsymbol{\Delta}_\perp|\Big(\overline{M}^2+2\bar{p}^+\Big(\sqrt{2s}-4\bar{p}^+\Big)\Big)}{4\sqrt{s}\,\bar{p}^+\,(\xi-1)} \tag{2.142}$$

$$q'\cdot\epsilon_\gamma(q,1)=\frac{|\boldsymbol{\Delta}_\perp|\Big(\overline{M}^2+2\bar{p}^+\Big(\sqrt{2s}-4\bar{p}^+\Big)\Big)}{4\sqrt{s}\,\bar{p}^+\,(\xi-1)} \tag{2.143}$$

$$q\cdot\epsilon_M(q',0)=\frac{\overline{M}^2\,(1+\xi)^2-\boldsymbol{\Delta}_\perp^2}{2\overline{M}\,(\xi^2-1)} \tag{2.144}$$

$$\epsilon_\gamma(q,1)\cdot\epsilon_M(q',0)=-\frac{|\boldsymbol{\Delta}_\perp|\,\Big(\overline{M}^2+8\bar{p}^{+2}-2\sqrt{2s}\,\bar{p}^+\Big)}{4\overline{M}\sqrt{s}\,\bar{p}^+\,(\xi-1)} \tag{2.145}$$

$$q\cdot p'=-\frac{1}{2}\Big(u-\overline{M}^2\Big) \tag{2.146}$$

$$p' \cdot \epsilon_M(q',0) = \frac{\left(\boldsymbol{\Delta}_\perp^2 + 8\bar{p}^{+2}\left(\xi-1\right)^2\right)^2 - 16\overline{M}^2}{64\overline{M}\bar{p}^{+2}\left(\xi-1\right)^2} \tag{2.147}$$

$$p \cdot \epsilon_M(q',0) = \frac{\left(\boldsymbol{\Delta}_\perp^2 - 2\overline{M}|\boldsymbol{\Delta}_\perp^2| + 8\bar{p}^{+2}\left(\xi^2-1\right)\right)\left(\boldsymbol{\Delta}_\perp^2 + 2\overline{M}|\boldsymbol{\Delta}_\perp^2| + 8\bar{p}^{+2}\left(\xi^2-1\right)\right)}{64\overline{M}\bar{p}^{+2}\left(\xi^2-1\right)} \tag{2.148}$$

$$p \cdot q = \frac{s}{2} \tag{2.149}$$

2.4.3.2 *The four Feynman diagrams*

In this section we examine the structure of the four Feynman diagrams contributing to the hard scattering amplitude. As we mentioned above it turns out that those diagrams can be expressed in terms of the spinor products and scalar products we have listed in the preceding section. Before we do that in detail we start with some preliminaries.

Color factor:
We used the color factor at the level of the hadronic amplitude, see Eq. (2.129).

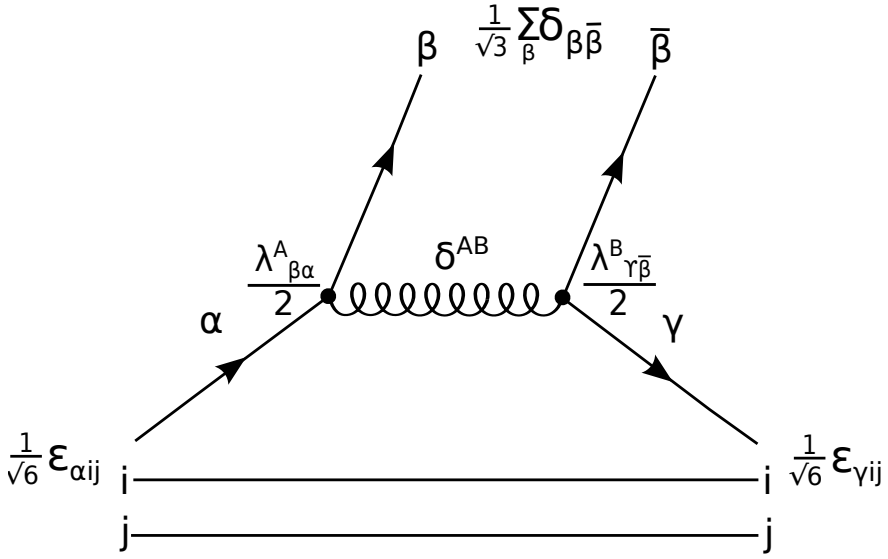

Figure 2.21: Calculation of the color factor.

From Fig. 2.21 it follows for the color factor

$$C = \sum_{A,B,\beta} \frac{1}{3!}\frac{1}{\sqrt{3}}\frac{1}{4}\epsilon_{\alpha ij}\,\epsilon_{\gamma ij}\,\delta^{AB}\,\delta_{\beta\bar{\beta}}\,\lambda^A_{\beta\alpha}\,\lambda^B_{\gamma\bar{\beta}} = \sum_{A,\beta} \frac{1}{3!}\frac{1}{\sqrt{3}}\frac{1}{4}\epsilon_{ij\alpha}\epsilon_{ij\gamma}\lambda^A_{\beta\alpha}\lambda^A_{\gamma\beta}$$

$$= \frac{1}{3!}\frac{1}{\sqrt{3}}\frac{1}{4}2\,\delta_{\alpha\gamma}\sum_{A,\beta}\lambda^A_{\beta\alpha}\,\lambda^A_{\gamma\beta} = 2\frac{1}{3!}\frac{1}{\sqrt{3}}\frac{1}{4}\,16 = \frac{4}{3}\frac{1}{\sqrt{3}} = \frac{C_F}{\sqrt{N_c}}, \tag{2.150}$$

where $C_F = (N_c^2 - 1)/(2N_c)$ is the usual SU(N) color factor.

Couplings:
For the strong coupling we use the one-loop expression [38]

$$\alpha(q^2) = \frac{4\pi}{\left(11 - \frac{2}{3}N_f(q^2)\right)\ln(-q^2/\Lambda^2)}, \tag{2.151}$$

where N_f is the number of quarks with $m^2_{quark} < |q^2|$ and $\Lambda = 234$ MeV. For $N_f = 4$ Eq. (2.151) reads

$$\alpha(q^2) = \frac{12\pi}{25\ln(-q^2/\Lambda^2)}. \tag{2.152}$$

We choose for the argument of Eq. (2.152) $q^2 = x'_{20}s$ which is roughly the average of the gluon and quark virtualities in the hard process.
The electromagnetic coupling strength g_e is given by

$$g_e = \frac{2}{3}\sqrt{4\pi\alpha} \quad \text{for u-quarks,} \tag{2.153}$$

$$g_e = \frac{2}{3}\sqrt{4\pi\alpha} \quad \text{for c-quarks.} \tag{2.154}$$

In the following we investigate individual Feynman diagrams.

Graph 1:

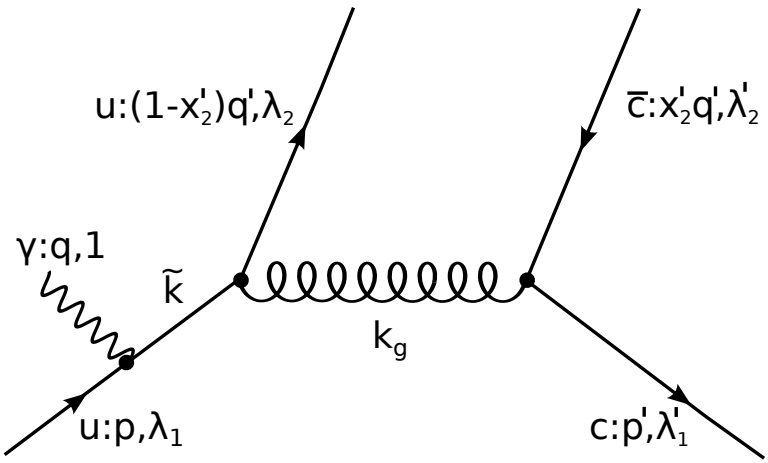

Figure 2.22: Graph 1

With the Feynman rules of App. F we obtain for graph 1 (see Fig. 2.22):

$$H^{(1),1}_{\lambda_1',\lambda_1} = \overline{u}\left(\left(1-x_2'\right)q',\lambda_2\right)\left(-ig_s\gamma^\mu\right)\frac{i\widetilde{\not{k}}}{\widetilde{k}^2}\Big(-ig_e\gamma^\sigma\Big)\epsilon_{\gamma\sigma}(q,1)u\left(p,\lambda_1\right)\left(-i\frac{g_{\mu\nu}}{k_g^2}\right) \times \overline{u}\left(p',\lambda_1'\right)\left(-ig_s\gamma^\nu\right)v\left(x_2'q',\lambda_2'\right). \tag{2.155}$$

Equation (2.155) can be written as

$$H^{(1),1}_{\lambda_1',\lambda_1} = i\,g_s^2\,g_e\frac{1}{k_g^2}\frac{1}{\widetilde{k}^2}\Big[\overline{u}\left(p',\lambda_1'\right)\gamma_\mu v\left(x_2'q',\lambda_2'\right)\overline{u}\left(\left(1-x_2'\right)q',\lambda_2\right)\gamma^\mu\left(\not{p}-\not{q}\right)\not{\epsilon}_\gamma(q,1)u\left(p,\lambda_1\right)\Big]. \tag{2.156}$$

The gluon momentum squared k_g^2 is given by

$$k_g^2 = \Big(p'+x_2'q'\Big)^2 = \overline{M}^2\Big(1+x_2'\Big)^2 + x_2'\Big(s-2\overline{M}^2\Big) \tag{2.157}$$

and the quark momentum squared $\widetilde{k}$ by

$$\widetilde{k}^2 = \Big(p+q\Big)^2 = s, \tag{2.158}$$

respectively. Before we continue to simplify the Dirac structure of Eq. (2.156), some remarks about the gluon and quark propagators are in order. In principle there are two different possibilities for the propagators. Using graph 1 as an example they are:

- *Momenta of external particles*:

  gluon propagator: $\Big(x_2'q'+p'\Big)^2$,

  quark propagator: $\Big(q+p\Big)^2$.

- *Using momenta of internal and external particles* :

  gluon propagator: $\Big(\widetilde{k}-\left(1-x_2'\right)q'\Big)^2$,

  quark propagator: $\Big(k_g+\left(1-x_2'\right)q'\Big)^2$.

As one can easily check, they all give the same results. Using the naive collinear approximation, i.e. $k_1 = x_1 p = \frac{\bar{x}_{10}+\xi}{1+\xi}p$ and $k_1' = x_1'p' = \frac{\bar{x}_{10}-\xi}{1-\xi}p'$ would violate momentum conservation. Only in the heavy quark limit, i.e. $\bar{x}_{10}\to 1$, momentum conservation is recovered and we can use any of the two possibilities for the propagators.

Using the Dirac equation and $p\cdot\epsilon_\gamma = 0$, Eq. (2.156) can be written as

$$H^{(1),1}_{\lambda_1',\lambda_1} = i\,g_s^2\,g_e\frac{1}{k_g^2}\frac{1}{\widetilde{k}^2}\Big[\overline{u}\left(p',\lambda_1'\right)\gamma_\mu\frac{1}{\sqrt{2}}\Big(\not{q}'-\overline{M}\Big)\not{\epsilon}_M(q',0)\gamma^\mu\not{q}\not{\epsilon}_\gamma(q,1)u\left(p,\lambda_1\right)\Big], \tag{2.159}$$

where we have replaced the spinors in the meson by its covariant spin wave function, cf. Eq. (2.127). With the relations for the Dirac matrices of App. E we get

$$H^{(1),1}_{\lambda_1',\lambda_1} = i\, g_s^2\, g_e \frac{1}{k_g^2}\frac{1}{\widetilde{k}^2}\Big[2\sqrt{2}\,\overline{M}\cdot ScP3\cdot SP2 - 2\sqrt{2}\,ScP4\cdot SP4 + \sqrt{2}\,\overline{M}\cdot SP8\Big]. \tag{2.160}$$

Graph 2:
The analytical expression for Fig. 2.23 is

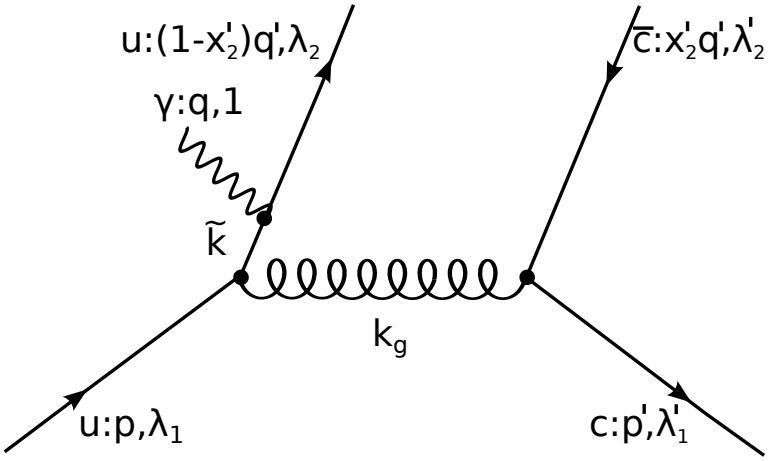

Figure 2.23: Graph 2

$$H^{(2),1}_{\lambda_1',\lambda_1} = i\, g_s^2\, g_e \frac{1}{k_g^2}\frac{1}{\widetilde{k}^2}\Big[\overline{u}\,(p',\lambda_1')\,\gamma_\mu v\,(x_2'q',\lambda_2')\,\overline{u}\,((1-x_2')\,q',\lambda_2)\,\not\epsilon_\gamma(q,1)((1-z)\not q' - \not q)\gamma^\mu u\,(p,\lambda_1)\Big]. \tag{2.161}$$

Together with the Dirac equation and the covariant spin wave function of the $\overline{D}^*$, Eq. (2.161) simplifies to

$$\begin{aligned} H^{(2),1}_{\lambda_1',\lambda_1} = i\, g_s^2\, g_e \frac{1}{k_g^2}\frac{1}{\widetilde{k}^2}\Big[&2(1-x_2')q'\cdot\epsilon_\gamma(q,1)\,\overline{u}\,(p',\lambda_1')\,\gamma_\mu\frac{1}{\sqrt{2}}\,(\not q' - \overline{M})\,\not\epsilon_M(q',0)\gamma^\mu u\,(p,\lambda_1) \\ &- \overline{u}\,(p',\lambda_1')\,\gamma_\mu\frac{1}{\sqrt{2}}\,(\not q' - \overline{M})\,\not\epsilon_M(q',0)\not\epsilon_\gamma(q,1)\not q\gamma^\mu u\,(p,\lambda_1)\Big]. \end{aligned} \tag{2.162}$$

Using standard relations for the Dirac matrices we obtain as the final result for graph 2

$$
\begin{aligned}
H^{(2),1}_{\lambda_1',\lambda_1} &= i\, g_s^2\, g_e \frac{1}{k_g^2}\frac{1}{\widetilde{k}^2} \\
&\Big[4\sqrt{2}\Big(ScP4\cdot ScP5 - ScP1\cdot ScP3\Big)\cdot SP1 \\
&+ 2\sqrt{2}\,\overline{M}\cdot ScP3\cdot SP2 + 2\sqrt{2}\,\left(1-x_2'\right)\overline{M}\cdot ScP2\cdot SP3 \\
&- 2\sqrt{2}\,\overline{M}\cdot ScP4\cdot SP4 - 2\sqrt{2}\,\Big(ScP5+ScP8\Big)\cdot SP5 \\
&- 2\sqrt{2}\,\Big(ScP6+ScP7\Big)\cdot SP6 + 2\sqrt{2}\cdot ScP1\cdot SP7 \\
&+ \sqrt{2}\,\overline{M}\cdot SP8\Big],
\end{aligned}
\tag{2.163}
$$

where the gluon momentum squared is given by Eq. (2.157) and the quark momentum squared is

$$
\widetilde{k}^2 = \Big((1-x_2'q') - q\Big)^2 = \Big(1-x_2'\Big)^2\overline{M}^2 + \Big(1-x_2'\Big)\Big(t-\overline{M}^2\Big). \tag{2.164}
$$

Graph 3:

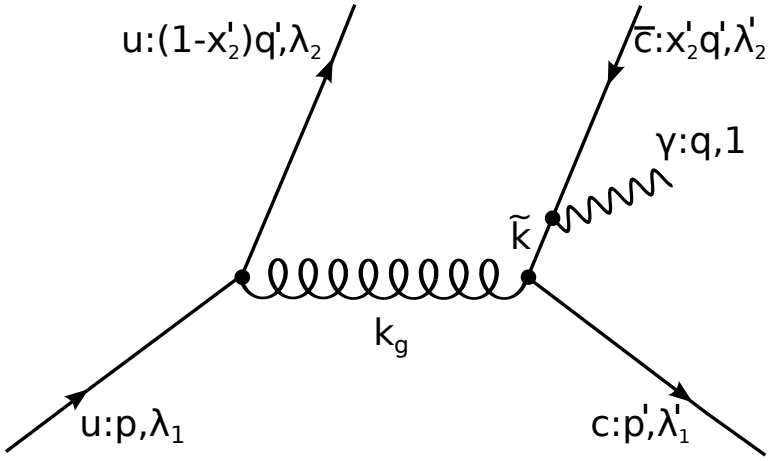

Figure 2.24: Graph 3

The analytical expression for Fig. 2.24 is

$$
\begin{aligned}
H^{(3),1}_{\lambda_1',\lambda_1} &= i\, g_s^2\, g_e \frac{1}{k_g^2}\frac{1}{\widetilde{k}^2 - x_2'\overline{M}^2}\Big[\overline{u}\left(p',\lambda_1'\right)\gamma_\mu(-x_2'\,\not{q}' + \not{q} + x_2'\,\overline{M})\not{\epsilon}_\gamma(q,1) \\
&\times v\left(x_2'q',\lambda_2'\right)\overline{u}\left(\left(1-x_2'\right)q',\lambda_2\right)\gamma^\mu u\left(p,\lambda_1\right)\Big].
\end{aligned}
\tag{2.165}
$$

Equation (2.165) can be written as

$$H^{(3),1}_{\lambda_1',\lambda_1} = i\,g_s^2\,g_e\frac{1}{k_g^2}\frac{1}{\widetilde{k}^2 - x_2'\overline{M}^2}\Big[\overline{u}\left(p',\lambda_1'\right)\gamma_\mu \not{q}\not{\epsilon}_\gamma(q,1)\frac{1}{\sqrt{2}}\left(\not{q}' - \overline{M}\right)\not{\epsilon}_M(q',0)\gamma^\mu u\left(p,\lambda_1\right) - 2x_2'(q'\cdot\epsilon_\gamma(q,1))\overline{u}\left(p',\lambda_1'\right)\gamma_\mu\frac{1}{\sqrt{2}}\left(\not{q}' - \overline{M}\right)\not{\epsilon}_M(q',0)\gamma^\mu u(p,\lambda_1).\tag{2.166}$$

The final result for graph 3 is

$$\begin{aligned} H^{(3),1}_{\lambda_1',\lambda_1} = i\,g_s^2\,g_e\frac{1}{k_g^2}\frac{1}{\widetilde{k}^2 - x_2'^2\overline{M}^2}\Big[&4\sqrt{2}\Big(ScP4\cdot ScP5 - ScP1\cdot ScP3\Big)\cdot SP1 \\ &+ 2\sqrt{2}\cdot ScP3\Big(\overline{M}-1\Big)\cdot SP2 - 2\sqrt{2}\,\overline{M}\,x_2'\cdot ScP2\cdot SP7 \\ &+ 2\sqrt{2}\cdot ScP4\Big(1-\overline{M}\Big)\cdot SP4 - 2\sqrt{2}\cdot ScP5\cdot SP5 \\ &- 2\sqrt{2}\Big(ScP6+ScP7\Big)\cdot SP6 + 2\sqrt{2}\cdot ScP1\cdot SP7 + \sqrt{2}\Big(2\overline{M}-1\Big)\cdot SP8\Big], \end{aligned}\tag{2.167}$$

where the gluon momentum squared k_g^2 is given by

$$k_g^2 = \Big(p - (1-x_2')q'\Big)^2 = \Big(1-x_2'\Big)^2\overline{M}^2 + \Big(1-x_2'\Big)\Big(u - \overline{M}^2\Big)\tag{2.168}$$

and the quark momentum squared $\widetilde{k}^2$ by

$$\widetilde{k}^2 = \Big(x_2'q' - q\Big)^2 = x_2'^2\overline{M}^2 + x_2'\Big(t - \overline{M}^2\Big),\tag{2.169}$$

respectively.

Graph 4:

Finally the analytical expression for graph 4 (Fig. 2.25) is

$$\begin{aligned} H^{(4),1}_{\lambda_1',\lambda_1} = i\,g_s^2\,g_e\frac{1}{k_g^2}\frac{1}{\widetilde{k}^2 - \overline{M}^2}\Big[&\overline{u}\left(p',\lambda_1'\right)\not{\epsilon}_\gamma(q,1)(\not{p}' - \not{q} + \overline{M})\gamma_\mu \\ &\times v\left(x_2'q',\lambda_2'\right)\overline{u}\left(\left(1-x_2'\right)q',\lambda_2\right)\gamma^\mu u\left(p,\lambda_1\right)\Big]. \end{aligned}\tag{2.170}$$

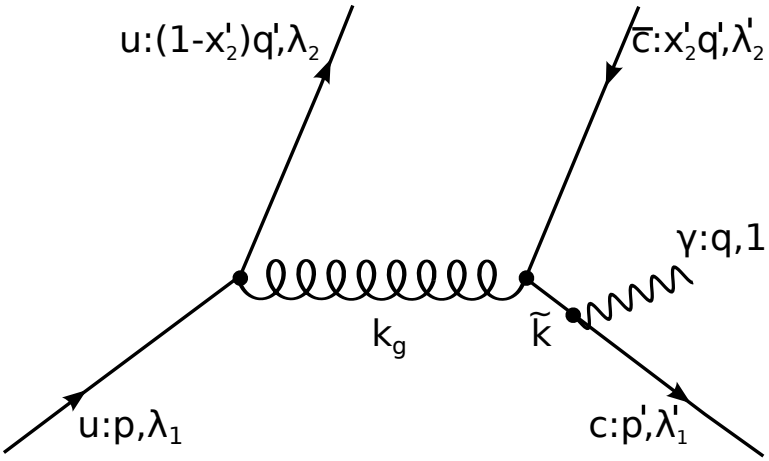

Figure 2.25: Graph 4

We can write Eq. (2.170) as

$$H^{(4),1}_{\lambda_1',\lambda_1} = i\,g_s^2\,g_e \frac{1}{k_g^2}\frac{1}{\widetilde{k}^2-\overline{M}^2}\Big[2(p'\cdot\epsilon_\gamma(q,1))\overline{u}(p',\lambda_1')\gamma_\mu\frac{1}{\sqrt{2}}\left(\not{q}'-\overline{M}\right)\not{\epsilon}_M(q',0)u\left(p,\lambda_1\right) - \overline{u}\left(p',\lambda_1'\right)\not{\epsilon}_\gamma(q,1)\not{q}\gamma_\mu\frac{1}{\sqrt{2}}\left(\not{q}'-\overline{M}\right)\not{\epsilon}_M(q',0)\gamma^\mu u\left(p,\lambda_1\right).$$

(2.171)

The final result for graph 4 reads

$$H^{(4),1}_{\lambda_1',\lambda_1} = i\,g_s^2\,g_e \frac{1}{k_g^2}\frac{1}{\widetilde{k}^2-\overline{M}^2}\Big[2\sqrt{2}\overline{M}\cdot ScP1\cdot SP3+\sqrt{2}\,\overline{M}\cdot SP8\Big], \qquad (2.172)$$

where the gluon momentum squared k_g^2 is given by Eq. (2.168) and the quark momentum squared $\widetilde{k}^2$ by

$$\widetilde{k}^2 = \left(p'-q\right)^2 = \overline{M}^2 + \left(u-\overline{M}^2\right). \qquad (2.173)$$

The full hard scattering amplitude is the sum

$$H^1_{\lambda_1',\lambda_1} = H^{(1),1}_{\lambda_1',\lambda_1} + H^{(2),1}_{\lambda_1',\lambda_1} + H^{(3),1}_{\lambda_1',\lambda_1} + H^{(4),1}_{\lambda_1',\lambda_1}. \qquad (2.174)$$

2.4.4 *Results*

Here we have to keep in mind that only longitudinally polarized $\overline{D}^+$ mesons are considered in the final state. The differential cross section for $\gamma\ p \to \Lambda_c^+\ \overline{D}^*_{\lambda=0}$ reads

[39]

$$\frac{d\sigma}{d\Omega} = \frac{1}{64\pi^2 s}\frac{|\mathbf{p}'|}{|\mathbf{p}|}\sigma_0 = \frac{1}{64\pi^2 s}\frac{\Lambda'}{\Lambda}\sigma_0 = \frac{1}{4\pi}s\Lambda\Lambda'\frac{d\sigma}{dt}, \tag{2.175}$$

with σ_0 defined as

$$\sigma_0 := \frac{1}{2}\sum_{\mu,\mu'}|\mathscr{M}_{\mu',\mu 1}|^2 \tag{2.176}$$

and Λ and Λ' are given by Eqs. (B.12) and (B.13). The differential cross sections for Mandelstam $s = 19,\ 21,\ 25$ and $30\ \text{GeV}^2$ are depicted in Fig. 2.26. In each of the figures we show the cross sections evaluated either with the KK mass exponential for both the Λ_c^+- and $\overline{D}^*$-LCWF or with the BB mass exponential for both. Before we discuss the cross sections we turn to the error assessment issue with respect to the model parameters: We vary a_Λ by $\pm 10\%$ around its central value of $0.75\ \text{GeV}^{-1}$. The valence Fock state probability of the Λ_c^+ is varied in the range 0.7 to 1. The errors of the parameters of the proton LCWF are not taken into account, since they lead to much smaller uncertainties compared to those of the Λ_c^+-LCWF. In fact, the proton LCWF that we use has been studied in detail in several processes. The uncertainties of f_{D^*} are taken from Ref. [36] and are $f_{D*} = 0.252 \pm 22.64$ MeV. The valence Fock state probability of the $\overline{D}^*$-meson, $P_{D^*} = 0.9$, is varied between 0.8 and 1, thus yielding different values for $a_{D^*} =$ and $N_{D^*} =$ as well. The gray bands in the plots show the variation of the cross section due to these uncertainties in the parameters.

The integrated cross section is displayed in Fig. 2.27. The larger cross section is obtained with the BB mass exponential, as already anticipated by the corresponding behavior of the differential cross sections. The difference of the cross sections when evaluated for the different mass exponentials is larger than the parametric errors. The absolute size of the integrated cross section is of the order of $10^{-1} - 1$ nb. Unfortunately there are no other model calculations to compare with. In Ref. [40] they calculate the (differential) cross section for $\gamma\ p \to \overline{D}^*\ \Lambda_c^+$, however, the sum over the helicities of the $\overline{D}^*$. According to the discussions of Sec. 2.5 we expect, using a hadronic model where SU(4) flavor symmetry is not broken at the wave function level, an integrated cross section in the range of $10 - 100$ nb. If SU(4) flavor symmetry is broken at the level of the hadronic wave functions we conjecture that the cross section is of comparable order to our estimate.

To make predictions for spin correlations we have to bear in mind that CMS observables are typically expressed in terms of CMS helicity amplitudes. Therefore we have to transform our LC helicity amplitudes $\mathscr{M}_{\mu' 0,\mu\nu}$ to CMS helicity amplitudes which we will denote by $\phi_{\mu' 0,\mu\nu}$. The relation between the two amplitudes is[39]

$$\phi_{\mu' 0,\mu\nu} = \frac{1}{\sqrt{1+\beta^2}} = \Big(\mathscr{M}_{\mu' 0,\mu\nu} + 2\mu'\beta\mathscr{M}_{-\mu' 0,\mu\nu}\Big), \tag{2.177}$$

[39] Although we use the same symbols for LC-helicities and "usual" helicities there should be no confusion which kind of helicity is meant, since it is clear that the subscripts of $\mathscr{M}$ refer to LC-helicities and subscripts of ϕ refer to "usual" helicities.

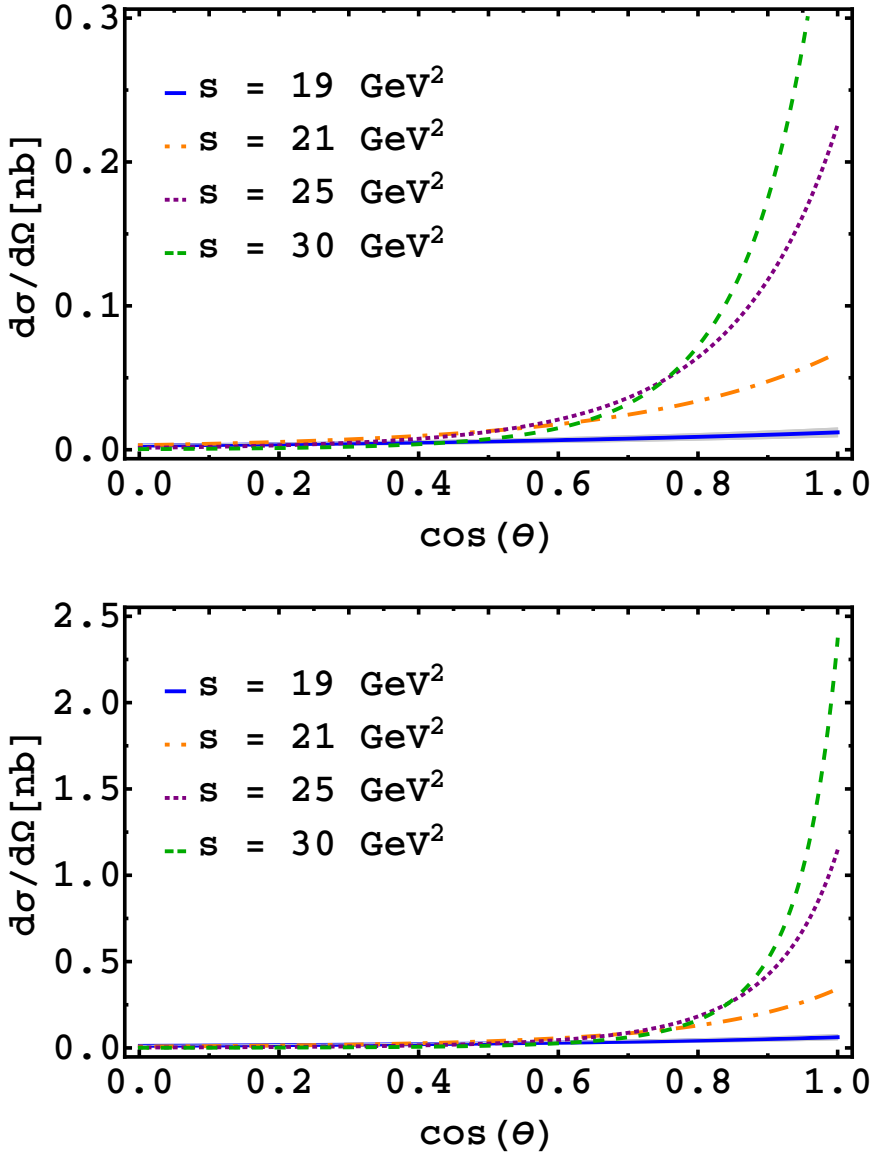

Figure 2.26: The differential $\gamma p \to \overline{D}^*_{\lambda=0}\Lambda_c^+$ cross section versus $\cos\theta$ for $s = 19, 21, 25, 30$ GeV^2 (solid, dash-dotted, dotted and dashed line). This plot has been obtained with the wave function parameterizations described in the text using the KK mass exponential (upper panel) and using the BB mass exponential (lower panel). The effects of uncertainties in the Λ_c and the D^* wave function parameters are indicated by the shaded band around the $s = 19$ GeV^2 curve (hardly visible).

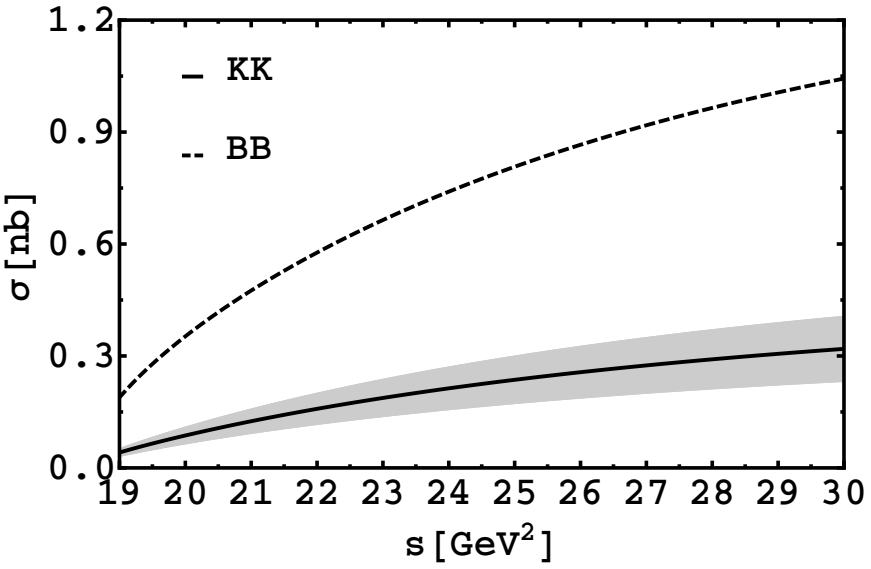

Figure 2.27: Our prediction for the integrated cross section σ versus Mandelstam s (solid line with error band). The solid line corresponds to the KK mass exponential and the dashed line corresponds to the BB mass exponential.

with $\beta := \frac{M_\Lambda}{p'^0 + |\mathbf{p}'|} \tan\frac{\theta}{2}$. In total there are 12 independent helicity amplitudes for the photoproduction of vector mesons [41]. As an example for spin observables for which our model provides nontrivial predictions, we will consider the beam asymmetry Σ_x (cf. [42])

$$\Sigma_x = \frac{\mathrm{d}\sigma}{\mathrm{d}t} = \frac{\mathrm{d}\sigma_\perp}{\mathrm{d}t} = \frac{\mathrm{d}\sigma_\parallel}{\mathrm{d}t} - \frac{1}{16\pi(s-m_p^2)^2}\mathscr{R}\Big(\phi^*_{-0,-1}\phi_{+0,+1} - \phi^*_{-0,+1}\phi_{+0,-1}\Big). \quad (2.178)$$

The result for the beam asymmetry is shown in Fig. 2.28. It hardly depends on the wave function model and thus its angular dependence is characteristic for the handbag mechanism.

2.4.5 *Summary*

The same conclusions as in Ref. [9] apply here, we repeat them in a slightly modified manner. In Sec. 2.4 we have investigated the exclusive process $\gamma\, p \to \overline{D}^*_{\lambda=0}\, \Lambda_c^+$ using a handbag mechanism. Thereby we have extended the range of applications of $p \to \Lambda_c^+$ transition GPDs, which have been introduced and used to describe $p\,\overline{p} \to \Lambda_c^+ \bar{\Lambda}_c^-$ in Ref. [11] and $\pi^- p \to D^- \Lambda_c^+$ in Ref. [7], by another exclusive reaction. We have argued that, under plausible physical restrictions on parton virtualities and intrinsic transverse momenta, one can "factorize" this process into a hard partonic subprocess and soft hadronic matrix elements. The partonic subprocess is the photoproduction of a $c\bar{c}$ pair off a u quark, i.e. $\gamma u \to u c\bar{c}$, and has been treated in leading order perturbative QCD. A numerical calculation reveals that all the propagators are highly virtual, so a perturbative treatment is justified. The soft hadronic matrix elements

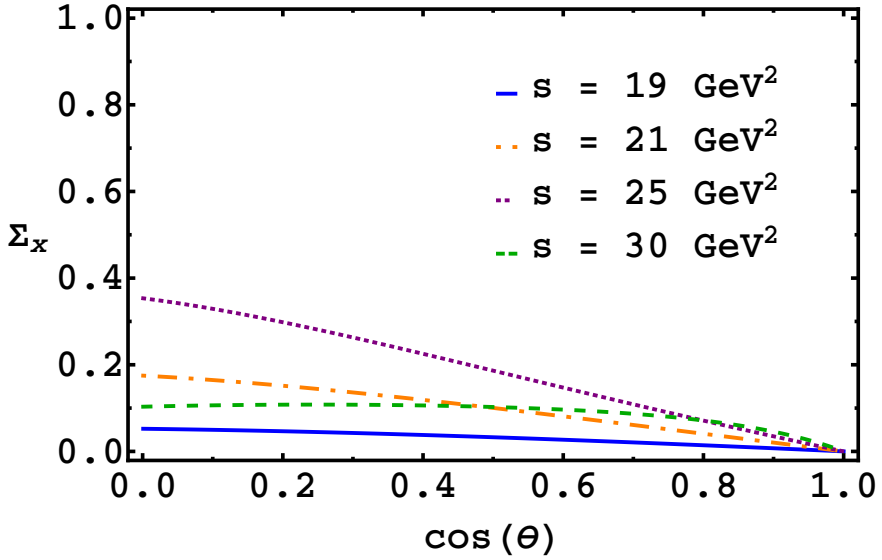

Figure 2.28: Beam asymmetry Σ_x for different values of Mandelstam s vs. $\cos\theta$.

are the non-perturbative ingredient of our photoproduction mechanism. One of them describes the $p \to \Lambda_c^+$ transition via emission of a u quark by the proton and reabsorption of a c quark by the remnant of the proton, the other one the formation of the outgoing u and $\bar{c}$ quarks to the $\overline{D^*}$ meson. The first one is parameterized in terms of eight GPDs, the second one in terms of a D^*-meson distribution amplitude. Our approach does not provide a rigorous proof of factorization. It is, at most, a first step in this direction.

In order to make numerical predictions we have adopted the overlap representation of Ref. [11] for the $p \to \Lambda_c^+$ transition GPDs and we have calculated the D-meson distribution amplitude from a simple Gaussian model for the light-cone wave function of the D^*-meson valence Fock state. The overlap representation makes sense for energies well above the reaction threshold and scattering into the forward hemisphere, where the momentum fractions of the active quarks have to be larger than the skewness (i.e. the DGLAP region) in order to produce the $c\bar{c}$-pair. The starting point of the overlap representation are also simple Gaussian-type light-cone wave functions for the valence Fock states of the proton and the Λ_c. The two parameters in each wave function were fixed by physical constraints which were taken to be the probabilities of the valence Fock states, the mean intrinsic transverse momenta and the D^*-meson decay constant. All the wave function models are pure s-wave. This reduces the number of non-vanishing $p \to \Lambda_c$ transition GPDs to three. These three non-vanishing GPDs are nearly identical if the contribution of helicity states with the c-quark helicity being opposite to the Λ_c helicity is assumed to be small (in agreement with experimental evidences). Plots for the GPDs show that they are strongly peaked at $x_0 = m_c/M_\Lambda$. This suggested to calculate the hadronic scattering amplitude by means of a peaking approximation. Thereby the variation of the hard-scattering amplitude is neglected in the relevant integration region (around x_0) when

it is convoluted with the GPDs and one can take it out of the integral. In this way the hadronic amplitude becomes a sum of products of generalized form factors, i.e. particular moments of the GPDs, with the hard scattering amplitude that has still to be convoluted with the D^*-meson DA.

With this model for the GPDs and the D^*-meson DA we have calculated (unpolarized) differential and integrated cross sections as well as the beam asymmetry. Our prediction for the integrated photoproduction cross section is of the order of $10^{-1} - 1$ nb. The spin correlation parameter is rather insensitive to details of the wave function model. This means it is mostly determined by the hard partonic subprocess and may thus give us some clues on how charm is produced on the partonic level.

2.5 Cross section in charmed hadron production: Discrepancies between different approaches

Exclusive production of charmed hadrons has been addressed with different models. As we have illustrated in Sec. 2.1 using the example of $\bar{p}\ p \to \bar{\Lambda}_c^-\ \Lambda_c^+$, there are differences up to three orders of magnitude in the estimates for the cross section [40]. In this section we try to understand how these differences come about with special emphasis on the differences compared to our model. However, we note right away, that the approaches are of completely different nature, so it is practically impossible to understand in detail where the drastic differences come from. But nonetheless we try to pin down what we think could be the main reasons for these differences.

To do so for single hadron exchange models we make reference to the case of strange particle production and discuss what kind of changes appear when we go to charm particle production. In Sec. 2.5.1 we discuss the differences of our model to single hadron exchange models. We will find that those are closely connected to the question how $SU(4)_f$-symmetry is broken. In the subsequent Sec. 2.5.2 we investigate the differences to reggeized hadron exchange models using the specific process of Sec. 2.3, i.e. $\pi^-\ p \to D^-\ \Lambda_c^+$. Here we will find that the differences are correlated with charm/strange suppression and how flavor symmetry is broken in the Regge residues and in the scale parameter. In the final chapter of this section we make some remarks on the intrinsic charm quark content of the proton.

2.5.1 *Single hadron-exchange models*

Exclusive charm production near threshold has been estimated within single hadron exchange models in Refs. [10, 43, 44], for example. As compared to the handbag mechanism, Refs. [11, 15], the predicted cross sections are about a factor of $100 - 1000$ larger.

To understand these differences we first look at the generic form of the transition potentials in these hadron exchange models. The transition potential for $\bar{p}\ p \to \bar{\Lambda}_c^-\ \Lambda_c^+$ is given by t-channel D and D^* exchanges, those for $\bar{p}\ p \to \bar{D}^0\ D^0$ is given by

[40] A similar conclusion can be made for other processes like $\bar{p}\ p \to \bar{D}^0\ D^0$, see Refs. [15, 43].

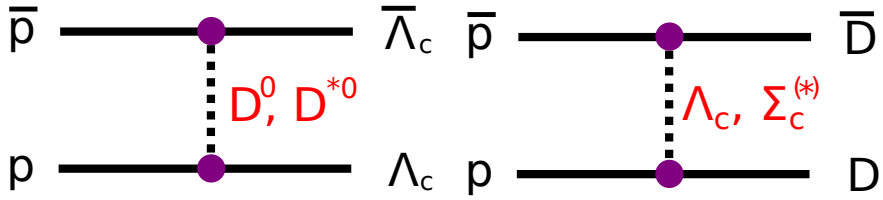

Figure 2.29: The transition potential for $\bar{p}\ p \to \bar{\Lambda}_c\ \Lambda_c$ (left figure) and for $\bar{p}\ p \to \bar{D}\ D$ (right figure), respectively.

t-channel Λ_c and $\Sigma_c^{(*)}$ exchanges, respectively. The transition potentials have the following generic form, see also Fig. 2.29,

$$V^{\bar{p}\ p\to\bar{\Lambda}_c\ \Lambda_c}(t) \sim \sum_{M=D,D^*} g^2_{p\,\Lambda_c\,M} \frac{F^2_{p\,\Lambda_c\,M}(t)}{t - m_M^2} \tag{2.179}$$

and

$$V^{\bar{p}\ p\to\bar{D}^0\ D^0}(t) \sim \sum_{B=\Lambda_c,\Sigma_c^{(*)}} g^2_{p\,D\,B} \frac{F^2_{p\,D\,B}(t)}{t - m_B^2}, \tag{2.180}$$

where $g_{p\,\Lambda_c\,M}$ and $g_{p\,D\,B}$ are the coupling constants at the respective hadronic vertex and $F_{p\,\Lambda_c\,M}$ and $F_{p\,D\,B}$ are the vertex form factors. Now, under the assumption of $SU(4)_f$-symmetry the coupling constants are the same as in the corresponding exchanges in $\bar{p}\ p \to \bar{\Lambda}\ \Lambda$ and $\bar{p}\ p \to \bar{K}\ K$, respectively [41]. With $SU(4)_f$-symmetry we can give a qualitative estimate for the size of the cross section coming from single hadronic exchange. Let us discuss this for $\bar{p}\ p \to \bar{\Lambda}_c\ \Lambda_c$. When one starts with $\bar{p}\ p \to \bar{\Lambda}\ \Lambda$ and goes to $\bar{p}\ p \to \bar{\Lambda}_c\ \Lambda_c$ the main change is due to the different meson propagator in the transition potential, i.e. the masses of $(K,\ K^*)$ are replaced by those of $(D,\ D^*)$, cf. Eqs. (2.179)-(2.180). The couplings stay the same because of the assumed $SU(4)_f$-symmetry. If one then considers the ratio of the transition potentials, one roughly gets

$$\frac{V^{\bar{p}\ p\to\bar{\Lambda}_c\ \Lambda_c}}{V^{\bar{p}\ p\to\bar{\Lambda}\ \Lambda}} = \frac{m^2_{M_s}}{m^2_{M_c}} \approx \frac{1}{4}. \tag{2.181}$$

So we expect that the cross section is smaller by a factor of around 16, i.e. one order of magnitude. It turns out that this is roughly what one finds in the full calculation [10, 44]. This explains why the cross section for $\bar{p}\ p \to \bar{\Lambda}_c\ \Lambda_c$ in a single hadron exchange model is smaller by about one order of magnitude as compared to $\bar{p}\ p \to \bar{\Lambda}\ \Lambda$. We want to remark that the variation of the cutoff parameter in the form factors of Eqs. (2.179)-(2.180) provides to some extent $SU(4)_f$-symmetry breaking, because it alters the t-dependence of the transition potential. In this way some $SU(4)_f$-symmetry breaking in the coupling is also mimicked [42].

[41] The cutoff parameter in the vertex factor cannot be taken over. The reason is that the masses of the exchanged particles in the charmed particle production are much larger than in strange particle production. The sensitivity of the cross section on the cutoff parameters is discussed in Refs.[10, 43].

[42] Indeed results from QCD sum rules show that the ratio of $g_{p\Lambda_c D}$ to $g_{p\Lambda K}$ is $1.47^{+0.58}_{-0.44}$, i.e. $SU(4)_f$-

Within our *factorization approach* we separate the process into a hard part (pQCD) and into a soft part (GPDs). To model the GPDs we employ an overlap representation in terms of LCWFs as was demonstrated in more detail in Sec. 2.2. We stress that in our model $SU(4)$-flavor-symmetry breaking (in addition to the one from the hadron and quark masses) occurs due to the flavor dependence of the hadron wave functions which diminishes the $p \to \Lambda_c$ overlap considerably as compared to the $p \to \Lambda$ and $\pi \to K$ ones [45], namely by three orders of magnitude.

Let us summarize

- Using hadronic models in the description of charmed particle production where $SU(4)_f$-symmetry is assumed for the coupling constants, we expect that the cross section is one order of magnitude smaller as compared to corresponding strange particle production.
- Using a factorization approach in the description of charmed particles production, where the non-perturbative part is described in terms of LCWFs which break $SU(4)_f$-symmetry, we expect that the cross section has to be three orders of magnitude smaller than in strange particle production.

We therefore expect that the cross section in models which break $SU(4)_f$-symmetry at the wave function level are closer to our cross section estimates.

2.5.2 *Reggeized hadron exchange models*

Exclusive production of charmed hadrons has also been addressed within Regge models. For $\pi^- p \to D^- \Lambda_c^+$ one has to consider the D^* trajectory. Its exchange leads to a characteristic factor

$$\sim \left(\frac{s}{s_0}\right)^{\alpha_{D^*}(t_0)} \tag{2.182}$$

for the forward scattering amplitude. With a typical trajectory $\alpha_{D^*}(t) \simeq -1 + t/2\,\mathrm{GeV}^{-2}$ [46, 47] and the still sizeable value of $|t_0|$ for s in the range $20 - 30$ GeV^2 one notices a strong suppression of the $D\Lambda_c$ channel as compared to the strangeness channel $K\Lambda$, where the K^* trajectory is exchanged. In the strangeness channel $|t_0|$ is very small for $s \simeq 20$ GeV^2. Thus, at $t = t_0 \simeq 0$ the K^* trajectory takes a value of about 0.4. In addition to the strong charm/strange suppression through the different trajectories and values of t_0 there is the issue of flavor symmetry breaking in the Regge residues and in the scale parameter, s_0. For the scale parameter it is usually relied on the quark-gluon string model of binary reactions [46]. In detail the differences in the Regge parameters and in the residues lead to substantial differences in the results for the charm/strange suppressions. Thus, in the recent work [48] a suppression factor of about 10^{-3} has been obtained and hence a cross section of the order of *nb* in agreement with our finding. In sharp contrast to [48] Khodjamirian *et al* [12] found a much milder charm/strange suppression. Thus, for instance, for the $\bar{p}p \to \bar{\Lambda}_c^- \Lambda_c^+$

symmetry is broken [12].

cross section they obtained a value which is about two orders of magnitude larger than the estimate in our partonic picture [11]. Results for $\pi^- p \to D^- \Lambda_c^+$, are not quoted in [12].
Using reggeized hadronic models one main issue can be identified which is responsible for the suppression of charmed particle production compared to strange particle production

- Depending on the differences in the Regge parameters one gets different results for charm/strange suppressions.

Before we turn briefly to the subject of the intrinsic charm content of the proton, let us summarize our findings of Sec. 2.5.1-2.5.2

- If one uses single hadron exchange models with $SU(4)_f$-symmetry to describe the production of charmed particles one gets a cross section which is roughly one order of magnitude smaller compared to the corresponding strange particle channel.

- If one uses reggeized hadron exchange models this difference strongly depends on the charm/strange suppression and can lead to cross sections which are one to three orders of magnitude smaller depending on the assumptions on $SU(4)_f$-symmetry breaking in the Regge residues an the scale parameter.

- If one uses an approach where the non-perturbative dynamics is modeled in terms of flavor dependent wave functions, due to $SU(4)_f$ symmetry breaking effects the cross section is about three orders of magnitude smaller than the one for the corresponding strange particle production process.

2.5.3 *Final remarks: intrinsic charm content of the proton*

To conclude the section of charmed hadron production, we discuss very briefly the topic of *intrinsic* charm in the nucleon. There are two distinct processes to produce charm in the nucleon

- *Extrinsic charm*: Through gluon radiation charm-anticharm pairs are produced. This perturbative process is a feature of QCD evolution. The charm is concentrated at very low momentum fractions x and with increasing Q^2 one expects to see more and more charm. Furthermore the charm and anticharm distributions are symmetric, i.e. $c(x) = \bar{c}(x)$.

- *Intrinsic charm*: Here the charm arises through non-perturbative fluctuations to a $|qqqc\bar{c}\rangle$ state. Compared to extrinsic charm, intrinsic charm tends to be valence-like, i.e.the extrinsic charm distribution is peaked at rather low values of the momentum fraction x. It is not necessary that charm and anticharm are equal.

Intrinsic charm was first introduced by Brodsky, Hoyer, Peterson, and Sakai [49]. They noticed that in order to describe the magnitude of the cross section of the first

direct measurements of charm production, one should add an intrinsic charm component. Since then there have been several theoretical studies on the intrinsic charm content of the nucleon but the magnitude of its charm content is still inconclusive: It ranges from 0.3 % to 2 % (see Ref. [50] for more details).

An example of a non-perturbative model to produce intrinsic charm in the nucleon is a meson-cloud model. The basic features of this model will be discussed in more detail in Sec. 3.2. In this model, say a proton, can fluctuate into a baryon plus a meson state. An example for a fluctuation to produce a charm-anticharm pair would be $p \to \Lambda_c^+ \overline{D}^0$. Here the charm is in the Λ_c^+ ($|udc\rangle$) and the anticharm is in the $\overline{D}^0(|u\bar{c}\rangle)$. The resulting charm probability distribution $c(x)$ can be written in the form of a convolution [50]

$$c(x) = \sum_{B,M} \Big[\int_x^1 \frac{\mathrm{d}y}{y} f^{p/BM}(y)\; c_B\left(\frac{x}{y}\right) + \int_x^1 \frac{\mathrm{d}y}{y} f^{p/MB}(y)\; c_M\left(\frac{x}{y}\right) \Big]. \tag{2.183}$$

In Eq. (2.183) $f^{p/BM}(y)$ ($f^{p/MB}(y)$) represents the slitting function[43] for a proton to fluctuate to a baryon (meson) B (M) with momentum fraction y of the proton momentum and with a spectator meson (baryon) M (B) carrying a momentum fraction $1-y$ of the proton momentum. c_B and c_M denote the charm distribution inside the baryon B and meson M, respectively. In analogy to Eq. (2.183) one can define an anticharm probability distribution $\bar{c}(x)$.

As we discussed in Secs. 2.5-2.5.2 the estimated cross sections in hadronic models are about a factor of $100-1000$ larger than ours. Cross sections as large as predicted by hadronic or some of the Regge models would also indicate that, in contrast to our assumption, charm is produced non-perturbatively which means that (non-perturbative) intrinsic charm of the proton must be taken into account. This could, in principle, be done within our approach (see Fig. 2.30 (left panel) for example), but it is hardly conceivable that the small amount of intrinsic charm in the proton that is compatible with inclusive data [50] could increase the cross section for the exclusive production of charmed hadrons by two or three orders of magnitude. In a similar way one could also think of intrinsic charm in the pion (see Fig. 2.30 (right panel)) Experimental data for processes like $\pi^- \; p \to D^- \; \Lambda_c^+$, $\bar{p} \; p \to \bar{\Lambda}_c^- \; \Lambda_c^+$, $\gamma \, p \to \overline{D}^0 \, \Lambda_c^+$ and $\bar{p} \; p \to D^0 \; \overline{D}^0$ up to several GeV above production threshold would thus be highly desirable to pin down the production mechanism of charmed hadrons and shed some more light on the question of non-perturbative intrinsic charm in the proton.

[43] Analogue to the quark-gluon splitting functions of perturbative QCD.

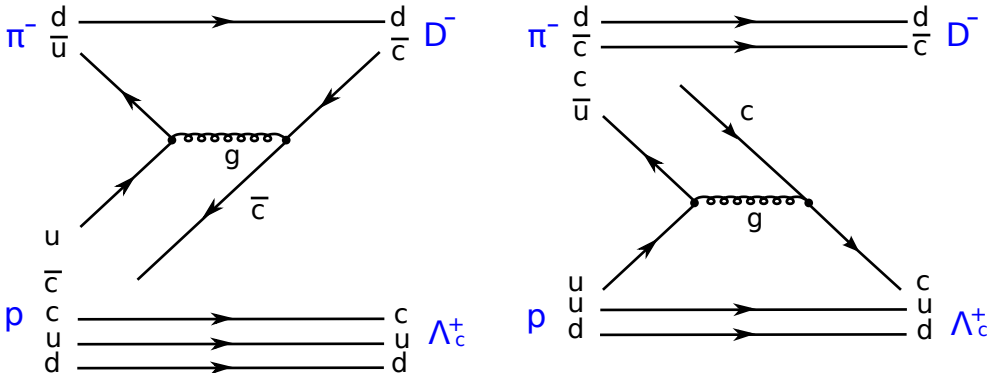

Figure 2.30: ERBL contributions to $\pi^- \; p \to D^- \; \Lambda_c^+$ with intrinsic charm content of the proton or pion, respectively.

3

Collinear parton distributions in a front form meson-cloud model

3.1 Introduction

The ideas of a pion cloud inside free nucleons emerged in the beginning of the 70's of the last century with the work of Drell, Yan and Levy [51] (1970) and Sullivan [52] (1972). Later it was realized that a (non-perturbative) pion cloud is a consequence of spontaneously broken chiral symmetry in QCD [53]. A renewed interest in the the meson-cloud model aroused because of experimental evidences that simple parton-model symmetries are broken such as the flavor symmetry in the sea of unpolarised nucleons[1] (related to the violation of Gottfried's sum rule) where it was found that $\bar{d} > \bar{u}$. We can explain this asymmetry naturally in the meson-cloud model: The wave function of the physical proton contains (many) virtual meson-baryon components. Via a convolution with the probability to find a meson-baryon component in the nucleon state, the valence anti-quark distribution of the meson contributes to the anti-quark distribution in the (physical) proton sea. In the proton wave function the probability of the Fock state $|n\pi^+\rangle$ is larger than that of the $|\Delta^{++}\pi^-\rangle$ Fock state. This naturally leads to an asymmetry $\bar{d} > \bar{u}$. We note, however, that the observed asymmetry cannot be fully ascribed to the meson-cloud. This does not question the value of the meson cloud model which has been extensively used in connection with parton distributions, see Ref. [54] for a review. The role of the meson-cloud model has also been discussed in connection with form factors [55], GPDs [56] and transition distribution amplitudes [57].

This section is organized as follows: In Sec. 3.2 we present the basics of the front form meson-cloud model. We continue to discuss in Sec. 3.3 how the meson-cloud model is applied to get a convolution formula for the PDFs. In Sec. 3.4 we discuss the model inputs and show in Sec. 3.5 our results.

3.2 Basics of the front form meson-cloud model

Before presenting the general formalism, we briefly discuss the main idea and the *assumptions* we make: To incorporate the meson-cloud effects into the wave function

[1] In Sec. 3.5.3 we discuss this issue in more detail and discuss the question whether this asymmetry extents to the polarized sea distributions.

of the physical nucleon, we picture the physical nucleon state $|\tilde{N}\rangle$ as being part of the time a bare nucleon state $|N\rangle$ and part of the time a nucleon dressed by a surrounding meson cloud. In the *one-meson approximation* this cloud is simply the higher order Fock state $|BM\rangle$ component in the Fock space expansion. Assuming that there are *no interactions* among the constituents of the baryon and the meson in the $|BM\rangle$-state during the interaction with the external probe, i.e. a hard photon, we can apply the convolution approach which enables us to relate the contribution of a certain $|BM\rangle$ Fock state to the parton distribution of the physical nucleon.

According to the derivation in Ref. [56], the physical nucleon state $|\tilde{N}\rangle$, characterized by the momentum $p_N = \left[p_N^+, p_N^-, \mathbf{p}_{N\perp}\right]$ and helicity μ, is an eigenstate of the light-cone Hamiltonian

$$H_{LC} = \sum_{B,M} \left[H_0^B + H_0^M + H_I^{(N,BM)}\right] : \tag{3.1}$$

$$H_{LC}\,|\tilde{N} : p, \mu\rangle = \frac{\mathbf{p}_{N\perp}^2 + M_N^2}{2p_N^+}\,|\tilde{N} : p, \mu\rangle\,. \tag{3.2}$$

$H_I^{(N,BM)}$ describes the nucleon-baryon-meson-interaction for all the possible baryon and meson states in which the nucleon can virtually fluctuate. H_0^B and H_0^M are (effective) Hamiltonians that govern the constituent quark dynamics inside the baryons and mesons, and lead to the confinement of the quarks inside baryons and mesons, respectively. Therefore the baryon state with three quarks, denoted by $|B : p_B, \lambda\rangle$, is an eigenstate of H_0^B , i.e.

$$H_0^B\,|B : p_B, \lambda\rangle = \frac{\mathbf{p}_{B\perp}^2 + M_B^2}{2p_B^+}\,|B : p_B, \lambda\rangle\,. \tag{3.3}$$

Similarly, a quark-antiquark state with the quantum numbers of a meson is an eigenstate of H_0^M:

$$H_0^M\,|M : p_M, \lambda\rangle = \frac{\mathbf{p}_{M\perp}^2 + M_M^2}{2p_M^+}\,|B : p_M, \lambda\rangle\,. \tag{3.4}$$

Treating $H_I^{(N,BM)}$ as a perturbation, we can expand the nucleon wave function in terms of eigenstates of the "free" bare Hamiltonian $H_0 = H_0^B + H_0^M$. We then get

$$\begin{aligned} |\tilde{N} : \tilde{p}, \mu\rangle = \Big(\sqrt{Z}\,|N : p_N, \mu\rangle + \sum_{n_1} \frac{|n_1\rangle\,\langle n_1|H_I|N : p_N, \mu\rangle}{E_N - E_{n_1} + i\epsilon} \\ + \sum_{n_1,n_2} \frac{|n_2\rangle\,\langle n_2|H_I|n_1\rangle\,\langle n_1|H_I|N : p_N, \mu\rangle}{(E_N - E_{n_2} + i\epsilon)\,(E_N - E_{n_1} + i\epsilon)} + \dots\Big), \end{aligned} \tag{3.5}$$

where Z is the wave function renormalization constant and the sum is a summation over the BM intermediate states. As we mentioned above, we are using the one-meson approximation. From that it follows that in the series expansion of Eq. (3.5) we only

take terms which are of first order in H_I:

$$\begin{aligned}|\tilde{N}:\tilde{p},\mu\rangle &= \sqrt{Z}\,|N:p_N,\mu\rangle + \sum_{B,M}|N(BM):p_N,\mu\rangle \\ &= \sqrt{Z}\,|N:p_N,\mu\rangle + \sum_{B,M}\Big[\int \frac{\mathrm{d}p_B^+\,\mathrm{d}^2\mathbf{p}_{B\perp}}{16\pi^3\,p_B^+}\frac{\mathrm{d}p_M^+\,\mathrm{d}^2\mathbf{p}_{M\perp}}{16\pi^3\,p_M^+} \\ &\times \sum_{\lambda_B,\lambda_M}\frac{\langle BM:p_B,p_M,\lambda_B,\lambda_M|H_I|N:p_N,\mu\rangle}{E_N-E_B-E_M}\,|BM:p_B,p_M,\lambda_B,\lambda_M\rangle\Big],\end{aligned} \tag{3.6}$$

where we have introduced $|BM:p_B,p_M,\lambda_B,\lambda_M\rangle$ as a shorthand notation for the tensor-product states $|B:p_B,\lambda_B\rangle\,|M:p_M,\lambda_M\rangle$. To calculate the energy denominator of Eq. (3.6) we write for the baryon and meson momenta

$$\begin{aligned}p_B^+ &= yp_N^+, & \mathbf{p}_{B\perp} &= \mathbf{k}_\perp + y\mathbf{p}_{N\perp},\\ p_M^+ &= (1-y)p_N^+, & \mathbf{p}_{M\perp} &= -\mathbf{k}_\perp + (1-y)\mathbf{p}_{N\perp},\end{aligned} \tag{3.7}$$

with y $(1-y)$ denoting the baryon (meson) longitudinal momentum fraction of the physical nucleon momentum and $\mathbf{k}_\perp(-\mathbf{k}_\perp)$ standing for the intrinsic transverse momentum of the baryon (meson) relative to the physical nucleon transverse momentum. The minus component can be identified by using the on-mass shell conditions. The energies in the denominator of Eq. (3.6) can now be written as

$$\begin{aligned}E_N &= \frac{1}{\sqrt{2}}\left(p_N^+ + p_N^-\right) = \frac{1}{\sqrt{2}}\Big(p_N^+ + \frac{M_N^2+\mathbf{p}_{N\perp}^2}{2p_N^+}\Big),\\ E_B &= \frac{1}{\sqrt{2}}\left(p_B^+ + p_B^-\right) = \frac{1}{\sqrt{2}}\left(yp_N^+ + \frac{M_B^2+(\mathbf{k}_\perp+y\mathbf{p}_{N\perp})^2}{2yp_N^+}\right),\\ E_M &= \frac{1}{\sqrt{2}}\left(p_M^+ + p_M^-\right) = \frac{1}{\sqrt{2}}\left((1-y)p_N^+ + \frac{M_M^2+(-\mathbf{k}_\perp+(1-y)\mathbf{p}_{N\perp})^2}{2(1-y)p_N^+}\right).\end{aligned} \tag{3.8}$$

If we use Eq. (3.8) the energy denominator reads

$$E_N - E_B - E_M = \frac{1}{2\sqrt{2}p_N^+}\Big(M_N^2 - M_{BM}^2\Big), \tag{3.9}$$

where we have defined the invariant mass of the baryon-meson fluctuation by

$$M_{BM}^2 = \frac{M_B^2+\mathbf{k}_\perp^2}{y} + \frac{M_M^2+\mathbf{k}_\perp^2}{1-y}. \tag{3.10}$$

Furthermore, the transition amplitude $\langle BM|H_I|N:p_N,\lambda\rangle$ in Eq. (3.6) has the following general expression:

$$\begin{aligned}\langle BM:p_B,p_M,\lambda_B,\lambda_M|H_I|N:p_N,\lambda\rangle &= 16\pi^3\delta\left(p_B^+ + p_M^+ - p_N^+\right)\delta^{(2)}\left(\mathbf{p}_{B\perp}+\mathbf{p}_{M\perp}-\mathbf{p}_{N\perp}\right)\\ &\times V^\mu_{\lambda_B,\lambda_M}(N,BM),\end{aligned} \tag{3.11}$$

with the vertex function $V^{\mu}_{\lambda_B,\lambda_M}(N,BM)$ being

$$V^{\mu}_{\lambda_B,\lambda_M}(N,BM) = \bar{u}_{N\alpha}\left(p_N,\mu\right) v^{\alpha\beta\gamma} \chi_{\beta}\left(p_M,\lambda_M\right) \Psi_{\gamma}\left(p_B,\lambda_B\right). \tag{3.12}$$

In Eq. (3.12) u_N is the spinor of the physical nucleon, χ and Ψ are the field operators of the virtual meson and baryon fluctuation, respectively, v denotes the structure we get (depending on momenta, derivatives, Dirac matrices, ...) if we work out Eq. (3.12) with a specified Lagrangian and α,β,γ are the bi-spinor and/or vector indices[2]. In App. H we show the results for the vertex functions.
Using the results of Eqs. (3.9) and (3.11), we find

$$\begin{aligned}|\tilde{N}:\tilde{p},\mu\rangle = \sqrt{Z}\,|N:p_N,\mu\rangle + \sum_{B,M}\int \frac{\mathrm{d}y\,\mathrm{d}^2\mathbf{k}_\perp}{16\pi^3}\frac{1}{\sqrt{y(1-y)}}\sum_{\lambda_B,\lambda_M}\phi^{\mu(N,BM)}_{\lambda_B,\lambda_M}(y,\mathbf{k}_\perp)\\ \times\,|B:yp_N^+,\mathbf{k}_\perp + y\mathbf{p}_{N\perp},\lambda_B\rangle\,|M:(1-y)p_N^+,-\mathbf{k}_\perp+(1-y)\mathbf{p}_{N\perp},\lambda_M\rangle\,,\end{aligned} \tag{3.13}$$

where we have introduced the probability amplitude $\phi^{\mu(N,BM)}_{\lambda_B,\lambda_M}(y,\mathbf{k}_\perp)$

$$\phi^{\mu(N,BM)}_{\lambda_B,\lambda_M}(y,\mathbf{k}_\perp) = \frac{1}{\sqrt{y(1-y)}}\frac{V^{\mu}_{\lambda_B,\lambda_M}(N,BM)}{M_N^2 - M_{BM}^2(y,\mathbf{k}_\perp)}. \tag{3.14}$$

The probability amplitude of Eq. (3.14) gives the amplitude that a nucleon with helicity μ fluctuates into a virtual BM system with the baryon having a longitudinal momentum fraction y, transverse momentum $\mathbf{k}_\perp$ and helicity λ_B, and the meson having a longitudinal momentum fraction $1-y$, transverse momentum $-\mathbf{k}_\perp$ and helicity λ_M. By imposing the normalization condition of the nucleon state of Eq. (3.13), we obtain a condition for Z:

$$1 = Z + P_{BM/N}, \tag{3.15}$$

where we have defined $P_{BM/N}$ by

$$P_{BM/N} = \sum_{B,M}\int \frac{\mathrm{d}y\,\mathrm{d}^2\mathbf{k}_\perp}{16\pi^3}\frac{1}{y(1-y)}\sum_{\lambda_B,\lambda_M}\frac{|V^{1/2}_{\lambda_B,\lambda_M}(N,BM)|^2}{M_N^2 - M_{BM}^2(y,\mathbf{k}_\perp)}. \tag{3.16}$$

$P_{BM/N}$ is the probability that a nucleon fluctuates into a baryon-meson state. In analogy, Z is the probability to find a bare nucleon in the physical nucleon.

3.3 Convolution model for the quark parton distribution functions

In this section we show how the meson-cloud model can be applied to calculate quark PDFs. The definition of the leading twist nucleon quark PDFs is given in Sec. 3.3.1.1. We can relate the quark PDFs to *helicity amplitudes* for which we can find an overlap representation in terms of LCWFs. As a side remark, we note that our discussion can

[2] E.g. for $B = N$ and $M = \pi$, the index β vanishes (since the pion is a pseudoscalar) and γ is a bi-spinor index. For $M = \rho$, β is a vector index.

be generalized also to GDPs in non-forward kinematics, as it was shown in Ref. [56].

3.3.1 *PDFs and helicity amplitudes*

3.3.1.1 *Definition of twist two quark PDFs of the nucleon*

For convenience we repeat the definition of the PDFs at twist two level:

- **unpolarised quark PDF**

$$f_1^q(x) = \frac{1}{2}\int \frac{\mathrm{d}z^-}{2\pi} e^{i\,x\,p^+\,z^-}\ \langle N:p,\mu|\ \bar{\Psi}^q\left(-z^-/2\right)\ \gamma^+\,\Psi^q\left(z^-/2\right)\ |N:p,\mu\rangle\,, \tag{3.17}$$

- **polarised quark PDF**

$$g_1^q(x) = \frac{1}{2}\int \frac{\mathrm{d}z^-}{2\pi} e^{i\,x\,p^+\,z^-}\ \langle N:p,\mu|\ \bar{\Psi}^q\left(-z^-/2\right)\ \gamma^+\gamma_5\,\Psi^q\left(z^-/2\right)\ |N:p,\mu\rangle\,, \tag{3.18}$$

- **transversity distribution**

$$h_1^q(x) = -\frac{1}{2}\int \frac{\mathrm{d}z^-}{2\pi} e^{i\,x\,p^+\,z^-}\ \langle N:p,\mu'_x|\ \bar{\Psi}^q\left(-z^-/2\right)\ i\sigma^{+1}\gamma_5\,\Psi^q\left(z^-/2\right)\ |N:p,\mu_x\rangle\,. \tag{3.19}$$

The nucleon state is characterized by the momentum p and the helicity $\mu(\mu_x)$[3].

Another way to define the leading twist PDFs is the following: We introduce the quark-quark correlator for a hadron target H

$$\Phi_{ab}(x,S) = \int \frac{\mathrm{d}\xi^-}{2\pi}\, e^{ik^+\xi^-}\,\langle H:p,S|\overline{\Psi}^q_b(0)\Psi^q_a(\xi)|H:p,S\rangle\big|_{\xi^+=\boldsymbol{\xi}_\perp=0}\,, \tag{3.20}$$

where $k^+ = xp^+$ and a,b are indices in the Dirac space. The target state is characterized by its four-momentum p and covariant spin four-vector S satisfying $p^2 = M^2$, $S^2 = -1$, and $p\cdot S = 0$. We choose a frame where the hadron momentum has no transverse components $P = \left[P^+, \frac{M^2}{2P^+}, \mathbf{0}_\perp\right]$, thus $S = \left[S_z\,\frac{p^+}{M}, -S_z\,\frac{M}{2P^+}, \boldsymbol{S}_\perp\right]$ with $\mathbf{S}^2 = 1$. From now on, we replace the dependence on the covariant spin four-vector S by the dependence on the unit three-vector $\mathbf{S} = (\mathbf{S}_\perp, S_z)$. The parton distribution functions can be obtained by performing the traces of the correlator (3.20) with suitable Dirac matrices. Using the abbreviation $\Phi^{[\Gamma]} \equiv \mathrm{Tr}[\Phi\Gamma]/2$, we have

$$\Phi^{[\gamma^+]}(x,\mathbf{S}) = f_1, \tag{3.21}$$

$$\Phi^{[\gamma^+\gamma_5]}(x,\mathbf{S}) = S_z g_1, \tag{3.22}$$

$$\Phi^{[i\sigma^{j+}\gamma_5]}(x,\mathbf{S}) = S^j_\perp h_1. \tag{3.23}$$

[3]The helicity μ_x refer to the helicities in the transversity basis in $\hat{x}$-direction, i.e. they are eigenstates of the transverse x-spin-projection operator, $\mathscr{Q}_\pm = \frac{1}{2}\left(1 \pm \gamma^1\gamma_5\right)$.

3.3.1.2 *Helicity amplitudes*

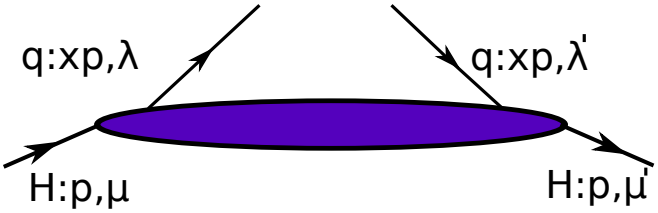

Figure 3.1: Representation of the helicity amplitudes defined in Eq. (3.24)

The helicity amplitudes are defined by (see also Fig. 3.1)

$$A^{q/H}_{\mu'\lambda',\mu\lambda} = \int \frac{\mathrm{d}z^-}{2\pi} e^{ix\,p^+\,z^-} \left\langle H:p,\mu' \right| \mathscr{O}^q_{\lambda'\lambda} \left| H:p,\mu \right\rangle |_{z^+=\mathbf{z}_\perp=0}, \tag{3.24}$$

with the various quark field operators given by

$$\begin{aligned}
\mathscr{O}^q_{++} &= \frac{1}{4}\bar{\psi}^q\left(-\frac{z}{2}\right)\gamma^+\left(1+\gamma_5\right)\psi^q\left(\frac{z}{2}\right) = \frac{1}{\sqrt{2}}\phi^\dagger_R\left(-\frac{z}{2}\right)\phi_R\left(\frac{z}{2}\right), \\
\mathscr{O}^q_{--} &= \frac{1}{4}\bar{\psi}^q\left(-\frac{z}{2}\right)\gamma^+\left(1-\gamma_5\right)\psi^q\left(\frac{z}{2}\right) = \frac{1}{\sqrt{2}}\phi^\dagger_L\left(-\frac{z}{2}\right)\phi_L\left(\frac{z}{2}\right), \\
\mathscr{O}^q_{-+} &= -\frac{i}{4}\bar{\psi}^q\left(-\frac{z}{2}\right)\sigma^{+1}\left(1+\gamma_5\right)\psi^q\left(\frac{z}{2}\right) \\
&= -\frac{i}{4}\bar{\psi}^q\left(-\frac{z}{2}\right)\left(\sigma^{+1}-i\sigma^{+2}\right)\psi^q\left(\frac{z}{2}\right) = \frac{1}{\sqrt{2}}\phi^\dagger_L\left(-\frac{z}{2}\right)\phi_R\left(\frac{z}{2}\right), \\
\mathscr{O}^q_{+-} &= \frac{i}{4}\bar{\psi}^q\left(-\frac{z}{2}\right)\sigma^{+1}\left(1-\gamma_5\right)\psi^q\left(\frac{z}{2}\right) \\
&= \frac{i}{4}\bar{\psi}^q\left(-\frac{z}{2}\right)\left(\sigma^{+1}+i\sigma^{+2}\right)\psi^q\left(\frac{z}{2}\right) = \frac{1}{\sqrt{2}}\phi^\dagger_R\left(-\frac{z}{2}\right)\phi_L\left(\frac{z}{2}\right).
\end{aligned} \tag{3.25}$$

$\phi_{R(L)}$ are the good field components with helicity $R(L)$. Following Ref. [23], we can express the helicity amplitudes of Eq. (3.24) in terms of LCWFs. To obtain the wave function representation of the helicity amplitudes we

1. insert the Fock state expansion into the matrix elements defining the helicity amplitudes,
2. express the quark field operators in terms of creation and annihilation operators of quarks and antiquarks,
3. use the anti-commutation relations of these operators.

The resulting formula is

$$\begin{aligned}
A^{q/H}_{\mu'\lambda',\mu\lambda}(x) = \sum_{N,\beta}\sum_{j=q}\int\left[\mathrm{d}x\right]_N\int\left[\mathrm{d}\mathbf{k}_\perp\right]_N fac(\lambda_j,\lambda'_j)\delta_{\lambda_j,\lambda}\delta_{\lambda'_j,\lambda'} \\
\times\,\delta\left(x-x_j\right)\Psi^{H*}_{\mu'}\left(\{x_i,\mathbf{k}_{\perp i},\lambda'_i,\beta'_i\}_{i=1,\ldots,N}\right)\Psi^H_\mu\left(\{x_i,\mathbf{k}_{\perp i},\lambda_i,\beta_i\}_{i=1,\ldots,N}\right),
\end{aligned} \tag{3.26}$$

where N specifies the number of partons in a Fock state, β is a collective label for flavor and color, j denotes the active quark and the global factor is given by

$$fac\left(\lambda_j, \lambda_j'\right) = \begin{cases} \delta_{\lambda_j,\lambda_j'} & \text{chiral even (unpolarised) ,} \\ sign(\lambda_j)\delta_{\lambda_j,\lambda_j'} & \text{chiral even (polarised) ,} \\ \delta_{\lambda_j,-\lambda_j'} & \text{chiral odd.} \end{cases} \tag{3.27}$$

3.3.1.3 *PDFs expressed in terms of helicity amplitudes*

The decomposition of the helicity amplitudes in terms of PDFs can be obtained by decomposing the target states $|H : p, \pm\mathbf{S}\rangle$ with light-cone polarization parallel or opposite to the generic direction $\mathbf{S} = (\sin\theta_S \cos\phi_S, \sin\theta_S \sin\phi_S, \cos\theta_S)$ in terms of the target light-cone helicity states $|H : p, \mu\rangle$,

$$\Big(|p, +\boldsymbol{S}\rangle, \quad |p, -\boldsymbol{S}\rangle\Big) = \Big(|p, +\rangle, \quad |p, -\rangle\Big)\, u(\theta_S, \phi_S), \tag{3.28}$$

where the $SU(2)$ rotation matrix $u(\theta_S, \phi_S)$ is given by

$$u(\theta_S, \phi_S) = \begin{pmatrix} \cos\frac{\theta_S}{2}\, e^{-i\phi_S/2} & -\sin\frac{\theta_S}{2}\, e^{-i\phi_S/2} \\ \sin\frac{\theta_S}{2}\, e^{i\phi_S/2} & \cos\frac{\theta_S}{2}\, e^{i\phi_S/2} \end{pmatrix}. \tag{3.29}$$

For a spin $1/2$ target like the proton one has:

$$A^{q/p}_{\mu'\lambda',\mu\lambda} = \left(\begin{array}{cc|cc} \frac{1}{2}\left(f_1^{q/p} + g_1^{q/p}\right) & 0 & 0 & h_1^{q/p} \\ 0 & \frac{1}{2}\left(f_1^{q/p} - g_1^{q/p}\right) & 0 & 0 \\ \hline 0 & 0 & \frac{1}{2}\left(f_1^{q/p} - g_1^{q/p}\right) & 0 \\ h_1^{q/p} & 0 & 0 & \frac{1}{2}\left(f_1^{q/p} + g_1^{q/p}\right) \end{array}\right), \tag{3.30}$$

where the elements of the 2×2 block matrices refer to hadron helicities (μ', μ) (quark helicities (λ', λ) fixed), whereas the different block matrices refer to the different contributions of quark helicities (λ', λ):

- 2×2 matrix:
  - upper left: $(\mu' = +, \mu = +)$
  - upper right: $(\mu' = -, \mu = +)$
  - lower left: $(\mu' = +, \mu = -)$
  - lower right: $(\mu' = -, \mu = -)$
- block matrices:
  - upper left: $(\lambda' = +, \lambda = +)$
  - upper right: $(\lambda' = -, \lambda = +)$
  - lower left: $(\lambda' = +, \lambda = -)$

– lower right: $(\lambda' = -, \lambda = -)$.

From Eq. (3.30) we read off that

$$\begin{aligned} f_1^{q/p}(x) &= A^{q/p}_{++,++}(x) + A^{q/p}_{-+,-+}(x), \\ g_1^{q/p}(x) &= A^{q/p}_{++,++}(x) - A^{q/p}_{-+,-+}(x), \\ h_1^{q/p}(x) &= A^{q/p}_{++,--}(x). \end{aligned} \tag{3.31}$$

For a spin 1 target like the ρ one has [58]:

$$A^{q/\rho}_{\mu'\lambda',\mu\lambda} = \left(\begin{array}{ccc|ccc} f_1 + g_1 - \frac{f_{1LL}}{3} & 0 & 0 & 0 & \sqrt{2}\,(h_1 + i h_{1LT}) & 0 \\ 0 & f_1 + \frac{2f_{1LL}}{3} & 0 & 0 & 0 & \sqrt{2}\,(h_1 - i h_{1LT}) \\ 0 & 0 & f_1 - g_1 - \frac{f_{1LL}}{3} & 0 & 0 & 0 \\ \hline 0 & 0 & 0 & f_1 - g_1 - \frac{f_{1LL}}{3} & 0 & \\ \sqrt{2}\,(h_1 - i h_{1LT}) & 0 & 0 & 0 & f_1 + \frac{2f_{1LL}}{3} & 0 \\ 0 & \sqrt{2}\,(h_1 + i h_{1LT}) & 0 & 0 & 0 & f_1 + g_1 - \frac{f_{1LL}}{3} \end{array}\right), \tag{3.32}$$

where the elements of the 3×3 block matrices refer to the ρ-helicity (μ', μ), whereas different blocks belong to different combinations of quark helicities (λ', λ). The definition of the helicity amplitudes in Ref. [58] differs from our definition in Eq. (3.24) by a factor of two. With our definition we obtain

$$\begin{aligned} f_1^{q/\rho}(x) &= \frac{2}{3}\Big(A^{q/\rho}_{1+,1+}(x) + A^{q/\rho}_{-1+,-1+}(x) + A^{q/\rho}_{0+,0+}(x)\Big), \\ f_{1LL}^{q\rho}(x) &= 2A^{q/\rho}_{0+,0+}(x) - (A^{q/\rho}_{1+,1+}(x) + A^{q/\rho}_{-1+,-1+}(x)), \\ g_1^{q/\rho}(x) &= A^{q/\rho}_{1+,1+}(x) - A^{q/\rho}_{-1+,-1+}(x), \\ h_1^{q/\rho}(x) &= \frac{1}{\sqrt{2}}\Big(A^{q/\rho}_{1+,0+}(x) + A^{q/\rho}_{0+,-1-}(x)\Big). \end{aligned} \tag{3.33}$$

For a spin 0 target, like the π, one has only one independent helicity amplitude, corresponding to the unpolarized PDF, i.e.

$$f_1^{q/\pi} = A^{q/\pi}_{0+,0+} + A^{q/\pi}_{0-,0-} = 2A^{q/\pi}_{0+,0+}. \tag{3.34}$$

3.3.2 *PDFs in the meson cloud model*

3.3.2.1 *Helicity amplitudes in the meson cloud model*

In DIS the virtual photon can hit either the bare proton[4] p or one of the constituents of the higher Fock states. As a consequence, a generic quark parton distribution function $PDF(x)$ can be obtained as a sum of two contributions:

$$PDF^{q/p}(x) = Z\, PDF^{q_V/p}_{bare}(x) + \delta PDF^{q}(x), \tag{3.35}$$

[4] We can restrict our discussion about the PDFs to the proton, since the PDFs of the neutron can be related to those of the proton by isospin invariance.

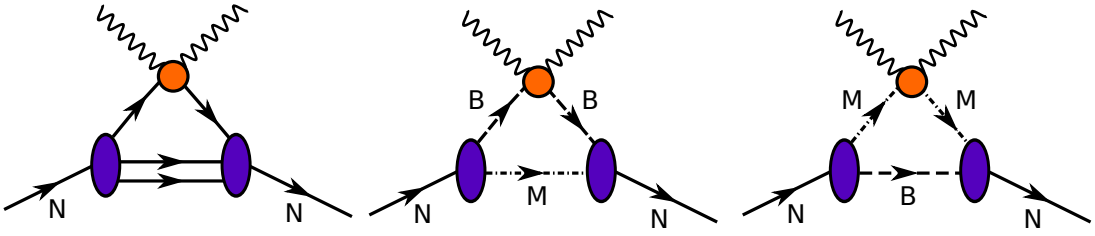

Figure 3.2: Deeply virtual scattering on the bare nucleon (left figure) and on the dressed nucleon: virtual baryon (middle figure, meson acting as a spectator) and on the virtual meson (right figure, baryon acting as a spectator).

where $PDF^{q_V/p}_{bare}$ is the valence quark distribution ($PDF = f_1, g_1$ or h_1, cf. Sec. 3.3.1.1 for their definition) of the bare proton described by $3q$ Fock states and $\delta PDF^{q/p}$ includes both valence and sea contribution coming from the BM Fock component of the proton state, i.e. $q = (u_V + \bar{u}, d_V + \bar{d})$. As we consider only the minimal $3q$ and $q\bar{q}$ configurations for the baryon and meson components in the BM fluctuation, respectively, only the meson can contribute to the sea of the physical proton. The last term in Eq. (3.35) can be further split into two contributions, with the active parton belonging either to the baryon ($\delta PDF^{q/BM}$) or to the meson ($\delta PDF^{q/MB}$), i.e.

$$\delta PDF^{q}(x) = \sum_{B,M} \left[\delta PDF^{q/BM}(x) + \delta PDF^{q/MB}(x) \right]. \tag{3.36}$$

To find the expression for $\delta PDF^{q}(x)$ we recall that the PDFs can be written in terms of helicity amplitudes, see the previous section. Therefore we need to find the helicity amplitudes in the meson cloud model. In the meson cloud model we can write the helicity amplitudes as

$$A^{q/p}_{\mu'\lambda',\mu\lambda}(x) = Z\, A^{q/(p,bare)}_{\mu'\lambda',\mu\lambda}(x) + \delta A^{q/p}_{\mu'\lambda',\mu\lambda}(x), \tag{3.37}$$

where $A^{q/(p,bare)}_{\mu'\lambda',\mu\lambda}$ is the contribution from the bare nucleon (described in terms of three valence quarks) and $\delta A^{q/p}_{\mu'\lambda',\mu\lambda}$ is the contribution from the higher Fock state, i.e. the baryon-meson fluctuation. $\delta A^{q/p}_{\mu'\lambda',\mu\lambda}$ can be split into two different parts: One where the active quark is in the baryon and another one where the active quark is in the meson:

$$\delta A^{q/p}_{\mu'\lambda',\mu\lambda}(x) = \sum_{B,M} \delta A^{q/BM}_{\mu'\lambda',\mu\lambda}(x) + \delta A^{q/MB}_{\mu'\lambda',\mu\lambda}(x). \tag{3.38}$$

In the first case a baryon is taken out (reinserted) from the initial (final) proton with a momentum fraction y_B of the plus momentum of the proton, a transverse momentum $\mathbf{p}_{B\perp}$ and helicity $\lambda_B(\lambda'_B)$. The meson is a spectator during the scattering process. In the second case a meson is taken out (reinserted) from the initial (final) proton with a momentum fraction y_M of the plus momentum of the proton, a transverse momentum $\mathbf{p}_{M\perp}$ and helicity $\lambda_M(\lambda'_M)$, respectively. The baryon now acts as the spectator.

To evaluate the baryon contribution $\delta A^{q/BM}_{\mu'\lambda',\mu\lambda}(x)$ we calculate the matrix element in Eq. (3.24) between the BM components of the initial and final proton. From the

nucleon wave function of Eq. (3.13) the contribution from the active baryon in the BM components reads[5]

$$\sum_{B,M} \int \frac{\mathrm{d}y_B}{y_B} \frac{\mathrm{d}y_M}{y_M} \delta\left(1 - y_B - y_M\right) \int \frac{\mathrm{d}^2\mathbf{k}_{B\perp} \mathrm{d}^2\mathbf{k}_{M\perp}}{16\pi^3} \delta^{(2)}\left(\mathbf{k}_{B\perp} + \mathbf{k}_{M\perp}\right) \\ \times \sum_{\lambda_B, \lambda_M} \phi^{\mu^{(\prime)}(p,BM)}_{\lambda_B^{(\prime)}, \lambda_M}\left(y_B, \mathbf{k}_{B\perp}\right) \left|B : y_B p_p^+, \mathbf{k}_{B\perp}, \lambda_B\right\rangle \left|M : y_M p_p^+, \mathbf{k}_{M\perp}, \lambda_M\right\rangle . \tag{3.39}$$

The final result for the baryon contribution to $\delta A^{q/BM}_{\mu'\lambda',\mu\lambda}(x)$ is given by

$$\delta A^{q/BM}_{\mu'\lambda',\mu\lambda}(x) = \sum_{\lambda_B^{(\prime)}, \lambda_M} \int_x^1 \frac{\mathrm{d}y_B}{y_B} \int \frac{\mathrm{d}\mathbf{k}_{\perp B}}{16\pi^3} A^{q/B}_{\lambda_B'\lambda',\lambda_B\lambda}\left(\frac{x}{y_B}\right) \\ \times \phi^{\mu(p,BM)}_{\lambda_B\lambda_M}\left(y_B, \mathbf{k}_{\perp B}\right) \left[\phi^{\mu'(p,BM)}_{\lambda_B'\lambda_M}\left(y_B, \mathbf{k}_{\perp B}\right)\right]^* , \tag{3.40}$$

with

$$A^{q/B}_{\lambda_B'\lambda',\lambda_B\lambda}\left(\frac{x}{y_B}\right) = \int \frac{\mathrm{d}z^-}{2\pi} e^{i\frac{x}{y_B} p_B^+ z^-} \left\langle B : p_B, \lambda_B'\right| \mathcal{O}_{\lambda'\lambda} \left|B : p_B, \lambda_B\right\rangle . \tag{3.41}$$

The quark field operator product $\mathcal{O}_{\lambda'\lambda}$ is defined in Eq. (3.25) for the different helicity combinations of (λ', λ). Analogous, we can calculate $\delta A^{q/MB}_{\mu'\lambda',\mu\lambda}(x)$. We find the following convolution

$$\delta A^{q/MB}_{\mu'\lambda',\mu\lambda}(x) = \sum_{\lambda_M^{(\prime)}, \lambda_M} \int_x^1 \frac{\mathrm{d}y_M}{y_M} \int \frac{\mathrm{d}\mathbf{k}_{\perp M}}{16\pi^3} A^{q/M}_{\lambda_M'\lambda',\lambda_M\lambda}\left(\frac{x}{y_M}\right) \\ \times \phi^{\mu(p,BM)}_{\lambda_B\lambda_M}\left(1 - y_M, -\mathbf{k}_{\perp M}\right) \left[\phi^{\mu'(p,BM)}_{\lambda_B\lambda_M'}\left(1 - y_M, -\mathbf{k}_{\perp M}\right)\right]^* , \tag{3.42}$$

with

$$A^{q/M}_{\lambda_M'\lambda',\lambda_M\lambda}\left(\frac{x}{y_M}\right) = \int \frac{\mathrm{d}z^-}{2\pi} e^{i\frac{x}{y_M} p_M^+ z^-} \left\langle M : p_M, \lambda_M'\right| \mathcal{O}_{\lambda'\lambda} \left|M : p_M, \lambda_M\right\rangle . \tag{3.43}$$

For equations (3.41) and (3.43) we can use the overlap formula of Eq. (3.26). Since we now have the expressions for the BM component of the helicity amplitudes, we can also calculate their contribution to the PDFs, i.e. we can calculate

$$\delta PDF^q(x) = \sum_{B,M} \left[\delta PDF^{q/BM}(x) + \delta PDF^{q/MB}(x)\right] . \tag{3.44}$$

We recall that the PDFs can be written in terms of helicity amplitudes, cf. Sec. 3.3.1.3.

3.3.2.2 *Convolution formula for the PDFs*

In this section we specify the convolution formula for the PDFs in the meson cloud model. The lowest lying fluctuations for the proton which we include in our calcula-

[5] The initial proton (baryon) has the helicity $\mu(\lambda_B)$ and the final proton (baryon) has the helicity $\mu'(\lambda_B')$.

tions are

$$\begin{aligned} p(uud) &\to n(udd)\,\pi^+(u\bar{d}), \\ p(uud) &\to p(uud)\,\pi^0\left(\frac{1}{\sqrt{2}}[d\bar{d}-u\bar{u}]\right), \\ p(uud) &\to n(udd)\,\rho^+(u\bar{d}), \\ p(uud) &\to p(uud)\,\rho^0\left(\frac{1}{\sqrt{2}}[d\bar{d}-u\bar{u}]\right). \end{aligned} \tag{3.45}$$

In what follows helicities $\pm\frac{1}{2}$ are denoted by $\pm$ for better legibility.

N π-fluctuation:
Let us start with[6] $\delta f_1^{q/BM}$:

- $B = N \to$ active, $M = \pi \to$ spectator

$$\begin{aligned} \delta f_1^{q/N\pi}(x) &= \delta A^{q/N\pi}_{++,++}(x) + \delta A^{q/N\pi}_{+-,+-}(x) = \int_x^1 \frac{\mathrm{d}y_B}{y_B} \int \frac{\mathrm{d}\mathbf{k}_{\perp B}}{16\pi^3} \\ &\times \Bigg[\Big[A^{q/N}_{++,++}\,\phi^{+(p,N\pi)}_{+0} \left(\phi^{+(p,N\pi)}_{+0}\right)^* + \underbrace{A^{q/N}_{-+,-+}}_{A^{q/N}_{+-,+-}}\,\phi^{+(p,N\pi)}_{-0} \left(\phi^{+(p,N\pi)}_{-0}\right)^* \Big] \\ &\quad + \Big[A^{q/N}_{+-,+-}\,\phi^{+(p,N\pi)}_{+0} \left(\phi^{+(p,N\pi)}_{+0}\right)^* + \underbrace{A^{q/N}_{--,--}}_{A^{q/N}_{++,++}}\,\phi^{+(p,N\pi)}_{-0} \left(\phi^{+(p,N\pi)}_{-0}\right)^* \Big] \Bigg] \\ &= \int_x^1 \frac{\mathrm{d}y_B}{y_B} \int \frac{\mathrm{d}\mathbf{k}_{\perp B}}{16\pi^3} \Bigg[\underbrace{\phi^{+(p,N\pi)}_{+0} \left(\phi^{+(p,N\pi)}_{+0}\right)^*}_{\left|(\phi^{+(p,N\pi)}_{+0}\right|^2} \Big[\underbrace{A^{q/N}_{++,++} + A^{q/N}_{+-,+-}}_{f_1^{q/N}} \Big] \\ &\qquad + \underbrace{\phi^{+(p,N\pi)}_{-0} \left(\phi^{+(p,N\pi)}_{-0}\right)^*}_{\left|(\phi^{+(p,N\pi)}_{-0}\right|^2} \Big[\underbrace{A^{q/N}_{++,++} + A^{q/N}_{+-,+-}}_{f_1^{q/N}} \Big] \Bigg] \\ &= \int_x^1 \frac{\mathrm{d}y_B}{y_B}\, f_1^{q/N}\left(\frac{x}{y_B}\right) \sum_{\lambda_N} \int \frac{\mathrm{d}\mathbf{k}_{\perp B}}{16\pi^3} \left|\phi^{+(p,N\pi)}_{\lambda_N 0}\,(y_B, \mathbf{k}_{\perp B})\right|^2. \end{aligned} \tag{3.46}$$

[6] We label the "pion helicity" with 0.

- $M = \pi \rightarrow$ active, $B = N \rightarrow$ spectator

$$\begin{aligned}\delta f_1^{q/\pi N}(x) &= \delta A^{q/\pi N}_{++,++}(x) + \delta A^{q/\pi N}_{+-,+-}(x) = \int_x^1 \frac{\mathrm{d}y_M}{y_M} \int \frac{\mathrm{d}\mathbf{k}_{\perp M}}{16\pi^3} \\ &\times \sum_{\lambda_N} \left[A^{q/\pi}_{0+,0+}\, \phi^{+(p,N\pi)}_{\lambda_N 0} \left(\phi^{+(p,N\pi)}_{\lambda_N 0}\right)^* + A^{q/\pi}_{0-,0-}\, \phi^{+(p,N\pi)}_{\lambda_N 0} \left(\phi^{+(p,N\pi)}_{\lambda_N 0}\right)^* \right] \\ &= \int_x^1 \frac{\mathrm{d}y_M}{y_M} \int \frac{\mathrm{d}\mathbf{k}_{\perp M}}{16\pi^3} \Big[\underbrace{A^{q/\pi}_{0+,0+} + A^{q/\pi}_{0-,0-}}_{f_1^{q/\pi}} \sum_{\lambda_N} \underbrace{\phi^{+(p,N\pi)}_{\lambda_N 0} \left(\phi^{+(p,N\pi)}_{\lambda_N 0}\right)^*}_{\left|(\phi^{+(p,N\pi)}_{\lambda_N 0}\right|^2} \Big] \\ &= \int_x^1 \frac{\mathrm{d}y_M}{y_M} f_1^{q/\pi}\left(\frac{x}{y_M}\right) \sum_{\lambda_N} \int \frac{\mathrm{d}\mathbf{k}_{\perp M}}{16\pi^3} \left| (\phi^{+(p,N\pi)}_{\lambda_N 0}\,(1-y_M, -\mathbf{k}_{\perp M}) \right|^2 .\end{aligned} \tag{3.47}$$

Only the active nucleon contributes to the polarized and transversity PDF since the pion has spin zero. We continue with $\delta g_1^{q/N\pi}$:

$$\begin{aligned}\delta g_1^{q/N\pi}(x) &= \delta A^{q/N\pi}_{++,++}(x) - \delta A^{q/N\pi}_{+-,+-}(x) = \int_x^1 \frac{\mathrm{d}y_B}{y_B} \int \frac{\mathrm{d}\mathbf{k}_{\perp B}}{16\pi^3} \\ &\times \Bigg[\left[A^{q/N}_{++,++}\, \phi^{+(p,N\pi)}_{+0} \left(\phi^{+(p,N\pi)}_{+0}\right)^* + \underbrace{A^{q/N}_{-+,-+}}_{A^{q/N}_{+-,+-}} \phi^{+(p,N\pi)}_{-0} \left(\phi^{+(p,N\pi)}_{-0}\right)^* \right] \\ &- \left[A^{q/N}_{+-,+-}\, \phi^{+(p,N\pi)}_{+0} \left(\phi^{+(p,N\pi)}_{+0}\right)^* + \underbrace{A^{q/N}_{--,--}}_{A^{q/N}_{++,++}} \phi^{+(p,N\pi)}_{-0} \left(\phi^{+(p,N\pi)}_{-0}\right)^* \right] \Bigg]\end{aligned} \tag{3.48}$$

$$\begin{aligned}&= \int_x^1 \frac{\mathrm{d}y_B}{y_B} \int \frac{\mathrm{d}\mathbf{k}_{\perp B}}{16\pi^3} \Bigg[\underbrace{\phi^{+(p,N\pi)}_{+0} \left(\phi^{+(p,N\pi)}_{+0}\right)^*}_{\left|(\phi^{+(p,N\pi)}_{+0}\right|^2} \Big[\underbrace{A^{q/N}_{++,++} - A^{q/N}_{+-,+-}}_{g_1^{q/N}} \Big] \\ &\qquad - \underbrace{\phi^{+(p,N\pi)}_{-0} \left(\phi^{+(p,N\pi)}_{-0}\right)^*}_{\left|(\phi^{+(p,N\pi)}_{-0}\right|^2} \Big[\underbrace{A^{q/N}_{++,++} - A^{q/N}_{+-,+-}}_{g_1^{q/N}} \Big] \Bigg] \\ &= \int_x^1 \frac{\mathrm{d}y_B}{y_B}\, g_1^{q/N}\left(\frac{x}{y_B}\right) \int \frac{\mathrm{d}\mathbf{k}_{\perp B}}{16\pi^3} \left[\left| (\phi^{+(p,N\pi)}_{+N0}\,(y_B, \mathbf{k}_{\perp B}) \right|^2 - \left| (\phi^{+(p,N\pi)}_{-0}\,(y_B, \mathbf{k}_{\perp B}) \right|^2 \right].\end{aligned} \tag{3.49}$$

The contribution $\delta h_1^{q/N\pi}$ of the $N\pi$-fluctuation to the transversity of the proton reads

$$\begin{aligned}\delta h_1^{q/N\pi}(x) = \delta A^{q/N\pi}_{++,--}(x) &= \int_x^1 \frac{\mathrm{d}y_B}{y_B} \int \frac{\mathrm{d}\mathbf{k}_{\perp B}}{16\pi^3} \underbrace{A^{q/N}_{++,--}\left(\frac{x}{y_B}\right)}_{h_1^{q/N}\left(\frac{x}{y_B}\right)} \\ &\times \phi_{-0}^{-(p,N\pi)}(y_B, \mathbf{k}_{\perp B}) \left(\phi_{+0}^{+(p,N\pi)}(y_B, \mathbf{k}_{\perp B})\right)^* \\ &= \int_x^1 \frac{\mathrm{d}y_B}{y_B} \int \frac{\mathrm{d}\mathbf{k}_{\perp B}}{16\pi^3} h_1^{q/N}\left(\frac{x}{y_B}\right) \\ &\times \phi_{-0}^{-(p,N\pi)}(y_B, \mathbf{k}_{\perp B}) \left(\phi_{+0}^{+(p,N\pi)}(y_B, \mathbf{k}_{\perp B})\right)^*.\end{aligned} \tag{3.50}$$

N ρ-fluctuation:
We now investigate the contribution of the $N\rho$ fluctuation to the PDFs of the proton. Since the ρ-meson is a vector particle it contributes to all three leading twist PDFs when the meson is active. Let us start with $\delta f_1^{q/BM}$:

- $B = N \rightarrow$ active, $M = \rho \rightarrow$ spectator

$$\begin{aligned}\delta f_1^{q/N\rho}(x) = \delta A^{q/N\rho}_{++,++}(x) + \delta A^{q/N\rho}_{+-,+-}(x) &= \int_x^1 \frac{\mathrm{d}y_B}{y_B} \int \frac{\mathrm{d}\mathbf{k}_{\perp B}}{16\pi^3} \\ &\times \sum_{\lambda_\rho} \Bigg[\Big[A^{q/N}_{++,++} \underbrace{\phi^{+(p,N\rho)}_{+\lambda_\rho} \left(\phi^{+(p,N\rho)}_{+\lambda_\rho}\right)^*}_{\left|\phi^{+(p,N\rho)}_{+\lambda_\rho}\right|^2} + \underbrace{A^{q/N}_{-+,-+}}_{A^{q/N}_{+-,+-}} \underbrace{\phi^{+(p,N\rho)}_{-\lambda_\rho} \left(\phi^{+(p,N\rho)}_{-\lambda_\rho}\right)^*}_{\left|\phi^{+(p,N\rho)}_{-\lambda_\rho}\right|^2} \Big] \\ &+ \Big[A^{q/N}_{+-,+-} \underbrace{\phi^{+(N,N\rho)}_{+\lambda_\rho} \left(\phi^{+(N,N\pi)}_{+\lambda_\rho}\right)^*}_{\left|\phi^{+(p,N\rho)}_{+\lambda_\rho}\right|^2} + \underbrace{A^{q/N}_{--,--}}_{A^{q/N}_{++,++}} \underbrace{\phi^{+(N,N\rho)}_{-\lambda_\rho} \left(\phi^{+(p,N\rho)}_{-\lambda_\rho}\right)^*}_{\left|\phi^{+(p,N\rho)}_{-\lambda_\rho}\right|^2} \Big] \Bigg]\end{aligned} \tag{3.51}$$

$$\begin{aligned}&= \int_x^1 \frac{\mathrm{d}y_B}{y_B} \int \frac{\mathrm{d}\mathbf{k}_{\perp B}}{16\pi^3} \sum_{\lambda_\rho} \Bigg[\left|(\phi^{+(p,N\rho)}_{+\lambda_\rho}\right|^2 \Big[\underbrace{A^{q/N}_{++,++} + A^{q/N}_{+-,+-}}_{f_1^{q/N}} \Big] \\ &\qquad + \underbrace{\phi^{+(p,N\rho)}_{-\lambda_\rho} \left(\phi^{+(p,N\rho)}_{-\lambda_\rho}\right)^*}_{\left|(\phi^{+(p,N\rho)}_{-\lambda_\rho}\right|^2} \Big[\underbrace{A^{q/N}_{++,++} + A^{q/N}_{+-,+-}}_{f_1^{q/N}} \Big] \Bigg] \\ &= \int_x^1 \frac{\mathrm{d}y_B}{y_B} f_1^{q/N}\left(\frac{x}{y_B}\right) \sum_{\lambda_N, \lambda_\rho} \int \frac{\mathrm{d}\mathbf{k}_{\perp B}}{16\pi^3} \left|(\phi^{+(p,N\rho)}_{\lambda_N\lambda_\rho}(y_B, \mathbf{k}_{\perp B})\right|^2.\end{aligned} \tag{3.52}$$

- $M = \rho \to$ active, $B = N \to$ spectator

$$\delta f_1^{q/\rho N}(x) = \delta A^{q/\rho N}_{++,++}(x) + \delta A^{q/\rho N}_{+-,+-}(x) = \int_x^1 \frac{\mathrm{d}y_M}{y_M} \int \frac{\mathrm{d}\mathbf{k}_{\perp M}}{16\pi^3}$$
$$\times \sum_{\lambda_N} \Bigg[\left|(\phi^{+(p,N\rho)}_{\lambda_N 1}\right|^2 \Big[\underbrace{A^{q/\rho}_{1+,1+} + A^{q/\rho}_{1-,1-}}_{f_1^{q/\rho} - \frac{1}{3} f_{1LL}^{q/\rho}} \Big] + \left|(\phi^{+(p,N\rho)}_{\lambda_N 0}\right|^2 \Big[\underbrace{A^{q/\rho}_{0+,0+} + A^{q/\rho}_{0-,0-}}_{f_1^{q/\rho} + \frac{2}{3} f_{1LL}^{q/\rho}} \Big]$$
$$+ \left|(\phi^{+(p,N\rho)}_{\lambda_N -1}\right|^2 \Big[\underbrace{A^{q/\rho}_{-1+,-1+} + A^{q/\rho}_{-1-,-1-}}_{f_1^{q/\rho} - \frac{1}{3} f_{1LL}^{q/\rho}} \Big] \Bigg]$$
$$= \int_x^1 \frac{\mathrm{d}y_M}{y_M} \int \frac{\mathrm{d}\mathbf{k}_{\perp M}}{16\pi^3} \Bigg[\sum_{\lambda_N, \lambda_\rho} f_1^{q/\rho}\left(\frac{x}{y_M}\right) \left|(\phi^{+(p,N\rho)}_{\lambda_N \lambda_\rho}\left(1 - y_M, -\mathbf{k}_{\perp M}\right)\right|^2$$
$$+ \sum_{\lambda_N} f_{1LL}^{q/\rho} \Big[\left(\frac{x}{y_M}\right) - \frac{1}{3}\left|\phi^{+(p,N\rho)}_{\lambda_N 1}\right|^2 + \frac{2}{3}\left|\phi^{+(p,N\rho)}_{\lambda_N 0}\right|^2 - \frac{1}{3}\left|\phi^{+(p,N\rho)}_{\lambda_N -1}\right|^2 \Big] \Bigg]. \tag{3.53}$$

We continue with the higher Fock state contribution to the polarised proton PDF:

- $B = N \to$ active, $M = \rho \to$ spectator

$$\delta g_1^{q/N\rho}(x) = \delta A^{q/N\rho}_{++,++}(x) - \delta A^{q/N\rho}_{+-,+-}(x) = \int_x^1 \frac{\mathrm{d}y_B}{y_B} \int \frac{\mathrm{d}\mathbf{k}_{\perp B}}{16\pi^3}$$
$$\times \sum_{\lambda_\rho} \Bigg[\Big[A^{q/N}_{++,++} \underbrace{\phi^{+(p,N\rho)}_{+\lambda_\rho} \left(\phi^{+(p,N\pi)}_{+\lambda_\rho}\right)^*}_{\left|\phi^{+(p,N\rho)}_{+\lambda_\rho}\right|^2} + \underbrace{A^{q/N}_{-+,-+}}_{A^{q/N}_{+-,+-}} \underbrace{\phi^{+(N,N\rho)}_{-\lambda_\rho} \left(\phi^{+(p,N\rho)}_{-\lambda_\rho}\right)^*}_{\left|\phi^{+(p,N\rho)}_{-\lambda_\rho}\right|^2} \Big]$$
$$- \Big[A^{q/N}_{+-,+-} \underbrace{\phi^{+(p,N\rho)}_{+\lambda_\rho} \left(\phi^{+(p,N\pi)}_{+\lambda_\rho}\right)^*}_{\left|\phi^{+(p,N\rho)}_{+\lambda_\rho}\right|^2} + \underbrace{A^{q/N}_{--,--}}_{A^{q/N}_{++,++}} \underbrace{\phi^{+(p,N\rho)}_{-\lambda_\rho} \left(\phi^{+(p,N\rho)}_{-\lambda_\rho}\right)^*}_{\left|\phi^{+(p,N\rho)}_{-\lambda_\rho}\right|^2} \Big] \Bigg] \tag{3.54}$$

$$= \int_x^1 \frac{\mathrm{d}y_B}{y_B} \int \frac{\mathrm{d}\mathbf{k}_{\perp B}}{16\pi^3} \sum_{\lambda_\rho} \Bigg[\left|(\phi^{+(p,N\rho)}_{+\lambda_\rho}\right|^2 \Big[\underbrace{A^{q/N}_{++,++} - A^{q/N}_{+-,+-}}_{g_1^{q/N}} \Big] \tag{3.55}$$
$$- \underbrace{\phi^{+(p,N\rho)}_{-\lambda_\rho} \left(\phi^{+(p,N\rho)}_{-\lambda_\rho}\right)^*}_{\left|(\phi^{+(p,N\rho)}_{-\lambda_\rho}\right|^2} \Big[\underbrace{A^{q/N}_{++,++} - A^{q/N}_{+-,+-}}_{g_1^{q/N}} \Big] \Bigg] \tag{3.56}$$

$$= \int_x^1 \frac{\mathrm{d}y_B}{y_B} g_1^{q/N}\left(\frac{x}{y_B}\right) \sum_{\lambda_\rho} \int \frac{\mathrm{d}\mathbf{p}_{\perp B}}{16\pi^3} \left[\left|(\phi^{+(p,N\rho)}_{+\lambda_\rho}\left(y_B, \mathbf{k}_{\perp B}\right)\right|^2 - \left|(\phi^{+(p,N\rho)}_{-\lambda_\rho}\left(y_B, \mathbf{k}_{\perp B}\right)\right|^2 \right]. \tag{3.57}$$

- $M = \rho \to$ active, $B = N \to$ spectator

$$\begin{aligned}\delta g_1^{q/\rho N}(x) &= \delta A^{q/\rho N}_{++,++}(x) - \delta A^{q/\rho N}_{+-,+-}(x) = \int_x^1 \frac{\mathrm{d}y_M}{y_M} \int \frac{\mathrm{d}\mathbf{k}_{\perp M}}{16\pi^3} \\ &\times \sum_{\lambda_N} \left[\left| (\phi^{+(p,N\rho)}_{\lambda_N 1} \right|^2 \Big[\underbrace{A^{q/\rho}_{1+,1+} - A^{q/\rho}_{1-,1-}}_{g_1^{q/\rho}} \Big] - \left| (\phi^{+(p,N\rho)}_{\lambda_N -1} \right|^2 \Big[\underbrace{A^{q/\rho}_{-1-,-1-} - A^{q/\rho}_{-1+,-1+}}_{g_1^{q/\rho}} \Big] \right] \\ &= \int_x^1 \frac{\mathrm{d}y_M}{y_M} \, g_1^{q/\rho}\left(\frac{x}{y_M}\right) \int \frac{\mathrm{d}\mathbf{k}_{\perp M}}{16\pi^3} \\ &\times \sum_{\lambda_N} \left[\left| (\phi^{+(p,N\rho)}_{\lambda_N 1}\left(1-y_M, -\mathbf{k}_{\perp M}\right) \right|^2 - \left| (\phi^{+(p,N\rho)}_{\lambda_N -1}\left(1-y_M, -\mathbf{k}_{\perp M}\right) \right|^2 \right].\end{aligned} \tag{3.58}$$

Finally, the contribution of the $N\rho$-fluctuation to the transversity reads

- $B = N \to$ active, $M = \rho \to$ spectator

$$\begin{aligned}\delta h_1^{q/N\rho}(x) &= \int_x^1 \frac{\mathrm{d}y_B}{y_B} \int \frac{\mathrm{d}\mathbf{k}_{\perp B}}{16\pi^3} \underbrace{A^{q/N}_{++,--}\left(\frac{x}{y_B}\right)}_{h_1^{q/N}\left(\frac{x}{y_B}\right)} \\ &\times \sum_{\lambda_\rho} \phi^{-(p,N\rho)}_{-\lambda_\rho}\left(y_B, \mathbf{k}_{\perp B}\right) \left(\phi^{+(p,N\rho)}_{+\lambda_\rho}\left(y_B, \mathbf{k}_{\perp B}\right)\right)^* \\ &= \int_x^1 \frac{\mathrm{d}y_B}{y_B} \int \frac{\mathrm{d}\mathbf{k}_{\perp B}}{16\pi^3} \, h_1^{q/N}\left(\frac{x}{y_B}\right) \sum_{\lambda_\rho} \phi^{-(p,N\rho)}_{-\lambda_\rho}\left(y_B, \mathbf{k}_{\perp B}\right) \left(\phi^{+(p,N\rho)}_{+\lambda_\rho}\left(y_B, \mathbf{k}_{\perp B}\right)\right)^*.\end{aligned} \tag{3.59}$$

- $M = \rho \to$ active, $B = N \to$ spectator

$$\begin{aligned}\delta A^{q/\rho N}_{++,--}(x) = \sum_{\lambda_N} \int_x^1 \frac{\mathrm{d}y_M}{y_M} \int \frac{\mathrm{d}\mathbf{k}_{\perp M}}{16\pi^3} \Big[& A^{q/\rho}_{1+,0-}\left(\frac{x}{y_M}\right) \phi^{-(p,\rho N)}_{0\lambda_N} \left(\phi^{+(p,\rho N)}_{1\lambda_N}\right)^* \\ & + A^{q/\rho}_{0+,-1-}\left(\frac{x}{y_M}\right) \phi^{-(p,\rho N)}_{-1\lambda_N} \left(\phi^{+(p,\rho N)}_{0\lambda_N}\right)^* \Big].\end{aligned} \tag{3.60}$$

Now we can use the following relation (parity invariance)

$$\begin{aligned}\phi^{+(p,\rho N)}_{\lambda_\rho \lambda_N} &= (-1)^{-\frac{1}{2}+\lambda_N+\lambda_\rho} \left(\phi^{-(p,\rho N)}_{-\lambda_\rho -\lambda_N}\right)^*, \\ \phi^{-(p,\rho N)}_{\lambda_\rho \lambda_N} &= (-1)^{\frac{1}{2}+\lambda_N+\lambda_\rho} \left(\phi^{+(p,\rho N)}_{-\lambda_\rho -\lambda_N}\right)^*\end{aligned} \tag{3.61}$$

and get

$$\sum_{\lambda_N} \phi^{-(p,\rho N)}_{-1\lambda_N} \left(\phi^{+(p,\rho N)}_{0\lambda_N}\right)^* = \sum_{\lambda_N} \phi^{-(p,\rho N)}_{0\lambda_N} \left(\phi^{+(p,\rho N)}_{1\lambda_N}\right)^*. \tag{3.62}$$

Thus

$$\begin{aligned}\delta h_1^{q/\rho N}(x) &= \delta A_{++,--}^{q/\rho N}(x) \\ &= \int_x^1 \frac{\mathrm{d}y_M}{y_M} \int \frac{\mathrm{d}\mathbf{k}_{\perp M}}{16\pi^3} \Big[\sqrt{2}\, h_1^{q/\rho}\left(\frac{x}{y_M}\right) \\ &\times \sum_{\lambda_N} \phi_{\lambda_N 0}^{-(p,\rho N)}(1-y_M, -\mathbf{p}_{\perp M}) \left(\phi_{\lambda_N 1}^{+(p,\rho N)}(1-y_M, -\mathbf{k}_{\perp M})\right)^* .\end{aligned} \tag{3.63}$$

Let us now summarize: The higher Fock state contribution to the different parton distribution functions of the proton can be written as the following convolutions:
• for the unpolarized PDF:

$$\delta f_1^{q/p}(x) = \sum_{B,M} \left[\int_x^1 \frac{dy}{y} f^{p/BM}(y)\, f_1^{q/B}\left(\frac{x}{y}\right) + \int_x^1 \frac{dy}{y} f^{p/MB}(y)\, f_1^{q/M}\left(\frac{x}{y}\right) \right] \tag{3.64}$$

with the splitting functions

$$f^{p/BM}(y) = f^{p/MB}(1-y) = \int \frac{d^2\mathbf{k}_\perp}{16\pi^3} \sum_{\lambda_B,\lambda_M} \left| \phi_{\lambda_B\lambda_M}^{\frac{1}{2}(p/BM)}(y, \mathbf{k}_\perp) \right|^2 . \tag{3.65}$$

When the ρ-meson is active there is an additional term in Eq. (3.64), namely

$$\sum_{B,\rho} \int_x^1 \frac{dy}{y} f_{LL}^{p/B\rho}(y) f_{1LL}\left(\frac{x}{y}\right), \tag{3.66}$$

with

$$f_{LL}^{p/B\rho}(y) = \sum_{\lambda_B} \Big[-\frac{1}{3} \left| \phi_{\lambda_B 1}^{+(p,N\rho)}(1-y, -\mathbf{k}_\perp) \right|^2 + \frac{2}{3} \left| \phi_{\lambda_B 0}^{+(p,N\rho)}(1-y, -\mathbf{k}_\perp) \right|^2 \tag{3.67}$$

$$- \frac{1}{3} \left| \phi_{\lambda_B -1}^{+(p,N\rho)}(1-y, -\mathbf{k}_\perp) \right|^2 \Big]. \tag{3.68}$$

The description of a nucleon as a sum of bare and BM Fock components is independent of whether the photon couples to the baryon or to the meson, so on general grounds the relation $f^{N/BM}(y) = f^{N/MB}(1-y)$ must hold. It simply means that when

a baryon which carries a momentum fraction y is struck by the photon, the remaining meson carries a momentum fraction $1-y$. Furthermore, this relation ensures charge conservation and momentum conservation automatically.

• for the longitudinally polarized PDF:

$$\delta g_1^{q/p}(x) = \sum_{B,M} \int_x^1 \frac{dy}{y} \Delta_L f^{p/BM}(y)\, g_1^{q/B}\left(\frac{x}{y}\right) + \sum_{B,\rho} \int_x^1 \frac{dy}{y} \Delta_L f^{p/\rho B}(y)\, g_1^{q/\rho}\left(\frac{x}{y}\right), \tag{3.69}$$

with the splitting functions

$$\Delta_L f^{p/BM}(y) = \int \frac{d^2\mathbf{k}_\perp}{16\pi^3} \sum_{\lambda_B \lambda_M} (-1)^{\frac{1}{2}-\lambda_B} \left|\phi^{\frac{1}{2}(p/BM)}_{\lambda_B \lambda_M}(y, \mathbf{k}_\perp)\right|^2, \tag{3.70}$$

$$\Delta_L f^{p/\rho B}(y) = \int \frac{d^2\mathbf{k}_\perp}{16\pi^3} \sum_{\lambda_B} \left[\left|\phi^{\frac{1}{2}(p/B\rho)}_{\lambda_B+1}(1-y, -\mathbf{k}_\perp)\right|^2 - \left|\phi^{\frac{1}{2}(p/B\rho)}_{\lambda_B-1}(1-y, -\mathbf{k}_\perp)\right|^2\right]. \tag{3.71}$$

• for the transversity:

$$\delta h_1^{q/p}(x) = \sum_{B,M} \int_x^1 \frac{dy}{y} \Delta_T f^{p/BM}(y)\, h_1^{q/B}\left(\frac{x}{y}\right) + \sum_{B,\rho} \int_x^1 \frac{dy}{y} \Delta_T f^{p/\rho B}(y)\, \sqrt{2} h_1^{q/\rho}\left(\frac{x}{y}\right), \tag{3.72}$$

with the splitting functions

$$\Delta_T f^{p/BM}(y) = \int \frac{d^2\mathbf{k}_\perp}{16\pi^3} \sum_{\lambda_M} \left[\phi^{-\frac{1}{2}(p/BM)}_{-\frac{1}{2}\lambda_M}(y, \mathbf{k}_\perp) \left(\phi^{\frac{1}{2}(p/BM)}_{\frac{1}{2}\lambda_M}(y, \mathbf{k}_\perp)\right)^*\right],$$

$$\Delta_T f^{p/\rho B}(y) = \int \frac{d^2\mathbf{k}_\perp}{16\pi^3} \sum_{\lambda_B} \left[\phi^{-\frac{1}{2}(p/BM)}_{\lambda_B 0}(1-y, -\mathbf{k}_\perp) \left(\phi^{\frac{1}{2}(p/B\rho)}_{\lambda_B+1}(1-y, -\mathbf{k}_\perp)\right)^*\right]. \tag{3.73}$$

In the convolution model an active meson (photon couples to the meson in the BM Fock component) with spin zero can only contribute to the unpolarised quark PDF f_1.

In the next section we present the model input and show explicitly the overlap formula for the baryonic and mesonic PDFs that appear in the convolution formula of Eqs. (3.64), (3.66), (3.69) and (3.72) respectively.

3.4 MODELING

We now specify the ingredients of the model calculation for the PDFs in the meson-cloud model. First of all, for the vertex function we use the results which have been explicitly derived in Refs. [56, 55] and are shown in App. H. These results were obtained using time-order perturbation theory (TOPT) in the infinite-momentum frame. In TOPT also intermediate particles are on their mass-shell. However, an additional off-shell dependence is introduced in the vertex function for the vector meson due to the derivative coupling. So, even using TOPT, we have a freedom on how to choose the meson energy in the vertex. In principle, there are two possible prescriptions:
A) $p_V^\mu = (E_V, \mathbf{p}_V)$, with the on-shell meson energy $E_V = \sqrt{m_V^2 + \mathbf{p}_V^2}$,
B) $p_V^\mu = (E_V, \mathbf{p}_V)$, with the off-shell meson energy $E_V = E_N - E_B$.
We will adopt the choice B), following the arguments of Ref. [59] to establish a correspondence between time-ordered perturbation theory in the infinite momentum frame and light-cone perturbation theory. The vertex functions, which we have defined in Eq. (3.12) read

- for the transition $p \to N\pi$

$$V^\mu_{\lambda_N,0}(p, N\pi) = i g_{pN\pi} \bar{u}\left(p_N, \lambda_N\right) \gamma_5 u\left(p_p, \mu\right), \tag{3.74}$$

- for the transition $p \to N\rho$

$$\begin{aligned} V^\mu_{\lambda_N,\lambda_M}(p, N\rho) = {} & g_{pN\rho}\, \bar{u}\left(p_N, \lambda_N\right) \gamma_\mu u\left(p_p, \mu\right) \epsilon^*_\mu(p_M, \lambda_V) \\ & - \frac{f_{NN\rho}}{2M_N}\, \bar{u}\left(p_N, \lambda_N\right) i\sigma^{\mu\nu} u\left(p_p, \mu\right) \epsilon^*_\mu(p_M, \lambda_V) p_{M\nu}. \end{aligned} \tag{3.75}$$

Furthermore, because of the extended structure of the hadrons involved, one has also to multiply the coupling constant for point-like particles in the vertex function by phenomenological vertex form factors. These form factors parametrize the unknown microscopic effects at the vertex and have to obey the constraint $F_{NBM}(y, k_\perp^2) = F_{NBM}(1-y, k_\perp^2)$ to ensure basic properties like charge and momentum conservation simultaneously [60]. To this aim we will use the following functional form

$$F_{NBM}(y, k_\perp^2) = \exp\left[\frac{M_N^2 - M_{BM}^2}{2\Lambda_{BM}^2}\right], \tag{3.76}$$

where Λ_{BM} is a cut-off parameter. Following the recent analysis of Refs. [61, 62], we take $\Lambda_{BM} = 0.8$ GeV for all the baryon-meson fluctuations entering our calculation. For the NBM coupling constants at the interaction vertex we used the numerical values

given in Refs. [63, 64], i.e. $g^2_{NN\pi}/4\pi = 13.6$, $g^2_{NN\rho}/4\pi = 0.84$ and $f_{NN\rho} = 6.1 g_{NN\rho}$[7]. With this choice of the parameters in the case of the $p \to N\pi$ and $p \to N\rho$ transitions one finds

$$P_{p/N\pi} = P_{p/p\pi^0} + P_{p/n\pi^+} = 3P_{p/p\pi^0} = 13.17\%, \tag{3.77}$$

$$P_{p/N\rho} = P_{p/p\rho^0} + P_{p/n\rho^+} = 3P_{p/p\rho^0} = 2.17\%. \tag{3.78}$$

For the hadron states of the bare nucleon and baryon-meson components in Eq. (3.13) we adopt the light-front constituent quark model of Ref. [55], that we briefly summarize here for convenience. A hadron state with momentum $\tilde{p}$ and helicity μ is given by

$$|H : \tilde{p}_H, \mu\rangle = \sum_{q_i,\lambda_i} \int \left[\frac{\mathrm{d}x}{\sqrt{x}}\right]_N [\mathrm{d}^2\mathbf{k}_\perp]_N \Psi^{[H]\mu;q_1\ldots q_N}_{\lambda_1\ldots\lambda_N}(\{\tilde{k}_i\}_{i=1,\ldots,N}) \prod_{i=1}^{N} |x_i p^+_H,\, \mathbf{p}_{i\perp}, \lambda_i, q_i\rangle\,, \tag{3.79}$$

where[8] $\Psi^{[H]\mu;q_1\ldots q_N}_{\lambda_1\ldots\lambda_N}(\{x_i, \mathbf{k}_{i\perp}\})$ is the LCWF which gives the probability amplitude for finding in the hadron with a light-front helicity μ, N partons with momenta $(x_i p^+_H, \mathbf{p}_{i\perp} = \mathbf{k}_{i\perp} + x_i \mathbf{p}_{\perp H})$ with x_i being the longitudinal momentum fraction of the i-th parton with respect to its parent hadron (the index i runs from 1 to N) and $\mathbf{k}_{i\perp}$ being the parton intrinsic transverse momentum. The index λ_i labels the (LC-)helicity and q_i the isospin of the i-th parton, respectively. In Eq. (3.79) and in the following, the integration measures are defined by

$$\left[\frac{\mathrm{d}x}{\sqrt{x}}\right]_N = \left(\prod_{i=1}^{N} \frac{\mathrm{d}x_i}{\sqrt{x_i}}\right) \delta\left(1 - \sum_{i=1}^{N} x_i\right), \tag{3.80}$$

$$\left[\mathrm{d}^2\mathbf{k}_\perp\right]_N = \frac{1}{(16\pi^3)^{N-1}} \left(\prod_{i=1}^{N} \mathrm{d}^2\mathbf{k}_{\perp i}\right) \delta\left(\sum_{i=1}^{N} \mathbf{k}_{\perp i}\right). \tag{3.81}$$

For valence Fock state components one has $N = 3$ and $N = 2$ for the baryon and meson, respectively. As explained in Ref. [66], the wave function $\Psi^{[H]\mu;q_1\ldots q_N}_{\lambda_1\ldots\lambda_N}$ can be obtained by transforming the ordinary equal-time (instant-form) wave function into one appropriate for front form. The instant-form wave function[9] $\Psi^{[H]c;q_1\ldots q_N}_{\mu_1\ldots\mu_N}$ is constructed as the product of a momentum wave function $\tilde{\psi}^{[H]}(\{\tilde{k}_i\})$, which is spherically symmetric and invariant under permutations, and a spin-isospin wave function $\phi^{[H]}(\{\mu_i\}, \{q_i\})$, which is uniquely determined by $SU(6)$-spin-flavor-symmetry requirements, i.e.

$$\Psi^{[H]c;q_1\ldots q_N}_{\mu_1\ldots\mu_N}(\{\tilde{k}_i\}) = \tilde{\psi}^{[H]}(\{\tilde{k}_i\}) \otimes \phi^{[H]}(\{\mu_i\}, \{q_i\})\,. \tag{3.82}$$

[7] Note that we follow Ref. [55] for the vertex interaction, where the coupling constant $f_{NN\rho}$ is dimensionless. In order to compare with the definition adopted in Refs. [65], $f_{NN\rho}$ has to be multiplied by a factor $4M_N$.

[8] We change the notation for the LCWF to a form which is very convenient to what follows.

[9] μ_i is the label for the "canonical" helicity of the i-th parton in the equal-time quantization.

The transformation to the front form is essentially accomplished by a Melosh-rotation, which acts on the particle spin

$$\Psi^{[H]\mu;\{q_i\}}_{\{\lambda_i\}}\left(\{x_i,\mathbf{k}_{\perp i}\}\right)=\tilde{\psi}^{[H]}\left(\{\tilde{k}_i\}\right)\sum_{\mu_1,\ldots,\mu_N}\phi^{[H]}\left(\{\mu_i\},\{q_i\}\right)\prod_{i=1}^{N}D^{1/2\,*}_{\mu_i\lambda_i}(R_{cf}(\tilde{k}_i)), \quad (3.83)$$

where $D^{1/2\,*}_{\mu_i\lambda_i}(R_{cf}(\tilde{k}_i))$ are the Wigner rotations matrices defined in Ref. [66].

In the case of the nucleon we adopt the momentum wave function of Ref. [67], which reads

$$\tilde{\psi}^{[N]}(\{\tilde{k}_i\}_{i=1,3})=16\pi^3\left[\frac{1}{M_0}\frac{\omega_1\omega_2\omega_3}{x_1x_2x_3}\right]^{1/2}\frac{N'}{(M_0^2+\beta^2)^{\gamma}}, \quad (3.84)$$

where $\omega_i=\sqrt{m_q^2+\mathbf{k}_i^2}$ is the energy of the i-th quark, $M_0=\sum_i\omega_i$ is the invariant mass of the system of N non-interacting quarks and N' is a normalization factor such that $\int d[x]_3 d[\mathbf{k}_\perp]_3|\psi(\{\tilde{k}_i\}_{i=1,2,3})|^2=1$. In Eq. (3.84), the scale β, the parameter γ for the power-law behavior, and the quark mass m_q are taken from the fit to the nucleon form factor of Ref. [68], i.e. $\gamma=3.21$, $\beta=0.489$ GeV and $m_q=0.264$ GeV.

The canonical wave function of the pion is taken from Ref. [69] and reads

$$\tilde{\psi}^{[\pi]}(\bar{x},\mathbf{k}_\perp)=[16\pi^3]^{1/2}\left[\frac{M_0}{4\bar{x}(1-\bar{x})}\right]^{1/2}\frac{i}{\pi^{3/4}\alpha^{3/2}}\exp\left[-k^2/(2\alpha^2)\right], \quad (3.85)$$

with $\mathbf{k}=\mathbf{k}_1=-\mathbf{k}_2$, $\bar{x}=x_1=1-x_2$ and the two parameters $\alpha=0.3124$ GeV and $m_q=0.25$ GeV fitted to the pion form factor data. The wave function of the ρ differs from the pion only in the spin part, with the canonical spin states of the $q\bar{q}$ pair coupled to $J=1$ instead of $J=0$.

We refer to the momentum wave functions of Eqs. (3.84)-(3.85), that were obtained adapting an analytical ansatz fitted to nucleon/pion form factors, as *model 1*. In addition we also use momentum wave functions that were obtained within a relativistic constituent quark model (CQM) by solving an eigenvalue equation for the mass operator. We refer to those LCWFs as *model 2*. The mass operator of the particular model we use has a hypercentral confining force and is given by [70]

$$M=\sum_{i=1}^{3}\sqrt{\mathbf{k}_i^2+m_i^2}-\frac{\tau}{y}+\kappa_l y, \quad (3.86)$$

with τ and κ_l being two parameters, $\sum_i\mathbf{k}_i=0$, $y=\sqrt{\boldsymbol{\rho}^2+\boldsymbol{\lambda}^2}$ is the radius of the hypersphere in six dimensions and $\boldsymbol{\rho}$ and $\boldsymbol{\lambda}$ are the Jacobi coordinates. The solutions have the general form of Eq. (3.82) with the momentum wave function (total orbital

angular momentum $L = 0$) [66]

$$\tilde{\psi}^{[N]}(\{\tilde{k}_i\}_{i=1,3}) = \psi_{00}(\tilde{y}) Y^{(0,0)}_{[0,0,0]}(\Omega)\,. \tag{3.87}$$

The solution of the the mass operator is the hyperradial wave function denoted by $\Psi_{\gamma,\nu}(\tilde{y})$. The function $Y^{(0,0)}_{[0,0,0]}$ is the hyperspherical harmonics defined on the hypersphere of unit radius.

The light-front formalism allows us to obtain a convenient representation of the hadron PDFs in terms of overlap of LCWFs. Labeling the active quark with $i = 1$, the hadron light-front helicity amplitudes introduced in Sec. 3.3.1.2 can be obtained as

$$A^{q/H}_{\mu'\lambda',\mu\lambda} = \int d[1\ldots N] \sum_{\lambda_2,\ldots,\lambda_N} \sum_{q_1\cdots q_N} \left(\psi^{[H]\mu';q_1\ldots q_N}_{\lambda'\lambda_2\ldots\lambda_N}\right)^* \psi^{[H]\mu;q_1\ldots q_N}_{\lambda\lambda_2\ldots\lambda_N}, \tag{3.88}$$

For $N = 3$

$$d[123] = [dx]_3 [d^2\mathbf{k}_\perp]_3\, 3\, \delta(x - x_1), \tag{3.89}$$

and for $N = 2$

$$d[12] = [dx]_2 [d^2\mathbf{k}_\perp]_2\, \delta(x - x_1) = \frac{\mathrm{d}x}{\sqrt{x(1-x)}} \frac{\mathrm{d}^2\mathbf{k}_\perp}{2(2\pi)^3}. \tag{3.90}$$

From the relations in Eq. (3.31) we then find the following LCWF overlap representation for the contribution of the $3q$ Fock state to the proton PDFs

$$\begin{aligned}
f_1^{q/p} &= \int \mathrm{d}[123] \sum_{\lambda_2\lambda_3} \sum_{q_2 q_3} \left[\left|\Psi^{[p]+;qq_2q_3}_{+\lambda_2\lambda_3}\right|^2 + \left|\Psi^{[p]+;qq_2q_3}_{-\lambda_2\lambda_3}\right|^2 \right], \\
g_1^{q/p} &= \int \mathrm{d}[123] \sum_{\lambda_2\lambda_3} \sum_{q_2 q_3} \left[\left|\Psi^{[p]+;qq_2q_3}_{+\lambda_2\lambda_3}\right|^2 - \left|\Psi^{[p]+;qq_2q_3}_{-\lambda_2\lambda_3}\right|^2 \right], \\
h_1^{q/p} &= \int \mathrm{d}[123] \sum_{\lambda_2\lambda_3} \sum_{q_2 q_3} \left(\Psi^{[p]+;qq_2q_3}_{+\lambda_2\lambda_3}\right)^* \Psi^{[p]-;qq_2q_3}_{-\lambda_2\lambda_3}.
\end{aligned} \tag{3.91}$$

The spin-/isospin part of the LCWF of Eq. (3.83) leads to the following result in Eq. (3.91) [71]

- $f_1^{q/p}$: iso,
- $g_1^{q/p}$: $iso\, \frac{\left(m_q + x_3 M_0\right)^2 - \mathbf{k}^2_{3\perp}}{\left(m_q + x_3 M_0\right)^2 + \mathbf{k}^2_{3\perp}}$,
- $h_1^{q/p}$: $iso \frac{\left(m_q + x_3 M_0\right)^2}{\left(m_q + x_3 M_0\right)^2 + \mathbf{k}^2_{3\perp}}$,

where $iso = 2(1)$ in $f_1^{q/p}$ for $q = u(d)$ and $iso = \frac{4}{3}\left(-\frac{1}{3}\right)$ in $g_1^{q/p}$ and $h_1^{q/p}$ for $q = u(d)$, respectively.

Analogously the contribution of the $q\bar{q}$ Fock state to the pion PDF reads

$$f_1^{q/\pi}(x) = f_1^{\bar{q}/\pi}(x) = \int \mathrm{d}[12] \sum_{\lambda_2} \left[\left| \Psi^{[\pi];q\bar{q}}_{+\lambda_2} \right|^2 + \left| \Psi^{[\pi];q\bar{q}}_{-\lambda_2} \right|^2 \right], \tag{3.92}$$

where $f^{q/\pi} = f^{q/\pi^+}$ refers to the parton distribution in the charged pion π^+, while the other PDFs can be obtained by isospin symmetry and charge symmetry, i.e. $f^{u/\pi^+} = f^{\bar{d}/\pi^+} = f^{d/\pi^-} = f^{\bar{u}/\pi^-} = 2f^{u/\pi^0} = 2f^{\bar{u}/\pi^0} = 2f^{d/\pi^0} = 2f^{\bar{d}/\pi^0}$.

Using the relations in Eq. (3.33) for the vector meson, we also obtain the following LCWF overlap representation for the contribution of the $q\bar{q}$ Fock state to the PDFs of the ρ meson

$$\begin{aligned}
f_1^{q/\rho}(x) &= f_1^{\bar{q}/\rho}(x) = \frac{2}{3} \int \mathrm{d}[12] \sum_{\lambda_2} \left[\left| \Psi^{[\rho]0;q\bar{q}}_{+\lambda_2} \right|^2 + \left| \Psi^{[\rho]+1;q\bar{q}}_{+\lambda_2} \right|^2 + \left| \Psi^{[\rho]+1;q\bar{q}}_{-\lambda_2} \right|^2 \right], \\
f_{1LL}^{q/\rho}(x) &= f_{1LL}^{\bar{q}/\rho}(x) = \int \mathrm{d}[12] \sum_{\lambda_2} \left[2\left| \Psi^{[\rho]0;q\bar{q}}_{+\lambda_2} \right|^2 - \left| \Psi^{[\rho]+1;q\bar{q}}_{+\lambda_2} \right|^2 - \left| \Psi^{[\rho]+1;q\bar{q}}_{-\lambda_2} \right|^2 \right], \\
g_1^{q/\rho}(x) &= g_1^{\bar{q}/\rho}(x) = \int \mathrm{d}[12] \sum_{\lambda_2} \left[\left| \Psi^{[\rho]+1;q\bar{q}}_{+\lambda_2} \right|^2 - \left| \Psi^{[\rho]+1;q\bar{q}}_{-\lambda_2} \right|^2 \right], \\
h_1^{q/\rho}(x) &= h_1^{\bar{q}/\rho}(x) = \frac{1}{\sqrt{2}} \int \mathrm{d}[12] \sum_{\lambda_2} \left[\Psi^{[\rho]0;q\bar{q}}_{-\lambda_2} \left(\Psi^{[\rho]+1;q\bar{q}}_{+\lambda_2} \right)^* + \Psi^{[\rho]-1;q\bar{q}}_{-\lambda_2} \left(\Psi^{[\rho]0;q\bar{q}}_{+\lambda_2} \right)^* \right].
\end{aligned} \tag{3.93}$$

Writing $j^{q/\rho} = j^{q/\rho^+}$ for the generic PDF j in the charged ρ meson ρ^+, the other PDFs can be obtained by isospin symmetry, i.e. $j^{u/\rho^+} = j^{\bar{d}/\rho^+} = j^{d/\rho^-} = j^{\bar{u}/\rho^-} = 2j^{u/\rho^0} = 2j^{\bar{u}/\rho^0} = 2j^{d/\rho^0} = 2j^{\bar{d}/\rho^0}$. The result of the Melosh-rotation in the different helicity amplitudes is given by

- $A^{q/\rho}_{1+,1+}$: $N_1 N_2 \left[\left(m_q + x_2 M_0 \right)^2 + \mathbf{k}_{\perp 2}^2 \right] \left(m_q + x_1 M_0 \right)^2$,
- $A^{q/\rho}_{-1-,-1-}$: equal to $A^{q/\rho}_{1+,1+}$,
- $A^{q/\rho}_{1-,1-}$: $N_1 N_2 \left[\left(m_q + x_2 M_0 \right)^2 + \mathbf{k}_{\perp 2}^2 \right] \mathbf{k}_{\perp 1}^2$,
- $A^{q/\rho}_{-1+,-1+}$: equal to $A^{q/\rho}_{1-,1-}$,
- $A^{q/\rho}_{0\pm,0\pm}$: $N_1 N_2 \frac{1}{2} \left[\left(m_q + x_2 M_0 \right)^2 + \mathbf{k}_{\perp 2}^2 \right] \left[\left(m_q + x_1 M_0 \right)^2 + \mathbf{k}_{\perp 1}^2 \right]$,
- $A^{q/\rho}_{1+,0-}$: $N_1 N_2 \frac{1}{\sqrt{2}} \left[\left(m_q + x_2 M_0 \right)^2 + \mathbf{k}_{\perp 2}^2 \right] \left[m_q + x_1 M_0 \right]^2$,
- $A^{q/\rho}_{0+,-1-}$: equal to $A^{q/\rho}_{1+,0-}$,

with the common prefactors N_1 and N_2 defined by

$$N_1 = \left[\left(m_q + x_1 M_0 \right)^2 + \mathbf{k}_{\perp 1}^2 \right]^{-1} \quad \text{and} \quad N_2 = \left[\left(m_q + x_2 M_0 \right)^2 + \mathbf{k}_{\perp 2}^2 \right]^{-1}. \tag{3.94}$$

3.5 Results

Before we discuss our results, we have to turn to the subject of finding the initial scale where our model calculations are valid. At the lowest hadronic scale μ_0^2 the bare nucleon is described by the valence quark model which we discussed in Sec. 3.4. When we include the meson cloud, the partonic content of the nucleon will be renormalized and a new scale $Q_0^2 > \mu_0^2$ must be defined. The scale Q_0^2 which depends on the partonic content we include is a priori not known. We now address the procedure how to obtain the initial scale Q_0^2: we calculate the second moment of the unpolarised PDF, i.e.[10] $\langle u_V(x, Q_0^2) + d_V(x, Q_0^2)\rangle_2$. Then we evolve back experimental data of the unpolarised valence PDF (at leading order) until it matches the value dictated by our model. Our model gives $\langle u_V(x, Q_0^2) + d_V(x, Q_0^2)\rangle_2 = 0.35$ which leads to $Q_0^2 = 0.19$ GeV^2.
Before we proceed to present our result we list the ingredients necessary for the calculation of the initial scale. It is convenient to discuss the evolution equations in the Mellin space, i.e. to consider the moments $\langle f(x, Q^2)\rangle_N$. The flavor non-singlet (NS) evolution equation of the valence PDF (at LO) reads [62]

$$\left.\frac{\langle q_{NS}(Q^2)\rangle_N}{\langle q_{NS}(Q_0^2)\rangle_N}\right|_{LO} = \left(\frac{\alpha_s(Q^2)}{\alpha_s(Q_0^2)}\right)^{\frac{P_{NS}^{(0)}(N)}{\beta_0}}, \tag{3.95}$$

with

- the strong coupling $\alpha_s(Q^2)$, for which we use the one-loop expression, i.e.

$$\alpha(Q^2) = \frac{4\pi}{(11 - \frac{2}{3}n_f(Q^2))\ln(Q^2/\Lambda_{QCD}^2)}, \tag{3.96}$$

  where $n_f(Q^2)$ is the number of quarks with $m_{quark}^2 < |Q^2|$ and the values of Λ_{QCD} are listed in footnote 11.

- $\beta_0 = 11 - \frac{2n_f}{3}$ is the lowest expansion coefficient of the QCD beta function

$$\beta_{N^mLO}(\alpha_s) = -\sum_{k=2}^{m} \beta_k \alpha_s^{k+2}. \tag{3.97}$$

- The N-th moment of the LO-NS-splitting function $P_{NS}^{(0)}(N)$ has the following form (see Ref. [72] for example)

$$P_{NS}^{(0)}(N) = \frac{8}{3}\Big[1 - \frac{2}{N(N+1)} + 4\sum_{j=2}^{N}\frac{1}{j}\Big]. \tag{3.98}$$

The evolution in the scale has been accomplished by modifying[11] the numerical procedures of Refs. [73, 74, 75].

[10] Using the notation $\langle f(x)\rangle_N = \int \mathrm{d}x x^{N-1} f(x)$.
[11] Modified to include the variable flavor-number scheme with heavy-quark mass thresholds

We now show our model calculations for the leading twist PDFs of the proton (valence and sea contributions), compare them with extractions from the experiment, discuss flavor asymmetries in the unpolarised and polarized sea and present our results for the tensor charge.

3.5.1 *Unpolarized quark PDF*

The unpolarised PDF f_1 is known with a very good precision. Many data exist to obtain PDF fits with a good accuracy, i.e. with small error bands. It is therefore very instructive to test how well our model calculation works for f_1 in order to be confident about the validity in the case of g_1 and in particular of h_1 where theoretical and experimental uncertainties are an issue. In Figs. 3.3-3.4 we show the valence part and the sea part of $xf_1(x)$, for both u-flavor and d-flavor, at the initial model scale $Q_0^2 = 0.19$ GeV^2 (dotted curves) and evolved to the scale $Q^2 = 2.4$ GeV^2 (solid curves). The differences between *model 1* and *model 2* for the valence f_1 are more pronounced at the initial scale. If we increase the scale the differences between the two model calculations become much smaller and we observe a good agreement with the PDF parametrization of Ref. [76]. We note, however, that the peak position of the up-distribution is at smaller values of x as compared to the peak position of the PDF parametrization and that the fall-off at larger values of x is better reproduced with *model 2*. For the down-distribution the peak position as well as the behavior at larger values of x is well reproduced with both models. The differences[12] of *model 1* and *model 2* for the unpolarised antiquark PDFs are so small that we decided to show only the result for *model 1*. With respect to the PDF parametrization of Ref. [76] the magnitude of the sea at intermediate values of x is smaller.

The cutoff dependence of the results has also been studied. Even in the case of the well investigated pion-nucleon coupling the cutoff parameter ranges from $\Lambda = 0.5$ GeV to $\Lambda = 1.3$ GeV [77]. With our model a cutoff of $\Lambda = 1.3$ GeV would lead to negative values of the unpolarized PDF, therefore we choose as an upper bound for the cutoff the value $\Lambda = 1.1$ GeV. In Fig. 3.5 we plot the cutoff dependence of $xf_1^{u_V/p}(x)$ and $xf_1^{\bar{u}/p}(x)$ (similar figures are obtained for d-flavor) for *model 1*. We observe that a larger cutoff shifts the peak of the valence distribution to smaller values of x and that the $x \to 1$ tail falls off stronger than the PDF-parameterization Ref. [76]. The sea distribution seems not to have a strong dependence on the choice of the cutoff.

$m_c = 1.4$ GeV, $m_t = 4.75$ GeV and $m_t = 175$ GeV. $\alpha_s(M_z) = 0.13939$ and, depending on the number of flavors n_f, $\Lambda_{QCD}(n_f)$ is $\Lambda_{QCD}(3) = 359$ MeV, $\Lambda_{QCD}(4) = 322$ MeV, $\Lambda_{QCD}(5) = 255$ MeV and $\Lambda_{QCD}(6) = 137$ MeV.

[12] At the initial scale the sea-quark distributions are the same in both models as they are generated by the antiquarks of the π and the ρ. After the LO-evolution the difference between the two models for the unpolarized seq-quark distributions is practically indistinguishable in the plot.

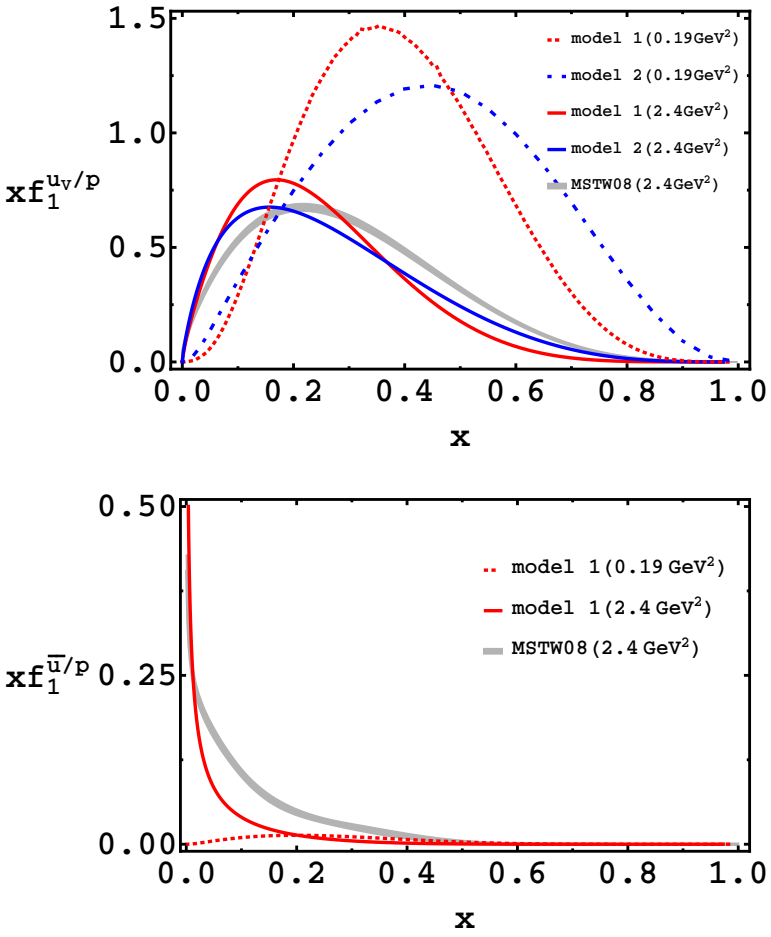

Figure 3.3: Unpolarised u-valence distribution (upper panel) and sea distribution (lower panel) using two different types of LCWFs as explained in the main text. The different scales are as indicated ($Q_0^2 = 0.19$ GeV^2 and $Q^2 = 2.4$ GeV^2). The gray band corresponds to the PDF parameterization of Ref. [76] at $Q^2 = 2.4$ GeV^2.

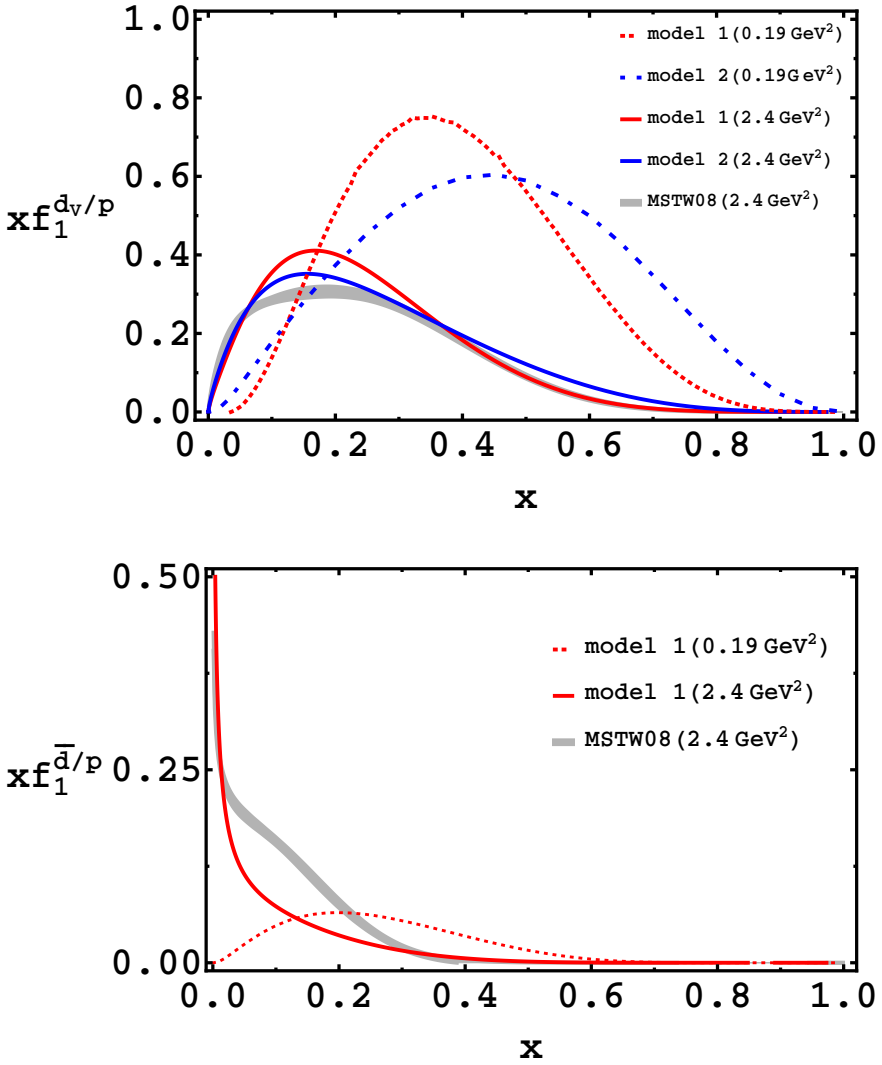

Figure 3.4: Unpolarised d-valence distribution (upper panel) and sea distribution (lower panel) using two different types of LCWFs as explained in the main text. The different scales are as indicated ($Q_0^2 = 0.19$ GeV^2 and $Q^2 = 2.4$ GeV^2). The gray band corresponds to the PDF parameterization of Ref. [76] at $Q^2 = 2.4$ GeV^2.

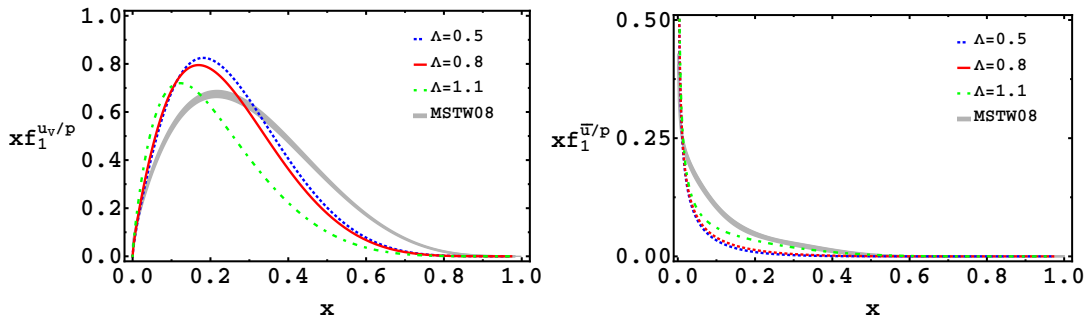

Figure 3.5: The cutoff dependence of the unpolarized u-valence distribution in the range $\Lambda = 0.5 - 1.1$ GeV (left panel) and the corresponding sea distribution (right panel) at $Q^2 = 2.4$ GeV^2. The gray band corresponds to the PDF parameterization of Ref. [76] at $Q^2 = 2.4$ GeV^2.

3.5.2 *Polarized quark PDF*

In Figs. 3.6-3.7 we plot our results for the (longitudinally) polarized PDF $xg_1(x)$ at $Q_0^2 = 0.19$ Gev^2 and $Q^2 = 2.4$ Gev^2 . Since we perform the scale evolution at LO, we can only compare our results to parameterizations of g_1 which are done at LO. The most recent parameterizations are all done at NLO, so we have to choose an older PDF set such as the one of Ref. [78]. We observe here that the agreement with our model calculation and the PDF parametrization is not as good as in the case of the unpolarised PDF. In particular the disagreement becomes most pronounced in the case of the the sea contributions to g_1: Especially we find that the qualitative behavior of our result for $xg_1^{\bar{u}/p}(x)$ and $xg_1^{\bar{d}/p}(x)$ is very different from the parameterization of Ref. [78] we compare with. Additionally we compare our model calculations for the valence and the sea part with experimental data from COMPASS [79], cf. Fig. 3.8. As we mentioned above the error bars for g_1 are much larger than for f_1, as there are not so much accurate data available. Our predictions of the valence g_1 are in fair agreement with the experiment but the huge error bars in the experimental data do not allow definite conclusions about the quantitative behavior of the sea contribution to g_1. Experimental data for the polarized d-sea (see lower right panel of Fig. 3.8) are afflicted by large error bars, but tend towards a small negative value, whereas our predictions are very small and positive. The PDF parameterization of Ref. [78] provides a small negative value of $xg_1^{\bar{u}/p}(x)$ at small x, see Fig. 3.7.

The cutoff dependence for *model 1* and u-flavor is shown in Fig. 3.9. Increasing the value of the cutoff decreases $xg_1^{u_V/p}$ in value but leaves the peak position approximately constant. However, for $xg_1^{\bar{u}/p}$ larger values of the cutoff significantly alter the functional behavior of $xg_1^{\bar{u}/p}$ as compared to smaller values of the cutoff.

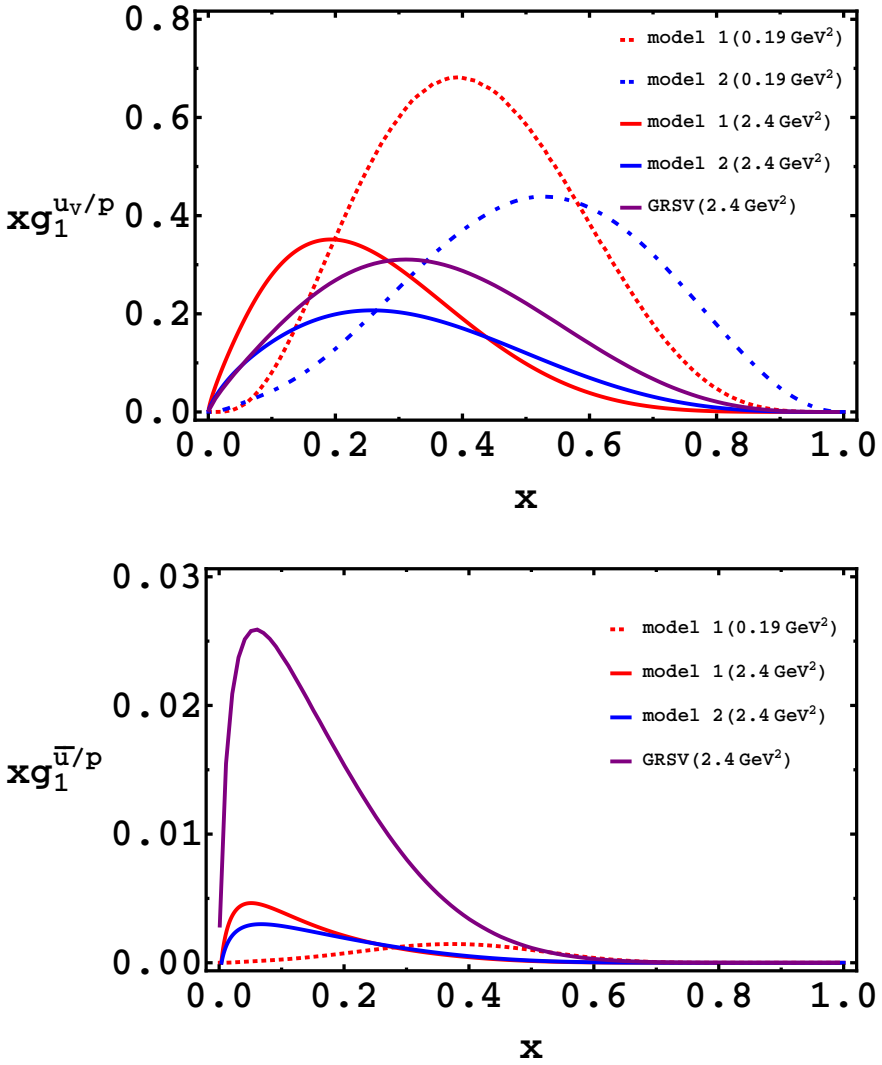

Figure 3.6: Polarized u-valence distribution (upper panel) and sea distribution (lower panel) using two different types of LCWFs as explained in the main text. The different scales are as indicated ($Q_0^2 = 0.19$ GeV^2 and $Q^2 = 2.4$ GeV^2). The solid purple line corresponds to the PDF parameterization of Ref. [78] at $Q^2 = 2.4$ GeV^2.

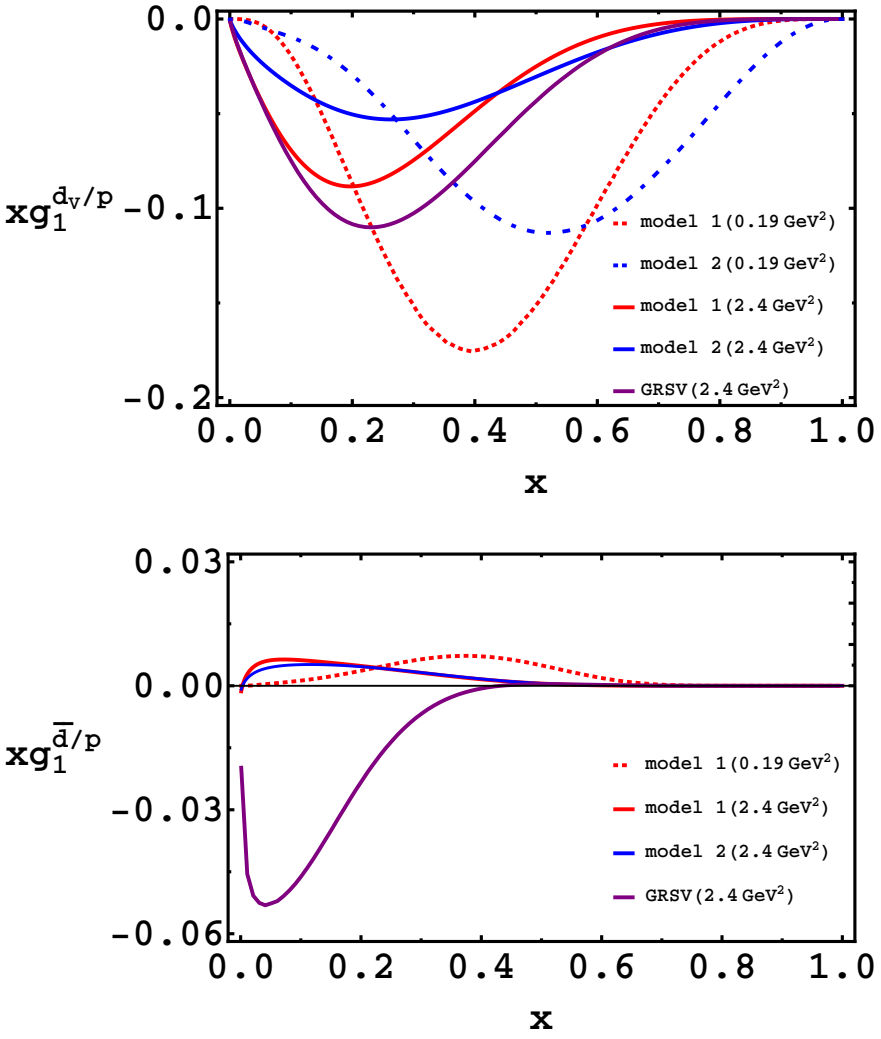

Figure 3.7: Polarized d-valence distribution (upper panel) and sea distribution (lower panel) using two different types of LCWFs as explained in the main text. The different scales are as indicated ($Q_0^2 = 0.19$ GeV^2 and $Q^2 = 2.4$ GeV^2). The solid purple line corresponds to the PDF set of Ref. [78].

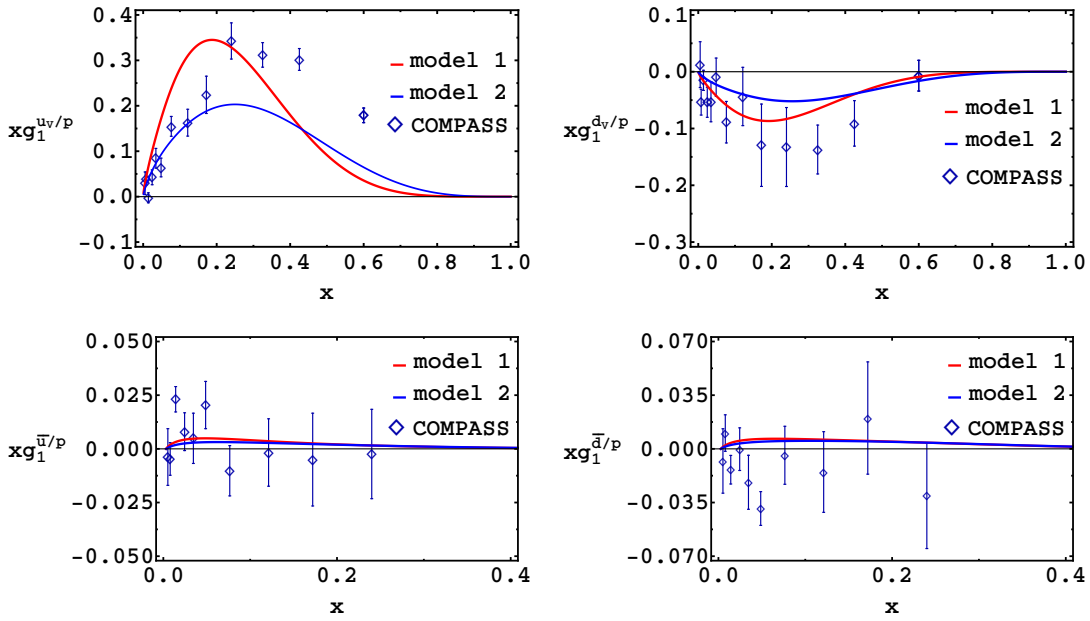

Figure 3.8: Comparison of our model calculation for the polarized PDF at a $Q^2 = 3.0$ GeV^2 with the experimental data taken from Ref. [79].

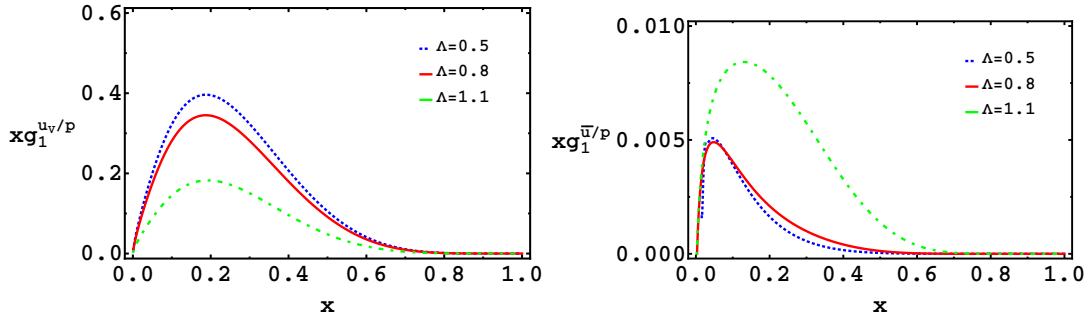

Figure 3.9: The cutoff dependence of the polarized u-valence distribution (left panel) in the range $\Lambda = 0.5 - 1.1$ GeV and the corresponding sea distribution (right panel) at $Q^2 = 3.0$ GeV^2.

3.5.3 *Flavor asymmetry in the nucleon sea*

We now discuss very briefly the topic of the flavor structure of the nucleon sea. We thereby focus on the breaking of the flavor symmetry $SU(2)_f$ in the light-quark sector. For a more detailed discussion on this topic (with an extension to breaking of $SU(3)_f$ we refer to Ref. [80].

The sea quarks in the nucleon are readily produced via the process shown in Fig. 3.10. Ignoring the small mass differences of the u- and d-quarks, the perturbatively produced sea is flavor symmetric, i.e. $\bar{u} = \bar{d}$. To explain a flavor asymmetry in the nucleon sea therefore requires a non-perturbative model[13].

[13]Strictly speaking also in perturbative QCD the flavor symmetry does not hold because the additional

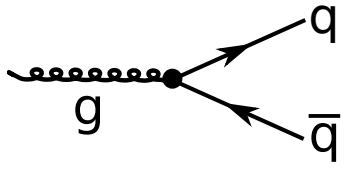

$$\bar{d}(x) = \bar{u}(x)$$

Figure 3.10: Perturbative production of the nucleon sea.

The first hint of $SU(2)_f$ breaking in the sea came from the Gottfried sum rule[14]

$$\begin{aligned}
&\int_0^1 \frac{\mathrm{d}x}{x}\Big[F_2^p(x) - F_2^n(x)\Big] \\
&= \sum_i e_i^2 \int_0^1 \mathrm{d}x\Big[q_i^p(x) + \bar{q}_i^p(x) - q_i^n(x) - \bar{q}_i^n\Big] \\
&= \frac{1}{3}\int_0^1 \mathrm{d}x\Big[u_v^p(x) - d_v^p(x)\Big] + \frac{2}{3}\int_0^1 \mathrm{d}x\Big[\bar{u}^p(x) - \bar{d}^p(x)\Big] \\
&= \frac{1}{3} + \frac{2}{3}\int_0^1 \mathrm{d}x\Big[\bar{u}^p(x) - \bar{d}^p(x)\Big].
\end{aligned} \tag{3.99}$$

In deriving Eq. (3.99) we used that $u^p(x) = d^n(x)$, $d^p(x) = u^n(x)$, $\bar{u}^p(x) = \bar{d}^n(x)$ and $\bar{d}^p(x) = \bar{u}^n(x)$. If the sea is flavor symmetric, the Gottfried sum rule value is equal to $\frac{1}{3}$. The new muon collaboration determined the Gottfried sum rule value to be 0.235 ± 0.026 at $Q^2 = 4$ GeV^2 [82, 83], which is significantly lower than $1/3$.
The *E*866/*NuSea* experiment [84] provides values for the unpolarised sea flavor asymmetry, namely for $f_1^{\bar{d}/p}(x) - f_1^{\bar{u}/p}(x)$ and $f_1^{\bar{d}/p}(x)/f_1^{\bar{u}/p}(x)$. In Figs. 3.11 and 3.12 we compare our results for $f_1^{\bar{d}/p}(x) - f_1^{\bar{u}/p}(x)$ and $f_1^{\bar{d}/p}(x)/f_1^{\bar{u}/p}(x)$, respectively, with the results from the *E*866/*NuSea* experiment.
Despite our simple model we observe a good agreement with the experimental data for $f_1^{\bar{d}/p}(x) - f_1^{\bar{u}/p}(x)$, however, the behavior $f_1^{\bar{d}/p}(x)/f_1^{\bar{u}/p}(x)$ for fairly large values of x is not well reproduced. However, as was pointed out in Ref. [80], all the different models have in common that they can describe the feature $\bar{d} > \bar{u}$ in the unpolarised sea very well, but fail to reproduce $f_1^{\bar{d}/p}(x)/f_1^{\bar{u}/p}(x)$ at larger values of x[15].
The large flavor asymmetry in the unpolarised sea naturally leads to the question whether the polarized sea is also asymmetric. We note right away that within our model this asymmetry cannot be very large, because only the rho fluctuation does contribute to the polarized sea and due to its large mass it is suppressed, see Eq. (3.14). Interestingly, although the different models can give a reasonable good explanation of the data of the $\bar{u}$- and $\bar{d}$-distributions, they tend to give different predictions on the sea in a (longitudinally) polarized nucleon. New data (with more precision as we will see in a moment) are therefore highly desirable to test the predictions of various models. Our estimate of the flavor asymmetry in the polarized sea is shown

u quark in the proton can lead to a suppression of $g \to u\bar{u}$ via Pauli-blocking [81]. NLO calculations later confirmed that the Pauli blocking cannot account for a sizable violation of the flavor symmetry in the sea.

[14] F_2 denotes the structure function in the standard analysis of DIS.

[15] Preliminary data from the $E-906$/*SeaQuest* collaboration show a better agreement with model calculation at larger x.

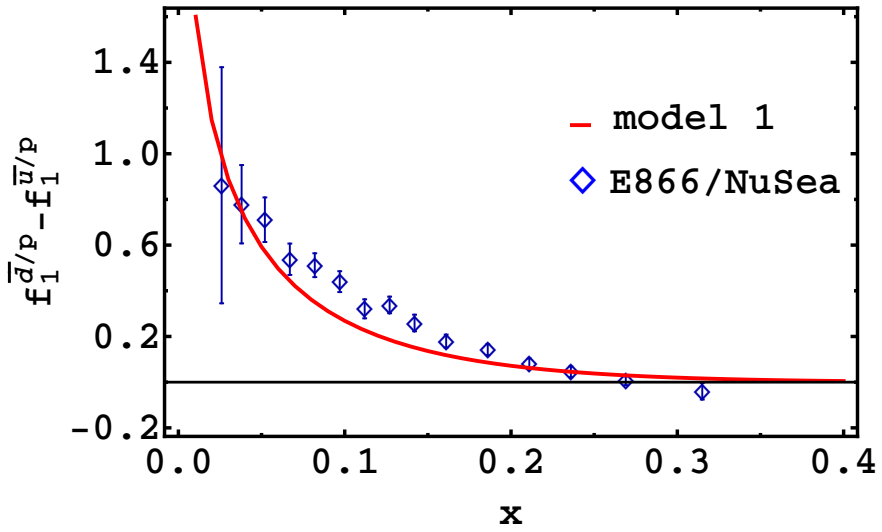

Figure 3.11: In this figure we show the $f_1^{\bar{d}/p}(x) - f_1^{\bar{u}/p}(x)$ distribution at the scale $Q^2 = 54\ \mathrm{GeV}^2$ in comparison to the experimental data taken from Ref. [84].

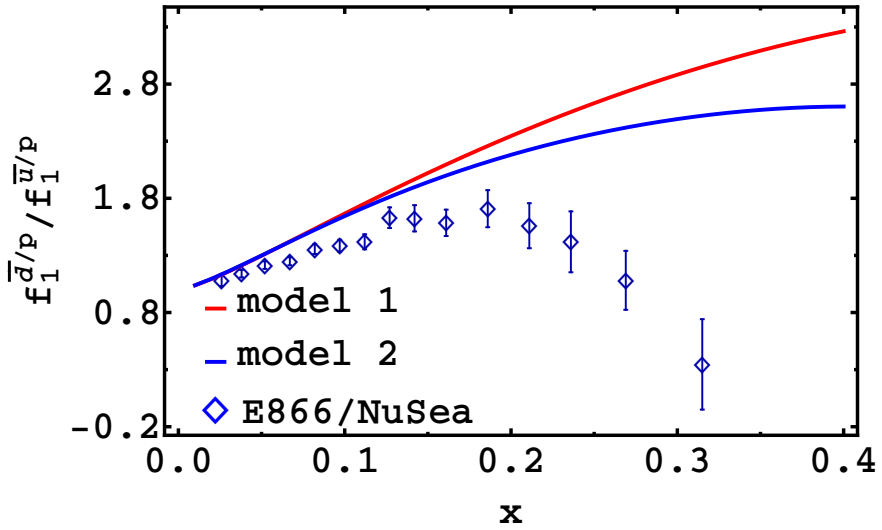

Figure 3.12: In this figure we show the $f_1^{\bar{d}/p}(x)/f_1^{\bar{u}/p}(x)$ distribution at the scale $Q^2 = 54\ \mathrm{GeV}^2$ in comparison to the experimental data taken from Ref. [84].

in Fig. 3.13. With our meson-cloud model we predict a small and negative value for $x\left(g_1^{\bar{u}/p}(x) - g_1^{\bar{d}/p}(x)\right)$. In Fig. 3.14 we compare our results with the experimental values from from COMPASS [79] and HERMES [85]. The accuracy of the data is limited, but the experiments seem to favor models which predict a small positive value.

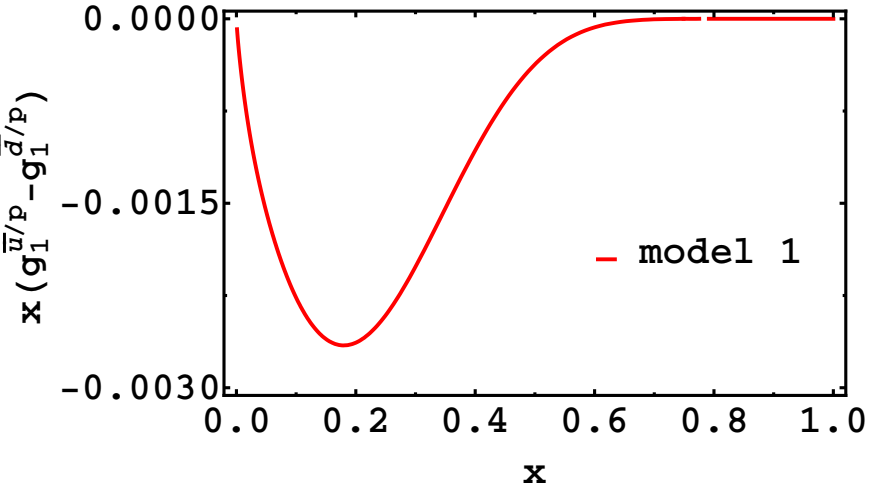

Figure 3.13: The flavor asymmetry of the polarized sea $x\left(g_1^{\bar{u}/p}(x) - g_1^{\bar{d}/p}(x)\right)$ at $Q^2 = 3.0\ \text{GeV}^2$ within our model.

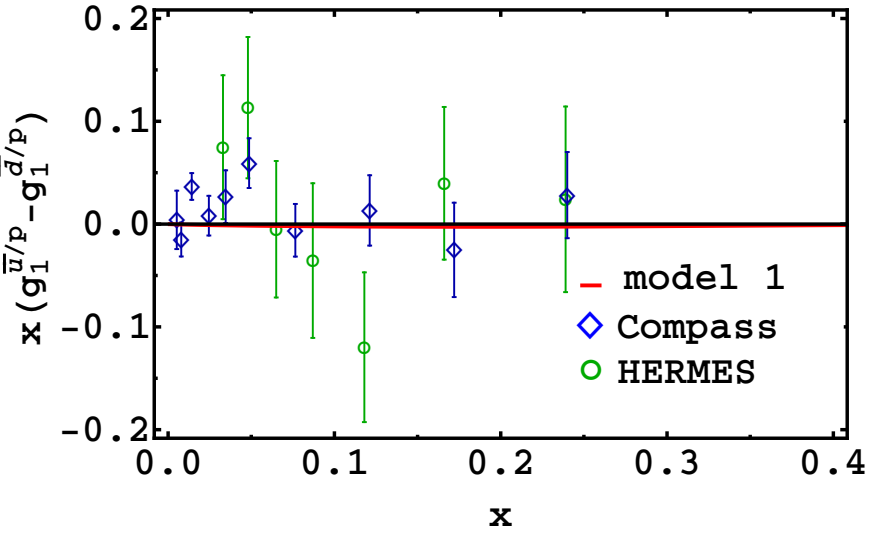

Figure 3.14: The flavor asymmetry of the polarized sea $x\left(g_1^{\bar{u}/p}(x) - g_1^{\bar{d}/p}(x)\right)$ within our model in comparison with the experimental data from COMPASS [79] and HERMES [85]. $Q^2 = 3.0\ \text{GeV}^2$.

3.5.4 *Transversity quark PDF*

We now discuss the third of the leading-twist quark distributions of the nucleon: The transversity distribution function. Due to its chiral-odd nature it involves a helicity flip of the struck quark. At leading twist it therefore decouples in DIS. It has to be coupled to another chiral-odd function to study it in a physical process such as in semi-inclusive DIS (SIDIS) or Drell-Yan processes. These processes involve at least another "soft" function such as a fragmentation function. Thus it is experimentally

very challenging to extract information about the transversity. We therefore also expect large uncertainties in the extractions from the experiment. From a phenomenological point of view, the unpolarized PDF is known very well, the polarized PDF to some extent and the transversity is poorly known.

In Fig. 3.15 we compare our model calculation (at the scales $Q_0^2 = 0.19$ Gev^2 and $Q^2 = 2.4$ Gev^2) of the valence transversity distribution of the proton with the experimental extractions from Refs. [86, 87, 88] (at $Q^2 = 2.4$ Gev^2). For values of $x \gtrsim 0.35$ our calculation of $xh_1^{u_V}$ is compatible with the various extractions within their error band and for values of $x \lesssim 0.35$, $xh_1^{u_V}$ with model 1 does not lie within the error bands anymore. The situation is different for $xh_1^{d_V}$: Both models lie approximately within the error bands of Ref. [87] for the whole x range.

The extracted functions themselves also are different. In Ref. [87] they used a tree-level expression (no scale evolution) and simultaneously extract information of the transversity and Collins function from azimuthal asymmetries in SIDIS and data on e^+e^--annihilation. Kang et al. [88] work with evolution equations within the standard transverse momentum distribution framework with next-to-leading-order (NLO) scale evolution. Since our scale evolution is done at leading order it is very encouraging to see that the tree level extractions and the NLO extractions yield similar results (see Fig. 3.15). We therefore expect that a scale evolution at NLO of our results from $Q_0^2 = 0.19$ Gev^2 to $Q^2 = 2.4$ Gev^2 does not alter our model calculations significantly. Radici et al. [86] extract the transversity using SIDIS with two hadrons in the final state within the standard collinear factorization framework and LO scale evolution.

The non-perturbative sea contribution to the transversity distribution is shown in Fig. 3.16. These predictions are the first calculations for the antiquark transversity distributions within a meson-cloud approach. We readily observe that its magnitude is very small as compared to the valence contribution. The transversity distribution is therefore dominated by its valence quarks. In the upper panel of Fig. 3.17 we show the isoscalar distribution $xh_1^{\bar{u}/p} + xh_1^{\bar{d}/p}$ and the isovector distribution $xh_1^{\bar{u}/p} - xh_1^{\bar{d}/p}$ and for comparison we plotted in the lower panel $xg_1^{\bar{u}/p} + xg_1^{\bar{d}/p}$ and $xg_1^{\bar{u}/p} - xg_1^{\bar{d}/p}$. The chiral quark soliton model satisfies in the large N_c limit the following inequalities [89, 90, 91]

$$\begin{aligned} |g_1^{\bar{u}} - g_1^{\bar{d}}| &> |g_1^{\bar{u}} + g_1^{\bar{d}}| \\ |h_1^{\bar{u}} - h_1^{\bar{d}}| &> |h_1^{\bar{u}} + h_1^{\bar{d}}| \end{aligned} \tag{3.100}$$

Analogous relations hold for the quark distributions. Equation (3.100) is not supported by the meson cloud model, while it holds for the quark distributions.

The cutoff dependence for *model 1* and u-flavor is shown in Fig. 3.18. We observe a similar cutoff-dependence as we have found for the polarized PDF.

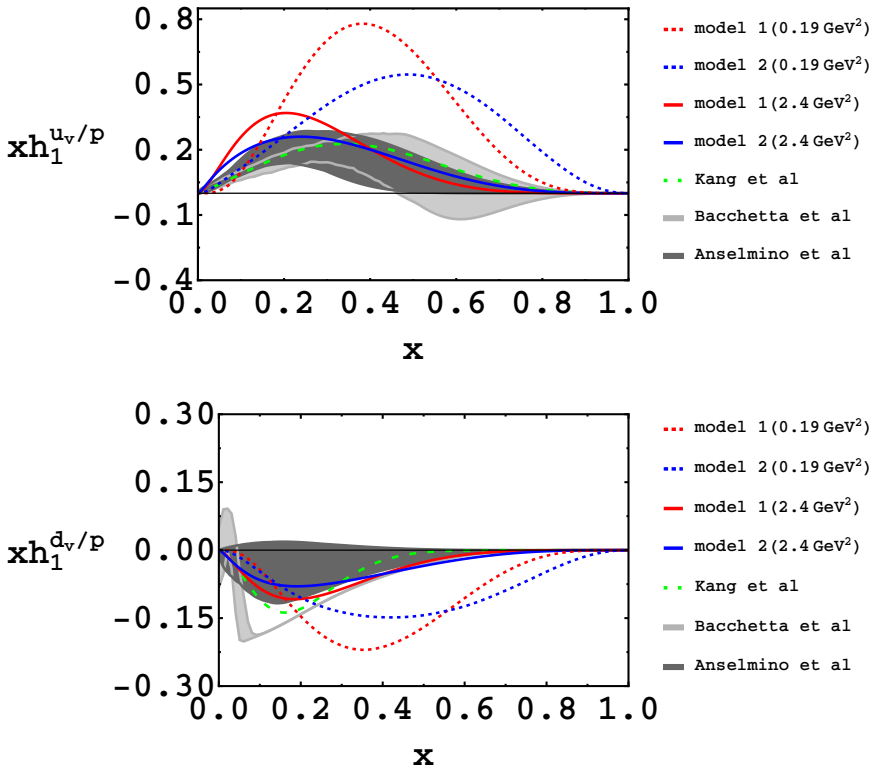

Figure 3.15: Comparison of our model calculation of the transversity PDF for u-flavor (upper panel) and d-flavor (lower panel) with experimental extractions of different groups. The model calculations are shown at the initial scale $Q_0^2 = 0.19$ GeV^2 and after LO evolution to $Q^2 = 2.4$ GeV^2. The experimental extractions for $Q^2 = 2.4$ GeV^2 are from references: Bachetta et al in Ref. [86], Anselmino et al in Ref. [87] and Kang et al in Ref. [88], respectively.

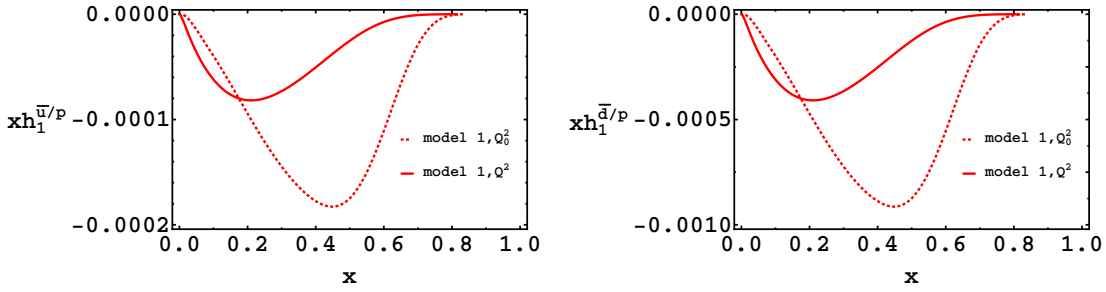

Figure 3.16: In this figure we show the sea part of the transversity for u-flavor (left panel) and d-flavor (right panel). The different scales are as follows: $Q_0^2 = 0.19$ GeV^2 and $Q^2 = 2.4$ GeV^2.

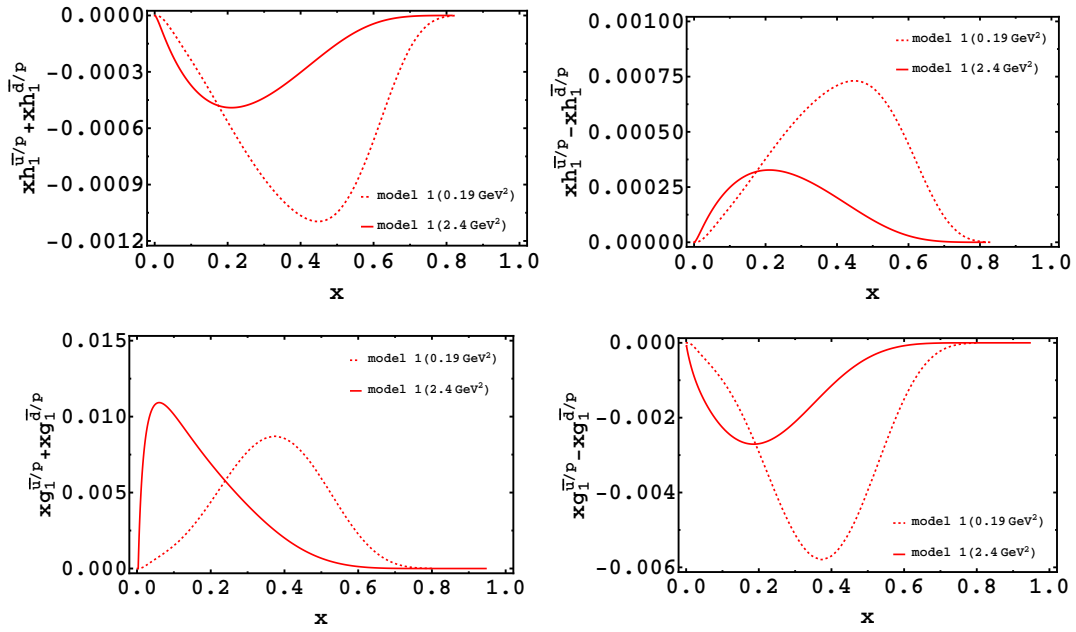

Figure 3.17: Top: Isoscalar distribution $xh_1^{\bar{u}/p} + xh_1^{\bar{d}/p}$ and the isovector distribution $xh_1^{\bar{u}/p} - xh_1^{\bar{d}/p}$ for $Q_0^2 = 0.19$ GeV^2 and $Q^2 = 2.4$ GeV^2. Bottom: Isoscalar distribution $xg_1^{\bar{u}/p} + xg_1^{\bar{d}/p}$ and the isovector distribution $xg_1^{\bar{u}/p} - xg_1^{\bar{d}/p}$.

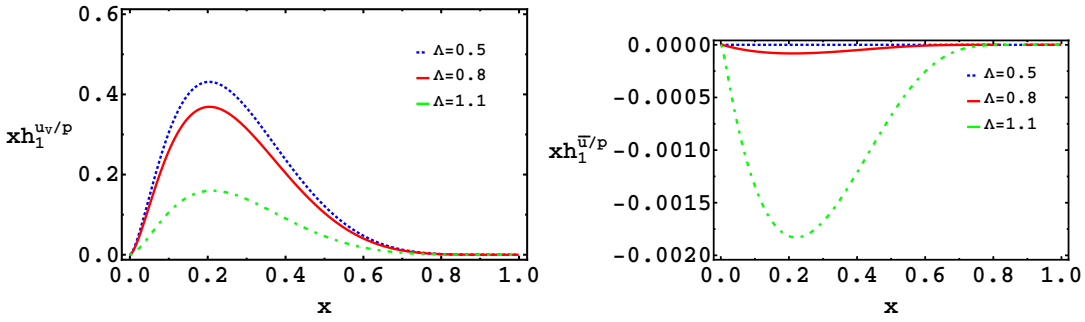

Figure 3.18: The cutoff dependence of the transversity u-valence distribution (left panel) in the range $\Lambda = 0.5 - 1.1$ GeV and the corresponding sea distribution (right panel) at $Q^2 = 2.4$ GeV^2.

We have also investigated the tensor charge. Like the isoscalar and axial vector charges, the tensor charge is an essential property for characterizing the momentum and spin structure of the nucleon. It is defined by the following forward matrix element [92]:

$$\langle N : p, S_T | i\bar{\Psi}^q \sigma^{\mu\nu} \gamma_5 \Psi^q | N : p, S_T \rangle = 2\delta q \left(Q_0^2\right) \left(p^\mu S_T^\nu - p^\nu S_T^\mu\right), \tag{3.101}$$

where the spin vector S_T is understood to be in the transversity basis and $\delta q \left(Q_0^2\right)$ is the tensor charge for flavor q at the scale Q_0^2. The tensor charge measures the net distribution of transversely polarized quarks in a transversely polarized proton [93].

It also enters the description of novel tensor interaction at the *TeV* scale [94]. Jaffe and Ji showed [95] that the tensor charge of the nucleon N can be related to the zeroth moment of the valence transversity, i.e.

$$\delta q = \int_0^1 \mathrm{d}x\, h_1^{N/q}(x). \tag{3.102}$$

Our results for the tensor charge at $Q^2 = 10\ \mathrm{GeV}^2$ are

- δu:

  model 1: 0.675,

  model 2: 0.560,

- δd:

  model 1: -0.208,

  model 2: -0.179.

The contribution of the u- and d-quarks to the tensor charge in our model and in comparison with various other model estimates is plotted in Fig. 3.19. Most notably it is interesting to compare our results with those of Refs. [96, 97, 98], because therein a three quark constituent model for the nucleon is used, so we can study the effect of the inclusion of the meson-cloud. For u-flavor the meson-cloud improves the agreement with the data analysis, whereas for d-flavor it gives only small corrections. Other results within a different theoretical framework are given as reported in the original works: QCD sum rule approach [92], chromodielectric model [99], axial-vector dominance model [100], chiral-quark soliton model [101, 102], light-front chiral quark soliton model [103], Dyson-Schwinger model [93] and lattice QCD [104, 105]. We remark that the dependence of the tensor charge on the scale is very mild so we can compare the tensor charge for different values of Q^2.

3.6 Summary

In this chapter we investigated the collinear PDFs within a front form meson cloud model. In Sec. 3.2 we formulated the basics of the meson cloud model. We expressed the wave function of the physical nucleon in terms of a bare nucleon and virtual meson-baryon components. At first order in the baryon-meson-nucleon interaction, the meson-baryon component consists of one meson M and one baryon B. We take $M = \pi, \rho$ and $B = p, n$ explicitly into account. With the expansion of the physical nucleon state in terms of a bare nucleon dressed by its virtual meson cloud we can obtain a convolution formula for the PDFs. In this convolution formula the splitting functions (which can be calculated using time-ordered perturbation theory) and the PDFs of the respective baryons and mesons enter, cf. Sec. 3.3.2.2. Those PDFs are modeled by a LCWF overlap representation. In Sec. 3.4 we presented explicitly the overlap formulas and discussed the model input to perform the overlaps. In the final section, 3.5, we showed various results:

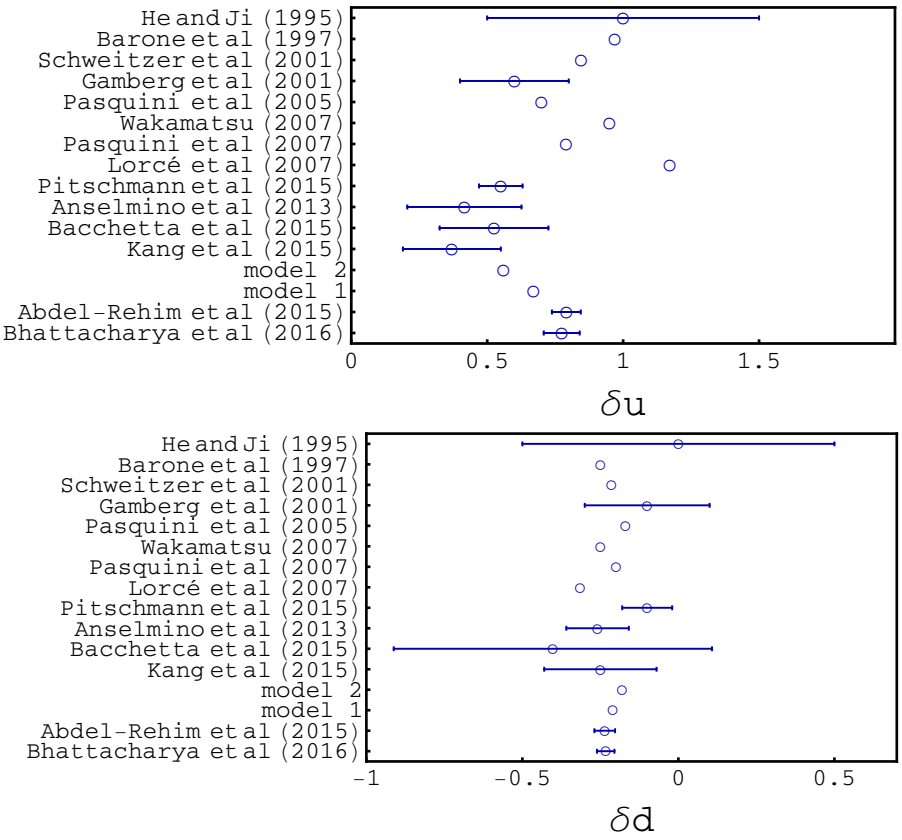

Figure 3.19: Comparison of our model calculation ($Q^2 = 2.4$ GeV^2) of the tensor charge δq with results from other references. The comparison is done with the following references: He and Ji [92] ($Q^2 \sim 1$ GeV^2), Barone et al. [99] ($Q^2 = 25$ GeV^2), Schweitzer et al. [102] ($Q^2 = 0.36$ GeV^2), Gamberg et al. [100] ($Q^2 \sim 1$ GeV^2), Pasquini et al. 2005 [96] ($Q^2 = 10$ GeV^2), Wakamatsu [101] ($Q^2 = 2.4$ GeV^2), Pasquini et al. 2007 [97, 98] ($Q^2 = 10$ GeV^2), Lorcé [103] ($Q^2 = 0.36$ GeV^2), Pitschmann [93] ($Q^2 = 4$ GeV^2), Anselmino et al. [87] ($Q^2 = 0.8$ GeV^2), Bacchetta et al [86] ($Q^2 = 10$ GeV^2), Kang et al. [88] ($Q^2 = 10$ GeV^2), Abdel-Rehim et al. [104] ($Q^2 = 4$ GeV^2) and Bhattacharya et al. [105] ($Q^2 = 4$ GeV^2). Upper figure for u-flavor and lower figure for d-flavor, respectively.

- ***Unpolarized PDF***: valence and sea contribution in comparison with the PDF-parameterization of Ref. [76].
  Our results are found to be in reasonable agreement with the PDF set we compare with.

- ***Polarized PDF***: valence and sea contribution in comparison with the PDF-parameterization of Ref. [78] and experimental data of Ref. [79].
  We note that the experimental error bars are much larger than for the unpolarized PDFs. Our results for the valence contributions to the polarized PDF follow the pattern set by the experimental data. For the sea contributions we find deviations from the experimental data, but due to the large error bars no definite conclusion can be drawn.

- Our estimate of the ***unpolarized and polarized sea*** in comparison with recent

experimental data.
The meson-cloud model is capable to describe the flavor asymmetry $f_1^{\bar{d}/p}(x) - f_1^{\bar{u}/p}(x)$ very well, but fails (as other models) to describe the observed asymmetry $f_1^{\bar{d}/p}(x)/f_1^{\bar{u}/p}(x)$ at larges values of x. For the polarized asymmetry the experimental data seem to favor models which predict a small positive value for $g_1^{\bar{d}/p}(x) - g_1^{\bar{u}/p}(x)$, whereas our model predicts a small negative value for it.

- ***Transversity PDF***: valence and sea contribution in comparison with the PDF-parameterizations of Refs. [86, 87, 88].
  The extractions from the experiments come along with huge error bands. Our model estimates for the transversity PDF lie within those error bands. We also find that the transversity PDF is dominated by valence degrees of freedom, i.e. the sea contribution is negligible.

- ***Tensor charge***: for u-flavor and d-flavor our predictions are within the range of experimental extractions and other model calculations.

Acknowledgements

I WANT TO THANK

. . . my parents for their love and support.

. . . my advisor, Wolfgang Schweiger, for giving me the opportunity to work in a very interesting field, for having always time to answer my questions, giving me guidance and for allowing me to work at my own pace. It has been a great pleasure for me to work with you.

. . . Barbara Pasquini and the hadron physics group at the University of Pavia for their hospitality.

. . . for the financial support by the Fond zur Förderung der wissenschaftlichen Forschung in Österreich via FWF DK $W1203 - N16$.

. . . my friends for having a great time the past years.

APPENDICES

A

Light-Cone Quantization

This appendix is a modified version of an appendix originally published in Ref. [9]. It is by no means complete but serves more as a short introduction into the topic and it introduces the notation.

A.1 Introduction

We first review some aspects of canonical field theory. The Lagrangian is the basic object from which the equations of motion (EOM) and constants of motion can be derived. Since the EOM are differential equations we need initial values for solving them. In a four dimensional space-time these initial conditions are formulated on a hypersphere. If we know them, i.e. all necessary field components $\phi(x^0, \mathbf{x})$ on a hypersphere that is, e.g., characterized by a fixed initial time x^0, we can propagate the initial configuration forward or backward in time with the help of the Hamiltonian[1] $H = P^0$. In a (classical) theory with a conjugate momentum[2] $\Pi[\phi] = \frac{\delta \mathscr{L}}{\delta(\partial_0 \phi)}$ and with the Hamiltonian $P_0 = P_0[\phi, \Pi]$ the EOM for a non-constrained system are given in terms of Poisson brackets:

$$\partial_0 \phi = \{P_0, \phi\}_{cl} \qquad \text{and} \qquad \partial_0 \Pi = \{P_0, \Pi\}_{cl}. \tag{A.1}$$

The transition to a quantum field theory can be obtained by making the field and its conjugate momentum operator-valued and replacing the Poisson brackets between them by commutators (or by the anti-commutator for fermionic fields)[3]

$$\{\phi(x), \Pi(y)\}_{cl} = \delta^3(\mathbf{x} - \mathbf{y}) \Rightarrow \frac{1}{i} \left[\phi(x), \Pi(y)\right]_{x^0 = y^0} = \delta^3(\mathbf{x} - \mathbf{y}). \tag{A.2}$$

The time derivatives of the field operators are given by the Heisenberg equations. These procedure is known as *canonical quantization* and it applies only for the *independent* fields. Therefore it can become very involved, especially for a gauge theory like

[1] Depending on the form of the Hamiltonian dynamics one can, however, choose a time parameter τ which differs from ordinary time $\tau = x^0 = t$. The Hamiltonian H will then generate the "time" evolution in the parameter τ, i.e. $H |\Psi_\tau\rangle = i \frac{\partial}{\partial_\tau} |\Psi_\tau\rangle$.

[2] For simplicity we assume that we have only one field, but the generalization to more fields is straightforward.

[3] We are not distinguishing between operators and their eigenvalues, but use the same symbol for both since it should be clear within the context if we either are talking about an operator or its associated eigenvalue.

QED or QCD: There can exist fields with no conjugate momentum (if not all fields are independent) and/or gauge) fields with redundant degrees of freedom.

One big disadvantage so far was that we have treated time t and space $\mathbf{x}$ as if they were different. In a covariant theory, however, time and space are only different aspects of a four dimensional space-time. Space can be defined as that hypersphere in space-time on which one choses the initial field configurations in accordance with microcausality. Time can be understood as the normal (or at least linear independent direction) to that hypersphere.

This can be phrased more formally by introducing generalized coordinates $\tilde{x}^\nu$. Starting from a basic parameterization of space-time x^μ with a metric tensor $g^{\mu\nu}$ (all elements are zero except of $g^{00} = 1$ and $g^{11} = g^{22} = g^{33} = -1$) one parameterizes space-time by the following relation

$$\tilde{x}^\nu = \tilde{x}^\nu(x^\mu). \tag{A.3}$$

The transformation Eq. $(A.3)$ is restricted by the condition that its inverse $x^\mu(\tilde{x}^\nu)$ exists and that it conserves the arc length, $(ds)^2 = g_{\mu\nu}dx^\mu dx^\nu = \tilde{g}_{\rho\sigma}d\tilde{x}^\rho d\tilde{x}^\sigma$. The two metric tensors are related by

$$\tilde{g}_{\rho\sigma} = g_{\mu\nu}\left(\frac{\partial x^\mu}{\partial \tilde{x}^\rho}\right)\left(\frac{\partial x^\nu}{\partial \tilde{x}^\sigma}\right). \tag{A.4}$$

The Lagrangian is independent of the parameterization, i.e. it can be expressed in terms of either x or $\tilde{x}$.

Now there are many possible ways to parameterize space-time by generalized coordinates $\tilde{x}(x)$ but all those which are connected by a Lorentz transformation should be excluded. This limits the freedom and following Dirac [106] there are at least three special parameterizations [4]. The difference between them is the hypersphere on which the fields are initialized and so one has correspondingly different time parameters and each of them also has its own Hamiltonian.

The question which hypersphere we should choose would in fact be an ill posed one, since, in principle, all should yield the same physical result. In high energy physics it is convenient to work in Dirac's, so-called, *front-form*. It is ideally suited for a description of high energy processes due to the following reasons:

- The ground state of the full theory nearly coincides (apart of zero modes[5]) with the ground state of the free theory.
- Wave functions in front form can be independent of the reference frame and are thus useful in the description of a wide range of high-energy scattering processes.
- In the light-cone gauge there are no ghosts.
- ...

The first two points will be discussed further in this appendix. Before we do so, let us introduce the notation we are using.

[4] There are actually 5 such parameterizations, see Ref. [107], but two of them seem to be less useful.

[5] Problems with quantization on a light-front, e.g. *zero modes*, are beyond the scope of this appendix.

A.2 Notation, metric and all That

For any four-vector $a^\mu = (a^0, a^1, a^2, a^3)$ (written in the "usual" coordinate) we write in LC-coordinates[6]

$$a^\mu = [a^+, a^-, \mathbf{a}_\perp] \tag{A.5}$$

with

$$a^\pm := \frac{a^0 \pm a^3}{\sqrt{2}} \quad \text{and} \quad \mathbf{a}_\perp := (a^1, a^2). \tag{A.6}$$

The metric tensor is now non-diagonal

$$g^{\mu\nu} = \begin{pmatrix} 0 & 1 & 0 & 0 \\ 1 & 0 & 0 & 0 \\ 0 & 0 & -1 & 0 \\ 0 & 0 & 0 & -1 \end{pmatrix}. \tag{A.7}$$

The scalar product of two four vectors in LC-coordinates is

$$a \cdot b = a^\mu b_\mu = g^{\mu\nu} a_\mu b_\nu = a^+ b^- + a^- b^+ - \mathbf{a}_\perp \cdot \mathbf{b}_\perp. \tag{A.8}$$

Due to the off-diagonal entries of the metric tensor the conversion of contravariant to covariant vectors is somewhat involved, we e.g. have: $a^\pm = a_\mp$ and $\partial^\pm \equiv \partial/\partial z_\pm = \partial/\partial z^\mp$.
For convenience we define two lightlike unit vectors

$$n_+ := \frac{1}{\sqrt{2}}(1,0,0,1) \equiv [1, 0, \mathbf{0}_\perp] \quad \text{and} \quad n_- := \frac{1}{\sqrt{2}}(1,0,0,-1) \equiv [0, 1, \mathbf{0}_\perp], \tag{A.9}$$

satisfying $n_+^2 = n_-^2 = 0$ and $n_+ \cdot n_- = 1$. Using Eq. $(A.9)$ LC-plus and -minus components can be projected out by

$$a^+ = n_- \cdot a \qquad \text{and} \qquad a^- = n_+ \cdot a, \tag{A.10}$$

respectively.

Light-cone coordinates depend on the particular choice of the z-axis but they transform simply under boosts along the z-axis. In "ordinary" coordinates a boost from the rest frame of a particle to a frame where the particle moves with velocity v into the z-direction changes the four vector components according to

$$x'^0 = \frac{x^0 - v x^3}{\sqrt{1-v^2}}, \qquad x'^3 = \frac{x^3 - v x^0}{\sqrt{1-v^2}}, \qquad x'^1 = x^1, \qquad x'^2 = x^2. \tag{A.11}$$

[6] The order of the index μ is now $\mu = +, -, 1, 2$. It has become common to speak of "light-cone coordinates", "light-cone quantization", "light-cone wave functions", etc., although all these terms rather refer to the light front, i.e. a hypersphere tangent to the light cone. We will stick to the common nomenclature, keeping in mind that it is not completely correct.

Equation $(A.11)$ in LC-coordinates reads

$$\tilde{x}^+ = x^+ e^{\psi}, \qquad \tilde{x}^- = x^- e^{-\psi}, \qquad \tilde{\mathbf{x}}_\perp = \mathbf{x}_\perp, \tag{A.12}$$

where the hyperbolic angle ψ is $\frac{1}{2}\ln\frac{1+v}{1-v}$, so that $v = \tanh\psi$ [108], i.e. plus and minus components are simply scaled by $e^{\pm\psi}$.
We consider now in particular the momentum p of a particle with mass m obtained by a boost with ψ from the rest frame into the z-direction:

$$p'^\mu = \left[p^+, \frac{m^2}{2p^+}, \mathbf{0}_\perp\right] = \left[\frac{m}{\sqrt{2}}e^{\psi}, \frac{m}{\sqrt{2}}e^{-\psi}, \mathbf{0}_\perp\right]. \tag{A.13}$$

If the boost in Eq. $(A.13)$ is very large, we see that the plus component of p^μ becomes large, whereas the minus component becomes small (using the "usual" components, p^0 and p^3 both become large).
A very useful Lorentz transformation is a *transverse boost* which leaves the plus component of a four vector a unchanged:

$$a^\mu = [a^+, a^-, \mathbf{a}_\perp] \to a'^\mu = \left[a^+, a^- - \frac{\mathbf{a}_\perp\cdot\mathbf{b}_\perp}{b^+} + \frac{a^+\mathbf{b}_\perp^2}{2(b^+)^2}, \mathbf{a}_\perp - \frac{a^+}{b^+}\mathbf{b}_\perp\right], \tag{A.14}$$

with b^+ and $\mathbf{b}_\perp$ being three parameters ($\mathbf{b}_\perp$ is a 2-vector).

For further purposes it will be convenient to define the following projectors

$$\mathscr{P}_\pm := \frac{1}{2}\gamma^\mp\gamma^\pm, \tag{A.15}$$

with

$$\mathscr{P}_+ + \mathscr{P}_- = 1, \quad \mathscr{P}_+\mathscr{P}_- = \mathscr{P}_-\mathscr{P}_+ = 0 \quad \text{and} \quad \mathscr{P}_\pm^2 = \mathscr{P}_\pm. \tag{A.16}$$

They further satisfy

$$\mathscr{P}_\pm\gamma^\mp = \gamma^\mp\mathscr{P}_\mp, \quad \mathscr{P}_\pm\gamma^\pm = 0 \quad \text{and} \quad \mathscr{P}_\pm\gamma_\perp = \gamma_\perp\mathscr{P}_\pm. \tag{A.17}$$

A.2.1 *Bound states on the light-cone, light-Cone wave functions and light-cone quantization*

Each hadronic state is an eigenstate of the QCD-Hamiltonian. If we denote the light-cone Hamiltonian by $H_{LC} = P^-$, each state of mass M must satisfy $P^-|\Psi\rangle = \frac{M^2+\mathbf{P}_\perp^2}{2P^+}|\Psi\rangle$. If we project this eigenvalue equation onto the various Fock states we get an infinite number of coupled integral equations. Solving these equations means solving the underlying field theory, i.e. QCD. Using the light-cone Fock state basis is particularly appealing because the vacuum is simple and the wave functions can be expressed in terms of frame independent coordinates.

A.2.1.1 *Light-cone vacuum*

Why is the vacuum simple? We first recall that in a quantum field theory the four-momentum P^μ of a *physical* particle has to satisfy the spectrum condition [109]

$$P^2 \geq 0 \qquad \text{and} \qquad P^0 \geq 0. \tag{A.18}$$

We can now immediately derive the inequalities ${P^0}^2 - {P^3}^2 \geq \mathbf{P}_\perp^2 \geq 0$ and $P^0 \geq |P^3|$ from Eqs. $(A.18)$, $(A.8)$ and the definition of light-cone coordinates, Eq. $(A.6)$. This implies for the plus component of the momentum

$$P^+ \geq 0. \tag{A.19}$$

The vacuum, defined as those state with the lowest possible energy eigenvalue, fulfills

$$P^+ |0\rangle = 0, \tag{A.20}$$

which means that the vacuum is an eigenstate of P^+ with eigenvalue zero. The consequence of this is, that the vacuum is also an eigenstate of the full light-cone Hamiltonian P^-. In other words the light-cone vacuum is also the ground state for the *interacting* theory [7]. As we will see later, we can therefore build a Fock state basis out of the vacuum.

A.2.1.2 *Bound states*

We want to solve the following eigenvalue problem[8]:

$$P^- |\Psi\rangle = \frac{M^2 + \mathbf{P}_\perp^2}{2P^+} |\Psi\rangle . \tag{A.22}$$

The operator P^+ is positive (having positive eigenvalues) as we showed above. As discussed in Refs. [107, 110] eigenfunctions of the Hamiltonian in the front-form can be labeled by six quantum numbers:

- the invariant mass M,
- the 3 momentum components P^+ and $\mathbf{P}_\perp$,
- the generalized total spin squared S^2 and its longitudinal projection S_z,

[7] These arguments hold for non-vanishing bare mass of the particles. For massless gauge fields the zero modes require some care

[8] Solving a relativistic bound state problem for a particle with mass M and wave function $|\Psi\rangle$ in a straightforward way within the usual equal-time formalism would require to solve the Schrödinger-like eigenvalue problem

$$H |\Psi\rangle = \sqrt{M^2 + \mathbf{P}^2} |\Psi\rangle , \tag{A.21}$$

where $H = P^0$ and $\mathbf{P}$ are second quantized Heisenberg operators and $|\Psi\rangle$ is expanded in multi-particle occupation number Fock states. This eigenvalue problem has several disadvantages like its complicated vacuum eigensolution (associated with a complicated vacuum structure) and the presence of a square root operator.

plus a collection of additional quantum numbers like charge, parity, color,... denoted by α.
A state $|\Psi\rangle$ can therefore be written as

$$|\Psi\rangle = |\Psi;\, M, P^+, \mathbf{P}_\perp, S^2, S_z, \alpha\rangle\,. \tag{A.23}$$

$|\Psi\rangle$ can be expanded in a complete set of functions, namely a complete basis of Fock states which are constructed in the usual way by applying creation operators to the vacuum state:

$$\begin{aligned} &|0\rangle\,, \\ &|q\bar{q} : k_i^+, \mathbf{k}_{\perp i}, \lambda_i\rangle &&= b^\dagger(k_1) d^\dagger(k_2)\,|0\rangle \\ &|q\bar{q}g : k_i^+, \mathbf{k}_{\perp i}, \lambda_i\rangle &&= b^\dagger(k_1) d^\dagger(k_2) a^\dagger(k_3)\,|0\rangle \\ &|gg : k_i^+, \mathbf{k}_{\perp i}, \lambda_i\rangle &&= a^\dagger(k_1) a^\dagger(k_1)\,|0\rangle\,, \\ &... \end{aligned} \tag{A.24}$$

The operators $b^\dagger(k)$, $d^\dagger(k)$ and $a^\dagger(k)$ create bare quarks, bare antiquarks and bare gluons (their anti-commutation relations are given in App. A.2.1.3. The notation keeps only track of the three-momenta $k_i^+, \mathbf{k}_{\perp i}$ and the helicity λ_i. The projections of $|\Psi\rangle$ on the basis vectors $|\mu_n\rangle := |n : k_i^+, \mathbf{k}_{\perp i}, \lambda_i\rangle$ (the index n labels the different Fock states) are called the wave functions (in this context the *light-cone wave functions* (LCWFs))

$$\Psi_n = \langle \mu_n | \Psi \rangle\,. \tag{A.25}$$

It therefore follows for the expansion of $|\Psi\rangle$ in Fock states

$$|\Psi\rangle = \sum_n \int \mathrm{d}[\mu_n]\, |\mu_n\rangle\, \Psi_n(\mu). \tag{A.26}$$

Each of the $|\mu_n\rangle = |n : k_i^+, \mathbf{k}_{\perp i}, \lambda_i\rangle$ is an eigenstate of P^+ and $\mathbf{P}_\perp$ with eigenvalues

$$\mathbf{P}_\perp = \sum_{i\in n} \mathbf{k}_{\perp i} \quad \text{and} \quad P^+ = \sum_{i\in n} k_i^+. \tag{A.27}$$

Now we introduce *relative* momentum coordinates x_i and $\hat{\mathbf{k}}_\perp$ via

$$\begin{aligned} k_i^+ &= x_i P^+, \\ \mathbf{k}_{i\perp} &= x_i\, \mathbf{P}_\perp + \hat{\mathbf{k}}_{i\perp}. \end{aligned} \tag{A.28}$$

x_i denotes the longitudinal momentum fraction of the i-th particle. Since $k_i^+ > 0$ and $P^+ > 0$, the values of x_i lie in the range of $0 < x_i < 1$. $\hat{\mathbf{k}}_{i\perp}$ is the relative transverse momentum of the i-th particle. In a frame where $\mathbf{P}_\perp = 0$ (which can be reached by a transverse boost, cf. Eq. $(A.14)$), we have $\mathbf{k}_{\perp i} = \hat{\mathbf{k}}_{i\perp}$. Therefore $\hat{\mathbf{k}}_{i\perp}$ can be considered as the *intrinsic* transverse momentum of the i-th particle. We note that the relative coordinates are invariant under light-front boosts. Comparing with Eq. $(A.27)$ we see

that the relative coordinates have to fulfill the following constraints:

$$\sum_i x_i = 1 \quad \text{and} \quad \sum_i \hat{\mathbf{k}}_{\perp i} = \mathbf{0}_\perp. \tag{A.29}$$

Before we proceed to write down the eigenvalue equation for the mass operator, we define the phase-space differential $\mathrm{d}[\mu_n]$. In our convention, where the anti-commutators are given by Eq. $(A.47)$ it reads

$$\int \mathrm{d}[\mu_n] ... = \int \left[\mathrm{d}x_i \mathrm{d}^2\hat{\mathbf{k}}_{\perp i}\right]_n ..., \tag{A.30}$$

with

$$\left[\mathrm{d}x_i \hat{\mathbf{k}}_{i\perp}\right]_n = \prod_{i=1}^n \mathrm{d}x_i \, \delta\left(1 - \sum_{i=1}^n x_i\right) \frac{1}{(16\pi^3)^{n-1}} \prod_{i=1}^n \mathrm{d}^2\,\hat{\mathbf{k}}_{i\perp} \delta^{(2)}\left(\sum_{i=1}^n \hat{\mathbf{k}}_{i\perp}\right). \tag{A.31}$$

In the case of interactions the front-form Hamiltonian P^- can be written as

$$P^- = P_0^- + V, \tag{A.32}$$

where P_0^- is the free front-form Hamiltonian and V the "potential" term. Since the minus momentum components are dynamical in front-form, the total minus momentum of the whole system is not equal to the sum of the minus momenta of the respective constituent particles. For the free case, the total light-cone energy reads in terms of relative coordinates (cf. Eq. $(A.28)$)

$$P_0^- = \sum_i k_i^- = \sum_i \frac{\mathbf{k}_{\perp i}^2 + m_i^2}{2k_i^+} = \frac{\mathbf{P}_\perp^2}{2P^+} + \sum_i \frac{\hat{\mathbf{k}}_{\perp i}^2 + m_i^2}{2x_i P^+}. \tag{A.33}$$

We observe in Eq. $(A.33)$ that P_0^- separates into a center-of-mass term (first term of Eq. $(A.33)$ which vanishes in hadron in/out frames) and a term containing only the relative coordinates (second term of Eq. $(A.33)$). Introducing the free invariant mass squared[9] $M_0^2 := P_0^2$ we can identify the relative momentum contribution with the free invariant mass squared, i.e.

$$M_0^2 = P_0^2 = 2P^+P_0^- - \mathbf{P}_\perp^2 = \sum_i \frac{\hat{\mathbf{k}}_{\perp i}^2 + m_i^2}{x_i}. \tag{A.34}$$

It is also possible to define an invariant mass squared in the interacting case,

$$M^2 := P^2 = 2P^+\left(P_0^- + V\right) - \mathbf{P}_\perp^2, \tag{A.35}$$

which can be rewritten in terms of the free invariant mass squared M_0^2

$$M^2 = P^2 = M_0^2 + 2P^+V. \tag{A.36}$$

[9] P_0 is the four momentum of the free system.

The difference between M and M_0 thus is

$$M^2 - M_0^2 = 2P^+V. \tag{A.37}$$

The front-form analogue of Eq. $(A.21)$ can now be stated as

$$\left(M^2 - M_0^2\right)|\Psi\rangle = W|\Psi\rangle\,, \tag{A.38}$$

with $W := 2P^+V$. Projecting the eigenvalue equation onto the various Fock states $\langle q\bar{q}|\,, \langle q\bar{q}g|\,, ...$ results in an infinite number of coupled integral eigenvalue equations. To conclude this section let us use Eq. $(A.38)$ to write for the LCWFs corresponding to the state $|\Psi\rangle$:

$$\Psi = \frac{W\Psi}{M^2 - M_0^2}. \tag{A.39}$$

With the help of the parameter

$$\epsilon := M^2 - M_0^2 = M^2 - \left(\sum_i k_i^-\right)^2 = M^2 - \sum_i \frac{\hat{\mathbf{k}}_{\perp i}^2 + m_i^2}{x_i}, \tag{A.40}$$

one sees that all LCWFs are of the form

$$\Psi = \frac{W\Psi}{\epsilon}. \tag{A.41}$$

ϵ measures how far off (light-cone) energy shell the bound state is since

$$P^- - \sum_i k_i^- = \frac{\epsilon}{P^+}. \tag{A.42}$$

We therefore learn from Eq. $(A.38)$ that there is only a small overlap of the bound state with Fock states that are far off the (light-cone) energy shell. This implies the restrictions

$$\Psi(x_i, \hat{\mathbf{k}}_{\perp i}) \to 0 \quad \text{for} \quad \hat{\mathbf{k}}_{\perp i}^2 \to \infty,\ x_i \to 0 \tag{A.43}$$

on the LCWFs.

A.2.1.3 *Canonical quantization of quark and gluon fields*

As mentioned in the introduction of this appendix, canonical quantization proceeds by imposing equal time commutation relations, here at LC-time $x^+ = 0$, on the *independent* dynamical fields. The independent fields are called "good" LC-field-components and the dependent fields are called "bad" LC-components, respectively. To make this statement clearer, we start with the Dirac equation for a quark field Ψ_q (suppressing spinor and color labels)

$$(i\not{D} - m)\Psi_q = 0, \tag{A.44}$$

with D being the covariant derivative, $D^\mu = \partial^\mu + igA^\mu$. With the help of the projection operators of. Eq. $(A.15)$, $\mathscr{P}^+$ and $\mathscr{P}^-$, we can rewrite the Dirac equation as a set of spinor equations

$$i\gamma^+ D^- \phi_q = (i\boldsymbol{\gamma}_\perp \cdot \mathbf{D}_\perp + m)\chi_q \quad \text{and} \quad i\gamma^- D^+ \chi_q = (i\boldsymbol{\gamma}_\perp \cdot \mathbf{D}_\perp + m)\phi_q, \tag{A.45}$$

where $\phi_q := \mathscr{P}^+ \Psi_q$ and $\chi_q := \mathscr{P}^- \Psi_q$. Since $D^\pm = \partial/\partial^\mp + igA^\pm$ it follows that in the second equation of Eq. $(A.45)$ "the light-cone time" x^+ does not occur and it is therefore not an EOM but rather constrains χ_q in terms of ϕ_q and $\mathbf{A}_\perp$. For light-cone gauge, $A^+ = 0$, it even takes on the simpler form $i\gamma^- \partial/\partial x^- \chi_q = \boldsymbol{\gamma}_\perp \cdot \mathbf{D}_\perp \phi_q + m\phi$. Hence ϕ_q describes the dynamically independent degree of freedom, referred to as the "good" field component, whereas the dependent field component χ_q is called the "bad" component. Thus the projection operators $\mathscr{P}^+$ and $\mathscr{P}^-$ project out "good" and "bad" field components of a Dirac field Ψ_q, respectively, i.e. $\Psi_q = (\mathscr{P}^+ + \mathscr{P}^-)\Psi_q = \phi_q + \chi_q$.

The independent free quark field can be expanded, at light-cone time $x^+ = 0$, as

$$\begin{aligned} \phi_q(x^-, \mathbf{x}_\perp) = \int \frac{\mathrm{d}k^+}{k^+} \frac{\mathrm{d}^2\hat{\mathbf{k}}_\perp}{16\pi^3} \theta(k^+) \sum_\lambda \\ \Big[b_q(k^+, \hat{\mathbf{k}}_\perp, w) u_+(k^+, \hat{\mathbf{k}}_\perp, w) e^{-ik^+x^- + i\hat{\mathbf{k}}_\perp \cdot \mathbf{x}_\perp} \\ + d_q^\dagger(k^+, \hat{\mathbf{k}}_\perp, w) v_+(k^+, \hat{\mathbf{k}}_\perp, w) e^{ik^+x^- - i\hat{\mathbf{k}}_\perp \cdot \mathbf{x}_\perp} \Big], \end{aligned} \tag{A.46}$$

with w being a collective index for helicity and color. The operator b is the annihilator of the "good" component of the quark field, the operator $d^\dagger$ the creator of the "good" component of the anti-quark field and for the quark and anti-quark spinors we consistently have to use $u_+(k^+, \hat{\mathbf{k}}_\perp, w) := \mathscr{P}^+ u(k^+, \hat{\mathbf{k}}_\perp, w)$ and $v_+(k^+, \hat{\mathbf{k}}_\perp, w) := \mathscr{P}^+ v(k^+, \hat{\mathbf{k}}_\perp, w)$.
The creation and annihilation operators fulfill the following anti-commutation relation

$$\begin{aligned} &\Big\{ b_{q'}(k'^+, \hat{\mathbf{k}}'_\perp, w'), b_q^\dagger(k^+, \hat{\mathbf{k}}_\perp, w) \Big\} = \Big\{ d_{q'}(k'^+, \hat{\mathbf{k}}'_\perp, w'), d_q^\dagger(k^+, \hat{\mathbf{k}}_\perp, w)) \Big\} \\ &= 16\pi^3 k^+ \delta(k'^+ - k^+) \delta^{(2)}(\hat{\mathbf{k}}'_\perp - \hat{\mathbf{k}}_\perp) \delta_{q'q} \delta_{w'w}. \end{aligned} \tag{A.47}$$

Similar considerations can be done for the gluonic field A^μ and they reveal that the "good" field components are the transverse ones, $\mathbf{A}_\perp$, whereas the bad one is A^-. The plus component can be fixed by the choice of the gauge, e.g. $A^+ = 0$ in light-cone gauge. The Fourier expansion of the independent gluonic field component is

$$\begin{aligned} \mathbf{A}_\perp(x^-, \mathbf{x}_\perp) = \int \frac{\mathrm{p}^+}{p^+} \frac{\mathrm{d}^2\hat{\mathbf{p}}_\perp}{16\pi^3} \theta(p^+) \sum_\lambda \\ \Big[a(p^+, \hat{\mathbf{p}}_\perp, w) \boldsymbol{\epsilon}_\perp(p^+, \hat{\mathbf{p}}_\perp, w) e^{-ip^+x^- + i\hat{\mathbf{p}}_\perp \cdot \mathbf{x}_\perp} + \\ + a^\dagger(p^+, \hat{\mathbf{p}}_\perp, w) \boldsymbol{\epsilon}_\perp^*(p^+, \hat{\mathbf{p}}_\perp, w) e^{+ip^+x^- - i\hat{\mathbf{p}}_\perp \cdot \mathbf{x}_\perp} \Big], \end{aligned} \tag{A.48}$$

where $\boldsymbol{\epsilon}_\perp$ is the transverse component of the gluon polarization vector and a, $a^\dagger$ are

the annihilation, creation operators for transverse gluons satisfying

$$\left[a(p'^+, \hat{\mathbf{p}}'_\perp, w'), a^\dagger(p^+, \hat{\mathbf{p}}_\perp, w)\right] = 16\pi^3 p^+ \delta(p'^+ - p^+)\delta^{(2)}(\hat{\mathbf{p}}'_\perp - \hat{\mathbf{p}}_\perp)\delta_{w'w}. \quad \text{(A.49)}$$

To conclude this section we repeat the Fock state decomposition of a hadronic state with momentum P and helicity λ. It can be written as a superposition of Fock states, that contain the free quanta of the "good" LC-components of quarks, antiquarks and gluon fields

$$|H : P, \mu\rangle = \sum_{n,\alpha} \int \left[\mathrm{d}x\mathrm{d}^2\hat{\mathbf{k}}_\perp\right]_n \Psi(x, \hat{\mathbf{k}}_\perp)_{n,\alpha} \, |n, \alpha : k_1, ..., k_n\rangle \,, \quad \text{(A.50)}$$

with the LCWFs $\Psi(x, \hat{\mathbf{k}}_\perp)_{n,\alpha}$ of the n-parton-Fock state $|n, \alpha : k_1, ..., k_n\rangle$ and α being a collective index for the parton content, helicity and color of each parton, respectively. The hadron states are normalized as

$$\langle H : P', \mu' | H : P, \mu\rangle = 16\pi^3 P^+ \delta(P'^+ - P^+)\delta^{(2)}(\mathbf{P}'_\perp - \mathbf{P}_\perp)\delta_{\mu'\mu}. \quad \text{(A.51)}$$

A.2.1.4 *Parton content of GPDs and PDFs*

In the last section of this appendix we want to study how (quark) GPDs and PDFs can be interpreted as quantities that give us information about how the partons are distributed inside the hadrons. To obtain this interpretation we employ the light-cone gauge, i.e. $A^+ = 0$.

Let us start with the GPDs. The GPDs are defined by the Fourier transform of a bilocal quark field operator product sandwiched between two non-forward hadron states. For the unpolarized GPDs the following quark field operator product occurs $\bar{\Psi}_q(z_1)\gamma^+\Psi(z_2)_q$. With the considerations of App. A.2.1.3 it can be written as

$$\bar{\Psi}_q(z_1)\gamma^+\Psi_q(z_2) = \Psi^\dagger\gamma^0\gamma^+\Psi(z_2) = \sqrt{2}\left(\mathscr{P}_+\Psi_q\right)(z_1)\left(\mathscr{P}_+\Psi\right)(z_2) = \sqrt{2}\phi_q^\dagger(z_1)\phi_q(z_2). \quad \text{(A.52)}$$

The good quark field operators can be expanded in terms of annihilation/creation operators. The density operator therefore reads

$$\begin{aligned}
\frac{1}{\sqrt{2}}\bar{\Psi}_q(z_1)\gamma^+\Psi(z_2) = \phi_q^\dagger(z_1)\phi_q(z_2) = 2\int \frac{\mathrm{d}k^+}{k^+}\frac{\mathrm{d}^2\mathbf{k}_\perp}{16\pi^3}\,\theta(k^+)\,\frac{\mathrm{d}k'^+}{k'^+}\frac{\mathrm{d}^2\mathbf{k}'_\perp}{16\pi^3}\,\theta(k'^+)\sum_{\lambda,\lambda'} \\
\times\Big[\exp\left(ik^+z_1^- - i\mathbf{k}_\perp\cdot\mathbf{z}_{\perp 1} - ik'^+z_2^- + i\mathbf{k}'_\perp\cdot\mathbf{z}_{\perp 2}\right) b^\dagger(w')b(w)\,u_+^\dagger(w')u_+(w) \\
+\exp\Big(-ik^+z_1^- + i\mathbf{k}_\perp\cdot\mathbf{z}_{\perp 1} + ik'^+z_2^- - i\mathbf{k}'_\perp\cdot\mathbf{z}_{\perp 2}\Big) d(w')d^\dagger(w)\,v_+^\dagger(w')v_+(w) \\
+\exp\Big(-ik^+z_1^- + i\mathbf{k}_\perp\cdot\mathbf{z}_{\perp 1} - ik'^+z_2^- + i\mathbf{k}'_\perp\cdot\mathbf{z}_{\perp 2}\Big) d(w')b(w)v_+^\dagger(w\prime)u_+(w) \\
+\exp\left(ik^+z_1^- - i\mathbf{k}_\perp\cdot\mathbf{z}_{\perp 1} + ik'^+z_2^- + -i\mathbf{k}'_\perp\cdot\mathbf{z}_{\perp 2}\right) b^\dagger(w')d^\dagger(w)u_+^\dagger(w')v_+(w),
\end{aligned} \quad \text{(A.53)}$$

with $w^{(\prime)} = \left(k^{+(\prime)}, \mathbf{k}_\perp^{(\prime)}, \lambda^{(\prime)}\right)$. The operators $b^\dagger(w')b(w)$ and $d^\dagger(w')d(w)$ count the number of quarks and antiquarks, whereas $d(w')b(w)$ and $b^\dagger(w')d^\dagger(w)$ annihilate/create a quark-/antiquark pair, respectively. Which of the four different terms of Eq. (A.53) does contribute in the defining matrix element of the unpolarized GPD is determined by the momentum fraction x, the constraint of positive $k^{+(\prime)}$ momenta and the constraint from momentum conservation, see for example Ref. [5]. We then recover the parton interpretation we have shown in Sec. 1. Similarly we can identify the parton content in the polarized and transversity GPDs. We note however, that the GPDs do not exhibit a probabilistic interpretation, since the the quarks can have different momenta. They are rather amplitudes which describe the correlation to find quarks with different momenta inside the hadrons.

We can furthermore easily include the chiral structure of the operators by defining the chiral projectors

$$\mathscr{P}_{R/L} = \frac{1}{2}\left(1 \pm \gamma_5\right). \tag{A.54}$$

The density operator $\bar{\Psi}_q(z_1)\gamma^+\Psi(z_2)$ "counts" the sum of right- and left-handed good quark field quanta:

$$\bar{\Psi}_q(z_1)\gamma^+\Psi(z_2) = \sqrt{2}\left(\phi^\dagger_{qR}(z_1)\phi_{qR}(z_2) + \phi^\dagger_{qL}(z_2)\phi_{qL}(z_2)\right). \tag{A.55}$$

The density operator for the polarized GPDs, $\bar{\Psi}_q(z_1)\gamma^+\gamma_5\Psi(z_2)$, is sensitive to the "net" helicity:

$$\bar{\Psi}_q(z_1)\gamma^+\Psi(z_2) = \sqrt{2}\left(\phi^\dagger_{qR}(z_1)\phi_{qR}(z_2) - \phi^\dagger_{qL}(z_2)\phi_{qL}(z_2)\right). \tag{A.56}$$

For the transversity GPDs with the density operator $\bar{\Psi}_q(z_1)i\sigma^{+i}\gamma_5\Psi_q(z_2)$, we change from the helicity basis, i.e. states that are eigenstates of the helicity operator introduced in Eq. (A.54),

$$\mathscr{P}_R\left|R\right\rangle = \frac{1}{2}\left|R\right\rangle \quad \text{and} \quad \mathscr{P}_L\left|L\right\rangle = -\frac{1}{2}\left|L\right\rangle \tag{A.57}$$

to the *transversity basis*, i.e. states that are eigenstates of $\mathscr{Q}_\pm = \frac{1}{2}\left(1 \mp \gamma_5\gamma_1\right)$:

$$\mathscr{Q}_+\left|\uparrow\right\rangle = \left|\uparrow\right\rangle \quad \text{and} \quad \mathscr{Q}_-\left|\downarrow\right\rangle = \left|\downarrow\right\rangle. \tag{A.58}$$

Those states are, of course, linear combinations of the helicity states,

$$\left|\uparrow\right\rangle = \frac{1}{\sqrt{2}}\left(\left|R\right\rangle + \left|L\right\rangle\right) \quad \text{and} \quad \left|\downarrow\right\rangle = \frac{1}{\sqrt{2}}\left(\left|R\right\rangle - \left|L\right\rangle\right). \tag{A.59}$$

In the transversity basis $\bar{\Psi}_q(z_1)i\sigma^{+i}\gamma_5\Psi_q(z_2)$ can be written as

$$\bar{\Psi}_q(z_1)i\sigma^{+i}\gamma_5\Psi_q(z_2) = \frac{1}{\sqrt{2}}\left(\phi^\dagger_{q\uparrow}(z_1)\phi_{q\uparrow}(z_2) - \phi^\dagger_{q\downarrow}(z_1)\phi_{q\downarrow}(z_2)\right). \tag{A.60}$$

The partonic and chiral structure of the bilocal quark field operators appearing in the definition of the PDFs is the same as for the GPDs. There is one change, however:

The PDFs are defined by forward matrix elements. So the quarks carry the same momentum. The number density interpretation (probabilistic interpretation) becomes then manifest: The operator $\bar{\Psi}_q(z_1)\gamma^+\Psi(z_2)$ counts the sum of right- and left-handed good quark field quanta, the operator $\bar{\Psi}_q(z_1)\gamma^+\gamma_5\Psi(z_2)$ counts the right-handed quarks minus the left-handed quarks and the operator $\bar{\Psi}_q(z_1)i\sigma^{+i}\gamma_5\Psi(z_2)$ counts the quarks in the $|\uparrow\rangle$ state minus the quarks in the $|\downarrow\rangle$ state.
This number operator idea corresponds to the particular choice of the light-cone gauge. There is also a further hitch here: The bilocal quark field operators, defining the PDFs are divergent in the ultraviolet[10]. Literally taken, this removes the possibility of interpreting the PDFs as number densities.
"The factorization formula merely permit them to be used as if they are number densities, since the factorizations have the form of PDFs convoluted with a short-distance cross section."-quote taken from Ref. [111].

[10]The renormalization of the UV singularities introduces the scale μ_F into the PDFs: Roughly speaking, the factorization scale is the upper cutoff for what momenta belong to the PDF.

B

Kinematics in a symmetric center-of-momentum-system

In this appendix we discuss the kinematics of a two particle scattering process of the form $a + b \to c + d$ in a symmetric center-of-momentum-system (CMS). A symmetric CMS is a frame in which the transverse momentum transfer of the incoming and outgoing particles is treated in a symmetric way. We denote the momentum and mass of the incoming particles a and b by p, m_a and q, m_b, respectively, those of the outgoing particles c and d by p', m_c and q', m_d, respectively, see Fig. B.1.

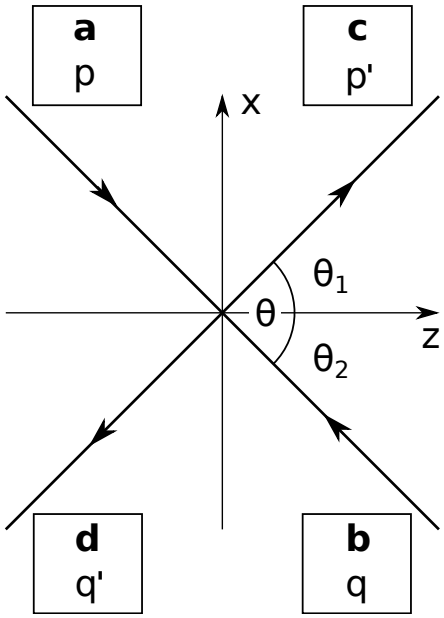

Figure B.1: CMS kinematics of $a + b \to c + d$. The z-axis of our symmetric CMS is aligned along the three vector part of $\bar{\mathbf{p}}$, defined in Eq. (B.2).

The momenta are parameterized in light-cone (LC) coordinates (cf. App. A for their definition). For the momenta of the particle a and particle b we write

$$p = \left[(1+\xi)\bar{p}^+, \frac{m_a^2 + \boldsymbol{\Delta}_\perp^2/4}{2(1+\xi)\bar{p}^+}, -\frac{\boldsymbol{\Delta}_\perp}{2}\right] \quad \text{and} \quad p' = \left[(1-\xi)\bar{p}^+, \frac{m_c^2 + \boldsymbol{\Delta}_\perp^2/4}{2(1-\xi)\bar{p}^+}, \frac{\boldsymbol{\Delta}_\perp}{2}\right], \tag{B.1}$$

where we have introduced the average momentum $\bar{p}$, the momentum transfer Δ and the "skewness" parameter ξ. The average momentum and the momentum transfer

are given by[1]

$$\bar{p} := \frac{1}{2}(p + p') \quad \text{and} \quad \Delta := p' - p = q - q'. \tag{B.2}$$

The minus components can be obtained by using the on-mass-shell conditions $p^2 = m_a^2$ and $p'^2 = m_c^2$. The parameter ξ gives the relative momentum transfer between the particle a and the particle c in the plus direction, i.e.

$$\xi := \frac{p^+ - p'^+}{p^+ + p'^+} = -\frac{\Delta^+}{2\bar{p}^+}. \tag{B.3}$$

The momenta of the particle b and the particle d are written as follows[2]

$$q = \left[\frac{m_b^2 + \boldsymbol{\Delta}_\perp^2/4}{2(1+\eta)\bar{q}^-}, (1+\eta)\bar{q}^-, \frac{\boldsymbol{\Delta}_\perp}{2}\right] \quad \text{and} \quad q' = \left[\frac{m_d^2 + \boldsymbol{\Delta}_\perp^2/4}{2(1-\eta)\bar{q}^-}, (1-\eta)\bar{q}^-, -\frac{\boldsymbol{\Delta}_\perp}{2}\right], \tag{B.4}$$

where we have introduced, in analogy to Eq. (B.2)

$$\bar{q} := \frac{1}{2}(q + q') \quad \text{and} \quad \eta := \frac{q^- - q'^-}{q^- + q'^-} = \frac{\Delta^-}{2\bar{q}^-}. \tag{B.5}$$

The "skewness"-parameter η gives now the relative momentum transfer in the minus direction between the particle b and the particle d.
$\bar{q}^-$ and η are not independent from $\bar{p}^+$ and ξ, but can be related to each other. After a straightforward calculation we find that

$$\bar{q}^- = \bar{p}^+ - \frac{m_a^2 - m_b^2 - m_d^2 + m_c^2}{2\sqrt{2}\sqrt{s}}. \tag{B.6}$$

If we insert the parameterizations of the momenta, cf. Eq. (B.1) and Eq. (B.4) into the definition of the momentum transfer, cf. Eq. (B.2) we find that

$$\eta = \frac{m_c^2\,(1+\xi) - m_a^2\,(1-\xi) + \xi\,\frac{\boldsymbol{\Delta}_\perp^2}{2}}{4\bar{p}^+\bar{q}^-\,(1-\xi^2)}. \tag{B.7}$$

The Mandelstam variable s is given by

$$s = (p+q)^2 = (p'+q')^2, \tag{B.8}$$

which is the invariant mass squared of our process. Mandelstam s has to be larger than $(m_c + m_d)^2$ to produce the particles c and d. The remaining two Mandelstam variables read

$$t = \Delta^2 = (p'-p)^2 = (q-q')^2 \tag{B.9}$$

[1] $\Delta = q - q'$ follows from momentum conservation, i.e. $p + q = p' + q'$.

[2] The role of the plus and minus components are now reversed, as compared to Eq. (B.1), since $q^3 = -p^3$ and $q'^3 = -p'^3$. The minus component is now the "large" component. To be more specific, for example: $q'^{\pm} = \frac{q'^0 \pm q'^3}{\sqrt{2}} = \frac{q'^0 \mp |p'^3|}{\sqrt{2}} = \frac{q'^0 \mp |q'^3|}{\sqrt{2}}$.

and

$$u = (q' - p)^2 = (p' - q)^2, \tag{B.10}$$

such that

$$s + t + u = m_a^2 + m_b^2 + m_c^2 + m_d^2. \tag{B.11}$$

Before we proceed to list the explicit expressions of the various kinematical variables in our symmetric CMS[3], it is convenient to introduce the following abbreviations

$$\Lambda := \sqrt{\left(1 - \frac{(m_a + m_b)^2}{s}\right)\left(1 - \frac{(m_a - m_b)^2}{s}\right)} \tag{B.12}$$

and

$$\Lambda' := \sqrt{\left(1 - \frac{(m_c + m_d)^2}{s}\right)\left(1 - \frac{(m_c - m_d)^2}{s}\right)}. \tag{B.13}$$

The three-momentum of the incoming particle a and its component into the z-direction can be written as

$$|\mathbf{p}| = \frac{\sqrt{s}}{2}\Lambda \quad \text{and} \quad p^3 = \frac{\sqrt{s}}{2}\sqrt{\Lambda^2 - \frac{\mathbf{\Delta}_\perp^2}{s}}. \tag{B.14}$$

The corresponding quantities for the outgoing particle c are

$$|\mathbf{p}'| = \frac{\sqrt{s}}{2}\Lambda' \quad \text{and} \quad |p'^3| = \frac{\sqrt{s}}{2}\sqrt{\Lambda'^2 - \frac{\mathbf{\Delta}_\perp^2}{s}}. \tag{B.15}$$

Note that in our CMS $|\mathbf{q}| = |\mathbf{p}|$, $q^3 = -p^3$, $|\mathbf{q}'| = |\mathbf{p}'|$ and $q'^3 = -p'^3$.
We have chosen our coordinate system in such a way, that p^3 is always positive, but p'^3 can become negative at large scattering angles. The sign change happens when $\mathbf{\Delta}_\perp^2$ reaches its maximum value, i.e.

$$\mathbf{\Delta}_{\perp\max}^2 = s\Lambda'^2. \tag{B.16}$$

We continue to find the expression for the scattering angle $\Theta = \Theta_1 + \Theta_2$, cf. Fig. B.1. The angle Θ_1 is given by

$$\begin{aligned}
\Theta_1 &= \arccos\left(\frac{p'^3}{|\mathbf{p}'|}\right) && = \arccos\left(\operatorname{sign}(p'^3)\sqrt{1 - \frac{\mathbf{\Delta}_\perp^2}{s\Lambda'^2}}\right) \\
&= \arcsin\left(\frac{|\mathbf{\Delta}_\perp|}{2|\mathbf{p}'|}\right) && = \arcsin\left(\frac{|\mathbf{\Delta}_\perp|}{\sqrt{s}\Lambda'}\right) \text{ for } p_3' \geq 0 \\
&= \pi - \arcsin\left(\frac{|\mathbf{\Delta}_\perp|}{2|\mathbf{p}'|}\right) && = \pi - \arcsin\left(\frac{|\mathbf{\Delta}_\perp|}{\sqrt{s}\Lambda'}\right) \text{ for } p_3' < 0,
\end{aligned} \tag{B.17}$$

[3]Since most of the calculations are only tedious (straightforward though) algebra, we do not present them in much detail.

where $\text{sign}(p'^3)$ takes care of the kinematical situation of scattering into the forward or backward hemisphere.
The angle Θ_2 reads

$$\begin{aligned}\Theta_2 = \quad & \arccos\left(\frac{p^3}{|\mathbf{p}|}\right) = \arccos\left(\sqrt{1-\frac{\boldsymbol{\Delta}_\perp^2}{s\Lambda^2}}\right) \\ = \quad & \arcsin\left(\frac{|\boldsymbol{\Delta}_\perp|}{2|\mathbf{p}|}\right) = \arcsin\left(\frac{|\boldsymbol{\Delta}|_\perp}{\sqrt{s}\Lambda}\right).\end{aligned} \tag{B.18}$$

With the help of Eqs. $(B.17)$ and $(B.18)$, the cosine and sine of Θ turn out to be

$$\cos\Theta = \frac{\text{sign}(p'^3)}{\Lambda\Lambda'}\left(\sqrt{\left(\Lambda^2-\frac{\boldsymbol{\Delta}_\perp^2}{s}\right)\left(\Lambda'^2-\frac{\boldsymbol{\Delta}_\perp^2}{s}\right)}-\text{sign}(p'^3)\frac{\boldsymbol{\Delta}_\perp^2}{s}\right) \tag{B.19}$$

and

$$\sin\Theta = \frac{1}{\Lambda\Lambda'}\frac{|\boldsymbol{\Delta}_\perp|}{\sqrt{s}}\left(\sqrt{\Lambda^2-\frac{\boldsymbol{\Delta}_\perp^2}{s}}+\text{sign}(p'^3)\sqrt{\Lambda'^2-\frac{\boldsymbol{\Delta}_\perp^2}{s}}\right). \tag{B.20}$$

Let us now find expressions for $\bar{p}^+$, ξ, $\bar{q}^-$ and η in a compact form. Starting from Eq. $(B.2)$ the plus component of the average momentum can be written with the help of Eqs. $(B.14)$, $(B.15)$, $(B.19)$ and $(B.20)$ as[4]

$$\begin{aligned}\bar{p}^+ &= \frac{1}{2}\left(p^+ + p'^+\right) = \frac{1}{2\sqrt{2}}\left((p^0+p^3)+(p'^0+p'^3)\right) \\ &= \frac{1}{4}\sqrt{\frac{s}{2}}\left(2+\frac{(m_a^2-m_b^2+m_c^2-m_d^2)}{s}+\Gamma\right),\end{aligned} \tag{B.21}$$

where Γ is given by

$$\Gamma = \sqrt{\Lambda^2+\Lambda'^2+2\Lambda\Lambda'\cos\Theta}. \tag{B.22}$$

For the "skewness" parameter ξ we obtain

$$\begin{aligned}\xi &= \frac{p^+-p'^+}{p^++p'^+} = \frac{\frac{1}{\sqrt{2}}\left(p^0-p^3-p'^0-p'^3\right)}{\frac{1}{\sqrt{2}}\left(p^0+p^3+p'^0+p'^3\right)} \\ &= \frac{\left(m_a^2-m_b^2-m_c^2+m_d^2\right)\Gamma+s\left(\Lambda^2-\Lambda'^2\right)}{\left(2s+m_a^2-m_b^2+m_c^2-m_D^2+s\Gamma\right)\Gamma}.\end{aligned} \tag{B.23}$$

[4]The explicit expressions for $p^{(\prime)3}$ were already given in Eqs. (B.14)-(B.15). The energy of the particle a and particle c is $p^0 = \frac{\sqrt{s}}{2}\left(1+\frac{m_a^2-m_b^2}{s}\right)$ and $p'^0 = \frac{\sqrt{s}}{2}\left(1+\frac{m_c^2-m_d^2}{s}\right)$, respectively.

For $\bar{q}^-$ and η we get[5]

$$\begin{aligned}\bar{q}^- &= \frac{1}{2}\left(q^- + q'^-\right) = \frac{1}{2\sqrt{2}}\left((q^0 - q^3) + (q'^0 - q'^3)\right) \\ &= \frac{1}{4}\sqrt{\frac{s}{2}}\left(2 + \frac{(m_b^2 - m_a^2 + m_d^2 - m_c^2)}{s} + \Gamma\right)\end{aligned} \tag{B.24}$$

and

$$\begin{aligned}\eta = \frac{q^- - q'^-}{q^- + q'^-} &= \frac{\frac{1}{\sqrt{2}}\left(q^0 - q^3 - q'^0 + q'^3\right)}{\frac{1}{\sqrt{2}}\left(q^0 - q^3 + q'^0 - q'^3\right)} \\ &= \frac{\left(m_b^2 - m_a^2 + m_c^2 - m_d^2\right)\Gamma + s\left(\Lambda^2 - \Lambda'^2\right)}{\left(2s - m_a^2 + m_b^2 - m_c^2 + m_d^2 + s\Gamma\right)\Gamma}.\end{aligned} \tag{B.25}$$

Next we consider the Mandelstam variables and write them in a more compact form with the help of Eqs. $(B.14)$, $(B.15)$, $(B.19)$ and $(B.20)$.
Mandelstam t can be written as

$$\begin{aligned}t &= m_a^2 + m_c^2 - 2\sqrt{m_a^2 + |\mathbf{p}|^2}\sqrt{m_c^2 + |\mathbf{p}'|^2} + \frac{s}{2}\Lambda\Lambda'\cos\Theta \\ &= \frac{(m_a^2 - m_b^2 - m_c^2 + m_d^2)^2}{4s} - \frac{s}{4}\left(\Lambda^2 + \Lambda'^2 - 2\Lambda\Lambda'\cos\Theta\right).\end{aligned} \tag{B.26}$$

We now specify Mandelstam t for forward $(\theta = 0)$ and backward $(\theta = \pi)$ scattering. For forward scattering it acquires the value

$$\begin{aligned}t_0 &:= t(\boldsymbol{\Delta}_\perp^2 = 0, p'^3 \geq 0) \\ &= \frac{(m_a^2 - m_b^2 - m_c^2 + m_d^2)^2}{4s} - \frac{s}{4}\left(\Lambda - \Lambda'\right)^2\end{aligned} \tag{B.27}$$

and for backward scattering

$$\begin{aligned}t_1 &:= t(\boldsymbol{\Delta}_\perp^2 = 0, p'^3 \leq 0) \\ &= \frac{(m_a^2 - m_b^2 - m_c^2 + m_d^2)^2}{4s} - \frac{s}{4}\left(\Lambda + \Lambda'\right)^2.\end{aligned} \tag{B.28}$$

Furthermore we can introduce a "reduced" Mandelstam variable t' that vanishes for forward scattering, i.e.

$$\begin{aligned}t' &:= t - t_0 \\ &= -\frac{s}{2}\Lambda\Lambda'(1 - \cos\Theta).\end{aligned} \tag{B.29}$$

[5] $q^{(\prime)3}$ are related to $p^{(\prime)3}$, cf. the statement after Eq. (B.15). The energy of the particle b and particle d is $q^0 = \frac{\sqrt{s}}{2}\left(1 + \frac{m_b^2 - m_a^2}{s}\right)$ and $q'^0 = \frac{\sqrt{s}}{2}\left(1 + \frac{m_d^2 - m_c^2}{s}\right)$, respectively.

Mandelstam u is given by

$$\begin{aligned} u &= -s - t + m_a^2 + m_b^2 + m_c^2 + m_d^2 \\ &= \frac{(m_a^2 - m_b^2 + m_c^2 - m_d^2)^2}{4s} - \frac{s}{4}\left(\Lambda^2 + \Lambda'^2 + 2\Lambda\Lambda'\cos\Theta\right). \end{aligned} \tag{B.30}$$

For forward scattering it becomes

$$\begin{aligned} u_0 &:= u(\boldsymbol{\Delta}_\perp^2 = 0, p'^3 \geq 0) \\ &= \frac{(m_a^2 - m_b^2 + m_c^2 - m_d^2)^2}{4s} - \frac{s}{4}\left(\Lambda + \Lambda'\right)^2 \end{aligned} \tag{B.31}$$

and for backward scattering

$$\begin{aligned} u_1 &:= u(\boldsymbol{\Delta}_\perp^2 = 0, p'^3 \leq 0) \\ &= \frac{(m_a^2 - m_b^2 + m_c^2 - m_d^2)^2}{4s} - \frac{s}{4}\left(\Lambda - \Lambda'\right)^2. \end{aligned} \tag{B.32}$$

The "reduced" Mandelstam variable u'

$$\begin{aligned} u' &:= u - u_1 \\ &= -\frac{s}{2}\Lambda\Lambda'(1 + \cos\Theta) \end{aligned} \tag{B.33}$$

vanishes for backward scattering.

We can write the transverse component of Δ as a function of the CMS scattering angle Θ, using Eqs. $(B.19)$ and $(B.20)$

$$\boldsymbol{\Delta}_\perp^2 = s\frac{\Lambda^2\Lambda'^2\,\sin^2\Theta}{(\Lambda^2 + \Lambda'^2 + 2\Lambda\Lambda'\cos\Theta)}, \tag{B.34}$$

or we solve Eq. $(B.26)$ for $\boldsymbol{\Delta}_\perp^2$ which gives

$$\boldsymbol{\Delta}_\perp^2 = -t'\frac{t' + s\Lambda\Lambda'}{t' + \frac{s}{4}\left(\Lambda + \Lambda'\right)^2}. \tag{B.35}$$

We now have expressions for the most important kinematical quantities in the most general case (unequal mass kinematics) for a two-body scattering process in the symmetric CMS system.

C

The $p \to \Lambda_c^+$ Generalized Parton Distributions

C.1 Introduction

In this appendix we discuss the $p \to \Lambda_c^+$ GPDs which were introduced for the first time in Ref. [11]. These GPDs parameterize the hadronic matrix element which describes the non-perturbative transition from the proton to the charmed Lambda that appears in the hadronic scattering amplitude Eqs. (2.34) and (2.95). For convenience we repeat it here

$$\bar{p}^+ \int \frac{\mathrm{d}z^-}{(2\pi)} e^{i\bar{x}\bar{p}^+ z^-} \langle \Lambda_c^+ : p', \mu' | \, \overline{\Psi}^c \left(-\frac{z^-}{2} \right) \Psi^u \left(\frac{z^-}{2} \right) \, | p : p, \mu \rangle \, . \tag{C.1}$$

The average momentum is denoted by $\bar{p} = \frac{p+p'}{2}$ and the average momentum fraction by $\bar{x} = \frac{\bar{k}^+}{\bar{p}^+}$, respectively, with $\bar{k} = \frac{k_1 + k_1'}{2}$. In Eq. (C.1) $\Psi^u(z^-/2)$ takes out a u-quark at space-time $z^-/2$ from the proton state $|p : p, \mu\rangle$, which then participates in the hard partonic subprocess, whereas $\overline{\Psi}^c(-z^-/2)$ reinserts the produced c-quark at space-time $-z^-/2$ into the remainder of the proton which gives the final Λ_c^+ hadron, see also Fig. C.1.

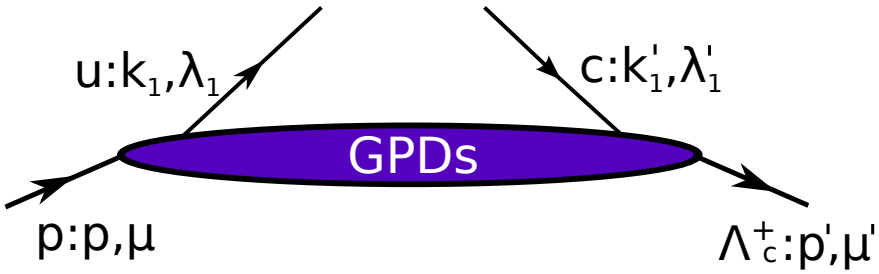

Figure C.1: Graphical representation of the $p \to \Lambda_c^+$ GPDs.

The procedure to project out the leading twist contributions of the quark field operator product in Eq. (C.1) is the following:
First, the quark field operators Ψ^u and Ψ^c are studied in the hadron-in frame of the proton and hadron-out frame of the Λ_c^+, respectively. These are frames in which the incoming or the outgoing hadron have no transverse momentum components. In such a frame, the dominant components of the quark fields are the, so called, "good" components, cf. Ref. [11] or Sec. 2.4.2 for more details. It turns out that in these frames

Ψ^u and Ψ^c can be written as

$$\Psi^u(z/2) = \frac{1}{2k_1^+} \sum_{\lambda_1} u(k_1, \lambda_1) \left(\overline{u}(k_1, \lambda_1) \gamma^+ \Psi^u(z/2) \right), \tag{C.2}$$

$$\Psi^c(-z/2) = \frac{1}{2k_1'^+} \sum_{\lambda_1'} u(k_1', \lambda_1') \left(\overline{u}(k_1', \lambda_1') \gamma^+ \Psi^c(-z/2) \right). \tag{C.3}$$

This is also true if one goes back to the CMS by a transverse boost, since a transverse boost does not change the plus components (of any 4-vector). With Eqs. (C.2) and (C.3) at hand we can write for the bilocal product

$$\begin{aligned}
&\overline{\Psi}^c(-z/2)\, \Psi^u(+z/2) = \\
&= \frac{1}{4k_1^+ k_1'^+} \sum_{\lambda_1} \Big[\Big(\overline{\Psi}^c(-z/2) \gamma^+ u(k_1', \lambda_1) \Big) \Big(\overline{u}(k_1, \lambda_1) \gamma^+ \Psi^u(z/2) \Big) \overline{u}(k_1', \lambda_1) u(k_1, \lambda_1) \\
&+ \Big(\overline{\Psi}^c(-z/2) \gamma^+ u(k_1', -\lambda_1) \Big) \Big(\overline{u}(k_1, \lambda_1) \gamma^+ \Psi^u(z/2) \Big) \overline{u}(k_1', -\lambda_1) u(k_1, \lambda_1) \Big],
\end{aligned} \tag{C.4}$$

where we have used $\lambda_1' = \pm\lambda_1$ to separate the product of quark fields into (LC) helicity non-flip and helicity flip configurations of the active quarks at the $p \to \Lambda_c^+$ vertex. The products of quark fields in Eq. (C.4) can be further simplified using appropriate LC spinor products and helicity projectors. In fact, inserting

$$\frac{\overline{u}(k_1', \lambda_1) \gamma^+ u(k_1, \lambda_1)}{2\sqrt{k_1^+ k_1'^+}} = 1, \tag{C.5}$$

between $u(k_1', \lambda_1)\overline{u}(k_1, \lambda_1)$ and

$$\frac{1}{i(2\lambda_1 i)^j} \frac{\overline{u}(k_1', -\lambda_1) i\sigma^{+j} u(k_1, \lambda_1)}{2\sqrt{k_1^+ k_1'}} = 1, \tag{C.6}$$

between $u(k_1', -\lambda_1)\overline{u}(k_1, \lambda_1)$ (with $j = 1, 2$ and $\sigma^{\pm j} = i\gamma^\pm \gamma^j$) we obtain for the non-helicity flip term in Eq. (C.4)

$$\begin{aligned}
&\overline{\Psi}^c(-z/2) \gamma^+ u(k_1', \lambda_1) \overline{u}(k_1, \lambda_1) \gamma^+ \Psi^u(z/2) = \\
&= \frac{1}{2\sqrt{k_1^+ k_1'^+}} \overline{\Psi}^c(-z/2) \gamma^+ u(k_1', \lambda_1) \overline{u}(k_1', \lambda_1) \gamma^+ u(k_1, \lambda_1) \overline{u}(k_1, \lambda_1) \gamma^+ \Psi^u(z/2)
\end{aligned} \tag{C.7}$$

and for the helicity flip term in Eq. (C.4)

$$\begin{aligned}
&\overline{\Psi}^c(-z/2) \gamma^+ u(k_1', -\lambda_1) \overline{u}(k_1, \lambda_1) \gamma^+ \Psi^u(z/2) = \\
&= \frac{1}{2\sqrt{k_1^+ k_1'^+}} \frac{1}{i(2\lambda_1 i)^j} \overline{\Psi}^c(-z/2) \gamma^+ u(k_1', -\lambda_1) \overline{u}(k_1' - \lambda_1) i\sigma^{+j} u(k_1, \lambda_1) \overline{u}(k_1, \lambda_1) \gamma^+ \Psi^u(z/2),
\end{aligned} \tag{C.8}$$

respectively. The reason for the insertions of Eqs. $(C.5)$ and $(C.6)$ is that we can now use the helicity projectors of the (massless) u-quark and the (heavy) c-quark. They explicitly read (they coincide for $m_c \to 0$)

$$u(k_1,\lambda_1)\overline{u}(k_1,\lambda_1) = k_1\cdot\gamma\frac{1-2\lambda_1\,\gamma_5}{2} \tag{C.9}$$

and

$$u(k_1',\lambda_1')\overline{u}(k_1',\lambda_1') = \Big(k_1'\cdot\gamma + m_c\Big)\frac{1+\gamma_5\,S_1\cdot\gamma}{2}. \tag{C.10}$$

The covariant spin vector

$$S_1 = \frac{2\lambda_1'}{m_c}\big(k_1'^{+} - \frac{m_c^2}{k_1'^{+}}n^-\big) \tag{C.11}$$

is needed for the c-quark with n^- being a unit vector pointing into the minus LC direction.

Now putting everything together, i.e. inserting the helicity projectors into Eqs. $(C.7)$ and $(C.8)$ and those further into Eq. $(C.4)$, we obtain after some algebra for our bilocal product of quark fields

$$\begin{aligned}
&\overline{\Psi}^c(-z/2)\Psi^u(z/2) = \\
&\frac{1}{2\sqrt{k_1^+k_1'^+}}\sum_{\lambda_1}\Big\{\overline{\Psi}^c(-z/2)\gamma^+\frac{1+2\lambda_1\gamma_5}{2}\Psi^u(z/2)\overline{u}(k_1',\lambda_1)u(k_1,\lambda_1) \\
&-\,i(-2\lambda_1 i)^j\overline{\Psi}^c(-z/2)i\sigma^{+j}\frac{1+2\lambda_1\gamma_5}{2}\Psi^u(z/2)\overline{u}(k_1',-\lambda_1)u(k_1,\lambda_1)\Big\}.
\end{aligned} \tag{C.12}$$

Thus we obtain as our final result for Eq. $(C.1)$

$$\begin{aligned}
&\bar{p}^+\int\frac{\mathrm{d}z^-}{(2\pi)}e^{i\bar{x}\bar{p}^+z^-}\,\langle\Lambda_c^+:p',\mu'|\overline{\Psi}^c\left(-\frac{z^-}{2}\right)\Psi^u\left(\frac{z^-}{2}\right)|p:p,\mu\rangle = \\
&\frac{1}{4\sqrt{k_1^+k_1'^+}}\sum_{\lambda_1}\bar{p}^+\int\frac{dz^-}{2\pi}e^{i\bar{x}\bar{p}^+z^-}\,\langle\Lambda_c^+:p',\mu'|\Big\{\overline{u}(k_1',\lambda_1)u(k_1,\lambda_1) \\
&\Big[\overline{\Psi}^c(-z^-/2)\gamma^+\Psi^u(z^-/2)+2\lambda_1\overline{\Psi}^c(-z^-/2)\gamma^+\gamma_5\Psi^u(z^-/2)\Big] \\
&-\,i\,(-2\lambda_1 i)^j\,\overline{u}(k_1',-\lambda_1)u(k_1,\lambda_1) \\
&\Big[\overline{\Psi}^c(-z^-/2)i\sigma^{+j}\Psi^u(z^-/2)+2\lambda_1\overline{\Psi}^c(-z^-/2)i\sigma^{+j}\gamma_5\Psi^u(z^-/2)\Big]\Big\}|p:p,\mu\rangle.
\end{aligned} \tag{C.13}$$

We have finally achieved that there are only leading twist quark field operator contributions. The advantage of Eq. $(C.13)$ is, that it is suitable for a parameterization in terms of GPDs after introducing an appropriate notation. Before we switch to the new notation, let us define vector, axial-vector and tensor currents of bilocal

quark-field-operator products

$$V^\mu(-z/2,z/2) := \overline{\Psi}^c(-z/2)\ \gamma^\mu\ \Psi^u(z/2) - \overline{\Psi}^u(z/2)\ \gamma^\mu\ \Psi^c(-z/2), \tag{C.14}$$

$$A^\mu(-z/2,z/2) := \overline{\Psi}^c(-z/2)\gamma^\mu\gamma_5\Psi^u(z/2) - \overline{\Psi}^u(z/2)\gamma^\mu\gamma_5\Psi^c(-z/2), \tag{C.15}$$

$$T^{\mu\nu}(-z/2,z/2) := \overline{\Psi}^c(-z/2)i\sigma^{\mu\nu}\Psi^u(z/2) - \overline{\Psi}^u(z/2)i\sigma^{\mu\nu}\Psi^c(-z/2) \tag{C.16}$$

and

$$T_5^{\mu\nu}(-z/2,z/2) := \overline{\Psi}^c(-z/2)i\sigma^{\mu\nu}\gamma_5\Psi^u(z/2) - \overline{\Psi}^u(z/2)i\sigma^{\mu\nu}\gamma_5\Psi^c(-z/2). \tag{C.17}$$

The antiparticle contribution has been added to have manifest charge-conjugation symmetry. Since we neglect the intrinsic charm content of the proton this can be done without getting any troubles. The new notation is the following

$$\mathscr{H}^{cu}_{\mu'\mu} := \bar{p}^+ \int \frac{dz^-}{2\pi} e^{i\bar{x}\bar{p}^+z^-} \left\langle \Lambda_c^+ : p',\mu' \right| V^+(-z^-/2,z^-/2) \left| p : p,\mu \right\rangle, \tag{C.18}$$

$$\widetilde{\mathscr{H}}^{cu}_{\mu'\mu} := \bar{p}^+ \int \frac{dz^-}{2\pi} e^{i\bar{x}\bar{p}^+z^-} \left\langle \Lambda_c^+ : p',\mu' \right| A^+(-z^-/2,z^-/2) \left| p : p,\mu \right\rangle, \tag{C.19}$$

$$\mathscr{H}^{Tcu}_{j\mu'\mu} := \bar{p}^+ \int \frac{dz^-}{2\pi} e^{i\bar{x}\bar{p}^+z^-} \left\langle \Lambda_c^+ : p',\mu' \right| T^{+j}(-z^-/2,z^-/2) \left| p : p,\mu \right\rangle, \tag{C.20}$$

$$\mathscr{H}^{Tcu}_{5j\mu'\mu} := \bar{p}^+ \int \frac{dz^-}{2\pi} e^{i\bar{x}\bar{p}^+z^-} \left\langle \Lambda_c^+ : p',\mu' \right| T_5^{+j}(-z^-/2,z^-/2) \left| p : p,\mu \right\rangle. \tag{C.21}$$

The action of V^+, A^+, T^{+j} and T_5^{+j} on the quark fields is that

- V^+ and A^+ do not flip the helicities of the active quarks, whereas
- T^{+j} and T_5^{+j} do.

$\mathscr{H}^{cu}_{\mu'\mu}$ and $\widetilde{\mathscr{H}}^{cu}_{\mu'\mu}$ are from now on referred to as quark helicity non-flip $p \to \Lambda_c^+$ transition matrix elements, whereas $\mathscr{H}^{Tcu}_{j\mu'\mu}$ and $\mathscr{H}^{Tcu}_{5j\mu'\mu}$ are called quark helicity flip $p \to \Lambda_c^+$ transition matrix elements.

With this new notation Eq. (C.13) reads

$$\begin{aligned}
&\bar{p}^+ \int \frac{\mathrm{d}z^-}{(2\pi)} e^{i\bar{x}\bar{p}^+z^-} \left\langle \Lambda_c^+ : p',\mu' \right| \overline{\Psi}^c\left(-\frac{z^-}{2}\right) \Psi^u\left(\frac{z^-}{2}\right) \left| p : p,\mu \right\rangle = \\
&\frac{1}{4\sqrt{k_1^+ k_1'^+}} \sum_{\lambda_1} \Big\{ \Big[\mathscr{H}^{cu}_{\mu'\mu} + 2\lambda_1 \widetilde{\mathscr{H}}^{cu}_{\mu'\mu} \Big] \overline{u}(k_1',\lambda_1) u(k_1,\lambda_1) \\
&-i(-2\lambda_1 i)^j \Big[\mathscr{H}^{Tcu}_{j\mu'\mu} + 2\lambda_1 \mathscr{H}^{Tcu}_{5j\mu'\mu} \Big] \overline{u}(k_1',-\lambda_1) u(k_1,\lambda_1) \Big\}.
\end{aligned} \tag{C.22}$$

Using

$$\sigma^{+1}\gamma_5 = -i\sigma^{+2} \qquad \text{and} \qquad \sigma^{+2}\gamma_5 = i\sigma^{+1}, \tag{C.23}$$

we can show that T_5^{+j} and T^{+j} are not independent. The relation between them is: $T_5^{+j} = (-1)^j T^{+k}$ with $k \neq j$ and $k, j = 1, 2$.

Thus the $p \to \Lambda_c^+$ transition matrix element finally becomes:

$$\bar{p}^+ \int \frac{\mathrm{d}z^-}{(2\pi)} e^{i\bar{x}\bar{p}^+ z^-} \langle \Lambda_c^+ : p', \mu' | \overline{\Psi}^c \left(-\frac{z^-}{2} \right) \Psi^u \left(\frac{z^-}{2} \right) | p : p, \mu \rangle = \frac{1}{4\sqrt{k_1^+ k_1'^+}} \sum_{\lambda_1} \left\{ \left[\mathscr{H}^{cu}_{\mu'\mu} + 2\lambda_1 \widetilde{\mathscr{H}}^{cu}_{\mu'\mu} \right] \overline{u}(k_1', \lambda_1) u(k_1, \lambda_1) - \lambda_1 \mathscr{H}^{Tcu}_{\lambda_1 \mu' \mu} \overline{u}(k_1', -\lambda_1) u(k_1, \lambda_1) \right\}. \tag{C.24}$$

We introduced

$$\mathscr{H}^{Tcu}_{\lambda_1 \mu' \mu} := \frac{1}{2} \left(\mathscr{H}^{Tcu}_{1\mu'\mu} - 2\lambda_1 i \mathscr{H}^{Tcu}_{2\mu'\mu} \right), \tag{C.25}$$

for later convenience. Equation (C.24) is separated into quark helicity non-flip contributions (involving $\mathscr{H}^{cu}_{\mu'\mu}$ and $\widetilde{\mathscr{H}}^{cu}_{\mu'\mu}$) and a quark helicity flip contribution (involving $\mathscr{H}^{Tcu}_{\lambda_1\mu'\mu}$). Both can be parameterized by GPDs as summarized in the following two subsections.

C.2 Quark helicity non-flip $p \to \Lambda_c^+$ transition matrix elements

The quark helicity-conserving distributions in the flavor-diagonal case have been considered for example in Ref. [112]. The Dirac structure in our case is the same as therein, though for our case we have to take the $u \to c$ transition in flavor space into account.
Let us start with the parameterization of $\mathscr{H}^{cu}_{\mu'\mu}$

$$\begin{aligned} \mathscr{H}^{cu}_{\mu'\mu} &= \bar{p}^+ \int \frac{dz^-}{2\pi} e^{i\bar{x}\bar{p}^+ z^-} \langle \Lambda_c^+ : p', \mu' | \, V^+(-z^-/2, z^-/2) \, | p : p, \mu \rangle \\ &= \overline{u}(p', \mu') \left[H^{cu}_{p\Lambda_c}(\bar{x}, \xi, t) \gamma^+ + E^{cu}_{p\Lambda_c}(\bar{x}, \xi, t) \, \frac{i\sigma^{+\nu}\Delta_\nu}{M_{\Lambda_c} + m_p} \right] u(p, \mu), \end{aligned} \tag{C.26}$$

with $H^{cu}_{p\Lambda_c}(\bar{x}, \xi, t)$ and $E^{cu}_{p\Lambda_c}(\bar{x}, \xi, t)$ being the GPDs. If we use the spinor product tables of App. C of Ref. [113] we can see that, although in the matrix element $\mathscr{H}^{cu}_{\mu'\mu}$ a quark helicity flip is not allowed, $\overline{u}(p', \mu') \frac{i\sigma^{+\nu}\Delta_\nu}{M_{\Lambda_c}+m_p} u(p, \mu)$ is associated with a hadron helicity flip. Consequently there is a mismatch between partonic and hadronic helicities. To resolve this mismatch we need a non-vanishing orbital angular momentum between active partons and spectators, in this case one unit of orbital angular momentum. As we discussed in Sec. 2.3.3 we are modeling our GPDs with LCWFs with zero orbital angular momentum. Thus, the GPD $E^{cu}_{p\Lambda_c}$ and in further consequence its associated transition form factor will vanish in our model.

Let us proceed with $\widetilde{\mathscr{H}}^{cu}_{\mu'\mu}$

$$\begin{aligned}\widetilde{\mathscr{H}}^{cu}_{\mu'\mu} &= \bar{p}^+ \int \frac{dz^-}{2\pi} e^{i\bar{x}\bar{p}^+ z^-} \langle \Lambda_c^+ : p', \mu' | A^+(-z^-/2, z^-/2) | p : p, \mu \rangle \\ &= \overline{u}(p', \mu') \left[\widetilde{H}^{cu}_{p\Lambda_c}(\bar{x}, \xi, t) \gamma^+ \gamma_5 + \widetilde{E}^{cu}_{p\Lambda_c}(\bar{x}, \xi, t) \frac{\Delta^+}{M_{\Lambda_c} + m_p} \gamma_5 \right] u(p, \mu).\end{aligned} \tag{C.27}$$

The GPDs are now $\widetilde{H}^{cu}_{p\Lambda_c}(\bar{x}, \xi, t)$ and $\widetilde{E}^{cu}_{p\Lambda_c}(\bar{x}, \xi, t)$. Comparison with the spinor table reveals that $\overline{u}(p', \mu') \frac{\Delta^+}{M_{\Lambda_c}+m_p} \gamma_5 u(p, \mu)$ is associated with a hadron helicity flip and we therefore conclude (see remarks above) that $\widetilde{E}^{cu}_{p\Lambda_c}(\bar{x}, \xi, t)$ can be neglected within our model framework.
The various occurring covariants in Eqs. (C.26) and (C.27) can be evaluated for our symmetric CMS system and thus our final results for the transition matrix elements are [11]

$$\mathscr{H}^{cu}_{\mu\mu} = 2\bar{p}^+ \sqrt{1-\xi^2} \left[H^{cu}_{p\Lambda_c} - \frac{\xi}{1-\xi^2} \widetilde{M} E^{cu}_{p\Lambda_c} \right], \tag{C.28}$$

$$\mathscr{H}^{cu}_{-\mu\mu} = 2\epsilon\bar{p}^+ \sqrt{1-\xi^2} \frac{1}{1-\xi^2} \frac{\boldsymbol{\Delta}_\perp}{M_{\Lambda_c} + m_p} E^{cu}_{p\Lambda_c}, \tag{C.29}$$

and

$$\widetilde{\mathscr{H}}^{cu}_{\mu\mu} = 2\epsilon\bar{p}^+ \sqrt{1-\xi^2} \left[\widetilde{H}^{cu}_{p\Lambda_c} - \frac{\xi}{1-\xi^2} \widetilde{M} \widetilde{E}^{cu}_{p\Lambda_c} \right], \tag{C.30}$$

$$\widetilde{\mathscr{H}}^{cu}_{-\mu\mu} = 2\bar{p}^+ \sqrt{1-\xi^2} \frac{\xi}{1-\xi^2} \frac{\boldsymbol{\Delta}_\perp}{M_{\Lambda_c} + m_p} \widetilde{E}^{cu}_{p\Lambda_c}, \tag{C.31}$$

with $\epsilon = (-1)^{\mu - 1/2}$ and $\widetilde{M} = \frac{(1+\xi)M_{\Lambda_c} - (1-\xi)m_p}{M_{\Lambda_c}+m_p}$.

C.3 Quark helicity flip $p \to \Lambda_c^+$ transition matrix elements

Quark helicity flip distributions for the flavor diagonal case have been considered in Ref. [4]. It was discussed in this paper that there are four independent distributions. $\mathscr{H}^{Tcu}_{j\mu'\mu}$ can be decomposed into the following Dirac structures:

$$\begin{aligned}\mathscr{H}^{Tcu}_{j\mu'\mu} &= \bar{p}^+ \int \frac{dz^-}{2\pi} e^{i\bar{x}\bar{p}^+ z^-} \langle \Lambda_c^+ : p', \mu' | T^{+j}(-z_1^-/2, z_1^-/2) | p : p, \mu \rangle \\ &= \overline{u}(p', \mu') \left[H^{cu}_{T\, p\Lambda_c}(\bar{x}, \xi, t) i\sigma^{+j} + \widetilde{H}^{cu}_{T\, p\Lambda_c}(\bar{x}, \xi, t) \frac{\bar{p}^+ \Delta^j - \Delta^+ \bar{p}^j}{M_\Lambda m_p} \right. \\ &\left. + E^{cu}_{T\, p\Lambda_c}(\bar{x}, \xi, t) \frac{\gamma^+ \Delta^j - \Delta^+ \gamma^j}{M_\Lambda + m_p} + \widetilde{E}^{cu}_{T\, p\Lambda_c}(\bar{x}, \xi, t) \frac{\gamma^+ \bar{p}^j - \bar{p}^+ \gamma^j}{(M_\Lambda + m_p)/2} \right] u(p, \mu).\end{aligned} \tag{C.32}$$

In Eq. (C.32) all four covariants, in general, contribute if the baryon helicity flips. If it is not flipped $\overline{u}(p', \mu') i\sigma^{+j} u(p, \mu)$ vanishes, the remaining three covariants still being non-zero. We recall that the mismatch between partonic and hadronic helicities is to be compensated by an appropriate number of units of orbital angular momentum in

the hadronic wave functions. We therefore expect the contributions parameterized by $\widetilde{H}^{cu}_{T\,p\Lambda_c}, E^{cu}_{T\,p\Lambda_c}$ and $\widetilde{E}^{cu}_{T\,p\Lambda_c}$ to be suppressed for ground state wave functions with zero orbital angular momenta.
After evaluating the spinor products in Eq. (C.32) we arrive at [11]

$$\mathscr{H}^{Tcu}_{\lambda_1\mu\mu} = \frac{\bar{p}^+}{\sqrt{1-\xi^2}}\frac{\boldsymbol{\Delta}^2_\perp}{M_{\Lambda_c}+m_p}\left\{(M_{\Lambda_c}+m_p)\frac{(1+\xi)M_{\Lambda_c}+(1-\xi)m_p}{2m_pM_{\Lambda_c}}\widetilde{H}^{cu}_{T\,p\Lambda_c}(\bar{x},\xi,t)\right.$$
$$\left. + [1+2\lambda_1\epsilon\xi]\,E^{cu}_{T\,p\Lambda_c}(\bar{x},\xi,t) - [\xi+2\lambda_1\epsilon]\,\widetilde{E}^{cu}_{T\,p\Lambda_c}(\bar{x},\xi,t)\right\}, \tag{C.33a}$$

$$\mathscr{H}^{Tcu}_{\lambda_1-\mu\mu} = -\frac{\bar{p}^+}{\sqrt{1-\xi^2}}\left\{(1-\xi^2)(\epsilon+2\lambda_1)H^{cu}_{T\,p\Lambda_c}(\bar{x},\xi,t) + \epsilon\frac{\Delta_\perp}{2M_{\Lambda_c}m_p}\widetilde{H}^{cu}_{T\,p\Lambda_c}(\bar{x},\xi,t)\right.$$
$$\left. - (\epsilon+2\lambda_1)\widetilde{M}\left[\xi\,E^{cu}_{T\,p\Lambda_c}(\bar{x},\xi,t) - \tilde{E}^{cu}_{T\,p\Lambda_c}(\bar{x},\xi,t)\right]\right\}. \tag{C.33b}$$

C.4 Transition form factors

Using the peaking approximation we need the integral over the GPDs rather than the GPDs themselves in the scattering amplitude. The transition form factors are defined by

$$\mathrm{FF}_i(\xi,t) = \int_\xi^1 \frac{\mathrm{d}\bar{x}}{\sqrt{\bar{x}^2-\xi^2}}\mathrm{GPD}_i(\bar{x},\xi,t), \tag{C.34}$$

where GPD_i stands for any of our transition GPDs and FF_i for their associated transition form factor (FF).
The correspondence between them is as follows

$$\begin{aligned} &H^{cu}_{T\,p\Lambda_c}, \widetilde{H}^{cu}_{p\Lambda_c},\ E^{cu}_{p\Lambda_c},\ \widetilde{E}^{cu}_{p\Lambda_c},\ H^{cu}_{T\,p\Lambda_c},\ \widetilde{H}^{cu}_{T\,p\Lambda_c},\ E^{cu}_{T\,p\Lambda_c},\ \widetilde{E}^{cu}_{T\,p\Lambda_c} \\ \leftrightarrow &R_V,\ R_A,\ R_T,\ R_P,\ S_T,\ S_S,\ S_{V1},\ S_{V2}. \end{aligned} \tag{C.35}$$

We see that taking ξ as the lower limit of integration in Eq. (C.34) leads to a ξ (or equivalently s) dependence of the FFs. Turning on the CMS energy, however, this dependence becomes weaker and in the limit $s \to \infty$ it disappears. The reason why we take for the $\bar{x}$-integration as a lower bound ξ instead of 0 is that we are interested in the GPDs in the *DGLAP*-region.

Finally we list explicit expressions for the integrals over the transition matrix

elements

$$\int_\xi^1 \frac{\mathrm{d}\bar{x}}{\sqrt{\bar{x}^2-\xi^2}} \mathscr{H}^{cu}_{\mu\mu} = 2\bar{p}^+ \sqrt{1-\xi^2}\left[R_V - \frac{\xi}{1-\xi^2}\widetilde{M} R_T\right], \tag{C.36}$$

$$\int_\xi^1 \frac{\mathrm{d}\bar{x}}{\sqrt{\bar{x}^2-\xi^2}} \mathscr{H}^{cu}_{-\mu\mu} = 2\epsilon\bar{p}^+ \sqrt{1-\xi^2}\frac{1}{1-\xi^2}\frac{\Delta_\perp}{M_{\Lambda_c}+m_p} R_T, \tag{C.37}$$

$$\int_\xi^1 \frac{\mathrm{d}\bar{x}}{\sqrt{\bar{x}^2-\xi^2}} \widetilde{\mathscr{H}}^{cu}_{\mu\mu} = 2\epsilon\bar{p}^+ \sqrt{1-\xi^2}\left[R_A - \frac{\xi}{1-\xi^2}\widetilde{M} R_P\right], \tag{C.38}$$

$$\int_\xi^1 \frac{\mathrm{d}\bar{x}}{\sqrt{\bar{x}^2-\xi^2}} \widetilde{\mathscr{H}}^{cu}_{-\mu\mu} = 2\bar{p}^+ \sqrt{1-\xi^2}\frac{\xi}{1-\xi^2}\frac{\Delta_\perp}{M_{\Lambda_c}+m_p} R_P, \tag{C.39}$$

$$\int_\xi^1 \frac{\mathrm{d}\bar{x}}{\sqrt{\bar{x}^2-\xi^2}} \mathscr{H}^{Tcu}_{\lambda_1\mu\mu} = \frac{\bar{p}^+}{\sqrt{1-\xi^2}}\frac{\Delta_\perp}{M_{\Lambda_c}+m_p}\left\{(M_{\Lambda_c}+m_p)\frac{(1+\xi)M_{\Lambda_c}+(1-\xi)m_p}{2m_p M_{\Lambda_c}} S_S \right. \tag{C.40}$$

$$\left. + \left[1+2\lambda_1\epsilon\xi\right] S_{V_1} - \left[\xi + 2\lambda_1\epsilon\right] S_{V_2}\right\},$$

$$\int_\xi^1 \frac{\mathrm{d}\bar{x}}{\sqrt{\bar{x}^2-\xi^2}} \mathscr{H}^{Tcu}_{\lambda_1-\mu\mu} = -\frac{\bar{p}^+}{\sqrt{1-\xi^2}}\left\{(1-\xi^2)(\epsilon+2\lambda_1)S_T + \epsilon\frac{\boldsymbol{\Delta}_\perp^2}{m_p M_{\Lambda_c}} S_S \right. \tag{C.41}$$

$$\left. -(\epsilon+2\lambda_1)\widetilde{M}\left[\xi\, S_{V_1} - S_{V_2}\right]\right\}.$$

D

Model parameters

Proton:
The normalization constant N_p and the oscillator parameter a_p are related to the valence Fock-state probability P_p as follows,

$$N_P = \sqrt{\frac{143360}{29}\,\pi^4\,a_P^4\,P_P}. \tag{D.1}$$

Lambda:
The normalization constant N_Λ and the r.m.s. of the intrinsic transverse momentum of the active c-quark $\sqrt{\langle \mathbf{k}_\perp^2 \rangle}_c$ in terms of P_Λ, a_Λ, ρ is given by

$$N_\Lambda = \sqrt{\frac{3\cdot 32^2\pi^4\,a_\Lambda^4\,P_\Lambda}{I_{12}^{KK}(a_\Lambda)}} + \frac{\rho^2}{10}\,I_{15}^{KK}(a_\Lambda) \quad \text{for } f_{KK}(x_1), \tag{D.2a}$$

$$N_\Lambda = \sqrt{\frac{3\cdot 32^2\pi^4\,a_\Lambda^4\,P_\Lambda}{I_{12}^{BB}(a_\Lambda)}} + \frac{\rho^2}{10}\,I_{15}^{BB}(a_\Lambda) \quad \text{for } f_{BB}(x_1), \tag{D.2b}$$

$$\sqrt{\langle \mathbf{k}_\perp^2 \rangle}_c^{KK} = \frac{1}{2a_\Lambda}\frac{I_{24}^{KK}}{I_{13}^{KK}}, \tag{D.3a}$$

$$\sqrt{\langle \mathbf{k}_\perp^2 \rangle}_c^{BB} = \frac{1}{2a_\Lambda}\frac{I_{24}^{BB}}{I_{13}^{BB}}, \tag{D.3b}$$

where we have introduced the abbreviations

$$I_{ij}^{(KK)}(a_\Lambda) := \int_0^1 \mathrm{d}x\, x^i (x-1)^j \exp\left[-2a_\Lambda^2 M_\Lambda^2 \frac{(x-x_0)^2}{x(x-1)}\right], \tag{D.4a}$$

$$I_{ik}^{(BB)}(a_\Lambda) := \int_0^1 \mathrm{d}x\, x^i (x-1)^j \exp\left[-2a_\Lambda M_\Lambda (1-x)\right]. \tag{D.4b}$$

Pi-meson:
The normalization constant N_π and the valence Fock-state probability P_π expressed in terms of a_π and f_π read,

$$N_\pi = \sqrt{\frac{3}{2}} f_\pi\,(4\pi a_\pi)^2 \quad \text{and} \quad P_\pi = \frac{N_\pi^2}{192 a_\pi^2 \pi^2}. \tag{D.5}$$

The r.m.s. is

$$\sqrt{\langle \mathbf{k}_\perp^2 \rangle} = \sqrt{\frac{1}{10}} \frac{1}{a_\pi}. \tag{D.6}$$

D-meson:
The normalization constant N_D and the valence Fock-state probability P_D expressed in terms of a_D and f_D read,

$$N_{D_{KK}} = \frac{\left(4\pi a_{D_{KK}}^2\right)^2 f_D}{2\sqrt{6} I_{11}^{(KK)}\left(a_{D_{KK}}/\sqrt{2}\right)} \quad \text{and} \quad P_D = \frac{N_{D_1}^2 I_{11}^{(KK)}\left(a_{D_{KK}}\right)}{32 a_{D_{KK}}^2 \pi^2}, \tag{D.7}$$

$$N_{D_{BB}} = \frac{\left(4\pi a_{D_{BB}}^2\right)^2 f_D}{2\sqrt{6} I_{11}^{(BB)}\left(a_{D_{BB}}/\sqrt{2}\right)} \quad \text{and} \quad P_D = \frac{N_{D_{BB}}^2 I_{11}^{(BB)}\left(a_{D_{BB}}\right)}{32 a_{D_{BB}}^2 \pi^2}, \tag{D.8}$$

where we have introduced the abbreviations

$$I_{ij}^{(KK)}\left(a_{D_{KK}}\right) := \int_0^1 \mathrm{d}x\, x^i (1-x)^j \exp\left[-2a_{D_{KK}}^2 M_D^2 \frac{(x-x_0)^2}{x(x-1)}\right], \tag{D.9a}$$

$$I_{ij}^{(BB)}\left(a_{D_{BB}}\right) := \int_0^1 \mathrm{d}x\, x^i (1-x)^j \exp\left[-2a_{D_{BB}} M_D\,(1-x)\right]. \tag{D.9b}$$

The r.m.s. of the active $\bar{c}$- quark is

$$\sqrt{\langle \mathbf{k}_\perp^2 \rangle_c^{(KK)}} = \frac{1}{2a_{D_{KK}}^2} \frac{I_{22}^{(KK)}\left(a_{D_{KK}}\right)}{I_{11}^{(KK)}\left(a_{D_{KK}}\right)} \quad \text{and} \quad \sqrt{\langle \mathbf{k}_\perp^2 \rangle_c^{(BB)}} = \frac{1}{2a_{D_{BB}}^2} \frac{I_{22}^{(BB)}\left(a_{D_{BB}}\right)}{I_{11}^{(BB)}\left(a_{D_{BB}}\right)}. \tag{D.10}$$

E

Dirac matrices and Dirac spinors

This appendix is taken from Ref. [9].

E.1 Dirac matrices

We are using the standard Dirac representation for the γ-matrices [114]

$$\gamma^0 = \begin{pmatrix} 1 & 0 \\ 0 & -1 \end{pmatrix}, \quad \gamma^i = \begin{pmatrix} 0 & \sigma^i \\ -\sigma^i & 0 \end{pmatrix}, \quad i = 1, 2, 3, \tag{E.1}$$

with σ^i being the Pauli matrices

$$\sigma^1 = \begin{pmatrix} 0 & 1 \\ 1 & 0 \end{pmatrix}, \quad \sigma^2 = \begin{pmatrix} 0 & -i \\ i & 0 \end{pmatrix} \text{ and } \sigma^3 = \begin{pmatrix} 1 & 0 \\ 0 & -1 \end{pmatrix}. \tag{E.2}$$

Its is useful to note that

$$g_{\mu\nu} g^{\mu\nu} = 4 \tag{E.3}$$

and to recall the fundamental anti-commutation relation for the γ-matrices and an associated rule for the "slash" products

$$\gamma^\mu \gamma^\nu + \gamma^\nu \gamma^\mu = 2g^{\mu\nu} \text{ and } \not{a}\not{b} + \not{b}\not{a} = 2a \cdot b, \tag{E.4}$$

where $\not{a} := a^\mu \gamma_\mu$. These relations entail a sequence of contraction theorems [115]:

$$\gamma_\mu \gamma^\mu = 4, \tag{E.5a}$$

$$\gamma_\mu \not{a} \gamma^\mu = -2\not{a}, \tag{E.5b}$$

$$\gamma_\mu \not{a}\not{b} \gamma^\mu = 4(a \cdot b), \tag{E.5c}$$

$$\gamma_\mu \not{a}\not{b}\not{c} \gamma^\mu = -2\not{c}\not{b}\not{a}. \tag{E.5d}$$

Finally, $\gamma^5 = i\gamma^0\gamma^1\gamma^2\gamma^3$ with $\{\gamma^\mu, \gamma^5\} = 0$.

E.2 Dirac spinors

E.2.1 *Helicity spinors*

In the Dirac representation a helicity spinor for a particle with mass m and momentum p moving in a direction parameterized by the angles ϕ and θ can be written as

$$u(p,\lambda) = \frac{1}{\sqrt{E+m}} \begin{pmatrix} (E+m)\mathscr{D}(\phi,\theta)\chi_\lambda \\ 2|\mathbf{p}|\lambda\mathscr{D}(\phi,\theta)\chi_\lambda \end{pmatrix}. \tag{E.6}$$

The rotation matrix $\mathscr{D}(\phi,\theta)$ is given by

$$\mathscr{D}(\phi,\theta) = \begin{pmatrix} \cos\frac{\theta}{2} & -e^{-i\phi}\sin\frac{\theta}{2} \\ e^{i\phi}\sin\frac{\theta}{2} & \cos\frac{\theta}{2} \end{pmatrix}, \tag{E.7}$$

where we have used the Jakob-Wick convention for the spin rotation [116].
χ_λ is a 2-component spinor which is given by

$$\chi_\lambda = \frac{1}{2}\begin{pmatrix} 1+2\lambda \\ 1-2\lambda \end{pmatrix}. \tag{E.8}$$

It is an eigenvector of σ_3, i.e.

$$\frac{1}{2}\sigma_3\chi_\lambda = \lambda\chi_\lambda, \tag{E.9}$$

with $\lambda = \pm\frac{1}{2}$. Its normalization is such that $\chi^\dagger_{\lambda'}\chi_\lambda = \delta_{\lambda'\lambda}$.

The helicity spinor for an antiparticle with mass m and momentum p moving in a direction parameterized by the angles ϕ and θ is

$$v(p,\lambda) = -\frac{1}{\sqrt{E+m}} \begin{pmatrix} 2|\mathbf{p}|\lambda\mathscr{D}^*(\phi,\theta)\chi_{-\lambda} \\ -(E+m)\mathscr{D}^*(\phi,\theta)\chi_{-\lambda} \end{pmatrix}. \tag{E.10}$$

$u(p,\lambda)$ satisfies the Dirac equation

$$(\not{p} - m)u(p,\lambda) = 0, \tag{E.11}$$

whereas $v(p,\lambda)$ fulfills

$$(\not{p} + m)v(p,\lambda) = 0. \tag{E.12}$$

The u-spinor and the v-spinor are related by charge conjugation:

$$u(p,\lambda) = \mathscr{C}\overline{v}^{\mathsf{T}}(p,\lambda), \tag{E.13}$$
$$v(p,\lambda) = \mathscr{C}\overline{u}^{\mathsf{T}}(p,\lambda), \tag{E.14}$$

where $\mathscr{C} = i\gamma^2\gamma^0$.

E.2.2 *Light-cone spinors*

For the sake of completeness we give a short overview of light-cone spinors, which coincide with the helicity spinors for zero mass, but are different if the mass is finite [4]. The corresponding set of spinors for $p^3 > 0$ is given by [110, 113, 117] (adjusted to our conventions of App. A)

$$u(p,\lambda) = \frac{1}{2^{1/4}}\frac{1}{\sqrt{p^+}}\left(\sqrt{2}p^+ + \beta m + \boldsymbol{\alpha}_\perp \cdot \mathbf{p}_\perp\right)\chi_\lambda, \tag{E.15}$$

and

$$v(p,\lambda) = -\frac{1}{2^{1/4}}\frac{1}{\sqrt{p^+}}\left(\sqrt{2}p^+ - \beta m + \boldsymbol{\alpha}_\perp \cdot \mathbf{p}_\perp\right)\chi_{-\lambda}, \tag{E.16}$$

where $\lambda = \pm\frac{1}{2}$ and $\chi_{\frac{1}{2}}$ and $\chi_{-\frac{1}{2}}$ are eigenstates of the projection operators $\mathscr{P}_+$ and $\mathscr{P}_-$ (cf. Eq. $(A.15)$), respectively. They are given by

$$\chi_{\frac{1}{2}} = \frac{1}{\sqrt{2}}\begin{pmatrix}1\\0\\1\\0\end{pmatrix}, \quad \chi_{-\frac{1}{2}} = \frac{1}{\sqrt{2}}\begin{pmatrix}0\\1\\0\\-1\end{pmatrix}. \tag{E.17}$$

Working in the Dirac representation we can write

$$\left(\sqrt{2}p^+ + \beta m + \boldsymbol{\alpha}_\perp \cdot \mathbf{p}_\perp\right) = \begin{pmatrix}\sqrt{2}p^+ + m & 0 & 0 & p^1 - ip^2\\ 0 & \sqrt{2}p^+ + m & p^1 + ip^2 & 0\\ 0 & p^1 - ip^2 & \sqrt{2}p^+ - m & 0\\ p^1 + ip^2 & 0 & 0 & \sqrt{2}p^+ - m\end{pmatrix}, \tag{E.18}$$

and

$$\left(\sqrt{2}p^+ - \beta m + \boldsymbol{\alpha}_\perp \cdot \mathbf{p}_\perp\right) = \begin{pmatrix}\sqrt{2}p^+ - m & 0 & 0 & p^1 - ip^2\\ 0 & \sqrt{2}p^+ - m & p^1 + ip^2 & 0\\ 0 & p^1 - ip^2 & \sqrt{2}p^+ + m & 0\\ p^1 + ip^2 & 0 & 0 & \sqrt{2}p^+ + m\end{pmatrix}. \tag{E.19}$$

If we use Eqs. $(E.18)$ and $(E.17)$ in $(E.15)$ and Eqs. $(E.19)$ and $(E.17)$ in $(E.16)$,

respectively, we get the desired light-cone spinors:

$$u\left(p,\frac{1}{2}\right)=\frac{1}{2^{1/4}}\frac{1}{\sqrt{p^+}}\begin{pmatrix}p^+ + m/\sqrt{2}\\ p_\perp/\sqrt{2}\\ p^+ - m/\sqrt{2}\\ p_\perp/\sqrt{2}\end{pmatrix},\quad u\left(p,-\frac{1}{2}\right)=\frac{1}{2^{1/4}}\frac{1}{\sqrt{p^+}}\begin{pmatrix}-p_\perp^*/\sqrt{2}\\ p^+ + m/\sqrt{2}\\ p_\perp^*/\sqrt{2}\\ -p^+ + m/\sqrt{2}\end{pmatrix} \tag{E.20}$$

and

$$v\left(p,\frac{1}{2}\right)=-\frac{1}{2^{1/4}}\frac{1}{\sqrt{p^+}}\begin{pmatrix}-p_\perp^*/\sqrt{2}\\ p^+ - m/\sqrt{2}\\ p_\perp^*/\sqrt{2}\\ -p^+ - m/\sqrt{2}\end{pmatrix},\quad v\left(p,-\frac{1}{2}\right)=-\frac{1}{2^{1/4}}\frac{1}{\sqrt{p^+}}\begin{pmatrix}p^+ - m/\sqrt{2}\\ p_\perp/\sqrt{2}\\ p^+ + m/\sqrt{2}\\ p_\perp/\sqrt{2}\end{pmatrix}, \tag{E.21}$$

where $p_\perp := p^1 + ip^2$. The light-cone spinors are again normalized such that $\overline{u}(p,\lambda')u(p,\lambda) = 2m\delta_{\lambda'\lambda}$ and $\overline{v}(p,\lambda')v(p,\lambda) = -2m\delta_{\lambda'\lambda}$.

Finally, we specify the light-cone spinors for the case that $p^3 < 0$ [113]. To do so, we rotate χ_λ with the help of the rotation matrix $\mathscr{D}$ and obtain

$$u\left(p,\frac{1}{2}\right)=\frac{1}{2^{1/4}}\frac{\mathrm{sign}(p^1)}{\sqrt{p^-}}\begin{pmatrix}p_\perp^*/\sqrt{2}\\ p^- + m/\sqrt{2}\\ p_\perp^*/\sqrt{2}\\ p^- - m/\sqrt{2}\end{pmatrix},\ u\left(p,-\frac{1}{2}\right)=-\frac{1}{2^{1/4}}\frac{\mathrm{sign}(p^1)}{\sqrt{p^-}}\begin{pmatrix}p^- + m/\sqrt{2}\\ -p_\perp/\sqrt{2}\\ -p^- + m/\sqrt{2}\\ p_\perp/\sqrt{2}\end{pmatrix}, \tag{E.22}$$

and

$$v\left(p,\frac{1}{2}\right)=\frac{1}{2^{1/4}}\frac{\mathrm{sign}(p^1)}{\sqrt{p^-}}\begin{pmatrix}p^- - m/\sqrt{2}\\ -p_\perp/\sqrt{2}\\ -p^- - m/\sqrt{2}\\ p_\perp/\sqrt{2}\end{pmatrix},\ v\left(p,-\frac{1}{2}\right)=-\frac{1}{2^{1/4}}\frac{\mathrm{sign}(p^1)}{\sqrt{p^-}}\begin{pmatrix}p_\perp^*/\sqrt{2}\\ p^- - m/\sqrt{2}\\ p_\perp^*/\sqrt{2}\\ p^- + m/\sqrt{2}\end{pmatrix}. \tag{E.23}$$

E.2.3 *Relation between helicity spinors and light-cone spinors*

The light-cone spinors and helicity spinors are related by a unitary transformation [4]:

$$\begin{pmatrix}u_H(\lambda=+1/2)\\ u_H(\lambda=-1/2)\end{pmatrix}=U\cdot\begin{pmatrix}u_{LC}(\lambda=+1/2)\\ u_{LC}(\lambda=-1/2)\end{pmatrix}, \tag{E.24}$$

$$\begin{pmatrix}v_H(\lambda=+1/2)\\ v_H(\lambda=-1/2)\end{pmatrix}=U^*\cdot\begin{pmatrix}v_{LC}(\lambda=+1/2)\\ v_{LC}(\lambda=-1/2)\end{pmatrix}, \tag{E.25}$$

with

$$U = \frac{\sqrt{p^0 + |\mathbf{p}|}}{\sqrt{2|\mathbf{p}|(|\mathbf{p}| + p^3)(p^0 + p^3)}} \begin{pmatrix} |\mathbf{p}| + p^3 & p_\perp \frac{m}{p^0+|\mathbf{p}|} \\ -p_\perp^* \frac{m}{p^0+|\mathbf{p}|} & |\mathbf{p}| + p^3 \end{pmatrix} \tag{E.26}$$
$$= \frac{\sqrt{p^0 + |\mathbf{p}|}}{\sqrt{p^0 + p^3}} \begin{pmatrix} \cos\frac{\theta}{2} & e^{i\phi} \frac{m}{p^0+|\mathbf{p}|} \sin\frac{\theta}{2} \\ -e^{-i\phi} \frac{m}{p^0+|\mathbf{p}|} \sin\frac{\theta}{2} & \cos\frac{\theta}{2} \end{pmatrix}.$$

For our CMS kinematics of App. B U can be written in a more convenient form

$$U = \frac{1}{\sqrt{1+\beta^2}} \begin{pmatrix} 1 & +\beta \\ -\beta & 1 \end{pmatrix}, \tag{E.27}$$

with

$$\beta := \frac{m}{p^0 + |\mathbf{p}|} \tan\frac{\theta}{2}. \tag{E.28}$$

F

Feynman rules

This appendix is a modified version of an appendix originally published in Ref. [9].

In this appendix we first recall the Feynman rules [115] used for calculating the hard-scattering amplitudes of Sec. 2.3 and Sec. 2.4.

In the following μ and ν are Lorentz indices, α and β color indices, respectively and we are omitting helicity labels.

F.0.4 *External lines*

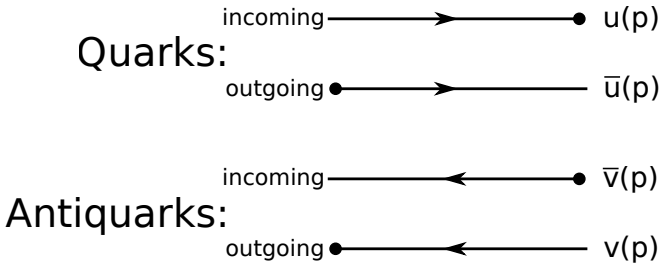

F.0.5 *Propagators*

Quarks and antiquarks

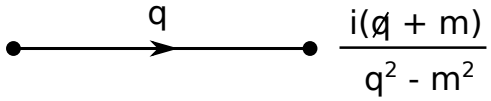

Gluons (Feynman gauge)

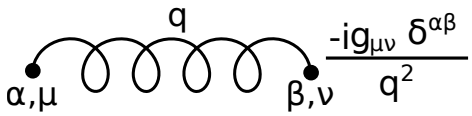

F.0.6 *Vertices*

Quark-gluon vertex

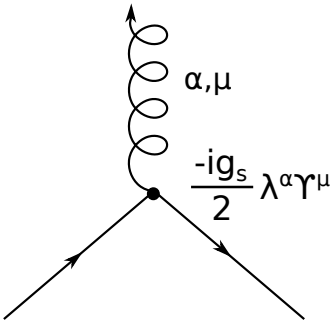

Quark-photon vertex

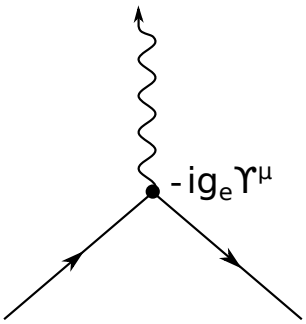

$g_e = |e|q$, where q is the fraction of the charge of the particle in units of the electron charge

F.0.7 *Gell-Mann matrices*

For the calculation of the color factor we need the Gell-Mann matrices which are the hermitian and traceless 3×3 matrices [118]

$$\lambda_1 = \begin{pmatrix} 0 & 1 & 0 \\ 1 & 0 & 0 \\ 0 & 0 & 0 \end{pmatrix}, \quad \lambda_2 = \begin{pmatrix} 0 & -i & 0 \\ i & 0 & 0 \\ 0 & 0 & 0 \end{pmatrix}, \quad \lambda_3 = \begin{pmatrix} 1 & 0 & 0 \\ 0 & -1 & 0 \\ 0 & 0 & 0 \end{pmatrix},$$

$$\lambda_4 = \begin{pmatrix} 0 & 0 & 1 \\ 0 & 0 & 0 \\ 1 & 0 & 0 \end{pmatrix}, \quad \lambda_5 = \begin{pmatrix} 0 & 0 & -i \\ 0 & 0 & 0 \\ i & 0 & 0 \end{pmatrix}, \quad \lambda_6 = \begin{pmatrix} 0 & 0 & 0 \\ 0 & 0 & 1 \\ 0 & 1 & 0 \end{pmatrix},$$

$$\lambda_7 = \begin{pmatrix} 0 & 0 & 0 \\ 0 & 0 & -i \\ 0 & i & 0 \end{pmatrix}, \quad \lambda_8 = \frac{1}{\sqrt{3}} \begin{pmatrix} 1 & 0 & 0 \\ 0 & 1 & 0 \\ 0 & 0 & -2 \end{pmatrix}. \tag{F.1}$$

They satisfy the following relations,

$$[\lambda_a, \lambda_b] = 2if_{abc}\lambda_c, \tag{F.2}$$

$$\mathrm{Tr}(\lambda_a\lambda_b) = 2\delta_{ab}, \tag{F.3}$$

with f_{abc} denoting the $SU(3)$ structure constants.

G

Update to diploma thesis

G.1 Introduction

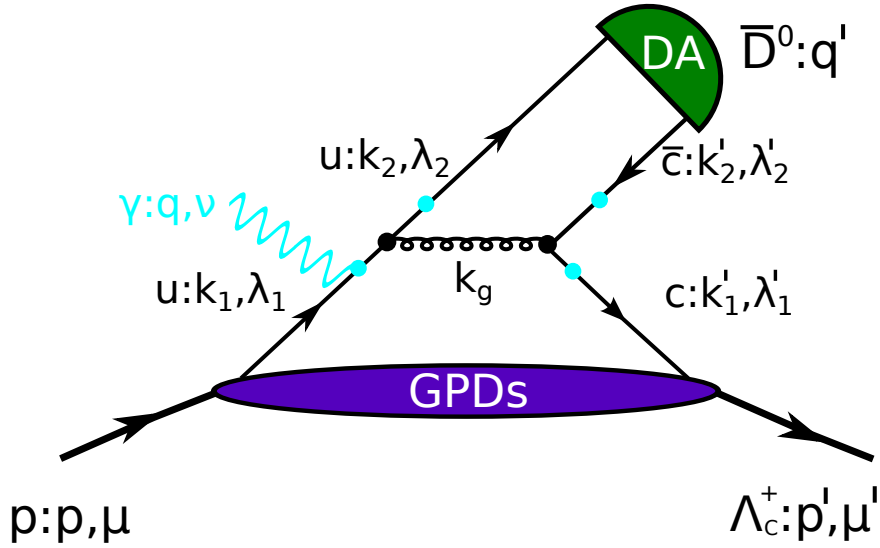

Figure G.1: Handbag contribution to the process $\gamma p \to \overline{D}^0 \Lambda_c^+$ (in the DGLAP region). The momenta and LC helicities of the quarks are specified. The photon can couple to either of the points indicated by the dots.

In this appendix we present the updated results for $\gamma\ p \to \overline{D}^0\ \Lambda_c^+$. This process can be investigated along the same lines as $\gamma\ p \to \overline{D}^*_{\lambda=0}\ \Lambda_c^+$ (see Sec. 2.4).

G.2 Kinematics

The kinematics is the same as in Sec. 2.4.1 with $m_d = M_D = 1.86484$ GeV^2. The threshold to produce the Λ_c^+ and the $\overline{D}^0$ is $s \sim (M_{\Lambda_c} + M_D)^2 = 17.23$ GeV^2.

G.3 THE HADRONIC SCATTERING AMPLITUDE

$$\begin{aligned}\mathscr{M}_{\mu',\mu\nu} = &\int \mathrm{d}\bar{x}_1\, \bar{p}^+ \int \frac{\mathrm{d}z_1^-}{(2\pi)} e^{i\bar{x}_1\bar{p}^+ z_1^-} \int \mathrm{d}k_2'^- \int \frac{\mathrm{d}z_2^+}{(2\pi)} e^{i\frac{z_2^+}{2}\left(-q'^- + 2k_2'^-\right)} \\ &\times \langle \Lambda_c^+ : p', \mu' | \overline{\Psi}^c \left(-\frac{z_1^-}{2}\right) \Psi^u \left(\frac{z_1^-}{2}\right) | p : p, \mu \rangle \, \widetilde{H}\left(\bar{x}_1\bar{p}^+, \bar{x}_2\bar{q}^-\right) \\ &\times \langle \overline{D}^0 : q' | \overline{\Psi}^u \left(\frac{z_2^+}{2}\right) \Psi^c \left(-\frac{z_2^+}{2}\right) | 0 \rangle \,,\end{aligned} \tag{G.1}$$

For the $p \to \Lambda_c$ transition we refer to App. C. The investigation of the meson matrix element is analogous to the one of Sec. 2.4.2 with the following changes, however:

- Equation (2.117) gets replaced by

$$\bar{\Psi}^u \Psi^c = -\frac{1}{4k_2^- k_2'^-} \sum_{\lambda_2} 2\lambda_2 \bar{\Psi}^u_- \gamma^- \gamma_5 \Psi^c_- \bar{u}\left(k_2, \lambda_2\right) v\left(k_2', -\lambda_2\right). \tag{G.2}$$

- The valence Fock state of the $\overline{D}^0$ reads

$$\begin{aligned}|\overline{D}^0 : q'\rangle = &\int \mathrm{d}\hat{x}_2' \int \frac{\mathrm{d}^2\hat{\mathbf{k}}_{\perp 2}'}{16\pi^3} \Psi_D(\hat{x}_2', \hat{\mathbf{k}}_\perp') \frac{1}{\sqrt{\hat{x}_2'(1-\hat{x}_2')}} \\ &\times \frac{1}{\sqrt{2}} \Big[|\bar{c} : \hat{x}_2' q'^-, \hat{\mathbf{k}}_\perp' + \hat{x}_2' \mathbf{q}_\perp', +\frac{1}{2}\rangle \, |u : (1-\hat{x}')q'^-, -\hat{\mathbf{k}}_\perp' + (1-\hat{x}')\mathbf{q}_\perp', -\frac{1}{2}\rangle \\ &\quad - |\bar{c} : \hat{x}_2' q'^-, \hat{\mathbf{k}}_\perp' + \hat{x}_2' \mathbf{q}_\perp', -\frac{1}{2}\rangle \, |u : (1-\hat{x}')q'^-, -\hat{\mathbf{k}}_\perp' + (1-\hat{x}')\mathbf{q}_\perp', \frac{1}{2}\rangle \Big].\end{aligned} \tag{G.3}$$

With these changes the final expression for the hadronic meson matrix element is given by

$$\begin{aligned}&-\int \frac{\mathrm{d}z_2^+}{2\pi} e^{i\frac{z_2^+}{2}\left(-q'^- + 2k_2'^-\right)} \frac{1}{4k_2^- k_2'^-} \langle \overline{D}^0 : q' | \sum_{\lambda_2} 2\lambda_2 \bar{\Psi}^u_- \left(\frac{z_2^+}{2}\right) \gamma^- \gamma_5 \Psi^c_- \left(-\frac{z_2^+}{2}\right) | 0 \rangle \\ &= \frac{f_{D^0}}{2\sqrt{6}} \phi_D\left(x_2'\right).\end{aligned}$$

The consequence of these changes is that the hadronic scattering amplitude gets an additional minus sign compared to the scattering amplitude for $\overline{D}^*$ production. For

convenience we state the expression for the hadronic scattering amplitude

$$\begin{aligned}
\mathscr{M}_{\frac{1}{2},\frac{1}{2}\nu} &= \frac{C}{4\sqrt{6}}\, f_D \sqrt{1-\xi^2} \\
&\quad \left[(R_V + R_A) \int \mathrm{d}z\, \phi_D(z) H^{\nu}_{\frac{1}{2},\frac{1}{2}} + (R_V - R_A) \int \mathrm{d}z\, \phi_D(z) H^{\nu}_{-\frac{1}{2},-\frac{1}{2}} \right], \\
\mathscr{M}_{-\frac{1}{2},-\frac{1}{2}\nu} &= \frac{C}{4\sqrt{6}}\, f_D \sqrt{1-\xi^2} \\
&\quad \left[(R_V - R_A) \int \mathrm{d}z\, \phi_D(z) H^{\nu}_{\frac{1}{2},\frac{1}{2}} + (R_V + R_A) \int \mathrm{d}z\, \phi_D(z) H^{\nu}_{-\frac{1}{2},-\frac{1}{2}} \right], \\
\mathscr{M}_{\frac{1}{2},-\frac{1}{2}\nu} &= \frac{C}{2\sqrt{6}}\, f_D \sqrt{1-\xi^2}\, S_T \int \mathrm{d}z\, \phi_D(z) H^{\nu}_{\frac{1}{2},-\frac{1}{2}}, \\
\mathscr{M}_{-\frac{1}{2},\frac{1}{2}\nu} &= \frac{C}{2\sqrt{6}}\, f_D \sqrt{1-\xi^2}\, S_T \int \mathrm{d}z\, \phi_D(z) H^{\nu}_{-\frac{1}{2},\frac{1}{2}},
\end{aligned} \tag{G.4}$$

with the color factor $C = \frac{4}{3}\frac{1}{\sqrt{3}}$. The functional form of the D meson DA that we use is the same as in Eq. (2.77).

G.4 The hard scattering amplitude

G.4.1 *Preliminaries*

The hard scattering amplitude of the photoproduction of the pseudoscalar meson can be written in terms of 4 spinor products and 2 scalar products. The respective spinor products are

- Spinor product 1 (SP1): $\bar{u}\,(p', \lambda_1')\, \gamma_5 u\,(p, \lambda_1)$,
- Spinor product 2 (SP2): $\bar{u}\,(p', \lambda_1')\, \not{q} \gamma_5 u\,(p, \lambda_1)$,
- Spinor product 3 (SP3): $\bar{u}\,(p', \lambda_1')\, \not{\epsilon}_\gamma(q,1) \gamma_5 u\,(p, \lambda_1)$,
- Spinor product 4 (SP4): $\bar{u}\,(p', \lambda_1')\, \not{q} \not{\epsilon}_\gamma(q,1) \gamma_5 u\,(p, \lambda_1)$.

Using the following parameterizations for the momenta and the photon polarization vectors (see Fig G.1 for the specification of the momenta and helicities labels and see also Sec. 2.4.3.2 for the kinematics in the hard scattering process)

$$\begin{aligned}
k_1 = p &= \Big[(1+\xi)\, \bar{p}^+, \ldots, -\frac{|\boldsymbol{\Delta}_\perp|}{2}, 0 \Big], \\
k_1' = p' &= \Big[(1-\xi)\, \bar{p}^+, \ldots, \frac{|\boldsymbol{\Delta}_\perp|}{2}, 0 \Big], \\
q &= \Big[\frac{\boldsymbol{\Delta}_\perp^2}{8\,(1+\xi)\,\bar{p}^+}, (1+\xi)\, \bar{p}^+, \frac{|\boldsymbol{\Delta}_\perp|}{2}, 0 \Big]
\end{aligned} \tag{G.5}$$

and

$$\begin{aligned} k_2 &= \left(1 - x_2'\right) q', \\ k_2' &= x_2' q', \\ \text{with } q' &= \Big[\frac{\overline{M}^2 + \boldsymbol{\Delta}_\perp^2/4}{2\left(1-\xi\right)\bar{p}^+}, \left(1-\xi\right)\bar{p}^+, -\frac{|\boldsymbol{\Delta}_\perp|}{2}, 0\Big],\ \bar{M} = \sqrt{M_{\Lambda_c} M_D} \end{aligned} \tag{G.6}$$

as well as

$$\epsilon_\gamma\left(q,1\right) = \Big[\frac{1}{2\sqrt{s}}|\boldsymbol{\Delta}_\perp|, -\frac{1}{2\sqrt{s}}|\boldsymbol{\Delta}_\perp|, \frac{2\left(1+\xi\right)\bar{p}^+}{\sqrt{s}} - \frac{1}{\sqrt{2}}, -\frac{I}{\sqrt{2}}\Big], \tag{G.7}$$

we can calculate the spinor and scalar products:

- $\bar{u}\left(p', \lambda_1'\right)\gamma_5 u\left(p, \lambda_1\right)$

$$\left(\lambda_1' = +, \lambda_1 = +\right): \quad \overline{M}\sqrt{\frac{1+\xi}{1-\xi}} \tag{G.8a}$$

$$\left(\lambda_1' = -, \lambda_1 = -\right): \quad -\overline{M}\sqrt{\frac{1+\xi}{1-\xi}} \tag{G.8b}$$

$$\left(\lambda_1' = +, \lambda_1 = -\right): \quad -\frac{|\boldsymbol{\Delta}_\perp|}{\sqrt{1-\xi^2}} \tag{G.8c}$$

$$\left(\lambda_1' = -, \lambda_1 = +\right): \quad -\frac{|\boldsymbol{\Delta}_\perp|}{\sqrt{1-\xi^2}} \tag{G.8d}$$

- $\bar{u}\left(p', \lambda_1'\right)\not{q}\gamma_5 u\left(p, \lambda_1\right)$

$$\left(\lambda_1' = +, \lambda_1 = +\right): \quad \left(2\sqrt{2s}\,\bar{p}^+ - s\right)\sqrt{\frac{1+\xi}{1-\xi}} \tag{G.9a}$$

$$\left(\lambda_1' = -, \lambda_1 = -\right): \quad -\left(2\sqrt{2s}\,\bar{p}^+ - s\right)\sqrt{\frac{1+\xi}{1-\xi}} \tag{G.9b}$$

$$\left(\lambda_1' = +, \lambda_1 = -\right): \quad -\frac{|\boldsymbol{\Delta}_\perp|\overline{M}\sqrt{s}}{2\sqrt{2}\,\bar{p}^+\sqrt{1-\xi^2}} \tag{G.9c}$$

$$\left(\lambda_1' = -, \lambda_1 = +\right): \quad -\frac{|\boldsymbol{\Delta}_\perp|\overline{M}\sqrt{s}}{2\sqrt{2}\,\bar{p}^+\sqrt{1-\xi^2}} \tag{G.9d}$$

- $\bar{u}\left(p', \lambda_1'\right) \not{\epsilon}_\gamma(q,1)\gamma_5 u\left(p, \lambda_1\right)$

$$(\lambda_1' = +, \lambda_1 = +): \quad -\frac{\sqrt{2}|\boldsymbol{\Delta}_\perp|}{\sqrt{1-\xi^2}} \tag{G.10a}$$

$$(\lambda_1' = -, \lambda_1 = -): \quad 0 \tag{G.10b}$$

$$(\lambda_1' = +, \lambda_1 = -): \quad 0 \tag{G.10c}$$

$$(\lambda_1' = -, \lambda_1 = +): \quad -\sqrt{2}\overline{M}\sqrt{\frac{1+\xi}{1-\xi}} \tag{G.10d}$$

- $\bar{u}\left(p', \lambda_1'\right) \not{q}\not{\epsilon}_\gamma(q,1)\gamma_5 u\left(p, \lambda_1\right)$

$$(\lambda_1' = +, \lambda_1 = +): \quad -\frac{|\boldsymbol{\Delta}_\perp|\overline{M}\sqrt{s}}{2\bar{p}^+\sqrt{1-\xi^2}} \tag{G.11a}$$

$$(\lambda_1' = -, \lambda_1 = -): \quad 0 \tag{G.11b}$$

$$(\lambda_1' = +, \lambda_1 = -): \quad 0 \tag{G.11c}$$

$$(\lambda_1' = -, \lambda_1 = +): \quad \left(\sqrt{2}\,s - 4\sqrt{s}\,\bar{p}^+\right)\sqrt{\frac{1+\xi}{1-\xi}} \tag{G.11d}$$

- scalar products

$$ScP1 = p' \cdot \epsilon_\gamma(q,1) = -\frac{|\boldsymbol{\Delta}_\perp|\left(\overline{M}^2 + 2\bar{p}^+\left(\sqrt{2s} - 4\bar{p}^+\right)\right)}{4\sqrt{s}\,\bar{p}^+\left(\xi - 1\right)} \tag{G.12}$$

$$ScP2 = q' \cdot \epsilon_\gamma(q,1) = \frac{|\boldsymbol{\Delta}_\perp|\left(\overline{M}^2 + 2\bar{p}^+\left(\sqrt{2s} - 4\bar{p}^+\right)\right)}{4\sqrt{s}\,\bar{p}^+\left(\xi - 1\right)} \tag{G.13}$$

Before we show the updated results we list the hard scattering amplitudes of the following 4 graphs:

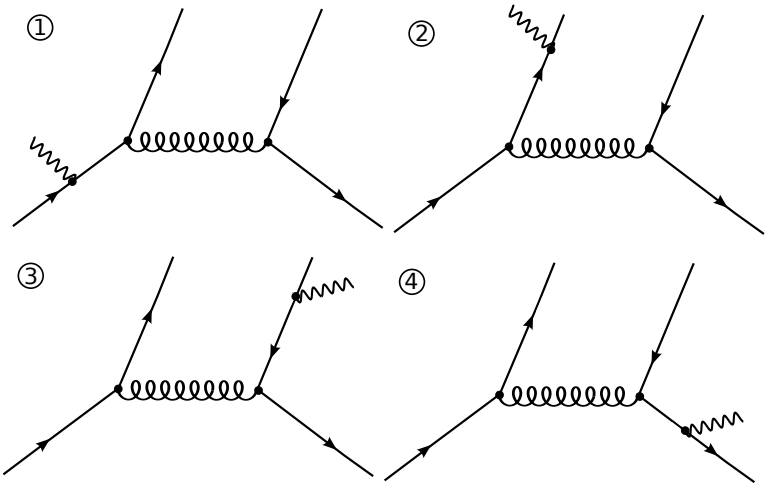

Figure G.2: The 4 leading order Feynman graphs contributing to the partonic subprocess.

- **Graph 1**
  The hard scattering amplitude for graph 1 reads[1]

$$H^{(1),1}_{\lambda_1',\lambda_1} = i\, g_s^2\, g_e \frac{1}{k_g^2}\frac{1}{\widetilde{k}^2}\Big[-\sqrt{2}\Big(s\cdot SP3 + \overline{M}\cdot SP4\Big)\Big], \tag{G.14}$$

  with

$$\begin{aligned} k_g^2 &= \Big(p + x_2' q'\Big)^2 = \overline{M}^2\Big(1 + x_2'\Big)^2 + x_2'\Big(s - 2\overline{M}^2\Big), \\ \widetilde{k}^2 &= \Big(p + q\Big)^2 = s. \end{aligned} \tag{G.15}$$

- **Graph 2**
  The hard scattering amplitude for graph 2 reads

$$\begin{aligned} H^{(2),1}_{\lambda_1',\lambda_1} = i\, g_s^2\, g_e \frac{1}{k_g^2}\frac{1}{\widetilde{k}^2}\Big[&2\sqrt{2}\,\overline{M}(x_2' - 1)\cdot ScP2\cdot SP1 \\ &- 2\sqrt{2}\Big(ScP1 + (1 - x_2')\cdot ScP2\Big)\cdot SP2 + \sqrt{2}\Big(\overline{M}^2 - u\Big)\cdot SP3 \\ &- \sqrt{2}\,\overline{M}\cdot SP4\Big], \end{aligned} \tag{G.16}$$

  where the gluon propagator has the same analytical expression as for graph 1 and the denominator of the quark propagator is given by

$$\widetilde{k}^2 = \Big((1 - x_2')q' - q\Big)^2 = \Big(1 - x_2'\Big)^2\overline{M}^2 + \Big(1 - x_2'\Big)\Big(t - \overline{M}^2\Big). \tag{G.17}$$

[1] The denominator of the gluon propagator is denoted by k_g^2 and the one of the respective quark propagator by $\widetilde{k}$, respectively.

- **Graph 3**
  The hard scattering amplitude for graph 3 reads

$$H^{(3),1}_{\lambda_1',\lambda_1} = i\, g_s^2\, g_e \frac{1}{k_g^2} \frac{1}{\widetilde{k}^2 - x_2'^2 \overline{M}^2} \Big[2\sqrt{2}\, \overline{M} x_2' \cdot ScP2 \cdot SP1 + 2\sqrt{2}\, x_2' \cdot ScP2 \cdot SP2 + \sqrt{2}\, s \cdot SP3 - \sqrt{2}\, \overline{M} \cdot SP4 \Big], \tag{G.18}$$

  with

$$\begin{aligned} k_g^2 &= \Big(p - (1 - x_2')q'\Big)^2 = \Big(1 - x_2'\Big)^2 \overline{M}^2 + \Big(1 - x_2'\Big)\Big(u - \overline{M}^2\Big), \\ \widetilde{k}^2 &= \Big(x_2' q' - q\Big)^2 = x_2'^2 \overline{M}^2 + x_2'\Big(t - \overline{M}^2\Big). \end{aligned} \tag{G.19}$$

- **Graph 4**
  The hard scattering amplitude for graph 4 reads

$$H^{(4),1}_{\lambda_1',\lambda_1} = i\, g_s^2\, g_e \frac{1}{k_g^2} \frac{1}{\widetilde{k}^2 - \overline{M}^2} \Big[-2\sqrt{2}\, \overline{M} \cdot ScP1 \cdot SP1 - \sqrt{2}\Big(\overline{M}^2 - u\Big) \cdot SP3 - \sqrt{2}\, \overline{M} \cdot SP4 \Big], \tag{G.20}$$

  where the denominator of the gluon propagator has the same analytical expression as for graph 3 and the denominator of the quark propagator is given by

$$\widetilde{k}^2 = \Big(p' - q\Big)^2 = \overline{M}^2 + \Big(u - \overline{M}^2\Big). \tag{G.21}$$

The full hard scattering amplitude is the sum

$$H^1_{\lambda_1',\lambda_1} = H^{(1),1}_{\lambda_1',\lambda_1} + H^{(2),1}_{\lambda_1',\lambda_1} + H^{(3),1}_{\lambda_1',\lambda_1} + H^{(4),1}_{\lambda_1',\lambda_1}. \tag{G.22}$$

G.5 Results

The differential cross section [39] for $\gamma\ p \to \Lambda_c^+\ \overline{D}^0$ (note the remark about the kinematics in Sec. G.2) is given by

$$\frac{d\sigma}{d\Omega} = \frac{1}{64\pi^2 s} \frac{|\mathbf{p}'|}{|\mathbf{p}|} \sigma_0 = \frac{1}{64\pi^2 s} \frac{\Lambda'}{\Lambda} \sigma_0 = \frac{1}{4\pi} s \Lambda \Lambda' \frac{d\sigma}{dt}, \tag{G.23}$$

with σ_0 defined as

$$\sigma_0 := \frac{1}{2} \sum_{\mu,\mu'} |\mathscr{M}_{\mu',\mu 1}|^2. \tag{G.24}$$

For the spin observables we need the "usual" helicity amplitudes. They can be

obtained by a Melosh-rotation of the LC-helicity amplitudes[2]

$$\phi_{\mu',\mu 1} = \frac{1}{\sqrt{1+\beta^2}}\Big(\mathscr{M}_{\mu',\mu 1} + 2\mu'\beta\mathscr{M}_{-\mu',\mu 1}\Big), \tag{G.25}$$

with $\beta := \frac{M_{\Lambda_c}}{p'^0+|\mathbf{p}'|}\tan\frac{\theta}{2}$. In general, exclusive photoproduction of pseudoscalar mesons can be described by four independent helicity amplitudes which are (following the notation of Ref. [119])

$$\begin{aligned} N &= \phi_{-\frac{1}{2},\frac{1}{2}1}, \quad & S_1 &= \phi_{-\frac{1}{2},-\frac{1}{2}1}, \\ D &= \phi_{\frac{1}{2},-\frac{1}{2}1}, \quad & S_2 &= \phi_{\frac{1}{2},\frac{1}{2}1}. \end{aligned} \tag{G.26}$$

N, S_1, S_2 and D represent independent non-flip, single-flip and double-flip amplitudes, respectively. There are in total 15 polarization observables [120]. Single-polarization observables will vanish within our approach, since we do not get complex phase factors. What we get, however, are non-vanishing spin correlations. Typical examples are the photon asymmetry

$$\Sigma\frac{d\sigma}{dt} = \frac{d\sigma_\perp}{dt} - \frac{d\sigma_\parallel}{dt} = \frac{1}{16\pi(s-m_p^2)^2}\mathscr{R}\left(S_1^* S_2 - N D^*\right) \tag{G.27}$$

and the double-polarization observable

$$E\frac{d\sigma}{dt} = \frac{1}{32\pi(s-m_p^2)^2}\left(|N|^2 - |S_1|^2 + |S_2|^2 - |D|^2\right). \tag{G.28}$$

Before we show the results we turn to the error assessment issue with respect to the model parameters: We vary a_Λ by $\pm 10\%$ around its central value of 0.75 GeV^{-1}. The valence Fock state probability of the Λ_c^+ is varied in the range 0.7 to 1. The errors of the parameters of the proton LCWF are not taken into account, since they lead to much smaller uncertainties compared to those of the Λ_c^+-LCWF. The uncertainties of f_D are taken from Ref. [16] and are $f_D = 0.2067 \pm 10$ MeV. The valence Fock state probability of the $\overline{D^0}$-meson, $P_D = 0.9$, is varied between 0.8 and 1, thus yielding different values for a_D and N_D as well. The "standard" values[3] for the oscillator parameter are $a_D = 0.86$ GeV$^{-1}(KK)$ and $a_D = 0.96$ GeV$^{-1}(BB)$. The gray bands in the plots show the variation of the cross section due to these uncertainties in the parameters.

The differential cross section is shown in Figs. G.3. The integrated cross section is plotted in Fig. G.4. If we compare our estimation with those of Ref. [121] where an effective Lagrangian approach has been used we find that there is a difference of about 2 orders of magnitude. This finding is in line with the discussions in Sec. 2.5

[2] Although we use the same symbols for LC-helicities and "usual" helicities there should be no confusion which kind of helicity is meant, since it is clear that the subscripts of $\mathscr{M}$ refer to LC-helicities and subscripts of ϕ refer to "usual" helicities.

[3] For $f_D = 0.2067$ MeV and $P_D = 0.9$.

where we argue that differences of about $2-3$ orders of magnitude in the cross sections using hadronic models and a perturbative treatment as we do are found.

Finally we show the spin observables in Figs. G.5-G.6, respectively. They hardly depend on the wave function model. Their angular dependence is thus most probably characteristic for the handbag mechanism.

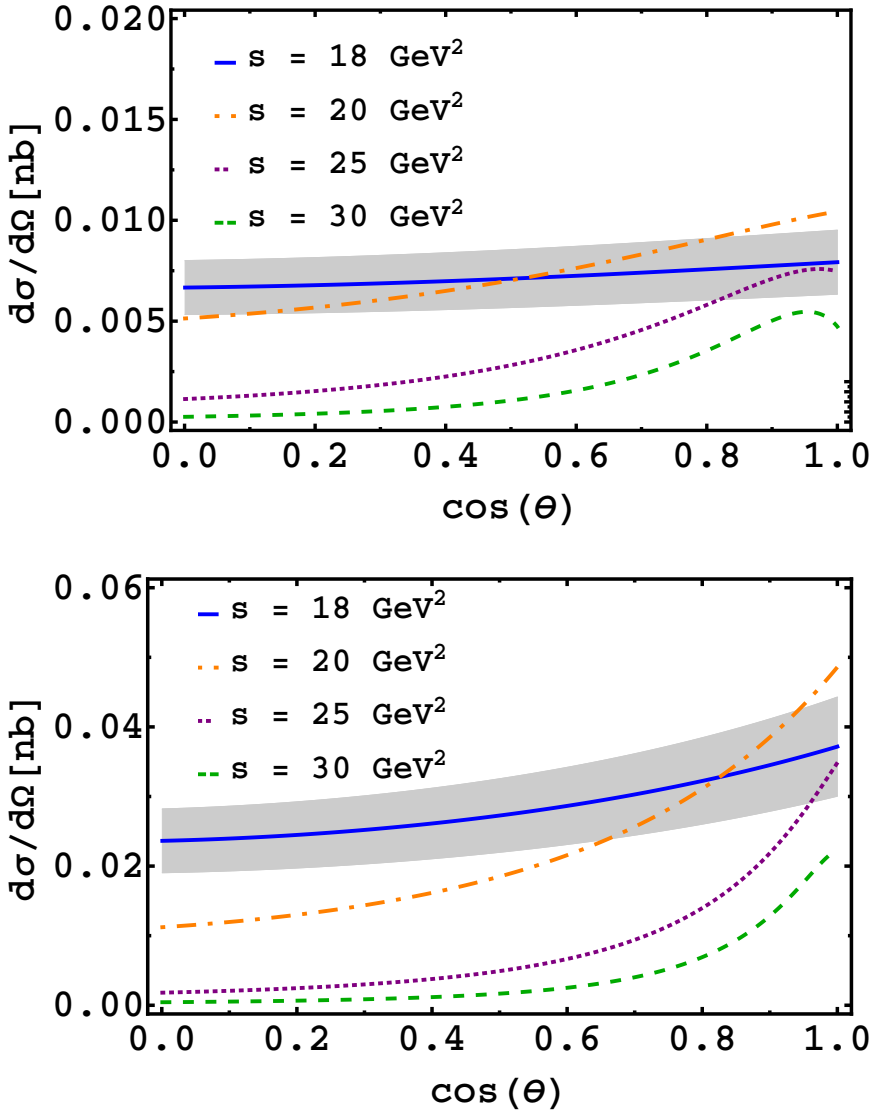

Figure G.3: The differential $\gamma p \to \overline{D}^0 \Lambda_c^+$ cross section versus $\cos\theta$ for $s = 18, 20, 25, 30$ GeV^2 (solid, dash-dotted, dotted and dashed line). This plot has been obtained with the wave function parameterizations described in the main text using the KK mass exponential (upper panel) and using the BB mass exponential (lower panel). The effects of uncertainties in the Λ_c and the D^0 wave function parameters are indicated by the shaded band around the $s = 18$ GeV^2 curve.

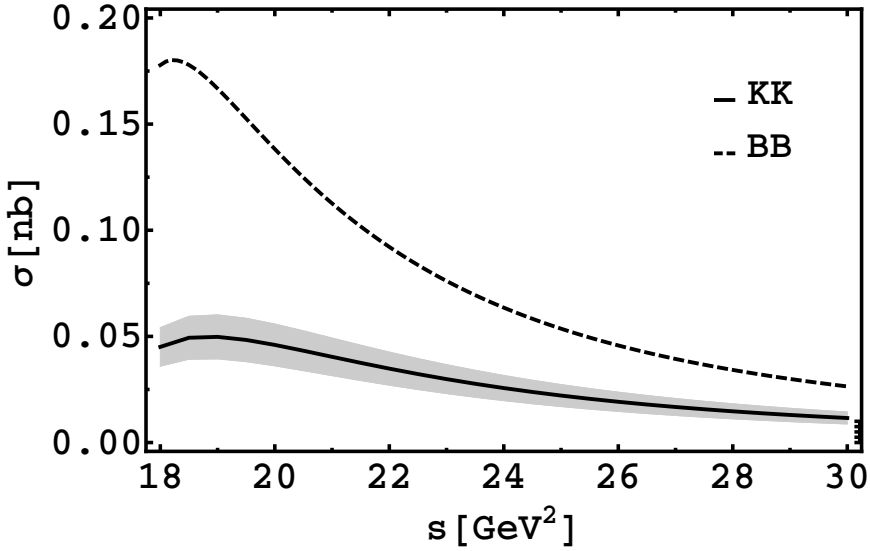

Figure G.4: Our prediction for the integrated cross section σ versus Mandelstam s (solid line with error band). Solid line corresponds to the KK mass exponentials and the dashed line corresponds to the BB mass exponential.

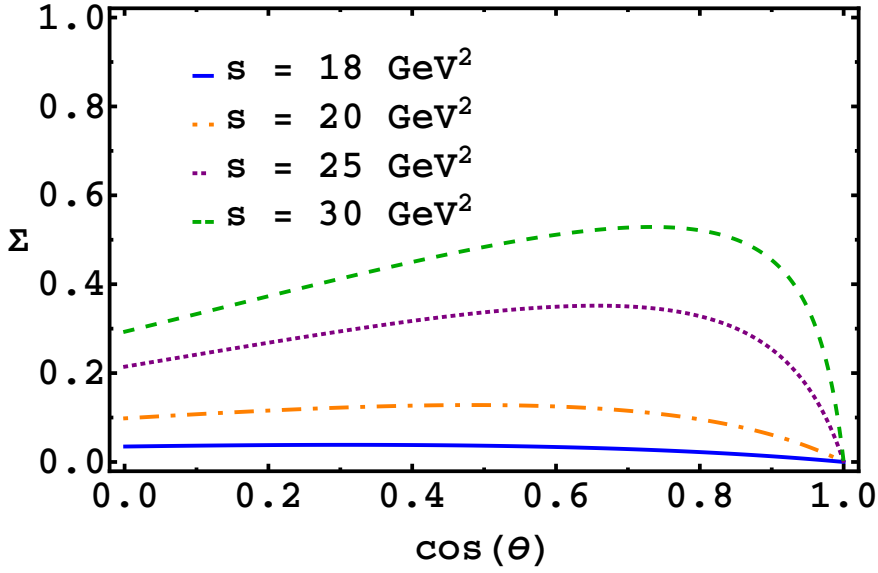

Figure G.5: Correlation function Σ for different values of Mandelstam s vs. $\cos\theta$.

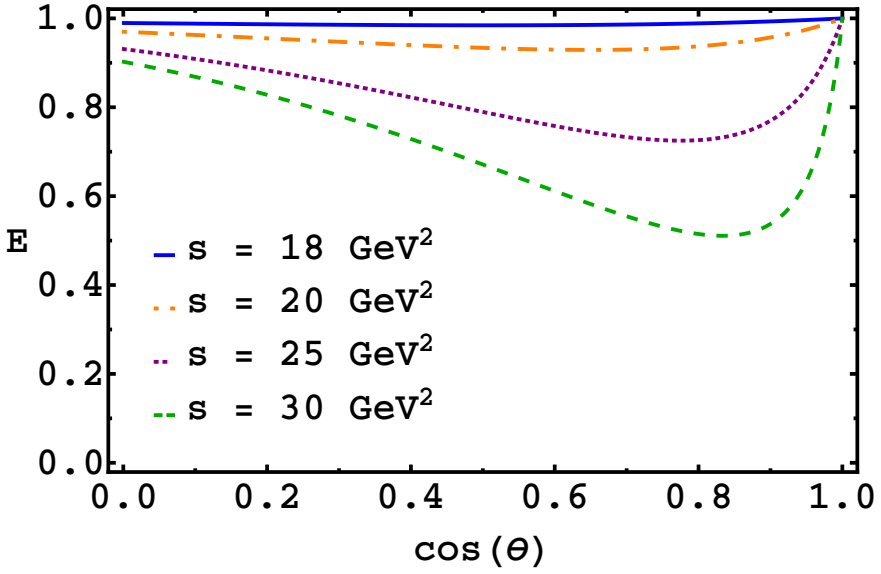

Figure G.6: Correlation function E for different values of Mandelstam s vs. $\cos\theta$.

H

Vertex functions

In this appendix we list the results for the vertex functions defined by

$$\langle BM : p_B, p_M, \lambda_B, \lambda_M | H_I | N : p_N, \lambda \rangle = 16\pi^3 \delta \left(p_B^+ + p_M^+ - p_N^+ \right) \delta^{(2)} \left(\mathbf{p}_{B\perp} + \mathbf{p}_{M\perp} - \mathbf{p}_{N\perp} \right) \times V^{\mu}_{\lambda_B, \lambda_M}(N, BM). \tag{H.1}$$

We consider only the transitions $p \to N\pi$ and $p \to N\rho$. The vertex functions are given

- for the transition $p \to N\pi$ by

$$V^{\mu}_{\lambda_N, 0}(p, N\pi) = i g_{pN\pi} \bar{u} \left(p_B, \lambda_B \right) \gamma_5 u \left(p_p, \mu \right), \tag{H.2}$$

- for the transition $p \to N\rho$ by

$$\begin{aligned} V^{\mu}_{\lambda_N, \lambda_M}(p, N\rho) = {} & g_{pN\rho} \, \bar{u} \left(p_B, \lambda_B \right) \gamma^{\rho} \left(p_p, \mu \right) \epsilon^*_{\rho}(p_M, \lambda_V) \\ & - \frac{f_{NN\rho}}{2M_N} \, \bar{u} \left(p_B, \lambda_B \right) i\sigma^{\rho\tau} u \left(p_p, \mu \right) \epsilon^*_{\rho}(p_M, \lambda_V) p_{M,\tau}. \end{aligned} \tag{H.3}$$

The momentum p_p is written as $p_p = \left[p_p^+, p_p^-, \mathbf{p}_{p\perp} \right]$, the momentum p_B as $p_B = \left[y p_p^+, p_B^-, \mathbf{k}_\perp + y \mathbf{p}_{p\perp} \right]$ and the momentum p_M as $p_M = \left[(1-y) p_p^+, p_M^-, -\mathbf{k}_\perp + (1-y) \mathbf{p}_{p\perp} \right]$, respectively. The polarization vector of the vector meson reads

- $\lambda_M = 0 : \; \epsilon = \frac{1}{M_V} \left[p_M^+, \frac{\mathbf{p}^2_{\perp M} - M_V^2}{2p_M^+}, \mathbf{p}_{\perp M} \right]$,
- $\lambda_M = 1 : \; \epsilon = \left[0, -\frac{p^1_{\perp M} + i p^2_{\perp M}}{\sqrt{2} p_M^+}, -\frac{1}{\sqrt{2}}, -\frac{i}{\sqrt{2}} \right]$,
- $\lambda_M = -1 : \; \epsilon = \left[0, \frac{p^1_{\perp M} - i p^2_{\perp M}}{\sqrt{2} p_M^+}, \frac{1}{\sqrt{2}}, -\frac{i}{\sqrt{2}} \right]$.

The final results for $p \to N\pi$ with proton helicity $\mu = \frac{1}{2}$ are given in Table. H.1. k_R is defined by $k_R = k^1_\perp + i k^2_\perp$. The vertex function for proton helicity $\mu = -\frac{1}{2}$ can be obtained via the parity relation

$$V^{-1/2(p,N\pi)}_{\lambda_N, 0}(y, \mathbf{k}_\perp) = (-1)^{1/2 - \lambda_N} V^{-\mu(p,N\pi)}_{-\lambda_B, 0}(y, \hat{\mathbf{k}}_\perp), \tag{H.4}$$

with $\hat{\mathbf{k}}_\perp = \left(k^1_\perp, -k^2_\perp \right)$.

The final results for $p \to N\rho$ with proton helicity $\mu = \frac{1}{2}$ in the prescription B are given in Table. H.2. The ones with $\mu = -\frac{1}{2}$ can be obtained by

$$V^{-1/2(p,N\rho)}_{\lambda_N,\lambda_\rho}(y,\mathbf{k}_\perp) = (-1)^{1/2+\lambda_N+\lambda_\rho} V^{1/2(p,N\rho)}_{-\lambda_N,-\lambda_\rho}(y,\hat{\mathbf{k}}_\perp). \tag{H.5}$$

$\mu \to \lambda_B$	$V(p,N\pi)$
$\frac{1}{2} \to \frac{1}{2}$	$ig_{NN\pi}\frac{M_p(1-y)}{\sqrt{y}}$
$\frac{1}{2} \to -\frac{1}{2}$	$-ig_{NN\pi}\frac{k_R}{\sqrt{y}}$

Table H.1: Vertex functions for $N \to N\pi$.

Table H.2: Vertex functions for $p \to NV$ and particle helicities $\frac{1}{2} \to \lambda'_N, \lambda_V$ in the prescription B.

λ'_N	λ_V	$V(N,NV)$
$+\frac{1}{2}$	$+1$	$\frac{\sqrt{2}k_L}{\sqrt{y}}\left[\frac{g}{1-y}+\frac{f}{2}\right]$
$-\frac{1}{2}$	$+1$	$g\frac{\sqrt{2}(M_B-yM_N)}{\sqrt{y}} + \frac{f}{2M_N}\frac{\sqrt{2}[k_\perp^2-(M_N+M_B)(1-y)(yM_N-M_B)]}{\sqrt{y}(1-y)}$
$+\frac{1}{2}$	0	$g\frac{k_\perp^2+(1-y)^2M_NM_B-yM_V^2}{M_V\sqrt{y}(1-y)}$ $+\frac{f}{2M_N}\frac{(yM_N-M_B)[k_\perp^2+y^2M_N^2-y(M_N^2+M_V^2+M_B^2)+M_B^2]}{2M_Vy\sqrt{y}}$
$-\frac{1}{2}$	0	$g\frac{(M_B-M_N)}{M_V\sqrt{y}} + \frac{f}{2M_N}\frac{k_R(1+y)[k_\perp^2-y(M_B^2+M_N^2+M_V^2)+M_B^2+y^2M_N^2]}{2M_Vy\sqrt{y}(1-y)}$
$+\frac{1}{2}$	-1	$-g\frac{\sqrt{2}yk_R}{\sqrt{y}(1-y)} + \frac{f}{2M_N}\frac{\sqrt{2}k_RM_B}{\sqrt{y}}$
$-\frac{1}{2}$	-1	$-\frac{f}{2M_N}\frac{\sqrt{2}k_R^2}{\sqrt{y}(1-y)}$

Bibliography

[1] CTEQ Collaboration, R. Brock *et al.*, Rev. Mod. Phys. (1994).

[2] C. Gattringer and C. B. Lang, *Quantum Chromodynamics on the Lattice - An Introductory Presentation*, 1st edition. ed. (Springer, Berlin, Heidelberg, 2009).

[3] M. Guidal, H. Moutarde and M. Vanderhaeghen, Rept. Prog. Phys. **76**, 066202 (2013), [1303.6600].

[4] M. Diehl, Eur. Phys. J. **C19**, 485 (2001), [hep-ph/0101335].

[5] M. Diehl, Phys. Rept. **388**, 41 (2003), [hep-ph/0307382].

[6] X.-D. Ji, Phys. Rev. Lett. **78**, 610 (1997), [hep-ph/9603249].

[7] S. Kofler, P. Kroll and W. Schweiger, Phys. Rev. **D91**, 054027 (2015), [1412.5367].

[8] S. Kofler, A. Goritschnig and W. Schweiger, PoS. , 061 (2014).

[9] S. Kofler, Hard exclusive production of charmed mesons, 2012.

[10] J. Haidenbauer and G. Krein, Phys. Lett. **B687**, 314 (2010), [0912.2663].

[11] A. Goritschnig, P. Kroll and W. Schweiger, Eur. Phys. J. **A42**, 43 (2009), [hep-ph/090525613].

[12] A. Khodjamirian, C. Klein, T. Mannel and Y. M. Wang, Eur. Phys. J. **A48**, 31 (2012), [1111.3798].

[13] M. Neubert, Phys. Rept. **245**, 259 (1994), [hep-ph/9306320].

[14] A. G. Grozin, hep-ph/9908366.

[15] A. T. Goritschnig, B. Pire and W. Schweiger, Phys. Rev. **D87**, 014017 (2013).

[16] Particle Data Group, K. A. Olive *et al.*, Chin. Phys. **C38**, 090001 (2014).

[17] M. Diehl, T. Feldmann, R. Jakob and P. Kroll, Eur. Phys. J. **C8**, 409 (1999), [hep-ph/9811253].

[18] B. A. Kniehl and G. Kramer, Phys. Rev. **D74**, 037502 (2006), [hep-ph/0607306].

[19] J. Bolz and P. Kroll, Z. Phys. **A356**, 327 (1996), [hep-ph/9603289].

[20] J. Körner and P. Kroll, Phys. Lett. **B293**, 201 (1992).

[21] J. Szwed, Nucl. Phys. **B229**, 53 (1983).

[22] D. Brommel, *Pion Structure from the Lattice*, PhD thesis, University of Regensburg, 2007.

[23] M. Diehl, T. Feldmann, R. Jakob and P. Kroll, Nucl. Phys. **B596**, 33 (2001), [hep-ph/0009255].

[24] N. Isgur and M. B. Wise, Nucl. Phys. **B348**, 276 (1991).

[25] M. G. Sotiropoulos and G. F. Sterman, Nucl. Phys. **B425**, 489 (1994), [hep-ph/9401237].

[26] Z. Dziembowski, Phys. Rev. **D37**, 768 (1988).

[27] B. Chibisov and A. R. Zhitnitsky, Phys. Rev. **D52**, 5273 (1995), [hep-ph/9503476].

[28] DELPHI Collaboration, P. Abreu *et al.*, Phys. Lett. **B474**, 205 (2000).

[29] J. Körner and P. Kroll, Z. Phys. **C57**, 383 (1993).

[30] P. Ball, V. M. Braun and E. Gardi, Phys. Lett. **B665**, 197 (2008), [hep-ph/08042424].

[31] T. Feldmann and P. Kroll, Eur. Phys. J. **C12**, 99 (2000), [hep-ph/9905343].

[32] R. Jakob and P. Kroll, Phys. Lett. **B315**, 463 (1993), [hep-ph/9306259], [Erratum: Phys. Lett.B319,545(1993)].

[33] G. Bell, T. Feldmann, Y.-M. Wang and M. W. Y. Yip, JHEP **11**, 191 (2013), [1308.6114].

[34] J. H. Christenson, E. Hummel, G. A. Kreiter, J. Sculli and P. Yamin, Phys. Rev. Lett. **55**, 154 (1985).

[35] M. Diehl, T. Gousset and B. Pire, Phys. Rev. **D59**, 034023 (1999), [hep-ph/9808479].

[36] W. Lucha, D. Melikhov and S. Simula, Phys. Lett. **B735**, 12 (2014), [1404.0293].

[37] A. Grozin and M. Neubert, Phys. Rev. **D55**, 272 (1997), [hep-ph/9607366].

[38] W. Greiner, S. Schramm and E. Stein, *Quantum Chromodynamics*, 3rd. rev. and enlarged ed. (Springer, Berlin, Heidelberg, 2007).

[39] A. D. Martin and T. D. Spearman, *Elementary particle theory* (North-Holland Pub. Co., Amsterdam, 1970).

[40] E. Tomasi-Gustafsson and M. P. Rekalo, Eur. Phys. J. **A21**, 469 (2004), [hep-ph/0401156].

[41] M. Pichowsky, C. Savkli and F. Tabakin, Phys. Rev. **C53**, 593 (1996), [nucl-th/9509022].

[42] C. F. Berger and W. Schweiger, Phys. Rev. **D61**, 114026 (2000), [hep-ph/9910509].

[43] J. Haidenbauer and G. Krein, Phys. Rev. **D89**, 114003 (2014), [1404.4174].

[44] R. Shyam and H. Lenske, Phys. Rev. **D90**, 014017 (2014), [1406.7071].

[45] P. Kroll, B. Quadder and W. Schweiger, Nucl. Phys. **B316**, 373 (1989).

[46] A. B. Kaidalov and P. E. Volkovitsky, Z. Phys. **C63**, 517 (1994).

[47] M. M. Brisudova, L. Burakovsky and J. T. Goldman, Phys. Rev. **D61**, 054013 (2000), [hep-ph/9906293].

[48] S.-H. Kim, A. Hosaka, H.-C. Kim, H. Noumi and K. Shirotori, PTEP **2014**, 103D01 (2014), [1405.3445].

[49] S. J. Brodsky, P. Hoyer, C. Peterson and N. Sakai, Phys. Lett. **B93**, 451 (1980).

[50] P. Jimenez-Delgado, T. J. Hobbs, J. T. Londergan and W. Melnitchouk, Phys. Rev. Lett. **114**, 082002 (2015), [1408.1708].

[51] S. D. Drell, D. J. Levy and T.-M. Yan, Phys. Rev. **D1**, 1035 (1970).

[52] J. D. Sullivan, Phys. Rev. **D5**, 1732 (1972).

[53] A. W. Thomas and W. Weise, *The Structure of the Nucleon* (Berlin, Germany: Wiley-VCH, 2001).

[54] J. Speth and A. W. Thomas, Adv. Nucl. Phys. **24**, 83 (1997).

[55] B. Pasquini and S. Boffi, Phys. Rev. **D76**, 074011 (2007), [0707.2897].

[56] B. Pasquini and S. Boffi, Phys. Rev. **D73**, 094001 (2006), [hep-ph/0601177].

[57] B. Pasquini, M. Pincetti and S. Boffi, Phys. Rev. **D80**, 014017 (2009), [0905.4018].

[58] A. Bacchetta and P. J. Mulders, Phys. Lett. **B518**, 85 (2001), [hep-ph/0104176].

[59] F. Bissey, F.-G. Cao and A. I. Signal, Phys. Rev. **D73**, 094008 (2006), [hep-ph/0512286].

[60] W. Melnitchouk, J. Speth and A. W. Thomas, Phys. Rev. **D59**, 014033 (1998), [hep-ph/9806255].

[61] G.-Q. Feng, F.-G. Cao, X.-H. Guo and A. I. Signal, Eur. Phys. J. **C72**, 2250 (2012), [1206.1688].

[62] M. Traini, Phys. Rev. **D89**, 034021 (2014), [1309.5814].

[63] R. Machleidt, K. Holinde and C. Elster, Phys. Rept. **149**, 1 (1987).

[64] H. Holtmann, A. Szczurek and J. Speth, Nucl. Phys. **A596**, 631 (1996), [hep-ph/9601388].

[65] F.-G. Cao and A. I. Signal, Phys. Rev. **D68**, 074002 (2003), [hep-ph/0306033].

[66] S. Boffi, B. Pasquini and M. Traini, Nucl. Phys. **B649**, 243 (2003), [hep-ph/0207340].

[67] F. Schlumpf, J. Phys. **G20**, 237 (1994), [hep-ph/9301233].

[68] S. J. Brodsky and F. Schlumpf, Phys. Lett. **B329**, 111 (1994), [hep-ph/9402214].

[69] H.-M. Choi and C.-R. Ji, Phys. Rev. **D59**, 074015 (1999), [hep-ph/9711450].

[70] P. Faccioli, M. Traini and V. Vento, Nucl. Phys. **A656**, 400 (1999), [hep-ph/9808201].

[71] B. Pasquini, S. Cazzaniga and S. Boffi, Phys. Rev. **D78**, 034025 (2008), [0806.2298].

[72] C. Fanelli, E. Pace, G. Romanelli, G. Salme and M. Salmistraro, Eur. Phys. J. **C76**, 253 (2016), [1603.04598].

[73] M. Miyama and S. Kumano, Comput. Phys. Commun. **94**, 185 (1996), [hep-ph/9508246].

[74] M. Hirai, S. Kumano and M. Miyama, Comput. Phys. Commun. **108**, 38 (1998), [hep-ph/9707220].

[75] M. Hirai, S. Kumano and M. Miyama, Comput. Phys. Commun. **111**, 150 (1998), [hep-ph/9712410].

[76] A. D. Martin, W. J. Stirling, R. S. Thorne and G. Watt, Eur. Phys. J. **C63**, 189 (2009), [0901.0002].

[77] S. Kumano and M. Miyama, Phys. Rev. **D65**, 034012 (2002), [hep-ph/0110097].

[78] M. Gluck, E. Reya, M. Stratmann and W. Vogelsang, Phys. Rev. **D63**, 094005 (2001), [hep-ph/0011215].

[79] COMPASS, M. G. Alekseev *et al.*, Phys. Lett. **B693**, 227 (2010), [1007.4061].

[80] W.-C. Chang and J.-C. Peng, Prog. Part. Nucl. Phys. **79**, 95 (2014), [1406.1260].

[81] R. D. Field and R. P. Feynman, Phys. Rev. **D15**, 2590 (1977).

[82] New Muon, P. Amaudruz *et al.*, Phys. Rev. Lett. **66**, 2712 (1991).

[83] New Muon, M. Arneodo *et al.*, Phys. Rev. **D50**, R1 (1994).

[84] NuSea, R. S. Towell *et al.*, Phys. Rev. **D64**, 052002 (2001), [hep-ex/0103030].

[85] HERMES, A. Airapetian *et al.*, Phys. Rev. **D71**, 012003 (2005), [hep-ex/0407032].

[86] M. Radici, A. Courtoy, A. Bacchetta and M. Guagnelli, JHEP **05**, 123 (2015), [1503.03495].

[87] M. Anselmino *et al.*, Phys. Rev. **D87**, 094019 (2013), [1303.3822].

[88] Z.-B. Kang, A. Prokudin, P. Sun and F. Yuan, Phys. Rev. **D93**, 014009 (2016), [1505.05589].

[89] P. V. Pobylitsa and M. V. Polyakov, Phys. Lett. **B389**, 350 (1996), [hep-ph/9608434].

[90] P. V. Pobylitsa, M. V. Polyakov, K. Goeke, T. Watabe and C. Weiss, Phys. Rev. **D59**, 034024 (1999), [hep-ph/9804436].

[91] P. V. Pobylitsa and M. V. Polyakov, Phys. Rev. **D62**, 097502 (2000), [hep-ph/0004094].

[92] H.-x. He and X.-D. Ji, Phys. Rev. **D52**, 2960 (1995), [hep-ph/9412235].

[93] M. Pitschmann, C.-Y. Seng, C. D. Roberts and S. M. Schmidt, Phys. Rev. **D91**, 074004 (2015), [1411.2052].

[94] T. Bhattacharya *et al.*, Phys. Rev. **D85**, 054512 (2012), [1110.6448].

[95] R. L. Jaffe and X.-D. Ji, Nucl. Phys. **B375**, 527 (1992).

[96] B. Pasquini, M. Pincetti and S. Boffi, Phys. Rev. **D72**, 094029 (2005), [hep-ph/0510376].

[97] B. Pasquini, M. Pincetti and S. Boffi, Phys. Rev. **D76**, 034020 (2007), [hep-ph/0612094].

[98] M. Pincetti, B. Pasquini and S. Boffi, Czech. J. Phys. **56**, F229 (2006), [hep-ph/0610051].

[99] V. Barone, T. Calarco and A. Drago, Phys. Lett. **B390**, 287 (1997), [hep-ph/9605434].

[100] L. P. Gamberg and G. R. Goldstein, Phys. Rev. Lett. **87**, 242001 (2001), [hep-ph/0107176].

[101] M. Wakamatsu, Phys. Lett. **B653**, 398 (2007), [0705.2917].

[102] P. Schweitzer *et al.*, Phys. Rev. **D64**, 034013 (2001), [hep-ph/0101300].

[103] C. Lorce, Phys. Rev. **D79**, 074027 (2009), [0708.4168].

[104] A. Abdel-Rehim *et al.*, Phys. Rev. **D92**, 114513 (2015), [1507.04936], [Erratum: Phys. Rev.D93,no.3,039904(2016)].

[105] PNDME, T. Bhattacharya *et al.*, Phys. Rev. **D92**, 094511 (2015), [1506.06411].

[106] P. A. Dirac, Rev. Mod. Phys. **21**, 392 (1949).

[107] T. Heinzl, Lect. Notes Phys. **572**, 55 (2001).

[108] J. C. Collins, hep-ph/9705393.

[109] R. F. Streater, R. F. Streater and A. S. Wightman, *PCT, Spin and Statistics, and All That* (Princeton University Press, Kassel, 2000).

[110] S. J. Brodsky, H.-C. Pauli and S. S. Pinsky, Phys. Rept. **301**, 299 (1998).

[111] J. C. Collins, Acta Phys. Polon. **B34**, 3103 (2003), [hep-ph/0304122].

[112] X.-D. Ji, J. Phys. **G24**, 1181 (1998), [hep-ph/9807358].

[113] A. T. Goritschnig, $p\overline{p} \to \Lambda_c^+ \overline{\Lambda}_c^-$ *within the Generalized Parton Picture*, PhD thesis, University of Graz, 2009.

[114] M. Maggiore, *A Modern Introduction To Quantum Field Theory* (Oxford University Press, New York, 2005).

[115] D. Griffiths, *Introduction to Elementary Particles* (John Wiley & Sons, 2008).

[116] M. Jacob and G. Wick, Annals Phys. **7**, 404 (1959).

[117] G. P. Lepage and S. J. Brodsky, Phys. Rev. D **22**, 2157 (1980).

[118] W. N. Cottingham and D. A. Greenwood, *An Introduction to the Standard Model of Particle Physics*, 2. aufl. ed. (Cambridge University Press, Cambridge, 2007).

[119] P. Kroll, M. Schürmann, K. Passek and W. Schweiger, Phys. Rev. **D55**, 4315 (1997), [hep-ph/9604353].

[120] I. Barker, A. Donnachie and J. Storrow, Nucl. Phys. **B95**, 347 (1975).

[121] E. Tomasi-Gustafsson and M. P. Rekalo, Phys. Rev. **D69**, 094015 (2004), [hep-ph/0310172].